AD-A096 078 WISCONSIN UNIV-MADISON DEPT OF GEOLOGY AND GEOPHYSICS F/G 8/10
STRATIGRAPHY AND GLACIAL-MARINE SEDIMENTS OF THE AMERASIAN BASI--ETC(U)
FEB 81 D L CLARK, R R WHITMAN, K A MORGAN N00014-76-C-0005
UNCLASSIFIED NL

1 OF 2
AD A096078

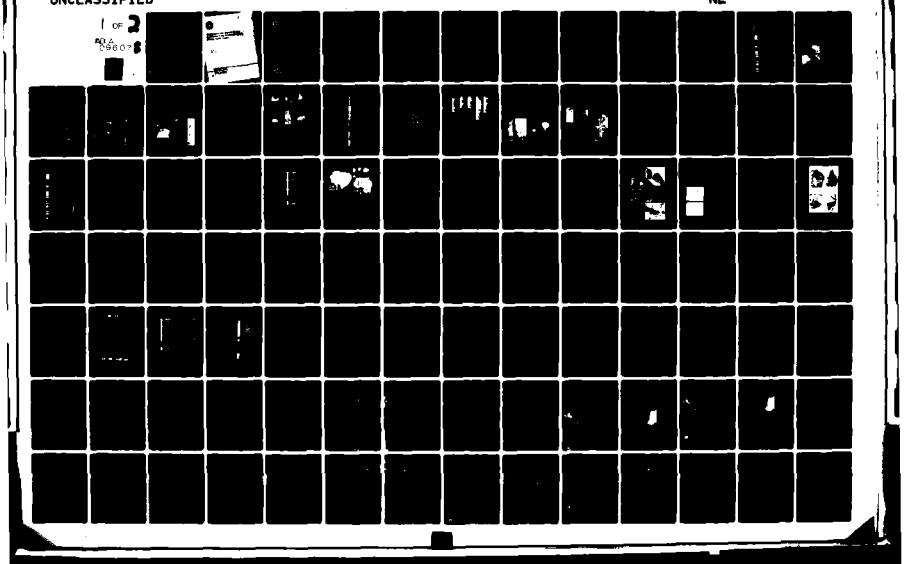

AD-A096078

AD A096078

DDC FILE COPY

(6)

(10) B [redacted] M [redacted]

(15)

(12)

(11) 1 Feb [redacted]

(12) 15

LEVEL

MAR 9 1981

C

Arctic paleoclimatology
sedimentology
sediment classification

404560

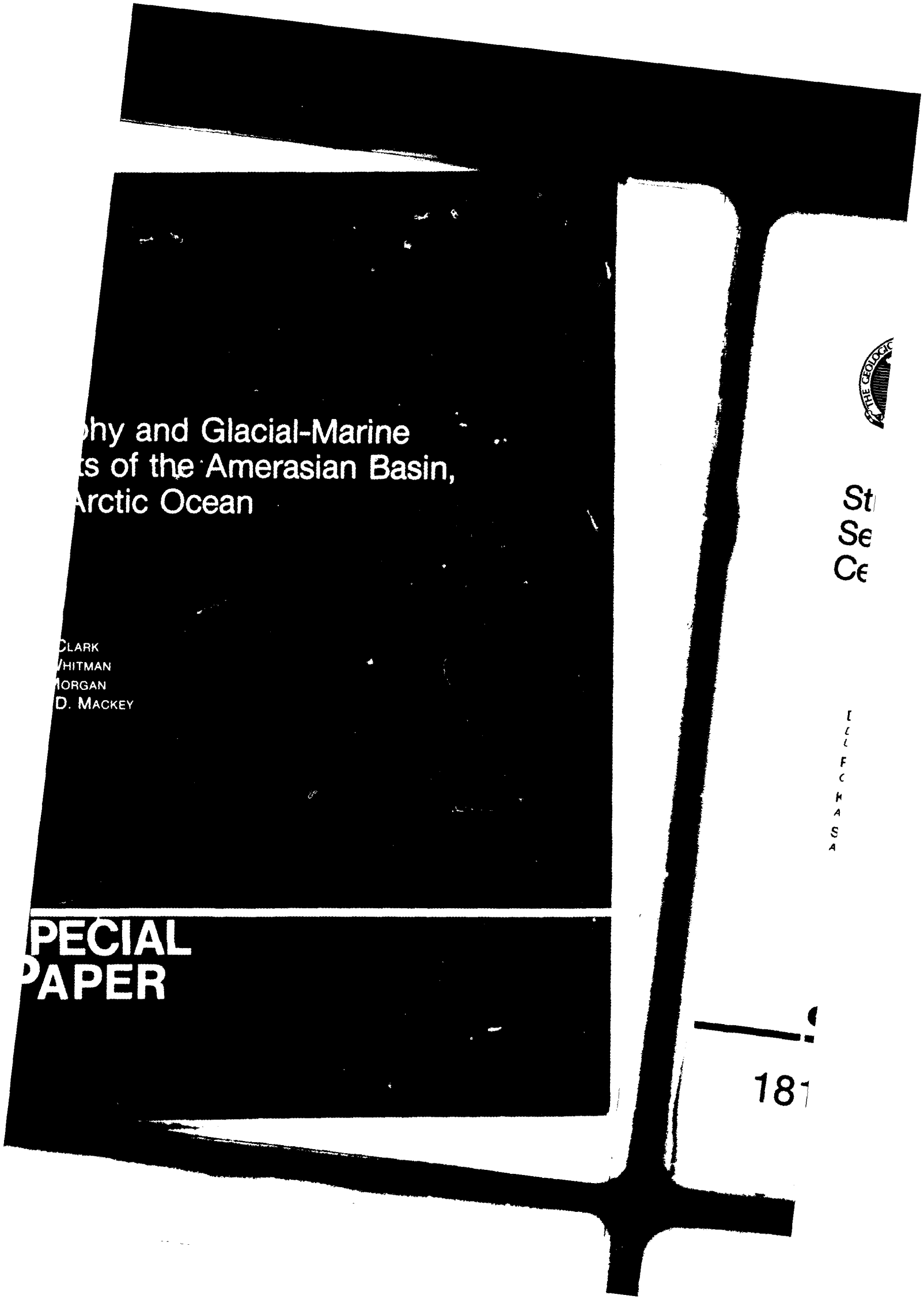
hy and Glacial-Marine
ts of the Amerasian Basin,
Arctic Ocean
CLARK
WHITMAN
MORGAN
D. MACKEY
PECIAL
PAPER
St
Se
Ce
181

(12)

Stratigraphy and Glacial-Marine Sediments of the Amerasian Basin, Central Arctic Ocean

DAVID L. CLARK
Department of Geology and Geophysics, University of Wisconsin, Madison, Wisconsin 53706

RICK R. WHITMAN
Continental Oil Company, Ponca City, Oklahoma 74601

KIRK A. MORGAN
Arco Oil and Gas Company, Anchorage, Alaska 99510

SCUDDER D. MACKEY
Arco Oil and Gas Company, Houston, Texas 77001

SPECIAL PAPER
181

THE GEOLOGICAL SOCIETY OF AMERICA
BOULDER, COLORADO

Library of Congress Catalog Card Number 80-65270
ISBN 0-8137-2181-4

Published by
THE GEOLOGICAL SOCIETY OF AMERICA, INC.
3300 Penrose Place, P.O. Box 9140
Boulder, Colorado 80301

Printed in the United States of America

Contents

ILLUSTRATIONS

Figure

Plate

Table

Acknowledgments

This study was made possible by support from the Office of Naval Research, Arctic Program, No. 00014-76-C-0005. J. Leonard Johnson was helpful in all phases on the study. The cores studied were collected by A. H. Lachenbruch and Vaughn Marshall, U.S. Geological Survey, Menlo Park, California, from ice-island T-3. Logistical support was provided by the Naval Arctic Research Laboratory, Point Barrow, Alaska.

The Deep Sea Drilling Project samples were obtained with the assistance of the National Science Foundation. Dennis S. Cassidy, Curator of the Antarctic Research Facility of Florida State University, provided information on the USNS *Eltanin* and Kara Sea samples. The East Pacific Ocean sediments were provided by Carl J. Bowser, University of Wisconsin Madison. David M. Mickelson, Lawrence J. Acomb, and Timothy A. Kessenich, also from Madison, provided the glacial till samples.

Various forms of aid on X-ray mineralogy data accumulation were provided by John A. Larson and Stephen J. Guggenheim. Paul B. Dombrowski, Donna Diederich, and Del Christensen provided drawings and sections. William A. Morgan, Ronald R. Charpentier, Julie A. Dumoulin, S. W. Bailey, Everett D. Glover, and Robert H. Dott, Jr., furnished constructive criticism. Charles W. Byers and Thomas B. Kellogg read the manuscript and suggested improvements.

Stratigraphy and glacial-marine sediments of the Amerasian Basin, central Arctic Ocean

DAVID L. CLARK
RICK R. WHITMAN*
KIRK A. MORGAN*
SCUDDER D. MACKEY*
Department of Geology and Geophysics, University of Wisconsin, Madison, Wisconsin 53706

ABSTRACT

Thirteen correlatable lithostratigraphic units are recognized in cores recovered from the central Arctic Ocean. The stratigraphic units range in age from late Miocene to Holocene and can be correlated over several hundred thousand square kilometres. Cores were taken from ice-island T-3 during its 1963 to 1973 drift in water depths ranging from 1,069 to 3,820 m. The 13 stratigraphic units, designated A to M, include silty and arenaceous lutites and carbonate-rich, pink-white layers. Three arenaceous lutites are important marker beds in the lower part of the section (A to H), and pink-white layers are distinctive units in the upper section (I to M).

Ages for the units can be calculated by the use of paleomagnetic reversal signatures and by extrapolation of sedimentation rates based on these figures. Units I to M have calculated sedimentation rates that average 1.14 mm/1,000 yr, whereas the sedimentation rates of the older units (A to H) average 0.5 mm/1,000 yr. Pebbles, probably ice-rafted, occur throughout the units. Extrapolation of the sedimentation rate from the Gilbert Polarity Interval 5 reversal indicates that the oldest erratic in undisturbed sediment may have been deposited 5.26 m.y. ago. In general, the arenaceous lutites and pink-white layers represent the highest sedimentation rate and are interpreted to have been deposited during times of increased glacial ice-rafting. Silty lutites may also be principally ice-rafted sediment, but they are believed to represent periods of reduced ice-rafting and lower sedimentation rates.

Four types of glacial-marine sediment can be characterized by silt-clay histograms. The four histogram types (type I, nonsorted, type II, bimodal, type III, clay mode, and type IV, silt mode) reflect differences in the environmental factors that influenced glacial-marine sedimentation. The major process that affected deposition of ice-rafted debris in the Arctic Ocean study area may have been mid-depth oceanic circulation. Little evidence was found to support the hypothesis that the reworking of central Arctic Basin glacial-marine sediment by bottom currents had any major effect on silt-clay distributions.

A mode was observed in the fine to coarse clay particles in most central Arctic Basin glacial-marine sediments. A similar mode was observed for East Pacific Ocean pelagic clay samples. A fine mode in both types of sediment suggests that deposition of clay and fine silt of pelagic or glacial origin occurs uniformly in the deep-sea environments that were sampled.

The geographic distribution of central Arctic Basin glacial-marine sediment types suggests that deposition of ice-rafted coarse sediment dominates sedimentation in the Alpha Cordillera region. In abyssal plain environments, deposition of ice-rafted debris also occurs but is partially masked by turbidite deposition.

The four types of glacial-marine sediment occur in units A to M and support the hypothesis that ice-rafting has been an important mechanism in contributing sediment to the Alpha Cordillera since the late Miocene. In addition, the stratigraphic distribution of these sediments supports the theory that arenaceous lutites represent periods of increased ice-rafting, while silty lutites represent periods of decreased ice-rafting. Central Arctic Basin and non-Arctic marginal sea glacial-marine sediments exhibit similar silt-clay histogram types.

Six intervals of increased Pleistocene glacial ice rafting are defined. Correlation with periods of continental glaciation is possible, but correlation with marine or terrestrial sequence is difficult because the central Arctic Ocean remained frozen while climatic changes more severely affected lower latitudes. Good correlation with glaciations defined by oxygen-isotope stratigraphy is possible for the most recent times of increased ice-rafting.

INTRODUCTION

Knowledge of the sediments and stratigraphy of the deep Arctic Ocean is based primarily on short cores taken during the drift of ice-island T-3 from 1963 to 1973. T-3 was abandoned in 1974, and

*Present address: Whitman, Continental Oil Company, Ponca City, Oklahoma 74601; Morgan, Arco Oil and Gas Company, Anchorage, Alaska 99510; Mackey, Arco Oil and Gas Company, Houston, Texas 77001.

because of the enormous problems inherent in working in an ice-covered ocean, there may not be a comparable program for decades to come. The T-3 cores may therefore remain unique.

This report is concerned with the identification of stratigraphic units and classification of the glacial-marine sediment that is the dominant sediment type in the central Amerasian Basin. The cores were selected from 580 successful casts made from T-3 by Vaughn Marshall and A. H. Lachenbruch of the U.S. Geological Survey, Menlo Park, California (Fig. 1). The location, water depth, and length of these cores are listed in Appendix 1A. The cores were recovered from most parts of the Alpha Cordillera, the dominant ridge of the Amerasian Basin. Canada Basin cores have a high percentage of turbidites and a different stratigraphy (Campbell and Clark, 1977) and are not included in this study. Cores from the eastern end of the Alpha Ridge contain a greater percentage of clastics and have significant stratigraphic differences from the cores of this study. The interpretation of these cores is in progress.

Details concerning the lithostratigraphy and glacial-marine sediment described in this report represent a synthesis of several separate projects at the University of Wisconsin. Previous work, more closely related to details of the fauna and paleoecology, has been summarized by Clark (1975, 1977a, 1977b), Joy and Clark (1977), Lagoe (1976, 1977), Gamber and Clark (1978), and Kitchell and Clark (1979).

In this report, we recognize 13 lithostratigraphic units ranging in age from late Miocene to Holocene. A textural classification of glacial-marine sediment and maps illustrating various sediment parameters of the modern Arctic Ocean surface are presented. The report is divided into sections that include the description and interpretation of the first lithostratigraphy of the central Arctic Ocean and a description and interpretation of the surface sediment. The final section illustrates the relationship of the surface and in-core sediment, both of which are largely glacial-marine. These sections lead to conclusions that pertain to the paleoclimatology of the central Arctic Ocean.

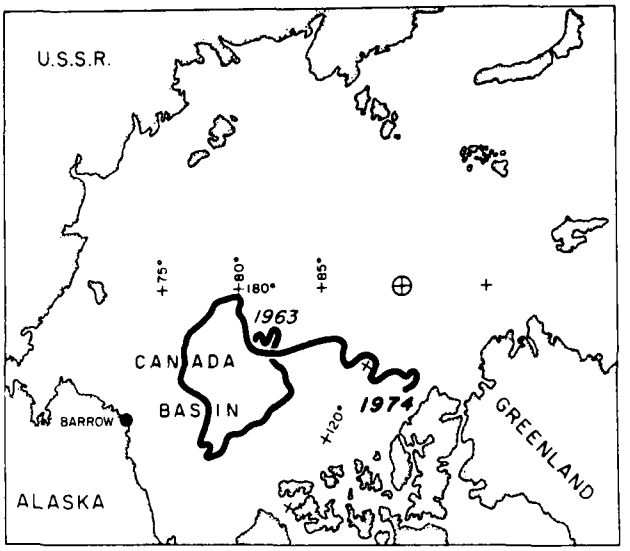

Figure 1. Track of ice-island T-3 drift. All cores were taken along the track of this drift.

PREVIOUS ATTEMPTS AT AN ARCTIC OCEAN STRATIGRAPHY

Previous attempts to develop a physical stratigraphy for the central Arctic Ocean have had little success. A few correlations based on a variety of sedimentary parameters have been only partially successful. For example, Frieson and others (1964) noted a correlation between alternating light brown and dark brown, Foraminifera-rich layers sampled on the Alpha Cordillera. Hunkins and Kutschale (1967) correlated similar units between the Wrangel Abyssal Plain and the Alpha Cordillera, but precise correlation was not achieved. Also, Herman (1964, 1974) used variations in color, texture, faunal abundance, and magnetics to correlate several T-3 cores from the Alpha Cordillera, but these factors have not been identified in other cores. Hunkins and others (1971) summarized previous correlation attempts and presented a synthesis of former work.

Darby (1971) determined changes in weight percent carbonate versus depth in core for 15 T-3 cores. At least 13 carbonate maxima and minima were identified and correlated in cores with a wide geographic distribution. Clark (1971) found a correlation between pelagic Foraminifera and ice-rafted erratics in 45 cores, and Larson (1975) was able to correlate several Foraminifera abundance peaks in five cores over a fairly wide geographic area.

The stratigraphy described herein emphasizes the differences between two major types of Arctic Ocean sediment: silty lutites and arenaceous lutites. The average weight percent of sand-sized material is considered to be the key sedimentary characteristic. Standard thin-section modal analysis, thin-section frequency analysis, plus X-ray and elemental analysis of the various units also were accomplished. The 13 lithostratigraphic units described have been correlated over several hundred thousand square kilometres and in several hundred cores. The uniformity of very thin units over such a large area is remarkable in that the units are of glacial-marine origin.

STRATIGRAPHY

The following stratigraphic descriptions are a composite study of the preserved halves of several hundred cores and of semiquantitative analysis of a few selected cores. Features such as gross sediment texture, burrowing, color mottling, layering, and erratics are easily observed with the unaided eye and permit visual differentiation of the units.

The oldest stratigraphic unit described (unit A) is the oldest normal sediment that has been penetrated in the central Amerasian Basin (Fig. 2). Older (Cretaceous and Paleocene) sediment has been described but represents parts of slump blocks that rest on and are covered by late Cenozoic sediment (Clark, 1974).

Unit A

Unit A, the oldest in situ sediment cored in the central Arctic Ocean, is composed of olive-brown silty lutite with rare (0.9- to 2.3-cm-thick layers of reddish-brown arenaceous lutite (Fig. 3). The olive-brown silty lutite is generally a mottled, light olive-brown to dark olive-brown color. Most of the cores studied in detail terminate in this unit, and the reported thickness is extremely variable. It is indeterminable how far unit A extends below the

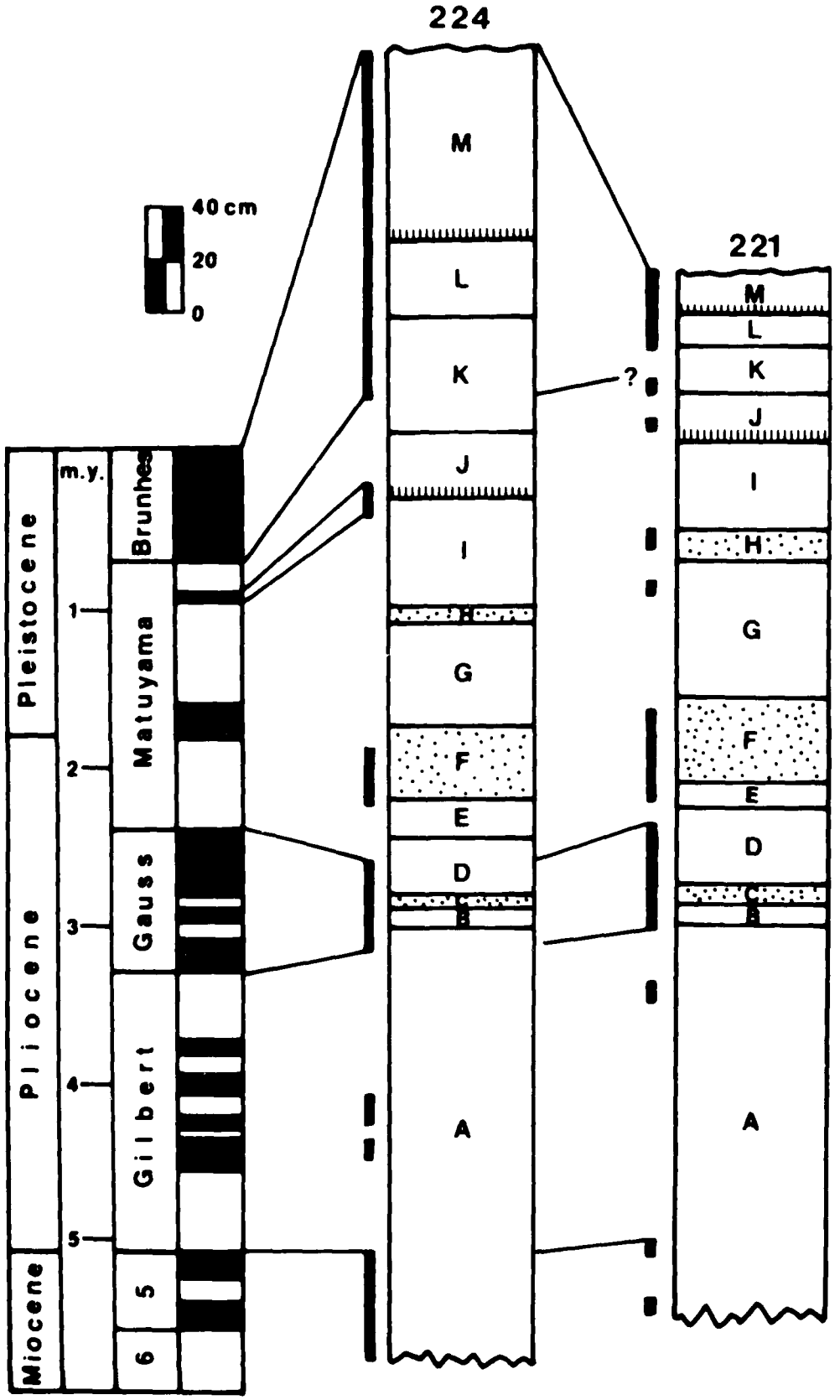

Figure 2. Lithostratigraphic units in two cores from the Alpha Ridge. Correlation with magnetic reversal stratigraphy and classification indicated. Strongest evidence of late Miocene age is from extrapolation of sedimentation rates fixed by Gauss-Gilbert and Matuyama-Gauss boundaries (explained in text). Stippled units are key arenaceous lutite beds in lower part of section. Hatches are key pink-white layers in upper part of section.

oldest sediment observed. In the two cores that made the deepest penetration (221 and 224), the thickness of unit A is 150 and 163.5 cm, respectively (Fig. 2).

Burrows, probably *Chondrites* (Chamberlain, 1975), are common. They generally range from 0.5 to 2.0 mm in diameter and 2.0 to 12.0 mm in length. Composite burrows (Chamberlain, 1975) are occasionally found (Fig. 4). They are commonly elliptical or round and range from 1.5 to 3.4 cm in their longest dimension.

The weight percent of the sand-sized fraction of the olive-brown silty lutite averages 5.0% for 26 cores (App. 2). The detrital sand-sized fraction is in the fine-sand range and is moderately well sorted. Monocrystalline quartz is the most abundant sand-sized particle (App. 3).

Authigenic ferromanganese sand-sized particles attain their greatest abundance in unit A. They occur in clusters associated with burrows or are uniformly distributed. These particles comprise between 2.1% and 43.4% of the sand-sized fraction of unit A. These dark brown to black ferromanganese particles impart a peppery or speckled appearance to the surface of the cores.

Arenaceous lutites are rare in unit A but have been found in cores (FI 283, FI 357, FI 381, FI 400) where the average weight percent of the sand-sized fraction is 26.35%. The mean size of the detrital sand fraction is in the fine-sand range and is moderately sorted. Ferromanganese particles are rare in the arenaceous lutites and average only 1.87% of the sand-sized fraction.

TABLE 1. DISTRIBUTION OF ERRATICS IN [illegible] ARCTIC [illegible]

Stratigraphic unit	Number of erratics	Average [illegible] (mm)	[illegible] erratics
M	442		
L	203		
K	205		
J	145		
I	250		
H	79		
G	153		
F	189		
E	83		
D	25		
C	22		
B	9		
A	15		
Total	[illegible]		

In the reference half of core FI 285, several very dark olive-brown, cohesive, silty lutite clasts occur (Fig. 3). These clasts are interspersed in segments two through five and are 18.0 to 65.5 cm from the bottom of the core. The clasts are as thick as 4.0 cm and extend beyond the boundaries of the core liner. One clast has 8.1% sand-sized material. This compares with an average of 5.86% sand-sized material for the surrounding olive-brown silty lutite. The sand is composed of 40% to 50% authigenic ferromanganese particles. This is similar to the maximum value of 41% ferromanganese parti

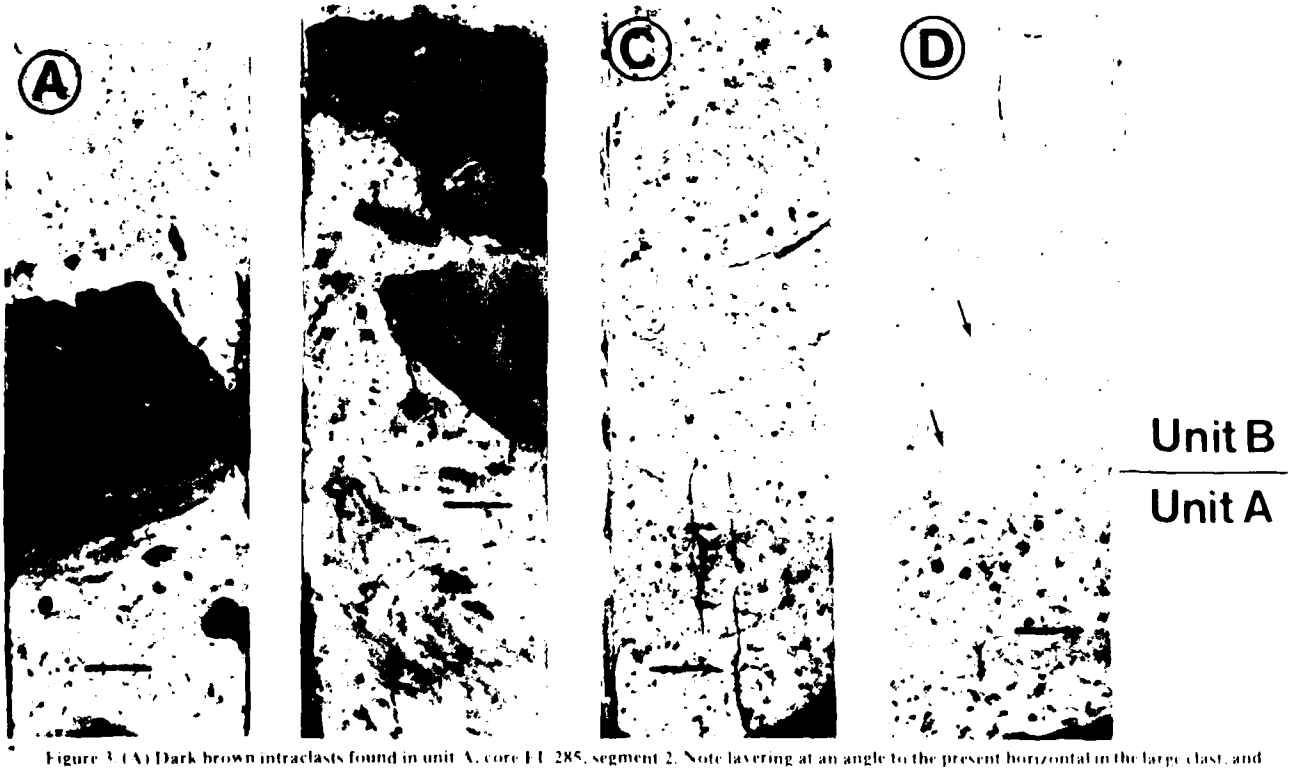

Figure 3. (A) Dark brown intraclasts found in unit A, core FI 285, segment 2. Note layering at an angle to the present horizontal in the large clast, and the contorted appearance of the surrounding light olive brown sediment. (B) Dark brown intraclasts in unit A, core FI 285, segment 4. Note the surrounding contorted, light olive-brown sediment. (C) Typical light olive-brown silty lutite found in unit A, core FI 430, segment 4. Note distinct burrows and change in sediment hue (color mottling). (D) Typical contact between light to medium olive-brown unit A and light olive brown unit B, core FI 430, segment 6. Note decrease in burrowing and more uniform appearance of unit B in contrast with unit A. The small arrows point to two possible composite burrows. Scale bars represent 1 cm.

cles in the sand-sized fraction in the surrounding olive-brown silty lutite. Foraminifera and other fossils are not present in the sand-sized fraction of the dark brown clasts. A very dark olive-brown clast at 3.0 to 7.0 cm in segment two is laminated or banded at an angle of 40° from the present horizontal. The adjacent olive-brown silty lutite is unlayered. However, it does show convolutions, contorted burrows, and general evidence of disturbance (Fig. 3).

Clasts in FL 285 probably are intraclasts that were locally derived from sediment stratigraphically below unit A. The dark olive-brown color of these clasts is very similar to the distinctively colored flow-in found in cores FL 221, FL 222, and FL 224. The clasts represent evidence of slumping and or current scour and redeposition of semiconsolidated sediment at the time that unit A was being deposited. Erratics are rare in unit A (Table 1).

Unit B

Overlying unit A is a thin silty lutite unit characterized by a uniform light brown color (Fig. 3). The thickness of unit B ranges from 2.0 to 14.5 cm, but the average thickness for 38 cores is 9.0 cm.

The lower contact of unit B is gradational and is placed approximately where burrowed sediment of unit A gradually ends and uniform unburrowed sediment begins. In some cores, indistinct, small, light olive-brown or olive-gray burrows appear. These burrows are *Chondrites* but are smaller than those in unit A. In many cases, some mottling of olive-gray or olive silty lutite with the olive-brown silty lutite occurs.

Black to dark brown ferromanganese particles are common in unit B and give the surface of the core a speckled appearance. The ferromanganese particles average 13.9% of the sand-sized fraction. They often occur in small clusters or are associated with burrows.

The weight percent of the sand-sized fraction averages 6.06% for 24 cores (App. 2). The detrital sand-sized fraction is generally in the fine-sand range and is moderately sorted. Monocrystalline quartz is the major constituent of the sand-sized fraction (App. 3).

Erratics are rare in this thin unit (Table 1).

Unit C

Above unit B is a thin but distinctive unit characterized by two thin, reddish olive-brown, arenaceous lutite layers and an intervening, slightly thicker, light olive-brown silty lutite (Fig. 4). The thickness of unit C ranges from 3.5 to 10.0 cm, but the average thickness for 40 cores is 6.03 cm. The thicknesses of the individual layers range from less than 1.0 cm for many of the arenaceous lutites to a maximum of 7.0 cm for the middle silty lutite.

The lower contact of unit C with unit B is at best irregular and often is diffuse and gradational. It is defined by a change in texture and a corresponding change in the shade of color from light olive-brown lutite to a darker, reddish olive-brown arenaceous lutite.

Unit C is the lowermost of three prominent arenaceous lutite key layers and in this context is referred to as the "lower coarse" layer.

The medial silty lutite resembles the underlying unit B in its overall light brown color. It has more and better developed burrows. In many cores it appears to have a relatively sandy

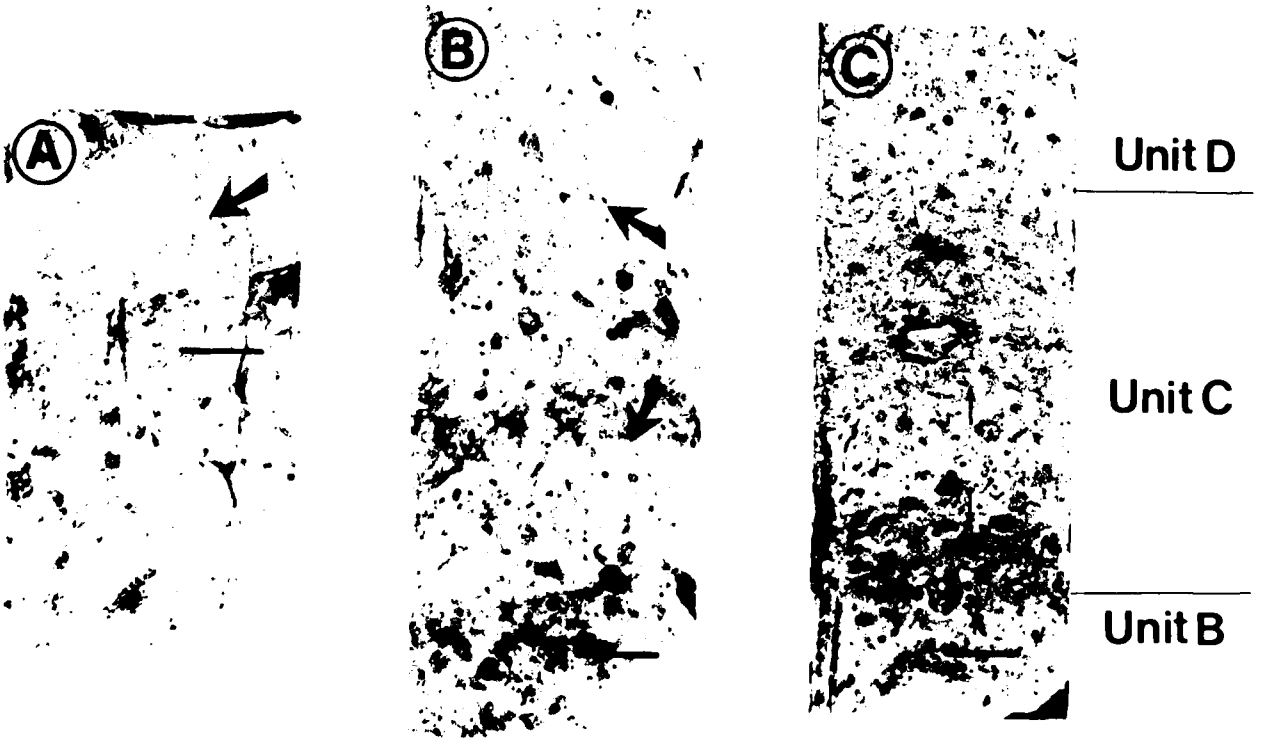

Figure 4. (A) Composite burrow (arrow) found in silty lutites of unit A, core FL 400, segment 2. (B) Composite burrows (arrows) found in unit A, core FL 400, segment 4. (C) Typical unit C and contacts with light olive-brown units B and D; core FL 283, segment 7. The contacts of the medial silty lutite layer in unit C are marked by the small arrows. Note the small pebble in the top of the lower coarse layer in unit C. All scale bars represent 1 cm.

texture. The contacts of the silty lutite with the overlying and underlying arenaceous lutites are moderately to extremely gradational.

The weight percent of the sand-sized fraction averages 16.73% for the lower part and 16.04% for the upper part of unit C for 22 cores (App. 2). The detrital sand-sized fraction is generally in the fine-sand range and is moderately sorted. Monocrystalline quartz is the major constituent of the sand-sized fraction (App. 3).

Ferromanganese particles are not obvious on the reference core halves. They constitute an average of only 2.0% of the sand-sized fraction for the lower part of unit C and 3.29% for the upper part.

Erratics occur at all levels in unit C (Table 1.)

Unit D

Unit D is a relatively thick, olive-brown to light olive-brown silty lutite (Fig. 5). The thickness of this unit ranges from 20.0 to 56.0 cm, but the average thickness for 40 cores is 34.17 cm. This unit is very similar in gross appearance to unit A.

The lower contact with the arenaceous unit C is gradational to moderately sharp and is irregular.

Burrows similar to *Chondrites* are very common in unit D. These burrows range from 2.0 to 20.0 mm in length and from 0.5 to 2.0 mm in diameter. The burrows are generally filled with sediment that is darker than the surrounding sediment. This feature augments the normal color mottling to produce some areas that are uniformly dark olive brown.

Ferromanganese particles are common and speckle the surface of the reference core halves. They are distributed evenly over the core surface, are found in clusters, or form rims on burrows. These particles average 8.8% of the sand-sized fraction.

The weight percent of the total sand-sized fraction averages 6.31% for 27 cores (App. 2). Detrital sand occurs in the fine-sand range and is moderately sorted. Monocrystalline quartz is the most abundant sand-sized grain type (App. 3).

Twenty-three erratics occur in cores studied in detail (Table 1).

Unit E

Above unit D is a thin, generally distinctive, uniform olive-gray to light olive-brown silty lutite (Fig. 5). The thickness of unit E ranges from 3.0 to 20.0 cm for 51 cores, with the average thickness being 9.44 cm. The characteristic feature of this unit is the uniform, unburrowed nature of the sediment. In cores where unit E is composed of a uniform olive-gray to olive silty lutite, a distinctive

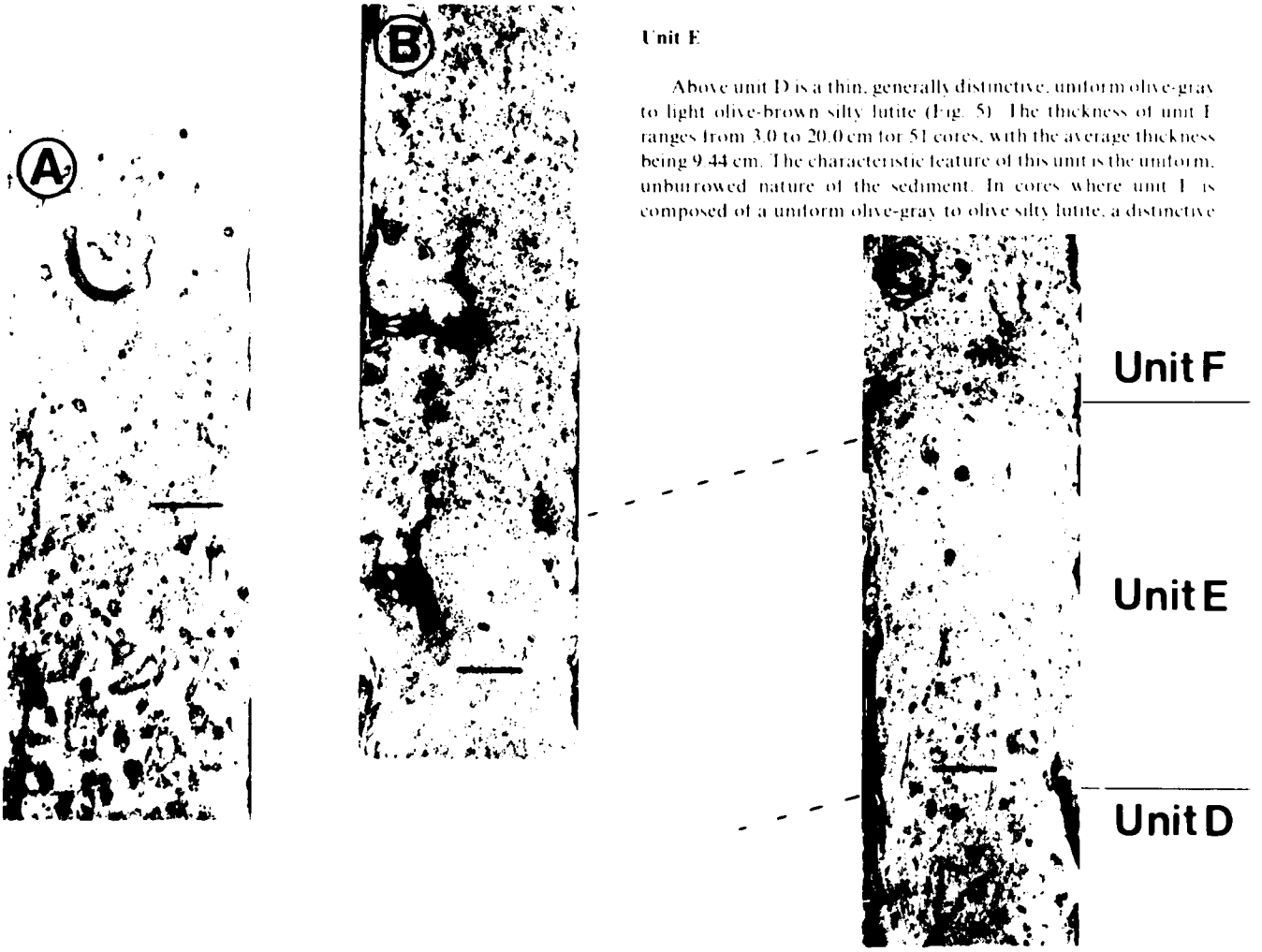

Figure 5. (A) Typical olive-brown, burrowed silty lutite of unit D; core EL 283, segment 9. (B) Contact between uniform olive-gray unit E and arenaceous unit F; core EL 221, segment 21. Note contact deformed concave downward. (C) Representative sample of units D, E, and F; core EL 283, segment 10. Note the downward-deformed contact between units E and F and the very gradational contact between uniform unit E and burrowed unit D. Correlation with (B) as shown. Scale bars represent 1 cm.

layer that contrasts with the generally olive-brown sediment above and below is formed. The upper portion of this unit, an arenaceous lutite, often is very sandy.

The lower contact of unit E with underlying unit D is gradational. The contact is at a level where most large and distinct burrows and dark mottled sediment have given way to a more uniform, light-colored sediment.

Mottling is very subtle in unit E. Burrows similar to *Chondrites* are rare and are usually very small, unobstrusive, and light colored. A long, vertical, more well defined burrow occasionally penetrates the greater part of the thickness of this unit.

Ferromanganese particles are present in most cases but are unobtrusive and minor and are not always easily noticed. In some cases, however, they do give a speckled appearance to the reference half of the core. These particles average 5.8% of the sand-sized fraction.

The weight percent of the sand-sized fraction for unit E averages 8.65% for 26 cores (App. 2). The average detrital sand-sized fraction is in the fine- to very fine-sand range and is moderately sorted. Monocrystalline quartz is the major sand-sized grain (App. 3).

Thirty-three erratics occur in the cores in which unit E was studied in detail (Table 1).

Unit F

Unit F is a distinctive, reddish olive-brown to light olive-brown arenaceous lutite (Fig. 5). The thickness of this unit which ranges from 2.5 to 36.5 cm, averages 13.76 cm for 49 cores. The sandy nature of this unit is readily apparent. Granules and coarse sand-sized grains of quartz, carbonates, and rock fragments are easily seen with the unaided eye on the surface of the reference core half. Cohesive mud clasts are common and often are abundant. These clasts are composed of a uniform clay to very fine silt. They are colored dark gray to black in most cases and pink to red in some rare instances. Occasionally they are finely banded or laminated. They are roughly spherical or have a polygonal outline with rounded corners. These clasts are significant for the glacial-marine genesis of the sediment and are discussed later.

Contact with the underlying unit E is exceedingly sharp, even under a microscope. The contact is well defined by a change in sorting and mean grain size that corresponds to the color change from olive-gray to light olive-brown silty lutite to reddish olive-brown arenaceous lutite.

Unit F is the second of the three key arenaceous lutite horizons. In relation to the stratigraphically lower and higher key units, this unit is referred to as the "middle coarse" layer. It forms an unmistakable combination when coupled with the often distinctive underlying unit E.

Unit F generally lacks internal bedding, lamination, or other primary sedimentary structures. In some cases there is a color change from light olive brown in the lower portion to reddish olive brown in the upper part of the unit.

Sediments in unit F are commonly subtly mottled. These mottles are a result of differing percentages of sand or differing mean grain size in the sand-sized fraction and are very vague with ill-defined boundaries. These mottles do not resemble burrowing but appear to be depositional or early diagenetic features.

In core FL 396, 84 cm from the base of the core, a small piece of wood was discovered (Fig. 6). The fragment is approximately 1.5

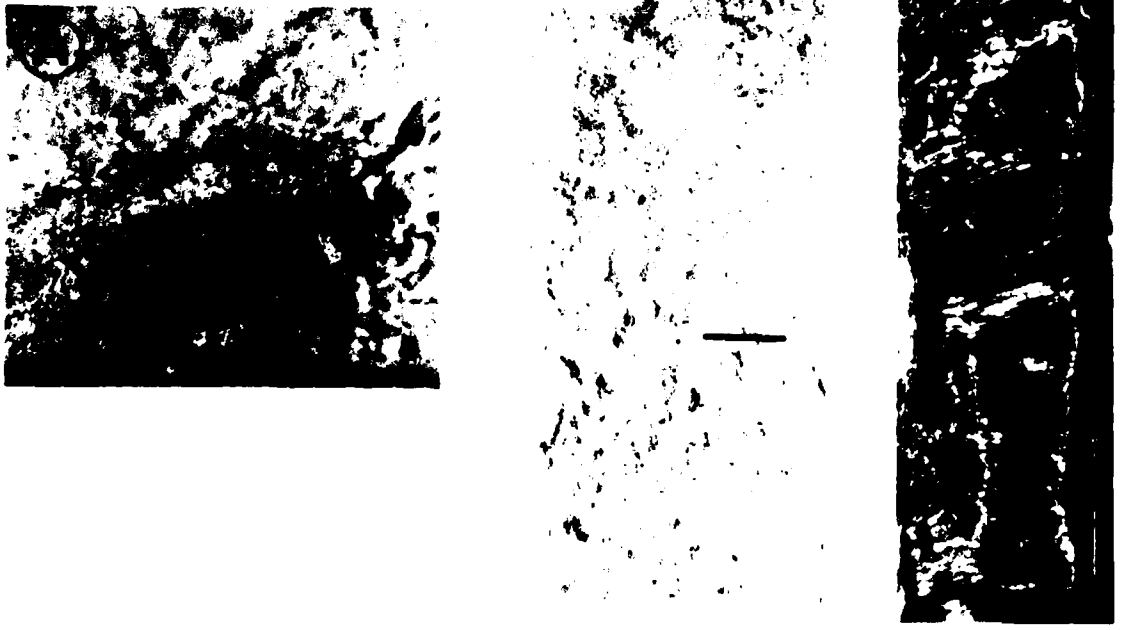

Figure 6. (A) Wood fragment found in unit F in core FL 396, segment 6. (B) Typical sediment in unit G; core FL 214, segment 9. Note burrows and change in sediment hue from light olive-brown to dark olive-brown (color mottling). (C) Typical Canada Abyssal Plain turbidite, core FL 63, segment 4 (see Campbell and Clark, 1977, for details). Compare with unit F in Figure 5. All scale bars represent 1 cm.

cm in length and 0.8 cm in width but is poorly preserved. Close study of thin sections reveals that the fragment is wood, but further identification is impossible (B. F. Kukachka, 1977, written commun.). This was the only plant fragment recovered from any Arctic core.

Ferromanganese particles are rare or absent in unit F. Their average weight percent of the sand-sized fraction for three cores is 2.0%.

The weight percent of the sand-sized fraction for this unit averages 23.00% for 27 cores (App. 2). The detrital sand-sized fraction has an average mean in the fine-sand range and is poorly sorted. Monocrystalline quartz is the most abundant sand-sized grain (App. 3).

Erratics are common in unit F. In the cores studied, 189 erratics were found (Table 1).

Unit G

This unit is a light olive-brown to dark olive-brown silty lutite (Fig. 6). Unit G ranges from 29.0 to 65.0 cm in thickness and averages 50.84 cm for 51 cores. This unit is similar to units A and D in overall appearance. It differs from both of these units in that Foraminifera tests are up to 20 times more abundant in the upper portion of unit G than they are in any stratigraphically lower unit. This large increase in Foraminifera tests is seen in 80% to 90% of the cores. The sudden appearance of abundant planktonic Foraminifera is easily recognized with a hand lens. This increase in the number of Foraminifera tests occurs at approximately one-third to two-thirds of the thickness of unit G from the lower contact with unit F.

The lower contact of unit G with the underlying middle coarse layer (that is, F) is gradational.

Unit G ranges in color from light olive brown to a very dark olive brown. There is general trend in the sediment color from a lighter olive brown at the bottom of the unit to a darker olive brown toward the top. The sediment is very color mottled. *Chondrites* type burrows are especially abundant in the upper two-thirds of this unit. The burrows are generally very large—up to 3.5 mm in diameter and 25.0 mm in length.

Ferromanganese particles are common. They rim a burrow and accentuate the burrow outline. These ferromanganese particles average more than 4.0% of the sand-sized fraction. Cohesive, dark-gray mud clasts, 1.0 to 3.0 mm in diameter, are occasionally present in this unit.

The weight percent of the sand-sized fraction averages 9.85% for 26 cores (App. 2). The detrital sand-sized fraction has an average mean value in the fine-sand range and is poorly sorted. Monocrystalline quartz is the major constituent of the sand-sized fraction (App. 3). Foraminifera tests average only 0.51% of the sand in the lower portion, but they constitute an average of 18.31% in the upper portion of this unit. They range from 8.5% to 35.42% of the sand-sized material of the Foraminifera-rich upper portion of unit G for three cores.

In unit G, 133 erratics occur in the cores (Table 1).

Unit H

Unit H is predominantly an arenaceous lutite. It is divided into five subunits—four thin arenaceous lutite layers and one thin, interstratified, silty lutite layer (Fig. 7). These layers have been designated subunits a through e, from bottom to top. Unit H ranges in thickness from 5.8 to 15.9 cm and averages 11.32 cm for 43 cores.

Unit H is the third and uppermost of the three key arenaceous lutites. In this context, it is known as the "top coarse" layer.

Erratics are common in unit H. Seventy-nine were found in the cores (Table 1).

Subunit Ha. This is a uniform, light olive-brown arenaceous lutite. It is absent in cores from the Chukchi Rise and western Alpha Cordillera areas (Fig. 8). This subunit is discontinuous and is very thin in many cores. It has a variable thickness that ranges from 0.8 to 6.0 cm and averages 3.07 cm for 14 cores.

The lower contact with unit G is usually sharp but often irregular. The contact is clearly defined by an upward change from usually dark brown silty lutite to light reddish olive-brown arenaceous lutite.

Ferromanganese particles are rare in subunit Ha and average 1.8% of the sand-sized fraction. No burrows or mottling were noted.

The weight percent of the sand-sized fraction has an average mean value in the fine-sand range and is moderately sorted. Monocrystalline quartz is by far the most abundant detrital grain type (App. 3).

Subunit Hb. This is a dark gray to reddish olive-brown arenaceous lutite characterized by an overall dark gray color. This subunit ranges in thickness from 1.0 to 4.3 cm and averages 2.75 cm for 20 cores.

The contact with subunit Ha is commonly sharp and irregular. In a few cores it is gradational. The boundary is usually sharply defined by a change in color and texture from a light reddish olive-brown arenaceous lutite below to a very coarse, grayish arenaceous lutite above.

Ferromanganese particles are rare in this subunit and average only 3.6% of the sand-sized fraction. Burrows are absent.

The weight percent of the sand-sized fraction averages 33.62% for 14 cores (App. 2). This value is the highest average percent sand-sized fraction of any of the other units in the study section. The detrital sand-sized fraction has an average mean value in the fine-sand range and is moderately sorted. Monocrystalline quartz is the major constituent of the sand-sized fraction (App. 3).

Subunit Hc. This is a light reddish olive-brown arenaceous lutite that is fairly uniform in overall appearance. The thickness of subunit Hc ranges from 0.7 to 7.17 cm and averages 3.36 cm for 22 cores.

The lower contact with subunit Hb ranges from gradational and indistinct to sharp and regular. This contact is defined by the change from grayish, very sandy and coarse arenaceous lutite below in subunit Hb to reddish, less sandy and coarse arenaceous lutite above in subunit Hc.

Ferromanganese particles are rare in this subunit and average only 3.0% of the sand-sized fraction. Burrows are rare.

The weight percent of the sand-sized fraction averages 20.70% for 22 cores (App. 2). The detrital sand-sized fraction has an average mean value in the fine-sand range and is poorly sorted. Monocrystalline quartz is the most abundant sand-sized grain (App. 3).

Subunit Hd. This olive-brown, often uniform silty lutite is the only silty lutite subunit in the generally arenaceous unit H. It ranges in thickness from 0.1 to 3.5 cm and averages 2.0 cm for 23 cores.

The lower contact with subunit Hc is very vague, diffuse, and gradational in most cases. This contact is largely defined by a

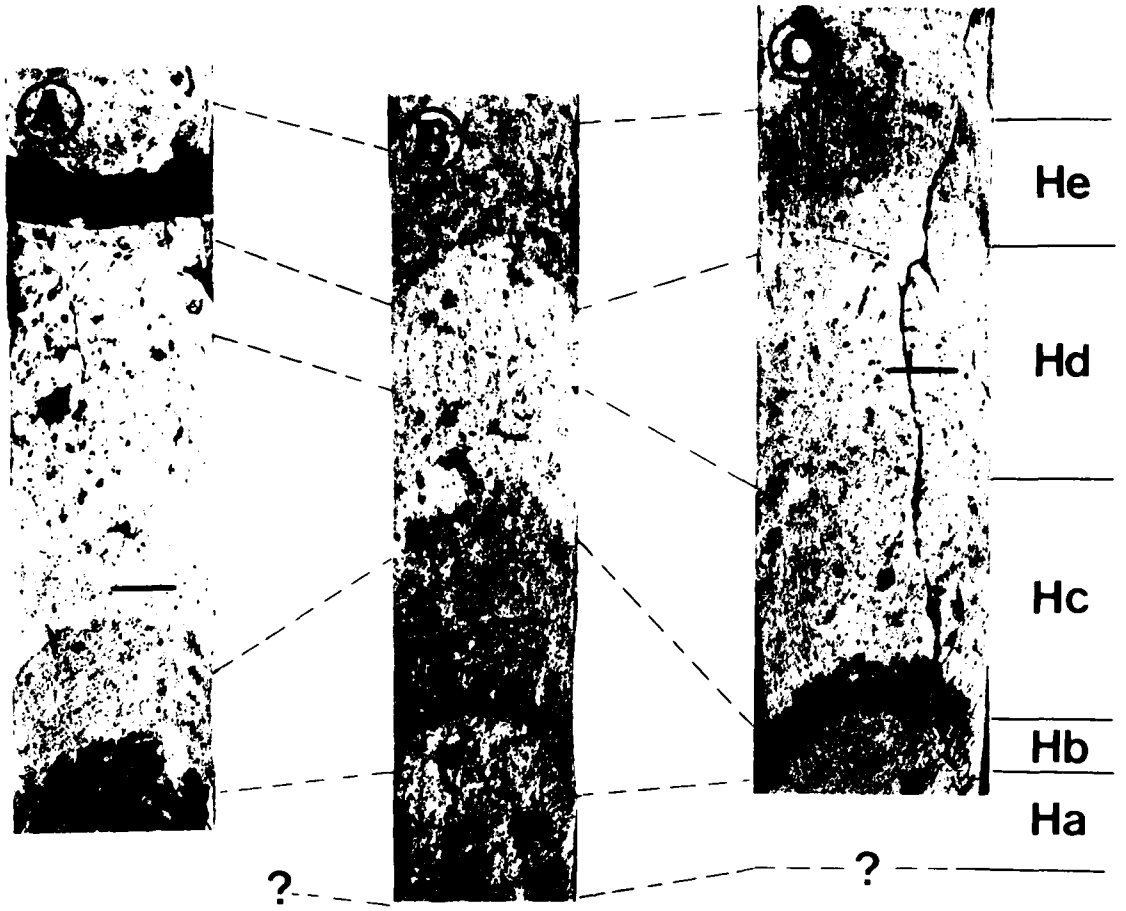

Figure 7. (A) Unit H, arenaceous lutite from core FI 283, segments 14 and 15. Subunit Ha is missing in this core. Note concave-downward deformation of contacts. Contact between subunits Hc and Hd is gradational. Sediment below subunit Hb is unit G. (B) Unit H from core FI 409, segment 7. Subunit Ha is present in this core. A small portion of unit G can be seen at the bottom of the photograph. Again, most contacts are deformed, and the contact between subunits Hc and Hd is poorly defined. (C) Unit H from core FI 308, segment 8. Subunit Ha is present; only its upper portion is shown. Most contacts are deformed. Correlation with (A) and (B) is as shown. Correlation lines drawn to deformed contacts. All scale bars represent 1 cm.

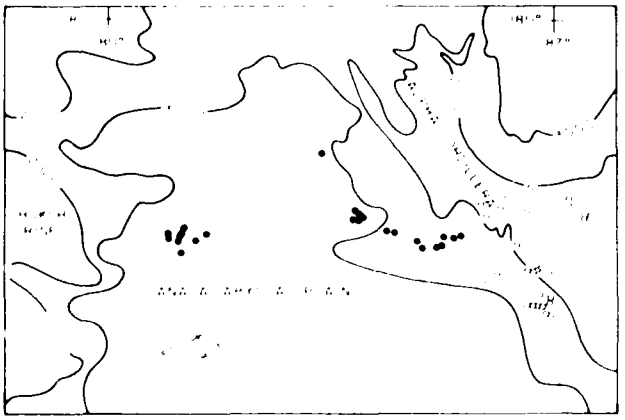

Figure 8. Map showing the distribution of subunit Ha. Closed circles represent cores with subunit Ha missing; open circles represent cores with subunit Ha present. Water depth in metres.

change in texture from predominantly arenaceous lutite below to silty lutite above.

Ferromanganese particles range from common to rare in this subunit and average 9.5% of the sand-sized fraction of the sediment.

Burrows similar to the *Chondrites* type are common in this subunit. The sediment is often color mottled with various shades of olive-brown sediment.

The average weight percent of the sand sized fraction is 7.8% for 24 cores (App. 2). The mean size of the detrital sand-sized fraction is in the fine sand range and is moderately sorted. The predominant sand sized grain is monocrystalline quartz (App. 3). Foraminifera are also common in this subunit in comparison to the other subunits in unit H. Foraminiferal tests average 6.3% of the sand sized fractions.

Subunit He. This is the uppermost subunit of unit H. It is a dark reddish olive brown arenaceous lutite. It is often discontinuous and irregular from one core to another. This subunit is generally the most poorly developed subunit in unit H.

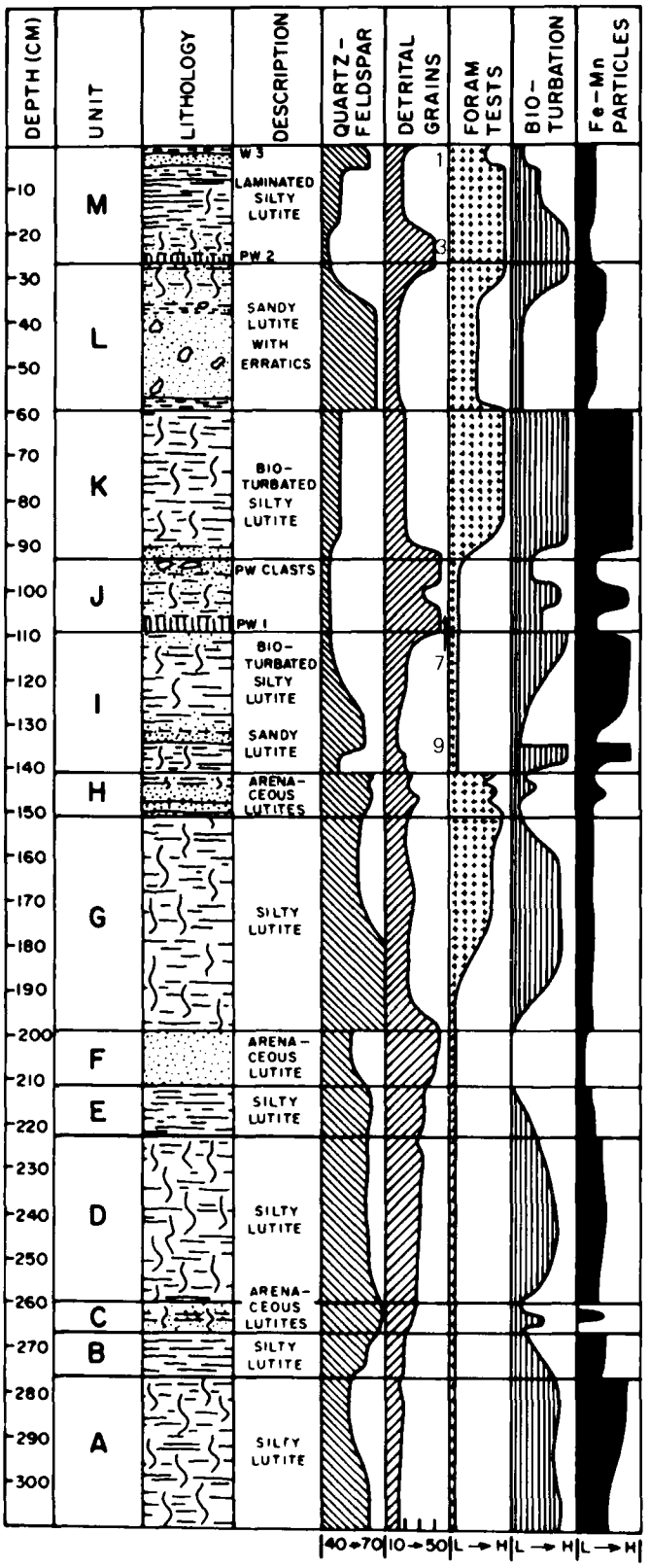

The lower contact is defined by a change in color and texture from olive-brown silty lutite below to reddish olive-brown arenaceous lutite above. The contact is usually sharp but irregular.

Ferromanganese particles are rare in this subunit and compose an average of 1.1% of the sand-sized fraction. Burrows are rare.

The average weight percent of the sand-sized fraction is 26.03% for 24 cores. (App. 2). The average detrital sand-sized fraction is in the fine-sand range and is moderately sorted. The most common sand-sized grain is monocrystalline quartz (App. 3).

The stratigraphy of the units and some of the important sedimentary parameters of each unit are summarized in Figure 9.

Unit I

Unit I is a silty lutite but contains a thin, arenaceous lutite subunit. At the base is an unmottled, olive silty lutite that grades upward into an intensively mottled, dark yellowish-brown silty lutite. The base is overlaid by a thin (2- to 4-cm), moderately mottled, olive-brown arenaceous lutite. Above this middle part is an unmottled to moderately mottled, yellowish-gray silty lutite that grades upward into an intensively mottled, dark yellowish-brown silty lutite.

The thickness of unit I ranges from 20 to 51 cm, with the average thickness being 33 cm. The base is marked by a sharp contact with the reddish olive-brown arenaceous lutite (unit H, Fig. 10).

Variations in percent coarse grains are plotted against depth in core for five "type" cores, and in Figure 11 a major peak near the center of the unit is associated with the thin arenaceous lutite. The middle of unit I (MI) has an average of 22% coarse grains (App. 2). These plots appear to be very important for units I to M.

Virtually all of the mottling is the result of bioturbation. Most of the burrows are *Chondrites*. The burrows range from 0.5 to 2 mm in width and are up to 30 mm in length. Rind burrows and composite burrows (Chamberlain, 1975) also occur in this unit but are rare. The most intensive burrowing is restricted to the silty lutite zones. Ferromanganese particles rim some burrows but generally comprise less than 7% of the sand-sized material.

The major arenaceous constituents are quartz-feldspar grains (~65%) and lithified rock fragments (~17%) (App. 3). Most of the grains or fragments are angular to subangular and appear to be poorly sorted.

Some 250 erratics occur in unit I cores (Table 1).

Unit J

At the base of unit J is a thin (1- to 4-cm) coarse, pink white layer designated PW1. This layer has a characteristic weak red (10YR 5/3) lower zone (0.5 to 2 cm) overlain by a white (10YR 8/2) upper zone (0.5 to 2 cm). In general, it is unburrowed and is associated with the prominent coarse percentage peak (Fig. 12). Unit J contains many angular clasts, the largest of which is 5 mm.

The PW1 layer is overlaid by an unmottled to moderately mottled, pale yellowish-brown silty lutite that grades into an arenaceous lutite. The contact usually is gradational and distorted. Small (1- to 4-mm) pink white clasts occasionally occur near the top of the unit.

Figure 9. Lithostratigraphic units A to M in central Arctic Ocean. Sedimentary parameters include percentages of quartz-feldspar and total detrital grains. L to H indicates low to high abundance. Descriptions indicated. Numbers in "detrital grains" column refer to carbonate maxima peaks of Darby (1975).

The thickness of unit J ranges from 11 to 38 cm, and the average thickness is 16 cm. This unit is an important key bed in the section (Fig. 11).

The percent coarse distribution is characterized by two peaks (units JL, JU, App. 2). The lower peak is associated with the pink-white layer, and the upper peak represents the overlying silty to arenaceous lutite (Fig. 11).

Most of the mottling is due to *Chondrites*-type burrowing organisms. The burrows are similar to those described in unit I and are outlined by small black, ferromanganese particles.

Hoffman (1972) gave a detailed description of the pink-white layers. He determined that the pink-white layers were rich in clastic carbonate and had lower proportions of iron and manganese oxide than the surrounding sediment. Petrographic study supports these results. The major sand-sized constituents are quartz-feldspar grains (~45%), detrital carbonate (~37%), and lithified rock fragments (~10%) (App. 3). Most of the grains are subangular to angular and are poorly sorted.

Some 135 erratics were recovered from the cores.

Unit K

Unit K is a mottled, dark yellowish-brown to dark grayish-brown, *Foraminifera-rich* silty lutite (Fig. 13). The thickness of unit K ranges from 14 to 53 cm, and the average thickness is 33 cm. The Brunhes-Matuyama magnetic boundary occurs in this unit.

The bottom contact is marked by a change from a light silty arenaceous lutite to dark silty lutite over a 2- to 5-cm interval.

Foraminifera, typically *Globoquadrina pachyderma*, are extremely abudant and can be easily observed in the upper two-thirds of the unit.

In general, unit K has a lower percent coarse distribution than the units immediately below (unit J) and above (unit I) (Fig. 11). The distribution averages 15% (App. 2).

This unit is intensively burrowed. *Chondrites* and horizontally stacked burrows similar to those in unit J are most abundant. *Zoophycos* occur in this unit. These burrows are backfilled, have a horizontal orientation, and are approximately 6 mm in width and up to 30 mm in length (width of core). Rind burrows and composite

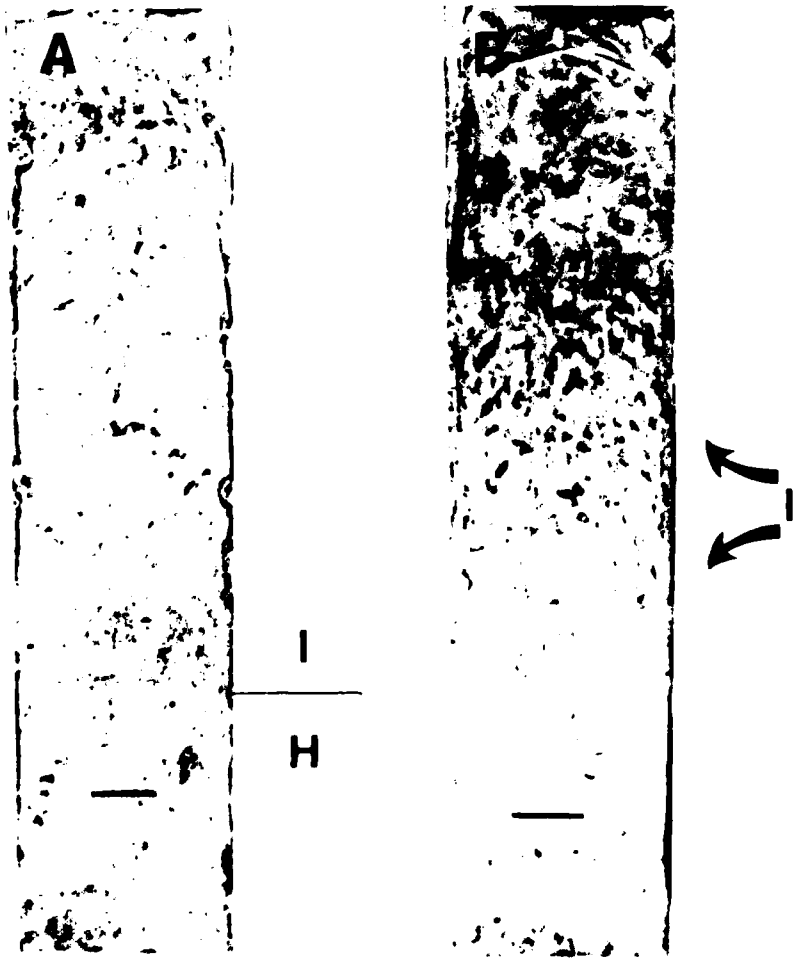

Figure 10. Typical lithology of unit I. (A) Unit H to I contact in FL 354, segment 15. Base of I is darker *zone of unburrowed olive silty lutite that grades* upward into a mottled, dark yellowish-brown silty lutite. (B) Middle and upper part of unit I from FL 354, segment 16. Middle part is only moderately burrowed, but it grades into the upper part of unit I, which is intensively burrowed, and a darker yellowish-brown silty lutite. Scale bars are 1 cm.

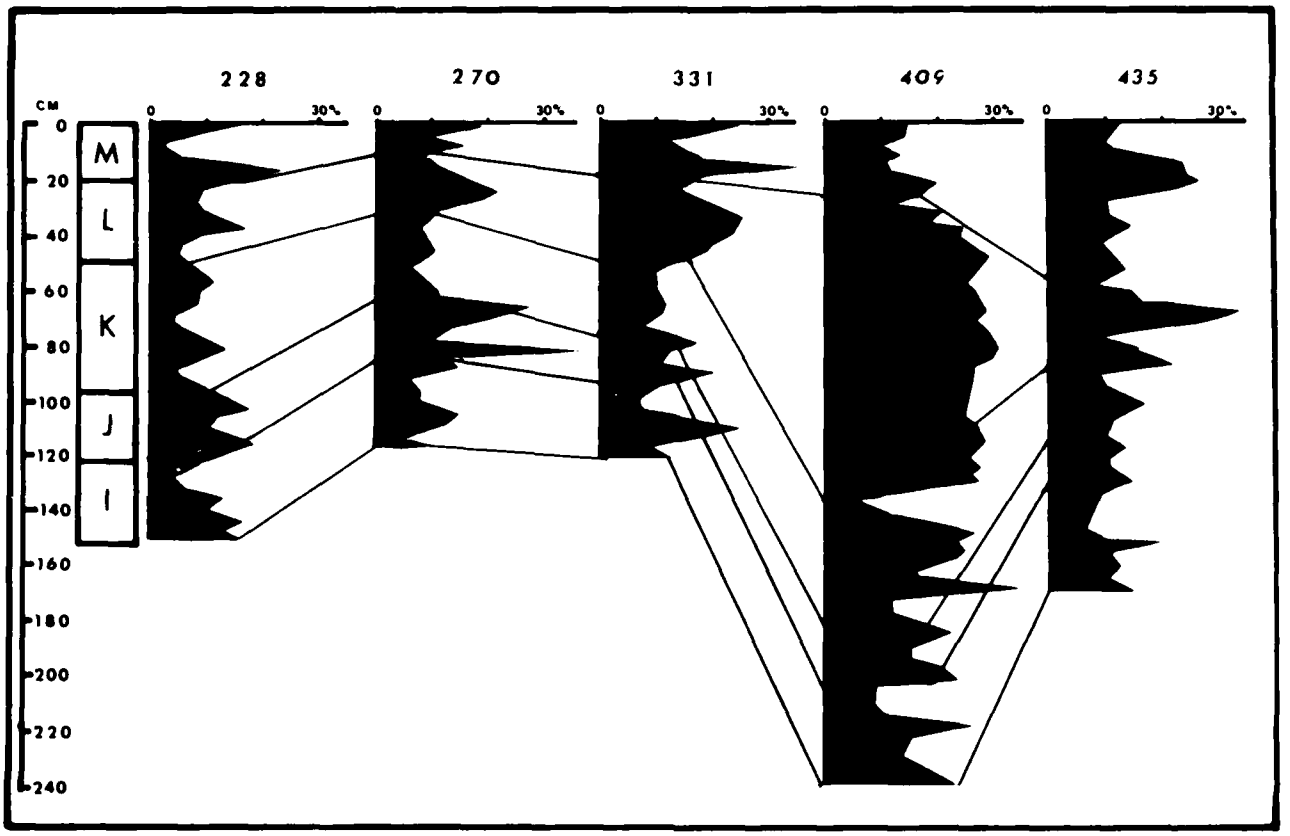

Figure 11. Correlation by lithostratigraphic units I to M of the percent coarse distribution (> 63 μm) between five cores. Each unit has a characteristic percent coarse distribution.

burrows (Chamberlain, 1975) occasionally occur but usually are rare. Small ferromanganese particles are evenly distributed throughout most of the unit and compose 7.7% by weight of the sediment in five cores.

Quartz-feldspar grains (~54%), detrital carbonate (~15%), and lithic fragments (~13%) are the major sand-sized particles in unit K (App. 3). Many of the grains are subangular to angular; the grains are poorly sorted.

In unit K, 204 erratics were found in the cores (Table 1).

Unit L

This unit is an arenaceous lutite with an upper silty lutite zone. The thickness of unit L ranges from 4 to 130 cm, with the average thickness being 33 cm.

The base of the unit is marked by a sharp contact between the dark, mottled silty lutite of unit K and a thin (1- to 3-cm), unmottled, olive to light yellowish-brown silty lutite (Fig. 12).

The percent coarse plots for unit L usually exhibit one major, continuous peak. The peak is easily distinguished in those cores that have a thick arenaceous lutite zone with erratics distributed evenly throughout (Fig. 11).

Chondrites and small rind burrows (Chamberlain, 1975) occur occasionally in the silty lutites of this unit. In addition, many large burrows filled with dark, *Foraminifera*-rich silty lutite or light silty lutite intermixed with small pink-white clasts are common in this zone. The large burrows range from 3 to 15 mm in width and reach 50 mm in length. The number of burrows and the burrowing intensity seem to increase toward the top of the unit. A distortion of the upper contact is due to this intensive burrowing activity in most cores. Ferromanganese particles average less than 4% in this unit.

The major sand-sized modes are quartz-feldspar grains (~66%) and lithic fragments (~17%) (App. 3). Unit L contains the highest proportion of quartz-feldspar grains of any Arctic lithologic unit studied.

Some 203 erratics were found in the cores (Table 1).

Unit M

The bottom of unit M, the uppermost lithologic unit in the central Arctic, is marked by a thin (0.5- to 2-cm), coarse, pink-white layer designated PW2 (Fig. 14). The PW2 layer, described by Hoffmann (1972), is similar to the PW1 layer found in unit L. In most of the cores, PW2 is distorted and is commonly intermixed with the surrounding darker sediment through an interval of 2 to 15 cm. Above the PW2 layer is a mottled, *Foraminifera*-rich yellowish-brown to brown silty lutite that grades into interlaminated light and dark silty lutites. The silty lutites are overlain by an unmottled olive to olive-gray arenaceous lutite. The top of the unit is marked by a thin (0.1- to 1-cm), white layer designated W3, which is overlain by a *Foraminifera*-rich, dark yellowish-brown silty lutite. In many of the cores, the upper several centimetres of section

are missing owing to loss of sample during the coring operation. Foraminifera, typically *Globoquadrina pachyderma*, are prominent in the dark silty lutites of this unit. Fine laminations <1 mm thick are the only primary sedimentary structures observed in unit M.

The thickness of unit M ranges from 2 to 82 cm, and the average thickness is 27 cm (Fig. 14).

The percent coarse grain distribution for this unit is variable. In general, there are two major peaks (units ML, MU, App. 2) a lower peak associated with the PW2 layer and an upper peak representing the olive to olive-gray arenaceous lutite (Fig. 12). A middle peak (unit MM, App. 2) averages only ~9% coarse.

The burrow types in this unit are similar to those described in unit L and are generally confined to the lower third of the unit. Burrowing is concentrated in PW2 and in the overlying silty lutite.

The PW2 and W3 layers contain quartz-feldspar grains (~40%), detrital carbonate (~32%), and Foraminifera tests (~15%) as the primary sand-sized constituents. The composition of these layers is similar to the PW1 layer of unit L. Ferromanganese particles are rare (2.2%).

The arenaceous lutite has quartz-feldspar grains (~58%), detrital carbonate (~18%), and lithic fragments (~11%) as the predominant sand-sized constituents (App. 3). This sediment is similar in composition to the arenaceous lutites in units L and J and the arenaceous lutites of units C, E, and H.

Unit M is relatively thick, and 442 erratics were recovered from the cores (Table 1).

DISTRIBUTION AND REGIONAL TRENDS OF STRATIGRAPHIC UNITS

The thicknesses of the individual units and the combined thicknesses of selected units were plotted (Figs. 15 to 22). The plot of thicknesses of unit E (middle coarse) shows a distinct pattern. This unit thickens dramatically from a minimum of 2.5 cm at the top of the Alpha Cordillera to a maximum of 36.5 cm at the base of the Chukchi Plateau (Fig. 15). Unit H (top coarse) shows a much less obvious trend toward thickening from shallower to deeper depths (Fig. 16). Unit C (bottom coarse) fails to show any significant trends in thickness (Fig. 17).

The thicknesses of the silty lutite intervals between the arenaceous lutite units show no geographic patterns (Fig. 18, 19). The plot of the total thickness of the section from unit C through unit H also fails to show any strong trend or pattern (Fig. 20). The thinnest values are found high on the Alpha Cordillera, but this distribution

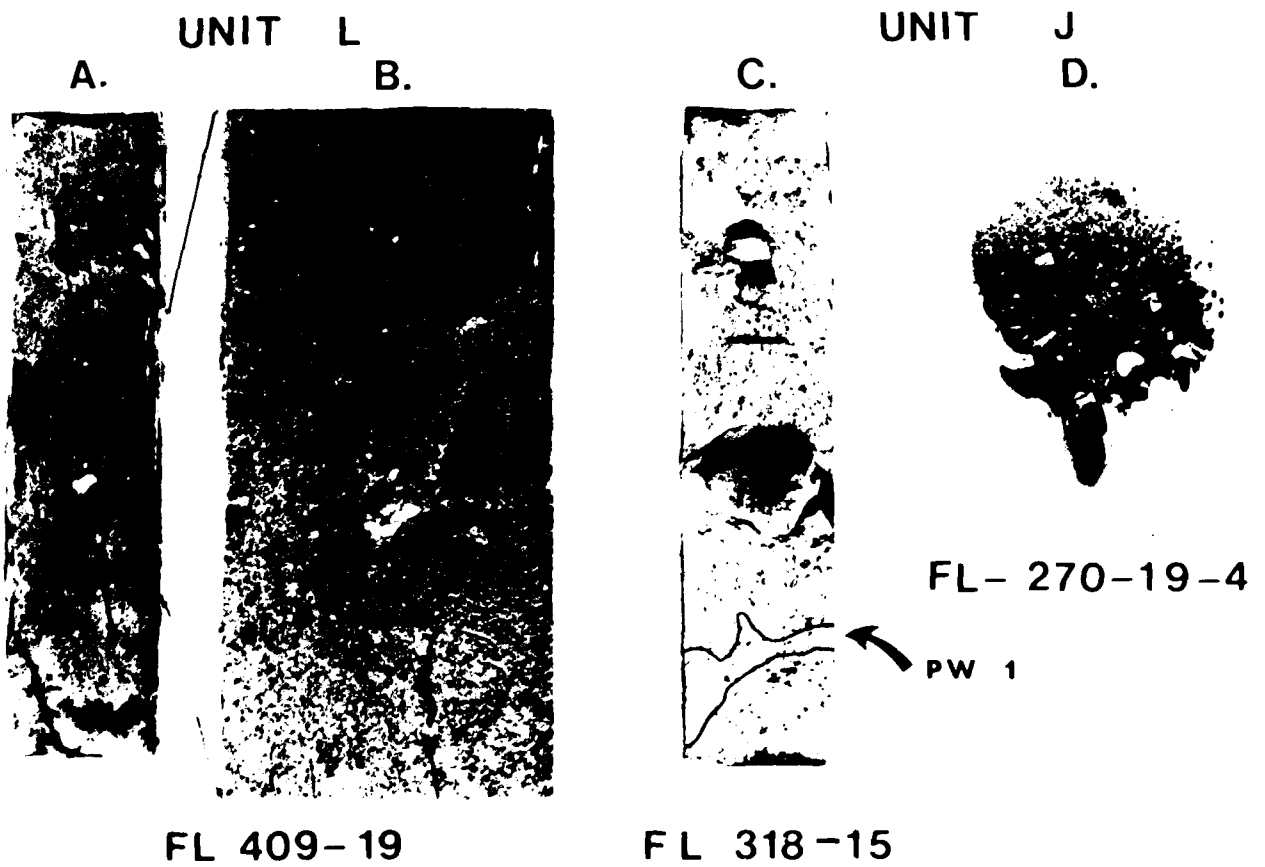

Figure 12. (A) Illustration of poorly sorted, ice-rafted sediment containing abundant erratics. Core segment is approximately 16 cm in length. (B) Enlargement of the center portion of Figure A. Note the coarse texture, poor sorting, and abundant erratics. This segment is typical of sediment in unit L. (C) This segment contains several erratics (unit J). The large erratic in the center of the segment is ~27 mm in diameter. Several small pink, white clasts occur in the PW1 layer. (D) Coarse fraction (>63 μm) of segment 270-19-4. Note the poor sorting and general angularity of coarse grains. The faceted erratic near the bottom of the photo is ~9 mm in diameter. Bar is 1 cm.

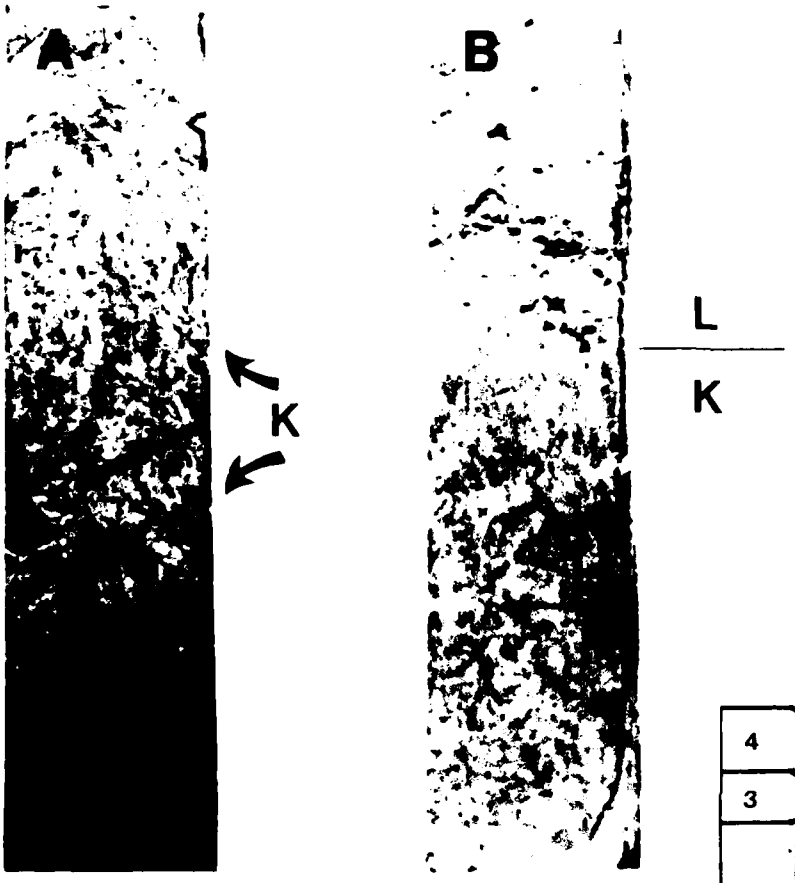

Figure 13. Typical lithology of unit K. (A) Dark yellowish-brown to dark grayish-brown silty lutite with some arenaceous material of lower and middle parts of unit K. FL 354, segment 19. Intense burrowing characterizes all parts of unit K. (B) Upper lighter portion of unit K and K to L contact in FL 354, segment 20. Notice relatively sharp contact of dark, burrowed unit K below and unburrowed, olive to light yellowish-brown silty lutite (unit L) above. Scale bars are 1 cm.

probably reflects the thickness pattern of unit F.

Examination of Figure 21 reveals a trend of gradual thinning toward the southern flank of the Alpha Cordillera for unit I.

No overall trends can be determined for unit J (Fig. 22). However, the PW1 layer is thickest (2 to 4 cm) and displays a distinct pink-white coloration in cores from the Chukchi Rise. It tends to thin and become less pink toward the Alpha Cordillera, where it is primarily a moderately burrowed, thin wisp of white sediment.

Unit K is thickest in cores from the Chukchi Rise and the southeast flank of the Alpha Cordillera (Fig. 23). It is thinnest in cores from the southwest flank and crest of the Alpha Cordillera.

The overall trend for unit L is a pronounced increase in thickness toward the crest and southeast flank of the Alpha Cordillera (Fig. 24) caused by an expansion of the light arenaceous lutite zone. The marked increase in the southeast flank area is a result of a local change in lithology. A moderately thick (5- to 30-cm), erratic-filled, dark olive-gray arenaceous lutite occurs above the light arenaceous lutite zone in the lower portion of unit L. This change in lithology occurs in cores FL 395, 396, 398, 408, 410, 413, and 417.

A definite trend in unit M is shown in Figure 25. There is a large increase in thickness toward the Alpha Cordillera. In general, this increase appears to be uniform throughout the entire unit.

Unit M exhibits some of the greatest variations in thickness between cores only in a short lateral distance apart. It is important to note that for both expanded and condensed sections, each of the

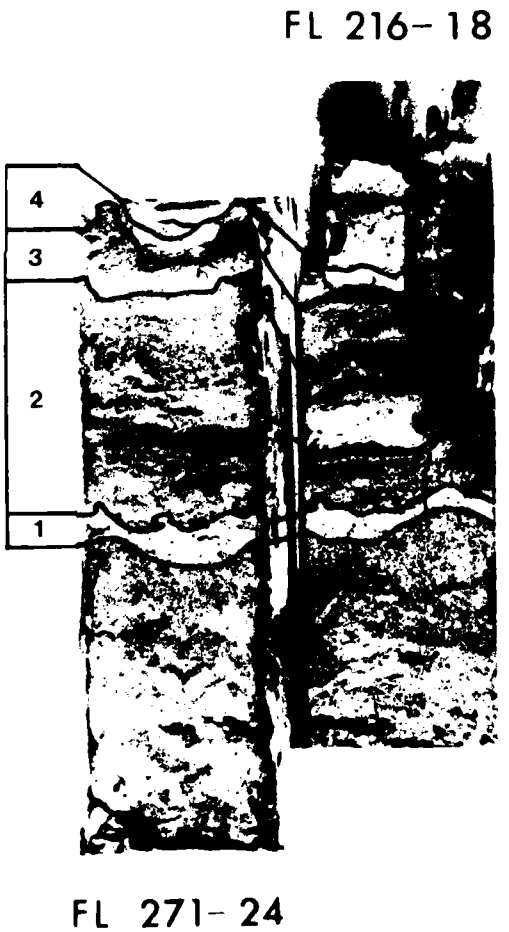

Figure 14. A comparison of unit M in two cores collected more than 200 km apart. Note the correlation of laminae in these segments. Core segment is 15 cm in length. (1) PW2 layer; (2) brown, Foraminifera-rich silty lutite grading into an interlaminated light and dark brown, Foraminifera-rich silty lutite; (3) gray to olive-gray arenaceous lutite; and (4) dark yellowish-brown, Foraminifera-rich silty lutite, overlain by the W3 layer.

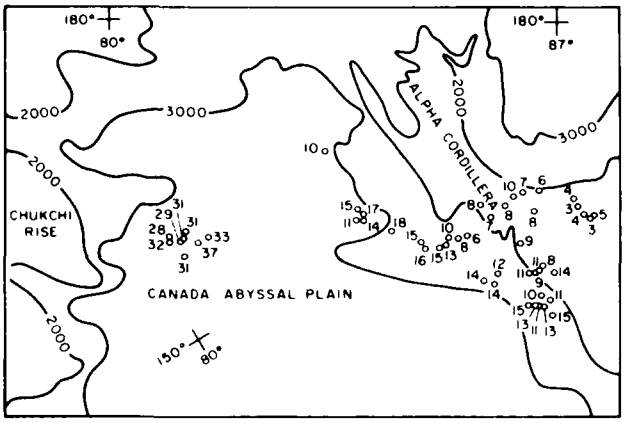

Figure 15. Thickness of unit F in centimetres. All fractional values are rounded to the nearest integer. A general trend from thin on the Alpha Cordillera to thick toward the Chukchi Plateau is apparent. Water depth in metres.

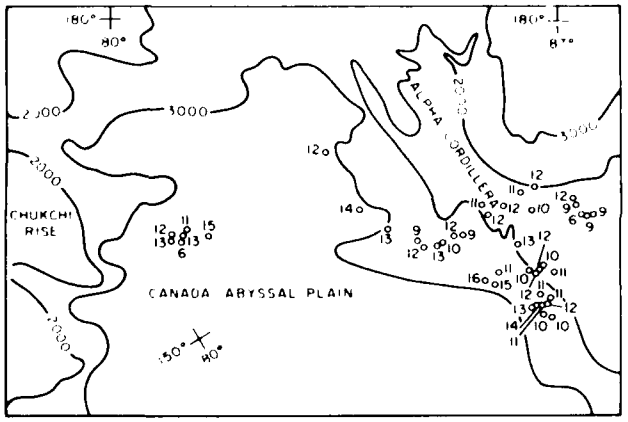

Figure 16. Thickness of unit H in centimetres. All fractional values are rounded to the nearest integer. There is some clustering of thin units on the Alpha Cordillera. Water depth in metres.

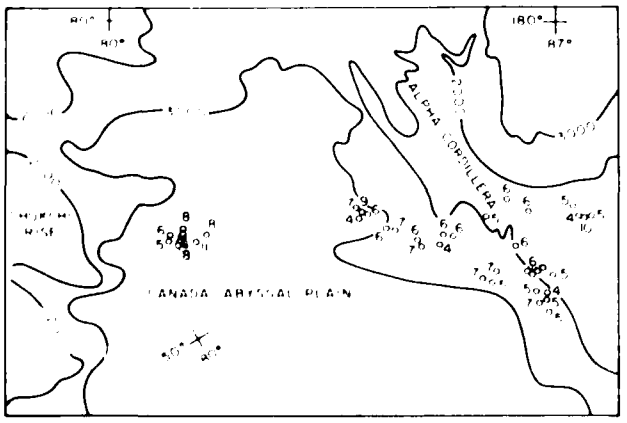

Figure 17. Thickness of unit C in centimetres. All fractional values are rounded to the nearest integer. Water depths in metres.

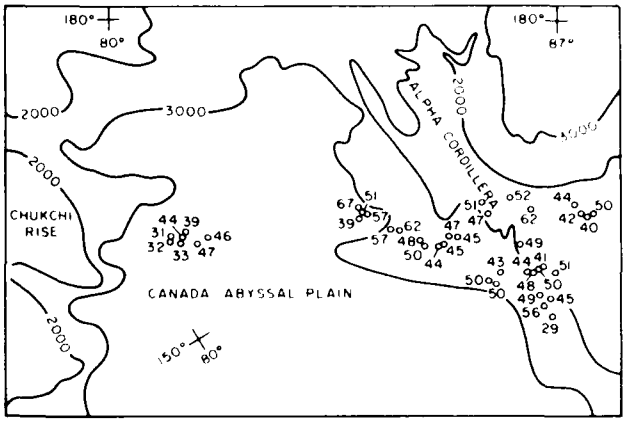

Figure 18. Distribution of the combined thicknesses of units D and E in centimetres. All fractional values are rounded to the nearest integer. There is a cluster of low values occurring in the group of cores near the Chukchi Plateau. Water depth in metres.

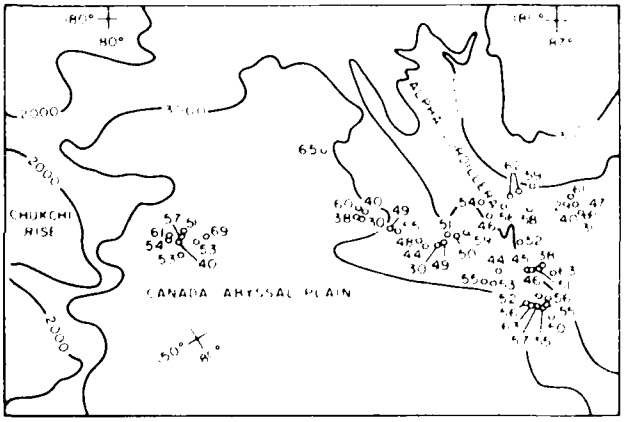

Figure 19. Thickness of unit G in centimetres. All fractional values are rounded to the nearest integer. There are low values high on the Alpha Cordillera. Water depth in metres.

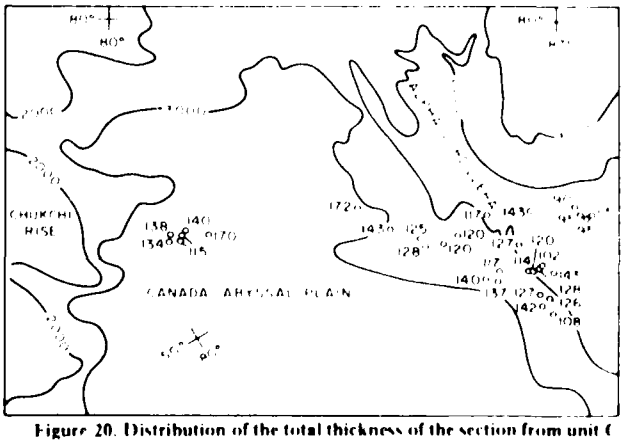

Figure 20. Distribution of the total thickness of the section from unit C through unit H, inclusive. All fractional values are rounded to the nearest integer. There is a clustering of low values on the Alpha Cordillera, which probably reflects the thinness of unit F in these cores. Water depth in metres.

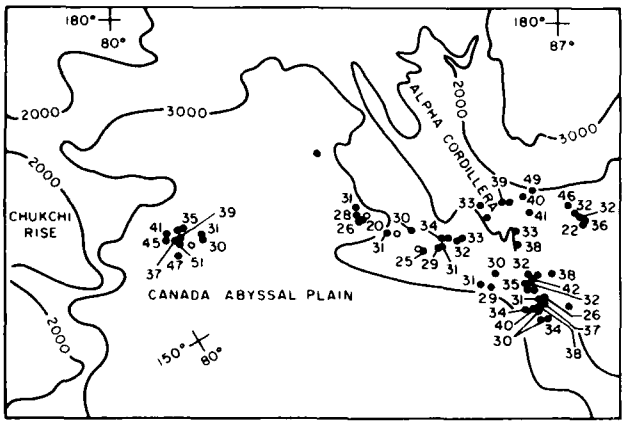

Figure 21. Distribution of the thickness of unit I in centimetres. Water depth in metres.

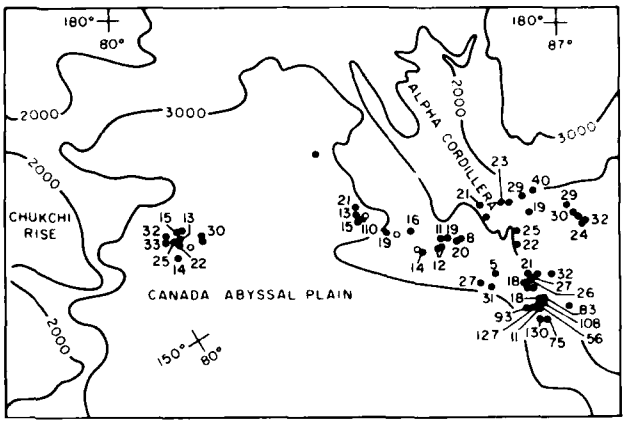

Figure 24. Distribution of the thickness of unit L in centimetres. Water depth in metres.

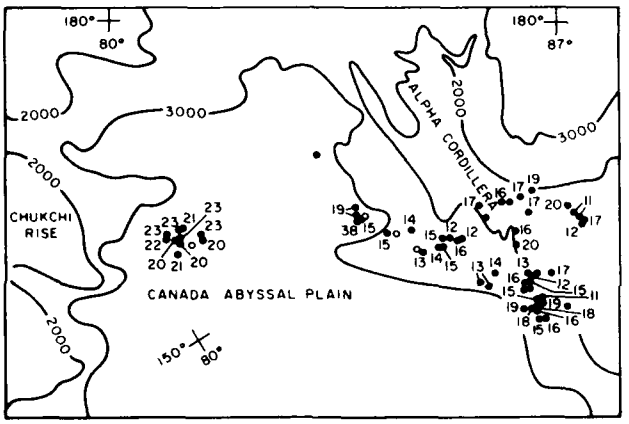

Figure 22. Distribution of the thickness of unit J in centimetres. Water depth in metres.

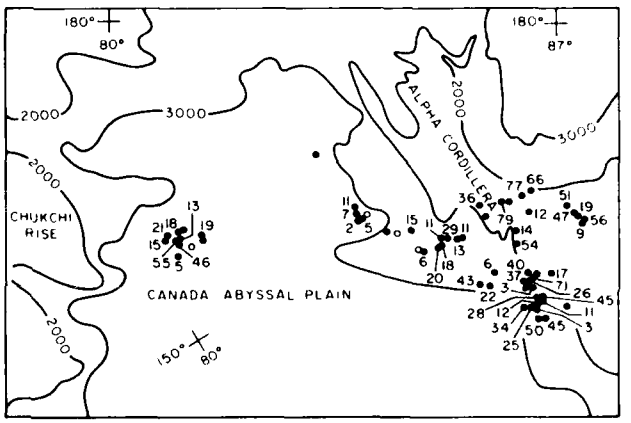

Figure 25. Distribution of the thickness of unit M in centimetres. Water depth in metres.

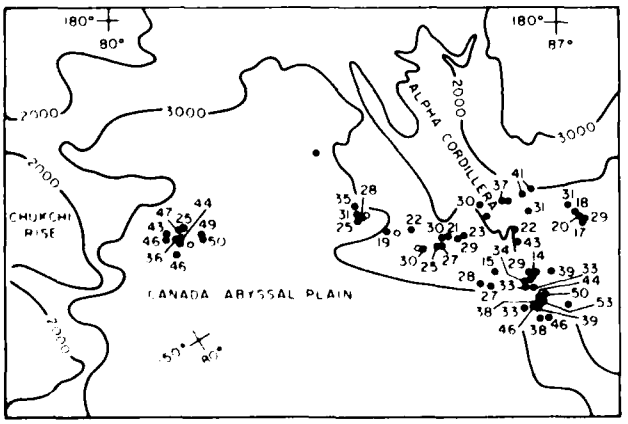

Figure 23. Distribution of the thickness of unit K in centimetres. Water depth in metres.

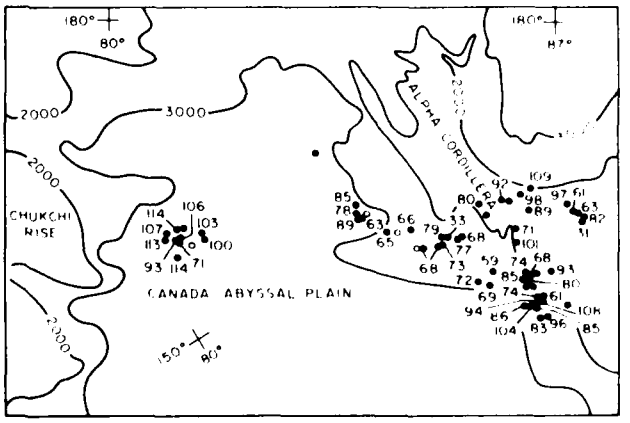

Figure 26. Distribution of the thickness for units I, J, and K combined. Thicknesses are in centimetres. These units are primarily silty lutites. Water depth in metres.

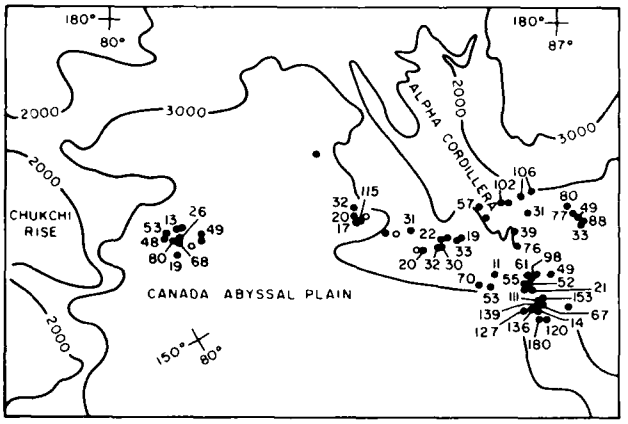

Figure 27. Distribution of the thickness for units I. and M combined. Thicknesses are in centimetres. These units are primarily arenaceous lutites. Water depth in metres.

subunits of unit M is present. It is possible to correlate 1- to 2-mm laminae with thicker, equivalent counterparts in a nearby expanded section, as shown in Figure 14. These local variations in thickness do not appear to be a function of bathymetry and are probably due to variations in the sedimentation rate.

The top of unit M is commonly marked by an olive-gray arenaceous lutite overlain by the W3 layer. However, several cores exhibit up to 5 cm of sediment overlying the W3 layer. This sediment can be characterized as a dark yellowish-brown silty lutite. The absence of this zone in a majority of cores probably is a result of truncation by the coring device during the coring operation. It is estimated that 3 to 5 cm of sediment was lost from the top of the section.

The distribution of thicknesses for units I, J, and K is shown in Figure 26. The sum of thicknesses for units I. and M is plotted in Figure 27. Units J and K generally seem to be thicker in cores from the Chukchi Rise. Units I, J, and M tend to thicken toward the crest of the Alpha Cordillera. All of the units are thicker in cores from the southeastern flank of the Alpha Cordillera.

UNCONFORMITIES

Only a few of the several hundred cores that have been studied have unconformities. Four of these are shown in Figure 28. Cores with unconformities are restricted to the extreme southwestern flank of the Alpha Cordillera and the northeastern flank of the

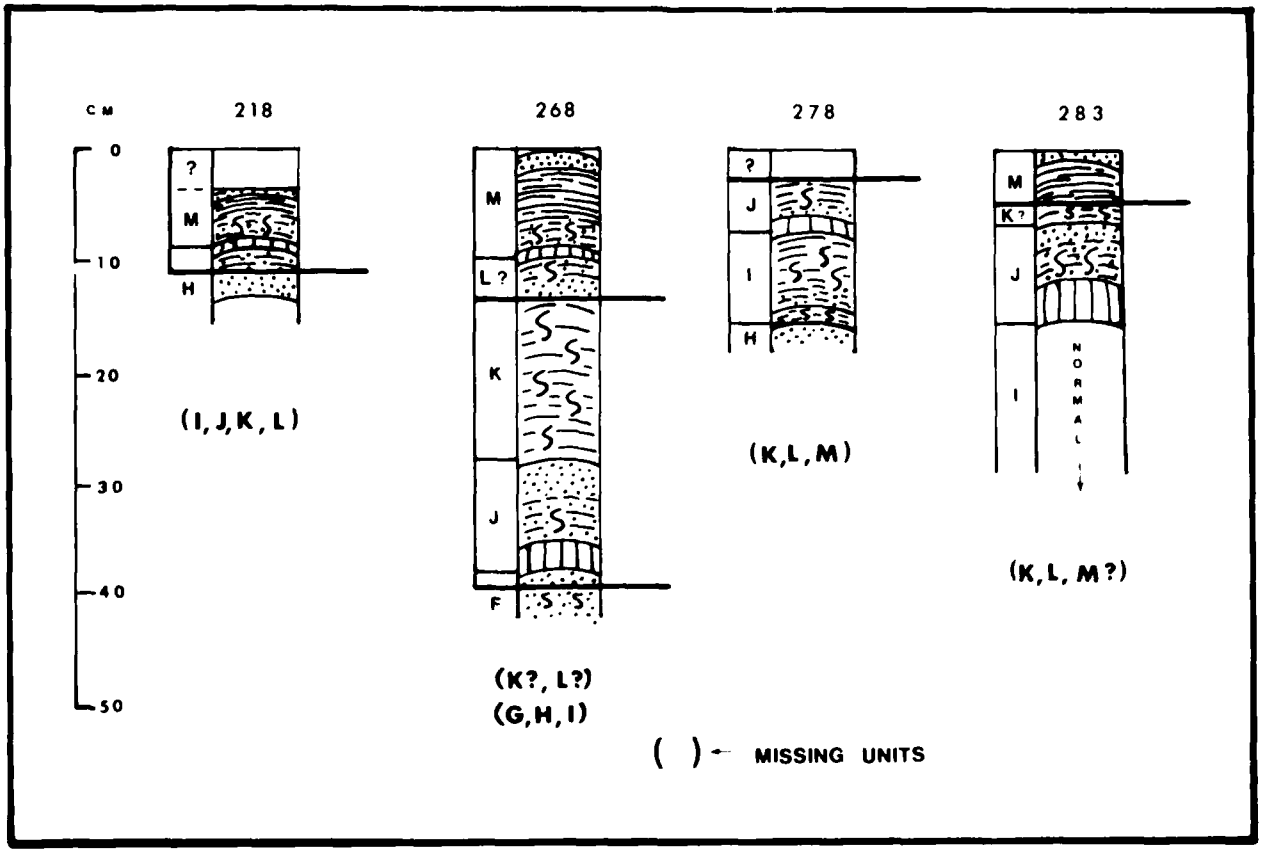

Figure 28. Lithologic and chronologic distribution of unconformities in the upper part of the section. Dark horizontal lines indicate the unconformities. Letters in parentheses are units missing from the section. Question marks indicate that only part of the unit is missing. The unconformity in core FL 218 and the unconformity near the top of core FL 268 have similar times of occurrence.

Chukchi Rise. The estimated date of occurrence (based on magnetic signature) for the unconformity in core FL 218 is 0.29 m.y. Two unconformities exist in FL 268. The upper unconformity occurred approximately 0.30 m.y. ago and may represent the same event as the one at the top of FL 218. The lower unconformity in core FL 268 shows a break where unit F is overlain by sediment of unit J. The precise nature of this unconformity is difficult to determine. The unconformity in core FL 278 is believed to have occurred in the Holocene. No sediment has accumulated above the unconformity. An alternate hypothesis is that this could be a result of the coring operation.

A lack of widespread unconformities implies that bottom sediments contain a continuous, complete record of depositional events for the Arctic. Extreme variations in unit thickness are probably not the result of unconformities but of local changes in the sedimentation rate.

CHRONOSTRATIGRAPHY

Introduction

Core FL 224 has what appears to be complete magnetic signatures that indicate the oldest sediment of any of the Arctic cores (Fig. 29). However, a major problem in working with sediment cores from the Arctic Ocean has been the lack of independent evidence to aid in correctly interpreting the paleomagnetics (Darby, 1975). Because of low species diversity in the Arctic Ocean, a biostratigraphic framework for the late Cenozoic has not been developed. Thus, interpretations of the paleomagnetics below the unmistakable Brunhes-Matuyama reversal are subjective. Subjectivity has increased with greater depth of core penetration.

Early attempts at Arctic paleomagnetic interpretations include Steuerwald and others (1968) and Clark (1969) for FL 224. Clark (1970) reinterpreted the paleomagnetic for FL 224 and FL 221 and concluded that the oldest sediment above flow-in was deposited during the Gauss Normal Epoch (~3.32 m.y.). This interpretation is refined in the present study. Interpretations in this paper were augmented by the study and interpretation of physical sedimentologic data not previously available.

Magnetic Stratigraphy

The Brunhes-Matuyama magnetic reversal occurs in a majority of the Arctic cores in stratigraphic unit K (Fig. 30). Determination of the Jaramillo subchronozone is more subjective because of its short duration (~60,000 yr), the relatively large sampling interval (5 cm), and the inconsistency of the magnetic data (the gradational zones in some cores). However, a relatively consistent normal polarity signal occurs near the bottom of unit J, and this is interpreted to represent the Jaramillo.

In addition to the Brunhes-Matuyama reversal, which is well documented in a majority of the Arctic cores in unit K, the Matuyama-Gauss reversal is a reliable horizon. The magnetic signature interpreted as the Matuyama-Gauss reversal is found consistently in unit D, approximately midway between units E and C, in all cores that penetrate through the section (Fig. 29). This reversal is generally very sharp and in this respect is as good a reference datum as the younger Brunhes-Matuyama boundary. Classification of older parts of the cores is more difficult.

Age of Stratigraphic Units

Introduction. Two approaches were used in determining the approximate age of each of the stratigraphic units: (1) use of selected sedimentary parameters and (2) use of sedimentation rates based on interpretations of paleomagnetic stratigraphy. The sedimentary parameters were studied for a first-order approximation of "fast" or "slow" rates of deposition. Magnetic stratigraphy yielded more quantitative data for calculating rates of sedimentation and approximating the age of units, but the data derived from (1) guided the selection of the several interpretations possible for (2).

Sedimentary Parameters Considered. (1) Figure 9 illustrates the vertical variation in ferromanganese-particle abundance in the units and demonstrates that it is greatest in silty lutites and lowest in the arenaceous lutites. It is the author's view that this suggests a major difference between these two sediment types in processes of depositon. It is suggested that an abundance of ferromanganese particles indicates low sedimentation rates (Moore, 1973; Watkins and Kennett, 1977). The possibility that the ferromanganese particles grew in the sediment below the sediment-water interface is discounted because if this were the case, the particles should be evenly distributed in all the units rather than being concentrated as they are in a few of the units. (2) The percentage of Foraminifera tests approaches zero in the lower (silty) portions of the section but shows a rapid increase in unit G and higher (arenaceous parts) (Fig. 9). The lack of Foraminifera tests lower in the section could be explained by post depositional solution due to corrosive bottom water or low sedimentation rates, low productivity, masking of abundance by high sedimentation rates, or a combination of factors. (3) The percentage of sand-sized material and erratics increases in the upper part of the cores studied (Fig. 9, Table 1). Most of the stratigraphic thickness of arenaceous lutite is found in the upper one-third to one-half of the cores. It is probable that greater percentages of sand represent relatively higher rates of deposition. The sharp, lower contacts of units H and F also suggest rapid deposition of these arenaceous units. (4) Most of the pebbles occurring in silty lutite have ferromanganese coatings in contrast to the rare occurrence of ferromanganese particles in arenaceous lutites. The extensive ferromanganese coatings on erratics in silty lutites support the hypothesis that silty lutites represent low sedimentation rates. If this is the case, the scarcity of coated pebbles in arenaceous lutites supports the theory that sedimentation rates were relatively high when the arenaceous lutites were being deposited. The erratics were buried faster than ferromanganese material could coat the exposed portions. (5) Burrowing is more intensive in silty lutites than in arenaceous lutites (Figs. 3, 4, 5, 6, 9), a factor that may indicate low sedimentation rates (Howard, 1975). A plot of burrow frequency versus depth shows good correlation between increased bioturbation and silty lutites (Fig. 9). A lack of burrows in arenaceous lutites (Figs. 4, 5, 7, 9) is probably a consequence of deposition rates that were higher than the ability of burrowing organisms to mix the sediment (Howard, 1975).

Conclusions. The portions of the cores below unit C consist mostly of silty lutites and a few thin arenaceous lutites. Evidence suggests that arenaceous lutites represent high sedimentation rates, whereas the paucity of sand-sized material in the silty lutites indicates low sedimentation rates. This assumption is supported by an abundance of ferromanganese particles, low amounts of Foraminifera and erratics, extensive ferromanganese coatings on

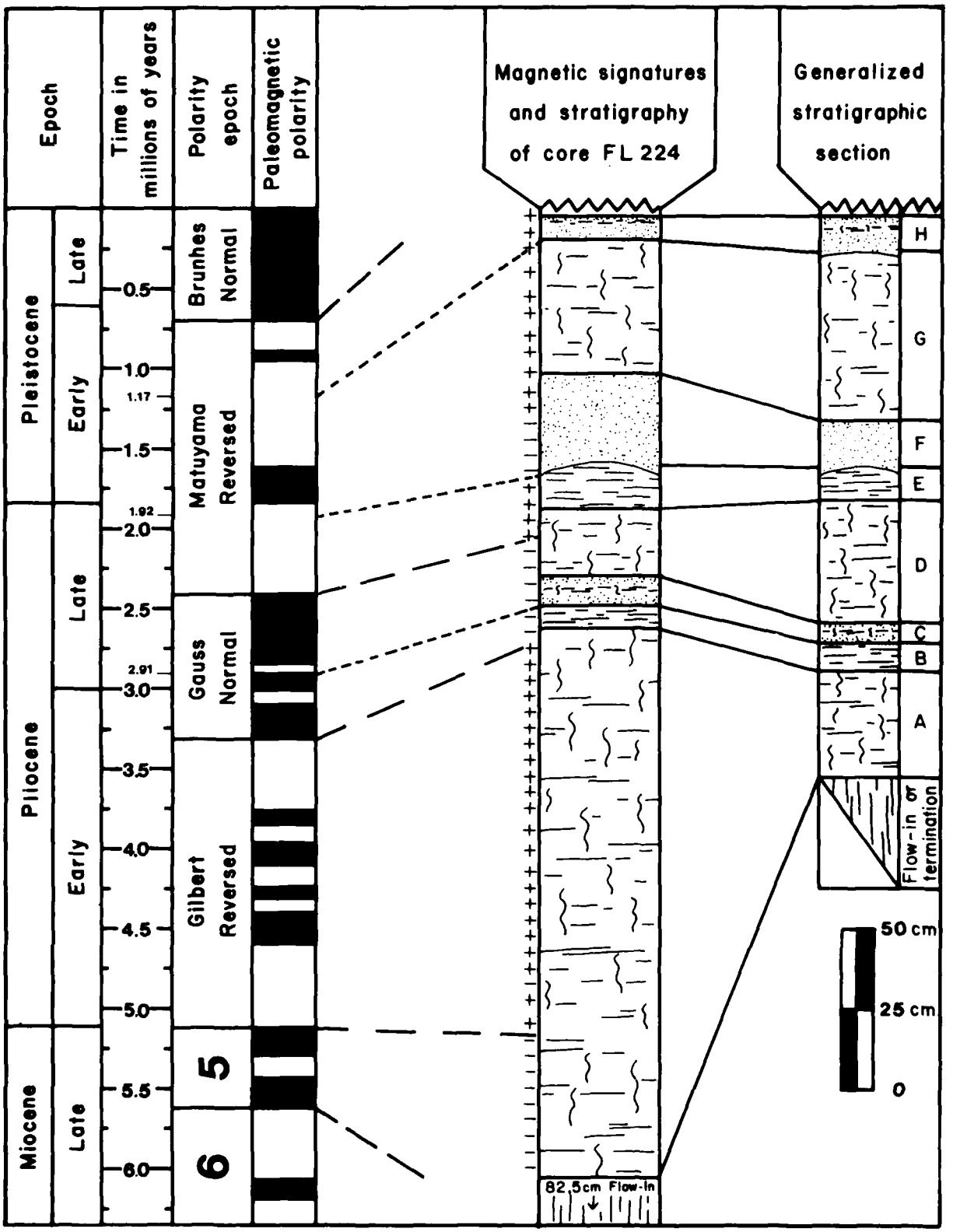

Figure 29. Correlation of the magnetic signatures of a portion of core FL 224 with the standard paleomagnetic time scale and the standard chronostratigraphic time scale. The ages of the bases of the arenaceous lutite layers are indicated by small numbers in the time column. The lithologic symbols are the same as in Figure 2.

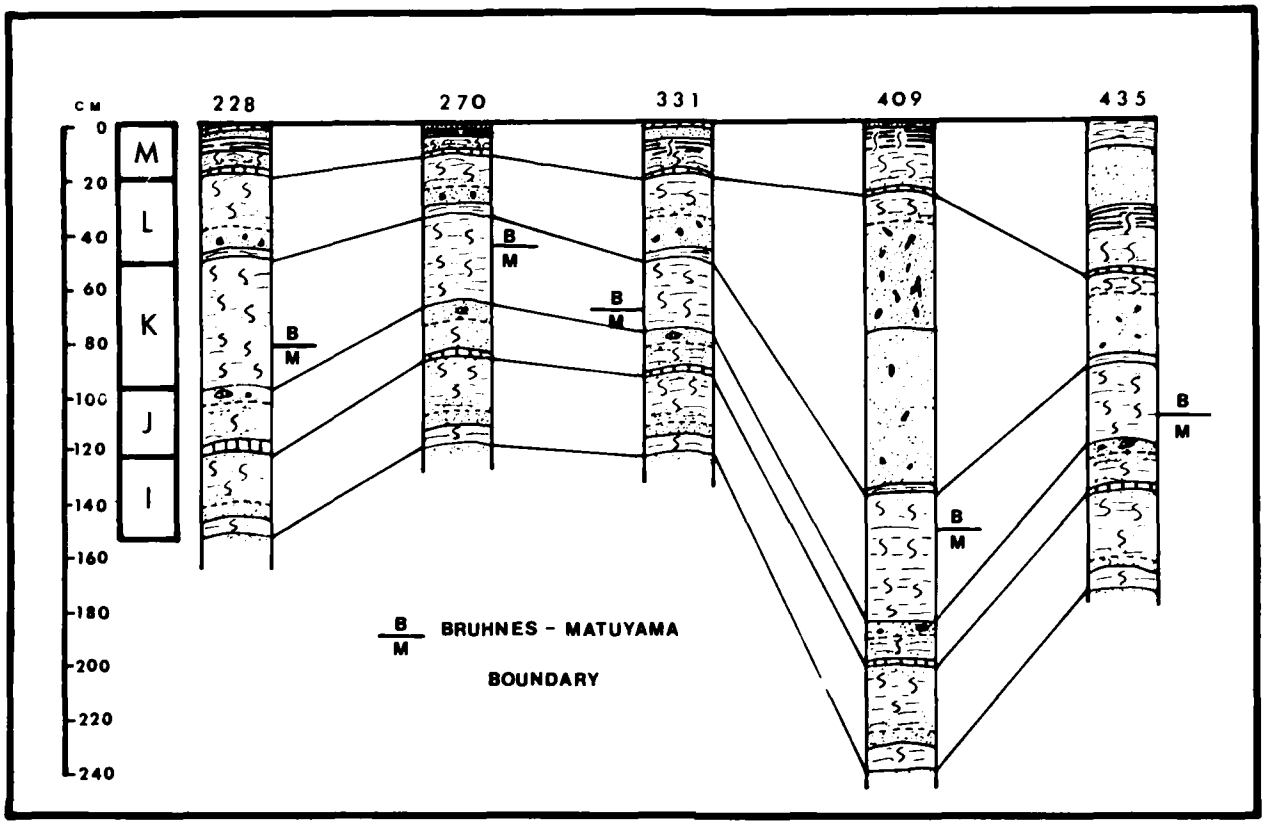

Figure 30. Lithologic correlation of I to M between five cores. End member cores (228, 435) are greater than 600 km apart. Note the occurrence of the Brunhes-Matuyama boundary in unit K.

larger pebbles, and more extensive burrowing in the silty lutites. These factors are considered good evidence of the low sedimentation rate for all silty lutites, including those of units A, B, and D in the part of the cores with poorest magnetic control.

Magnetic Stratigraphy Interpretations. Semiquantitative sedimentation rates can be calculated from interpretations based on major paleomagnetic epoch boundaries. The Brunhes-Matuyama boundary can be identified in the lower-middle part of stratigraphic unit K. This major polarity reversal was recognized in the majority of the Arctic cores. The boundary between the Brunhes and Matuyama commonly is marked at 0.7 m.y. Dates for this boundary in the literature range from 0.69 to 0.73 m.y. This boundary is the most distinctive and widespread paleomagnetic signature recognized in the Arctic cores (Figs. 2, 30; Clark, 1970).

Typically, the change from normal to reversed polarity is gradational over a 15- to 40-cm interval for the Brunhes-Matuyama boundary. A comparison of the lithologic details of the part of unit K in cores in which a sharp, distinctive Brunhes-Matuyama boundary occurs, with other cores in which a gradational magnetic signature was recorded, was helpful. The part of unit K in which a sharp, well-defined magnetic reversal is present correlates with a thin, light-colored zone of coarser sediment in the cores for which a gradational magnetic change is recorded. The uppermost or first reversed reading also correlated with the same light-colored, coarser sediment of unit K. Thus, by selecting the first reversed polarity signature in the gradational interval, a consistent method of identification of the Brunhes-Matuyama boundary in all of the cores was accomplished.

TABLE 2. SEDIMENTATION RATES FOR SELECTED INTERVALS IN THE SEDIMENT CORES

Interval	Average rate (mm/1,000yr)	Range in rates (mm/1,000yr)
Brunhes 0.0 to 0.70 m.y.	1.14	0.55 to 2.92
Base of unit B to Matuyama-Gauss reversal 1.17 to 2.41 m.y.	0.70	0.53 to 1.01
Gauss 2.41 to 3.32 m.y.	0.53	0.34 to 0.74
Gilbert 3.32 to 5.12 m.y.	0.46	0.39 to 0.66

Sedimentation rates for the Brunhes Epoch were then calculated on the basis of this paleomagnetic-lithologic correlation. Rates ranged from 0.55 to 2.92 mm/1,000 yr (Table 2) and averaged 1.32 mm/1,000 yr for the cores studied.

The Jaramillo subchronozone is also recognized in at least half of the cores. The Jaramillo occurs in the lower portion of unit I and the upper portion of unit I. To check the validity of this occurrence, ages for the Jaramillo were calculated based on the sedimentation

rate for the Brunhes in each core. The calculated ages for the Jaramillo bracket the actual age (0.89 to 0.95 m.y.) consistently. This supports the idea that sedimentation rates changed very little in the upper part of the Matuyama.

Ages of *unit* boundaries were calculated by extrapolation of the Brunhes sedimentation rate into older parts of the cores. Because the Brunhes-Matuyama boundary is the most reliable magnetic signature in the upper parts of the cores (lithologic units I to M), it was used as the base line for age determination of depositional units (Table 3). Farther from the Brunhes-Matuyama boundary in the cores, the calculated ages are less accurate. For example, the base of unit I, on the calculated sedimentation rate, ranges from 0.94 to 3.02 m.y. in different cores. In many of the cores in which unit I occurs, a tentative Matuyama-Gauss boundary has been recognized. The actual age of the Matuyama-Gauss boundary is 2.43 to 2.48 m.y. Because this magnetic boundary occurs in unit D, ~100 cm below the base of unit I, it is apparent that several of the calculated ages for the base of unit I are spurious. The problem can be explained on the basis of the sedimentary makeup of the units.

TABLE 3. CHRONOLOGY OF UPPER UNITS

Unit	Age interval (m.y.)	Error (m.y.)*
M	0.000 to 0.264	± 0.037
L	0.264 to 0.558	± 0.060
K	0.558 to 0.822	± 0.083
J	0.822 to 0.946	± 0.093
I	0.946 to 1.200	± 0.105

*Estimated error calculated by subtracting the average age from the age calculated using the average unit thickness.

About 70% of the 100-cm section (below unit I) is silty lutite. Silty lutites represent low sedimentation rates. The sediments deposited during the Brunhes are predominantly arenaceous lutites and represent higher sedimentation rates. Therefore, the calculated Brunhes sedimentation rate most likely is greater than the actual sedimentation rate for the section of predominantly silty lutite above and below unit I (units A, B, D, F, G, I, K, and part of M).

If it is assumed that the sedimentation rate based on the Brunhes-Matuyama reversal represents a maximum figure, the minimum time needed to deposit 100 cm of sediment is 0.88 m.y. Subtracting the minimum time of deposition for the actual age of the Matuyama-Gauss boundary (2.43 m.y.) gives a maximum possible age of 1.55 m.y. for the base of unit I.

Re-examination of the thickness data reveals the reason for the spurious dates. Figure 31 shows distribution of sedimentation rates. Comparison of this with the thickness trend of units I and M (Fig. 27) indicates a close similarity. Cores with condensed I and M units have extremely low sedimentation rates. Because the total unit thickness of the Matuyama is relatively constant,

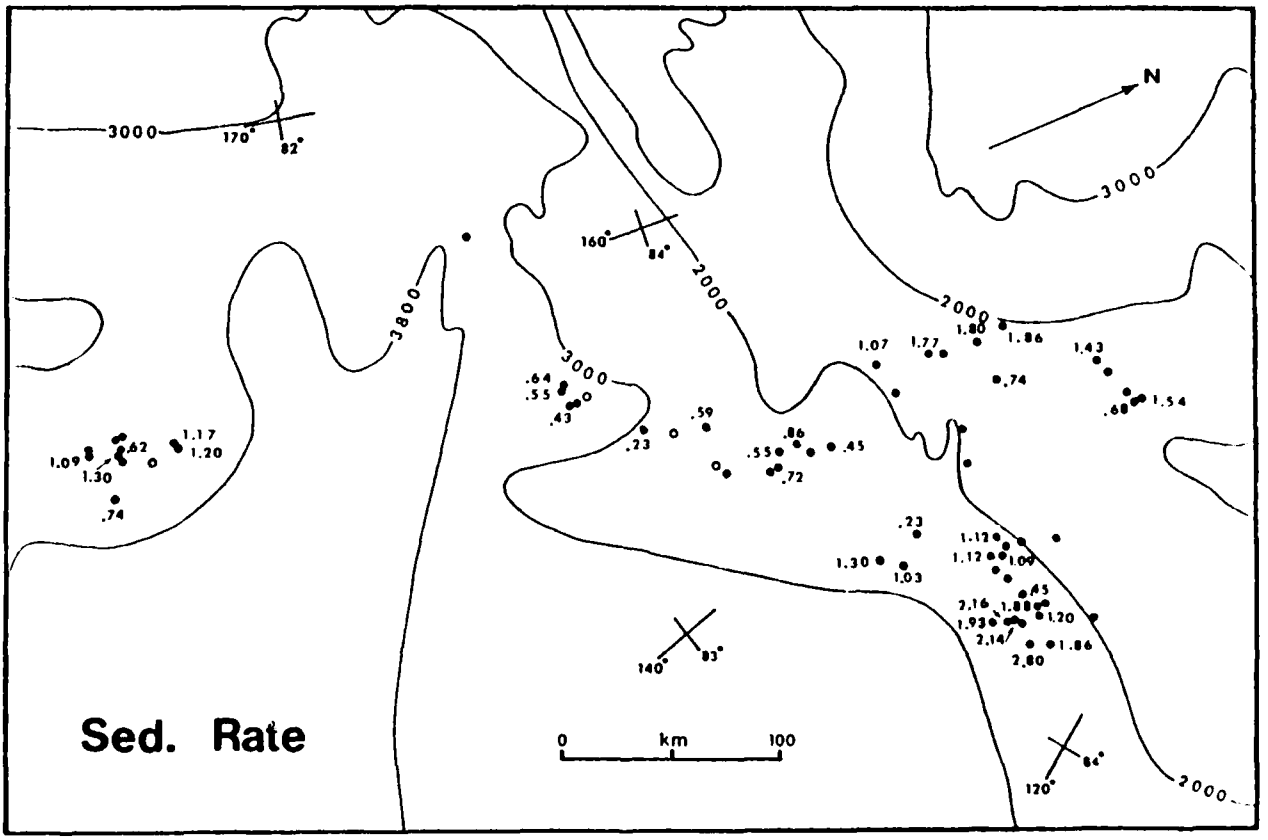

Figure 31. The geographic distribution of calculated sedimentation rates for units I to M for cores with interpretable magnetics. Sedimentation rates are in millimetres/1,000 yr. Note similarity of distribution pattern with Figure 27.

extrapolation of the resultant low sedimentation rates results in inflated ages for the lower units. About 35% of the cores have calculated dates greater then 1.5 m.y. for the bottom contact of unit I. All of these cores have condensed L and M units.

The average sedimentation rate and age for each unit were recalculated after elimination of cores in which calculated ages for the base of unit I were greater than 1.5 m.y. The average sedimentation rate that results is 1.14 mm/1,000 yr. Table 3 lists the ages for units I to M. The relationship of calculated ages to lithology for the upper parts of the cores and the apparent sedimentation rate are illustrated in Figure 32.

The next most reliable magnetic signature is in the middle of unit D. In order to check on the identification of this signature, assumed to be the Matuyama-Gauss boundary, the sedimentation rates were extrapolated downward. The calculated age of the base of unit H averages 1.17 m.y. ± 100,000 yr with a 95% degree of confidence and a range in values from 0.92 m.y. to 1.37 m.y. Using 1.17 m.y. as the age for the base of unit H, the sedimentation rate was calculated from the base of unit H to the assumed Matuyama-Gauss boundary in unit D for 25 cores. Using this sedimentation rate for each core and interpolating from the base of unit H, the base of unit F was calculated to average 1.92 m.y. ± 30,000 yr with a 95% degree of confidence and a range in values from 1.85 m.y. to 2.19 m.y.

The calculated sedimentation rate for the interval from the base of unit H to the assumed Matuyama-Gauss reversal is ~0.5 mm 1,000 yr. This includes units D, E, F, and G, which are predominantly silty lutite. This is an extremely important calculation because it contrasts with the higher sedimentation rate of the predominantly arenaceous lutites higher in the section (units H to M). The contrast convinces us that silty lutites represent lower sedimentation rates and that arenaceous lutites resulted from higher sedimentation rates—an idea developed separately on sedimentologic grounds.

A value of 0.5 mm 1,000 yr for silty lutites is important because four-fifths of the sediment in the lower part of the section (units D, E, F, and G) is silty lutite. Using this calculated value (0.5 mm 1,000 yr), the less distinctive magnetic signatures for the Gauss and Gilbert Epochs (which include nearly all silty lutites) can be verified (Figs. 2, 29).

An alternate interpretation of the paleomagnetics is that all of the interval below the Matuyama chron represents the Gauss and that the polarity reversal of unit D, believed to be the Matuyama-Gauss, is of Kaena and or Mammoth age. At 0.5 mm 1,000 yr, the expected thicknesses are 44.5 cm for the Gauss and 89.0 cm for the Gilbert. These values are exceedingly close to the average measured values of 46.9 cm for the probable Gauss in 25 cores and 83.1 cm for the probable Gilbert in 7 cores. If the reversed interval of unit D were Kaena and or Mammoth, sedimentation rates of at least 3.2 mm 1,000 yr would be necessary to achieve sufficient thicknesses. This value for sedimentation rates seems unlikely in view of the conclusions concerning low sedimentation rates for silty lutites. The average sedimentation rate for the Brunhes (including abundant arenaceous units) is 1.14 mm 1,000 yr (Table 2). Therefore, 0.5 mm 1,000 yr seems a more reasonable sedimentation rate for the lower silty lutite portion of the section than 3.2 mm 1,000 yr, which is a greater sedimentation rate then that found in the generally arenaceous Brunhes chron.

The sum of the evidence stongly implies low sedimentation rates for the lower stratigraphic units in the Arctic Ocean in general and specifically for silty lutites. Low sedimentation rates for the lower portion of the cores suggest adoption of the paleomagnetic interpretation shown (Fig. 29).

Average calculated sedimentation rates for various intervals consistent with the interpretation shown in Figure 29 are listed in Table 2. The range of sedimentation rates calculated for the Brunhes is in line with previously reported, nonturbidite sedimentation rates in the Arctic Ocean (Hunkins and Kutschale, 1967; Ku and Broecker, 1967; Ku and Opdyke, 1968; Steuerwald and others, 1968; Clark, 1970; Hunkins and others, 1971). It is clear from Table 2 that sedimentation rates have fluctuated during the late Cenozoic in the Arctic Ocean.

The paleomagnetic signature suggesting the age of 3.32 or 3.40 m.y. for the Gauss-Gilbert boundary was tested with a further extrapolation of sedimentation rates. The interval in the cores designated unit A includes the assumed Gauss-Gilbert boundary. In addition, a few cores have signatures that could be interpreted as being basal Gilbert as well as Polarity Anomaly 5. This interval consists of silty lutites, and the sedimentation rate of 0.5 mm 1,000 yr, shown to be reasonably accurate for the immediately overlying silty lutites, was applied. Using this sedimentation rate, the calculated age of the 49 magnetic signatures assumed to be Gauss-Gilbert and Gilbert Polarity Anomaly 5 boundaries was consistent (Fig. 2). On this basis, the oldest part of unit A in cores 224 and 221 is interpreted to include sediment of Miocene age. This age is tentative, and the combination of sedimentary parameters and magnetic signatures is the best present method of age determination.

Conclusions. Interpretation of the oldest sediment in core FI 224 as being upper Miocene (Fig. 29) has major implications for interpretation of the paleoclimatic history of the Arctic Ocean. An angular pebble, 1.1 × 0.7 cm (Fig. 33), was found in segment 8 of core FI 221 ~14.0 cm above flow-in and 8.5 cm below the base of the Gilbert. This segment is in an interval of normal polarity interpreted as Miocene Polarity Anomaly 5. This age interpretation is supported by physical correlations with core FI 224 and others. The pebble is partly coated with what appears to be a ferromanganese crust. This coating is similar to that on pebbles described by Schwarzacher and Hunkins (1961). The pebbles were from the surface of the Arctic Ocean floor and were interpreted as glacial erratics.

In addition to the pebble in segment 8, a larger pebble, 1.6 × 1.15 cm (Fig. 33) was found in dark brown flow-in near the base of the core in the middle of segment 1. This pebble is also coated with a ferromanganese crust. Both pebbles are angular to subangular with many facets. It is reasonable to assume that both of these pebbles are ice-rafted, and their presence suggests the existence of some type of ice-rafting transport at the time the sediment accumulated. Extrapolation of the Gilbert sedimentation rate for FI 221 (which is 0.54 mm 1,000 yr) from the Gilbert reversal to the pebble in segment 8 resulted in an age for the deposition of the pebble of 5.26 m.y. This value currently is the oldest date for the initiation of ice-rafting in the Arctic. The pebble found in flow-in below segment 8 supports the idea of even earlier ice-rafting.

The age of the oldest sediment recovered (which is in FI 224) was calculated in a similar manner. Extrapolation of the Gilbert sedimentation rate (0.54 mm 1,000 yr) for FI 224 from the Gilbert reversal to the sediment just above flow-in segment 6 resulted in a minimum age for this sediment of ~5.89 m.y. This value places the oldest sediment in Miocene reversed interval 6 (LaBrecque and others, 1977) (Fig. 29), which does not correspond to the normal

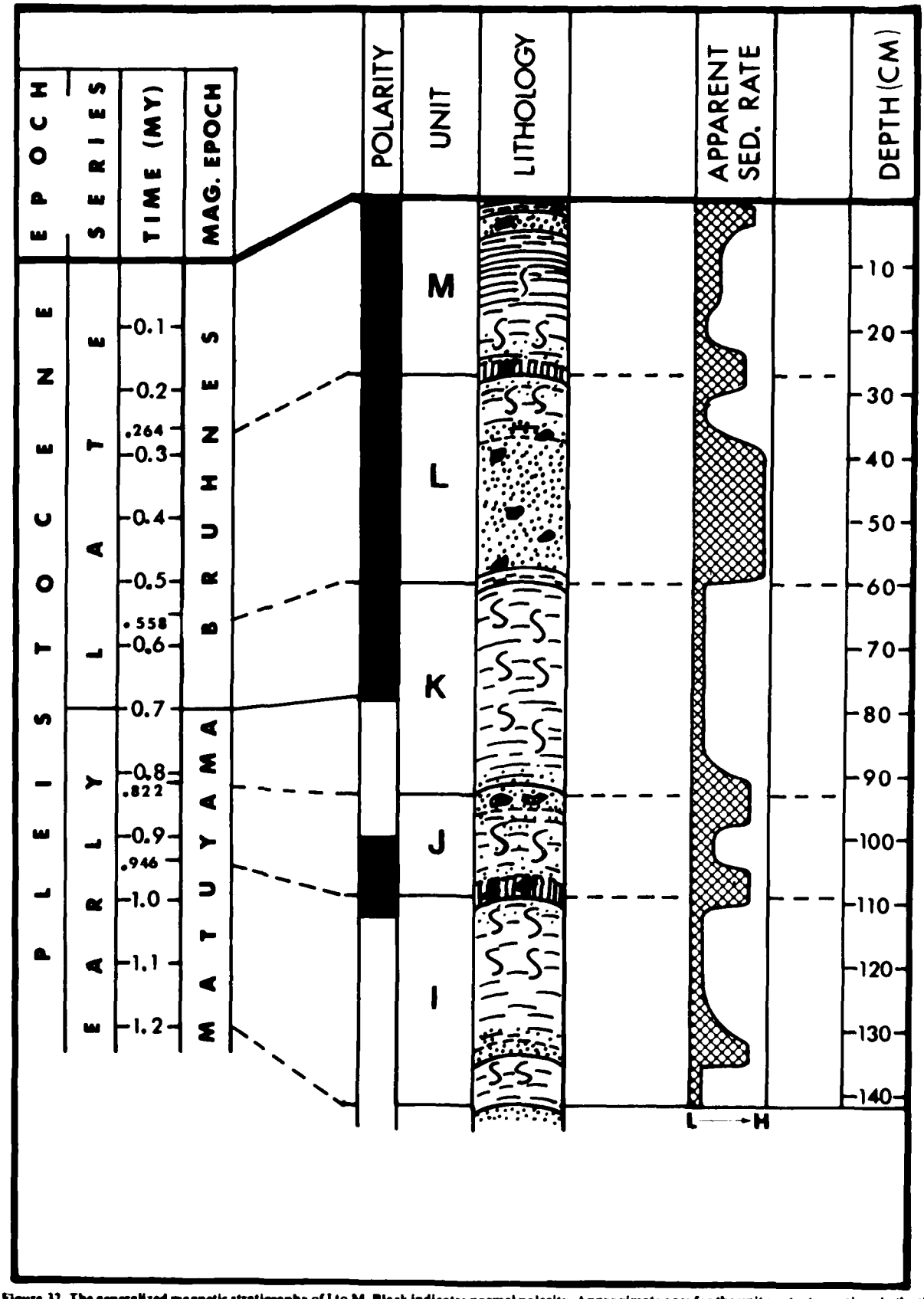

Figure 32. The generalized magnetic stratigraphy of I to M. Black indicates normal polarity. Approximate ages for the unit contacts are given in the time column (smaller numbers) and average sedimentation rates.

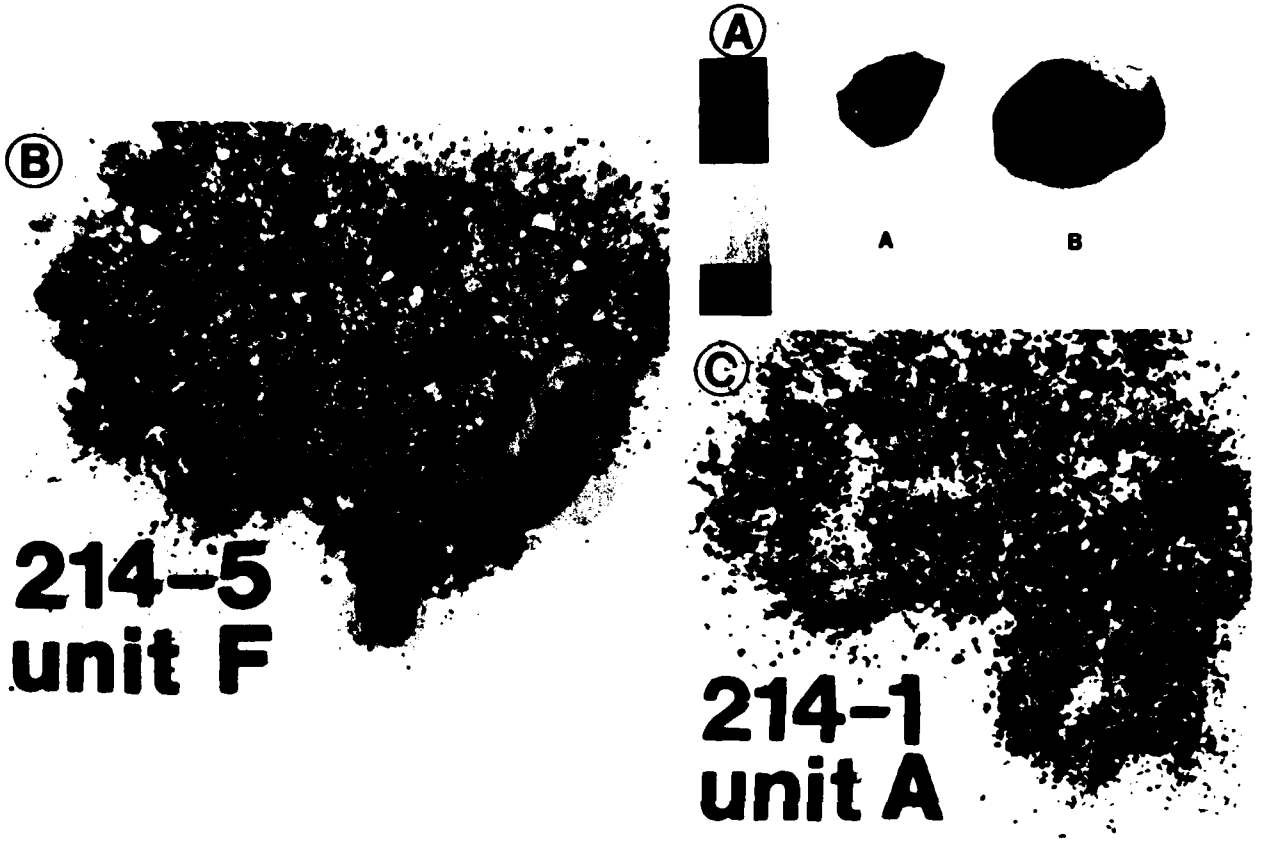

Figure 33. (A) Pebbles from core FL 221. Pebble A is from unit A, segment 8, top sample. Pebble B is from flow-in, segment 1, middle of the core. The scale is in centimetres. (B) A portion of the coarse fraction (<63 μm) from unit F, core FL 214, segment 5, sample 2. (C) A portion of the coarse fraction (<63 μm) from unit A, core FL 214, segment 1, sample 1. The black particles are ferromanganese particles. For both (B) and (C) the numeral 1 is 2.85 mm high.

polarity magnetic signatures of this sediment. This inconsistency may have resulted from an increase in sedimentation rates in the Miocene or from unreliable paleomagnetics in the bottom of core FL 224. The normal polarity magnetic signatures suggest a *maximum* age of the oldest undisturbed sediment in FL 224 to be 5.62 m.y. This age is the oldest reliable date for in-place sediment in the Arctic Ocean.

While we believe that these age approximations are sound, we concede that isotope data for the oldest parts of our cores would make our position more comfortable. The Arctic sediment has not yielded such data to date.

SURFACE-SEDIMENT CHARACTERISTICS

Bottom photographs from several parts of the central Arctic Ocean show two prominent features: (1) primary sedimentary structures in a silty lutite matrix and (2) pebble fields. The sedimentary structures, mostly trace fossils, were described and interpreted by Kitchell and others (1978a, 1978b) Kitchell (1979), and Kitchell and Clark (1979). The conclusion of this work challenges previous ideas concerning trace fossils and bathymetry.

No bathymetric gradient in behavioral complexity can be interpreted from the Arctic photographs (Kitchell and Clark, 1979). Those traces identified in the fossil record to represent efficient foraging strategies are conspicuously absent at all depths in the central Arctic. In contrast, the efficient foraging strategies of the *Nereites* group were shown to be present at all depths in the Antarctic (Kitchell and others, 1978b). These findings suggest that, despite the trace-fossil paradigm that increasing behavioral complexity and sediment exploitation correlate with a decrease in food availability, the presence or absence of surface-grazing organisms is more important than depth or nutrient supply in modifying sediment. Trace-fossil patterns may be better understood by reference to resource-optimization theory and the effect of predation (Kitchell, 1979).

Also prominent in bottom photos are pebble fields, interpreted as accumulations of ice-rafted debris (Schwarzacher and Hunkins, 1961). This conclusion is in harmony with our own work summarized in the following pages.

ARCTIC SURFACE-SEDIMENT TEXTURE

Introduction

In addition to photographic study of surface trace fossils and pebble fields, several hundred core tops were studied texturally.

The surface sediment generally consists of less than 15% sand-sized material. The remaining 85% of the surface sediment was studied to determine the relative importance and abundance of silt- and clay-sized particles. Some 93 core tops were selected for detailed textural analysis (App. 1B). The uppermost 3 cm of the cores was considered to be surface sediment.

The result of this study is a silt-clay textural classification of glacial-marine sediment. The samples were selected to provide a wide geographic distribution representing glacial-marine sediment in varying depositional environments in the modern central Arctic Ocean. Figure 34 shows the geographic distribution of the surface-sediment samples as well as the bathymetric configuration of the central Arctic Basin.

Sediment and Geomorphic Structure of Study Area

Thirty-one of the surface-sediment samples were collected from the flanks of the Alpha Cordillera and its western extension, the Mendeleyev Ridge. The Alpha Cordillera is a broad bathymetric high that reaches its crest at a depth of 1,800 m below the ocean surface (Hunkins and Kutschale, 1967). Although a few persistent linear trends occur, most of the 250- to 800-km width of the Alpha Cordillera consists of small discontinuous ridges and small peaks (Hall, 1973). The sediment thickness over the Alpha Cordillera, measured by seismic reflection techniques, is ~300 m (Hall, 1973).

The Canada Abyssal Plain and its northwestern extension, the Mendeleyev Abyssal Plain, lie to the south of the Alpha Cordillera (Fig. 34). Hunkins (1968) reported that this abyssal plain has a uniform depth of ~3,800 m and covers an area of almost 255,000 km². At its western boundary, the Canada Abyssal Plain impinges on the steep slopes of the Chukchi Rise and the Northwind Escarpment. The gradual slopes of the Canadian Continental Rise form the southern and eastern boundaries. Hunkins (1968) and Hunkins and Kutschale (1967) have hypothesized that the occurrence of more gradual slopes and shallower depths at the eastern boundary of this abyssal plain indicates that the principal source of sediment is the eastern portion of the Canadian Continental Shelf. Campbell and Clark (1977) reported higher turbidite concentrations in cores from the southeastern and northeastern portions of the abyssal plain. This turbidite concentration indicates a sediment source in the Canadian Archipelago in support of the earlier theory of Hunkins (1968).

Sediments in the Canada Abyssal Plain differ from those of the Alpha Cordillera in that they have lower concentrations of Foraminifera and are dark olive-gray to gray in color (Hunkins and Kutschale, 1967). More significantly, Campbell and Clark (1977)

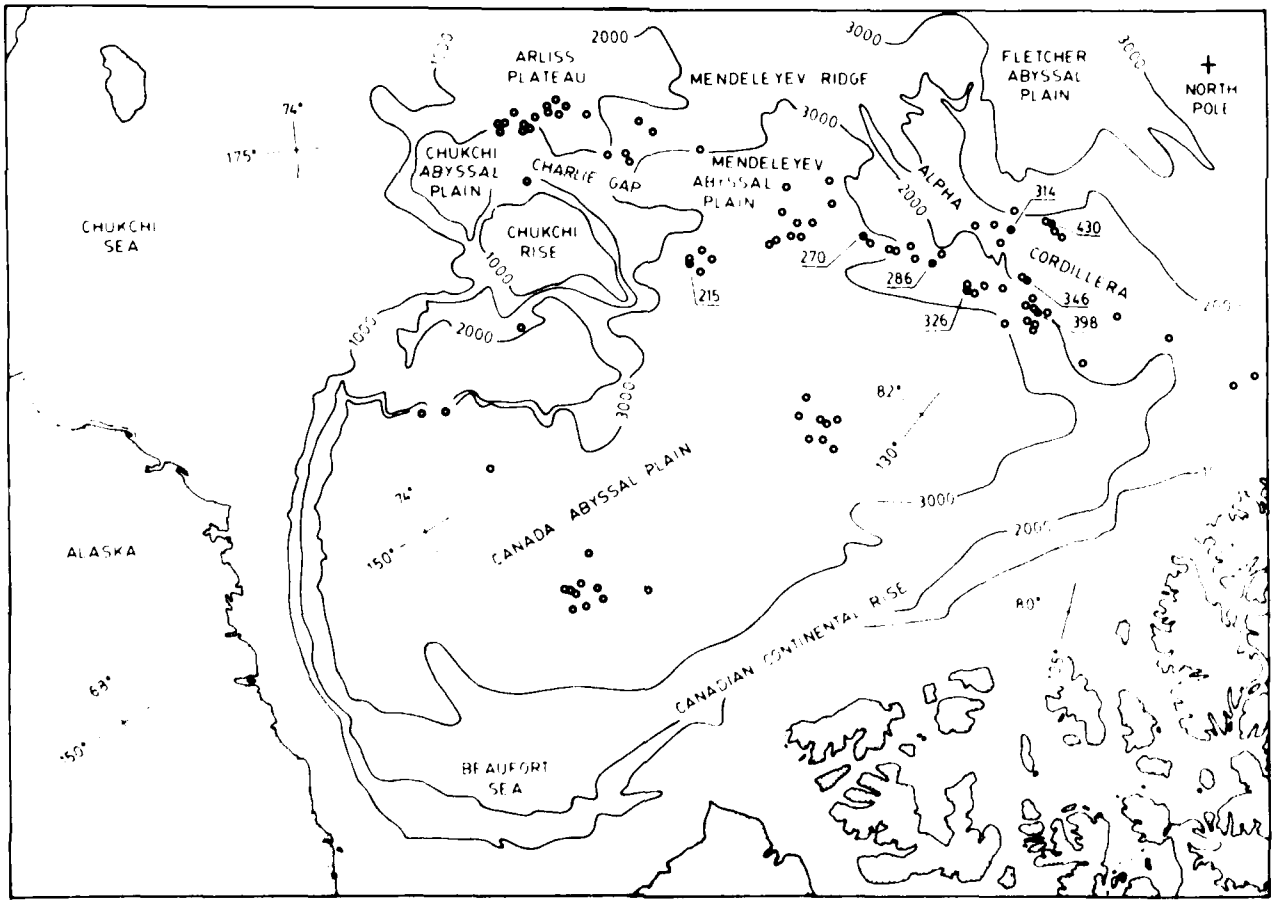

Figure 34. Geomorphic map of a portion of the Arctic Ocean showing the geographic distribution of surface samples (that is core tops) and the bathymetric configuration of the central Arctic Basin. Open circles represent locations of surface-sediment samples. Locations of the eight cores used in the stratigraphic analysis are indicated by numbered closed circles. The water-depth contour interval in 1,000 m.

concluded that well-sorted sandy layers comprising as much as 27% of the sediment in some cores are the product of turbidity currents. These deposits exhibit better sorting than those of the Alpha Cordillera and are deposited at higher rates. Sedimentation rates as high as 83 mm/1,000 yr have been calculated for some sites in the Canada Abyssal Plain (Campbell and Clark, 1977). The high rate of sedimentation has resulted in the deposition of a 2-km layer of sediment (Hunkins and Kutschale, 1967) in the abyssal plain, compared to only 300 m of sediment for the Alpha Cordillera (Hall, 1973). A total of 39 sediment samples from the Canada Abyssal Plain was analyzed.

The Chukchi Abyssal Plain lies to the west of the Canada Abyssal Plain. It is bounded on the west by the Arliss Plateau and on the south and east by Chukchi Rise. The average depth of this abyssal plain, which covers an area of 5,000 km^2, is ~2,200 m (Hunkins, 1968). A narrow canyon called the Charlie Gap connects the Chukchi Abyssal Plain with the northwestern extremities of the Canada Abyssal Plain. Hunkins (1968) suggested that minor amounts of sediment may flow through the Charlie Gap from the Chukchi Abyssal Plain and be deposited on the Canada Abyssal Plain.

Little information is available on the sediments of the Chukchi Abyssal Plain. Their textural characteristics are assumed to be similar to those of the Canada Abyssal Plain because the depositional environments of those two regions are similar. Sedimentation rates determined from seismic and paleomagnetic data for the Chukchi Abyssal Plain are ~2.4 mm/1,000 yr. A group of 13 samples from the northern edge of the Chukchi Plain was analyzed.

The remaining 11 surface sediment samples were taken from locations scattered on the southern flank of the Northwind Escarpment and the northwestern boundary of the Canada Abyssal Plain.

In addition to the Arctic Ocean core-top samples, 17 samples of normal pelagic and hemipelagic clays, calcareous ooze, and siliceous ooze from other oceans and 20 samples of continental glacial till were analyzed. Grain-size distributions were determined to contrast marine, glacial, and glacial-marine sediment characteristics. The locations of these comparative samples are listed in Appendix 1C and 1D.

Study consisted of sieving samples on a 63-μm (micrometre) sieve for removal of sand and larger-sized particles and conducting an electronic size analysis of the material that passed through the sieve using a TA II Coulter counter. The Coulter counter measured the percentages of particles in 19 class intervals between 0.63 and 63 μm, or ~11 to 4 phi. Data from the Coulter counter and sieve were normalized. The term "coarse" (as applied to particles, modes, distributions, and so forth) hereafter refers to particles larger than 63 μm in diameter.

Silt-Clay Grain-Size Histograms

Four types of silt-clay grain-size distributions were observed in the histograms constructed for the Arctic Ocean surface sediments.

Type I Sediment. Sediments with silt-clay histograms having a flat distribution over the entire fine-clay to coarse-silt range (0.63 to 63.0 μm) (Fig. 35) are referred to as type I sediment. These sediments are nonsorted and consist of nearly equal amounts of silt and finer material. The amount of fine to coarse clay, hereafter referred to as the clay-sized fraction, has a mean of 39.4% by weight, whereas the mean silt content is 46.4%. The mean percentage of coarse material is 14.1% for type I sediment.

Type II Sediment. Bimodal silt-clay histograms (Fig. 36) are characteristic of type II sediments. The finer mode consistently occurs in the 1.26- to 2.52-μm (medium- to coarse-clay) range. The coarse mode is more variable in position, generally in the 6.35- to 63.0-μm (fine- to coarse-silt) range. In a few cases, only the fine tail of the coarse mode occurs in the silt-sized fraction; this indicates that the peak and coarse tail occur in the coarse fraction. For type II sediment, the mean contents of silt-, clay-, and coarse-sized particles are 16.0%, 48.3%, and 35.6%, respectively. A gradational change was noted between type I and type II sediments. Some poorly sorted sediments show slight bimodality, and some bimodal sediments are poorly sorted.

Type III Sediment. The third type of sediment histogram (Fig. 37) exhibits a strong mode in the medium- to coarse-clay range with a coarse tail extending through the silt range. In some cases, a secondary mode is found in the fine- to coarse-silt range, which

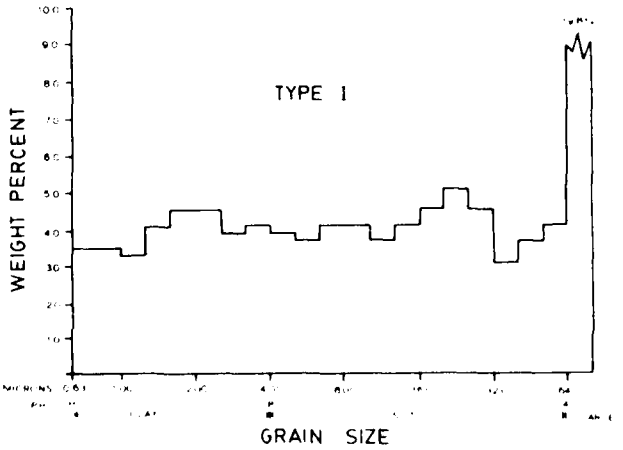

Figure 35. Typical Arctic Ocean type I silt-clay grain-size histogram (sample 17-19-1). *The percentage of grains with diameters greater than* 63 μm, that is, the coarse fraction, is represented by the column labeled "Coarse" at the right side of the histogram. Not that the distribution is constant over the entire fine-clay to coarse-silt (0.63- to 63.0-μm) range.

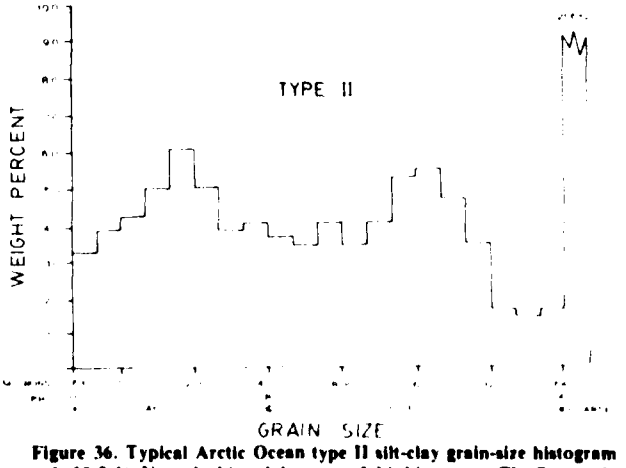

Figure 36. Typical Arctic Ocean type II silt-clay grain-size histogram (sample 19-8-1). Note the bimodal nature of this histogram. The fine mode occurs in the medium- to coarse-clay (1.26- to 2.52-μm) range. The coarse mode is found in the fine- to coarse-silt (6.35- to 63-μm) range.

suggests that type III sediments are related to the bimodal sediments characteristic of type II. The relative abundances of coarse-, silt-, and clay-sized particles for type III sediments are influenced by the geographic locations from which the samples were taken. Type III sediments of the Canada Abyssal Plain (Fig. 37) tend to have low mean contents of coarse particles (2.0%) and silt particles (31.2%) and a high mean clay content (68.8%). Alpha Cordillera type III sediments (Fig. 38) have higher mean coarse percentages (15.2%) and a lower mean clay content (47.7%). Type III sediments of the Chukchi Abyssal Plain tend to have relative coarse, silt, and clay proportions intermediate between those of the Alpha Cordillera and the Canada Abyssal Plain. Generally, type III sediments have a low mean coarse content and a high mean clay content in comparison to other sediment types.

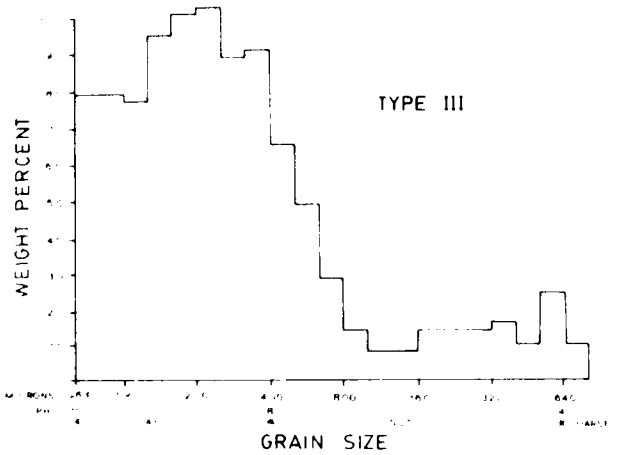

Figure 37. Silt-clay grain-size histogram representing a typical Canada Abyssal Plain type III sediment (sample 50-14-1). Note the occurrence of a mode in the medium- to coarse-clay (1.26- to 2.52-μm) range with a coarse tail extending through the silt range. The fine mode in type III sediments of the Canada Abyssal Plain is probably composed of fine sediments associated with turbidity-current deposits.

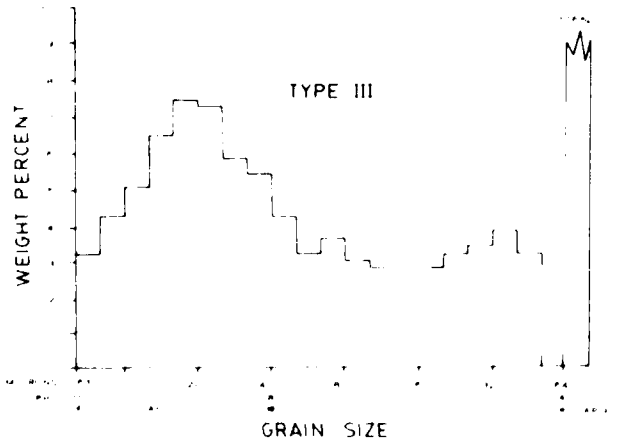

Figure 38. Typical type III silt-clay grain size histogram representing a sediment sample from the Alpha Cordillera (sample 395-16-1). Comparison of Alpha Cordillera and Canada Abyssal Plain type III histograms revealed that type III sediments from the cordillera have larger relative proportions of silt and coarse material. Type III histograms representing Alpha Cordillera sediments are assumed to indicate low influx rates for glacial ice-rafted medium to coarse silt.

Type IV Sediment. Type IV sediments have a mode in the coarse-sized or coarse-silt sized fraction and a fine tail extending through the fine-silt and coarse-clay class intervals. Some type IV sediments are bimodal with a secondary mode in the medium- to coarse-clay range. The geographic location of samples shows some influence on the relative proportions of coarse-, silt-, and clay-sized particles occurring in type IV sediment. Samples from the Canada Abyssal Plain (Fig. 39) tend to have more silt and fewer coarse grains (mean silt content = 74.6%; mean coarse content = 11.9%) than do those from the Alpha Cordillera (Fig. 40) (mean silt content = 63.6%; mean coarse content = 25.7%). Overall, type IV sediments have a high mean coarse-silt content and a low mean clay content in comparison to other sediment types.

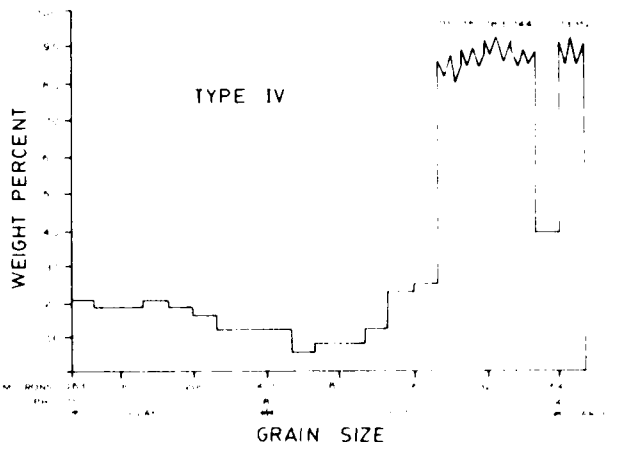

Figure 39. Silt-clay grain-size histogram representing a typical type IV sediment from the Canada Abyssal Plain (sample 75-8-1). Note the presence of a mode in the coarse-silt fraction with a fine tail extending through the fine-silt-sized and clay-sized fraction. The occurrence of the silt mode in Canada Abyssal Plain type IV sediments is believed to result from deposition of silt by turbidity currents.

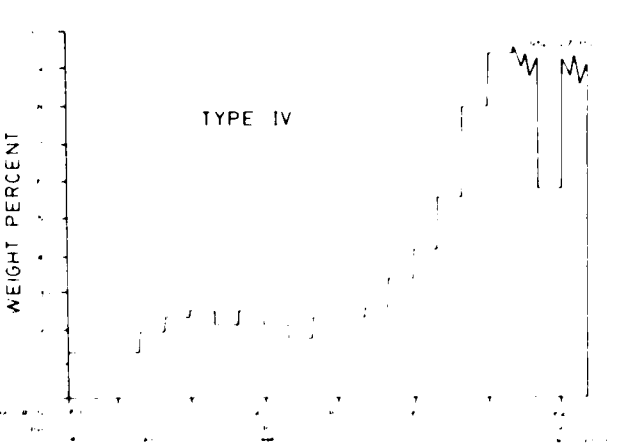

Figure 40. Typical type IV silt-clay histogram representing sediment from the Alpha Cordillera (sample 533-20-1). When compared to Canada Abyssal Plain type IV histograms, Alpha Cordillera type IV histograms were found to exhibit higher relative proportions of clay and coarse particles. Type IV sediments of the Alpha Cordillera probably result from high rates of deposition of glacial ice-rafted silt and coarse material.

Statistical Parameters

The mean, standard deviation (sorting coefficient), and skewness were calculated graphically for the 0.63- to 63.0-μm (fine-clay to coarse-silt) histograms in order to describe the size distribution of the particles of each Arctic Ocean surface-sediment sample. These parameters should not be considered representative of the entire sample because they do not include the coarse fraction or particles finer than 0.63 μm. They are useful for comparisons between sediment types, however. The mean values of each statistical parameter and the mean coarse, silt, and clay percentages typifying each sediment type are listed in Table 4.

Statistical tests were used to evaluate the validity of this classification. The t test was used to determine the significance of differences in the mean statistical parameters of the sediment types at the 0.95 confidence level. The significance of differences in standard deviations of the mean statistical parameters was determined, at the 0.95 confidence level, using the F test. Unless otherwise noted, differences described in this discussion were found to be significant.

Skewness coefficients of type I sediments are among the highest encountered in Arctic Ocean surface sediments; these samples deviate the most from a symmetrical, normal distribution. Positive skewness usually indicates the presence of a coarse tail in a unimodal distribution. This is not apparent in the histograms of type I sediments. Perhaps the silt distribution of these sediments should be thought of as a poorly sorted coarse tail of a unimodal distribution with its mode in the clay-sized fraction.

The bimodal distributions of type II yield a mean skewness of 1.2 with a standard deviation of 0.3. This mean value suggests that the silt mode of some bimodal histograms may represent the coarse tail of a predominantly clay-sized sediment.

The mean grain size of type I sediment is smaller than that of type II, which reflects the absence of the silt mode in type I histograms. The mean sorting coefficient of type II sediment is somewhat higher than that of type I. The variability in the size range covered by the silt mode in the type II histogram is demonstrated by the greater standard deviation of the mean sorting coefficient for type II sediments.

Regardless of geographic influences, type III sediments have the smallest mean grain sizes of the four sediment types. This is a result of the high clay content reflected by the mode in the clay-sized fraction of type III histograms. These sediments also show the best sorting of all Arctic Ocean surface samples. The presence of a coarse tail or secondary mode in the silt-sized fraction gives these samples high positive skewness values.

Mean grain sizes of type IV sediments are the largest encountered for Arctic Ocean surface sediments. The coarse nature of these deposits is also reflected by the high percentage of silt and coarse sediment (Table 4). Although type IV grain-size distributions show a pronounced silt mode, the sorting is poor owing to the wide grain-size range in which this mode occurs. Negative mean skewness coefficients were calculated for type IV sediments of the Canada Abyssal Plain and the Alpha Cordillera. This effect was produced by the presence of a fine tail or secondary mode in the clay fraction. Type IV sediments have mean skewness coefficients near zero, which indicates that their grain-size distributions are nearly symmetrical about the mean grain size, that is, they approach a normal distribution.

Conclusions

Four textural categories of Arctic Ocean surface sediment are recognizable: (1) type I, sediment with a nonsorted silt-clay histogram; (2) type II, sediment with a bimodal silt-clay histogram; (3) type III, sediment with a strong mode in the coarse-clay range; and (4) type IV, sediment with a strong mode in the coarse silt range.

FERROMANGANESE MICRONODULES

Description

Dark brown to black ferromanganese micronodules are common in the sand-sized fraction of the silty lutites in the cores studied. These particles are friable and easy to crush with the point of a dissecting needle. They occur in a variety of shapes and growth habits, but irregular, angular particles predominate. Rounded, nearly spherical shapes and elongated, smooth cylindrical forms are common. Often it is clear that two particles have merged after initial separate and independent growth (Fig. 4I). Quartz, mica, and other detrital grains as well as whole or fragmented Foraminifera tests are often incorporated into the ferromanganese particles.

Ferromanganese material commonly speckles the surface of Foraminifera, both benthic and planktonic, and in many cases encrusts the whole test. Pebbles in the sediment are generally wholly or partly coated with a thin ferromanganese layer. Scanning electron microscope photographs show clearly the detrital grains incorporated into the particles and the secondary nature of the coatings on Foraminifera tests (Fig. 4I).

The ends of several thin section plugs were ground, polished, and studied in reflected light, but the ferromanganese particles displayed no laminations. Broken particles observed with the scanning electron microscope show a crumbly, irregular, broken surface but no layering. It appears that these particles are loose

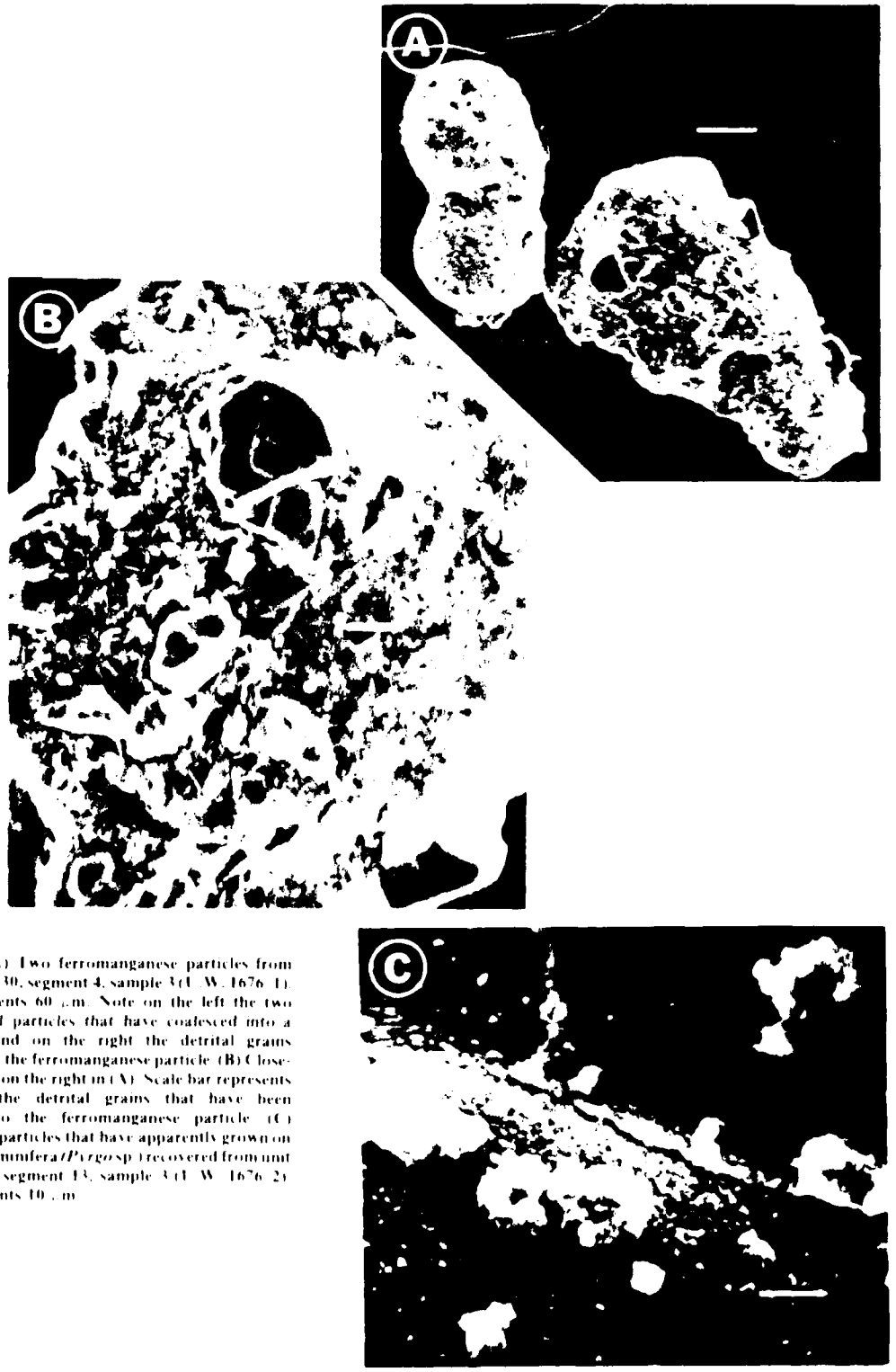

Figure 41. (A) Two ferromanganese particles from unit A, core EE-430, segment 4, sample 3 (USGS-W-1676-1). Scale bar represents 60 μm. Note on the left the two roughly spherical particles that have coalesced into a single particle and on the right the detrital grains incorporated into the ferromanganese particle. (B) Close-up of the particle on the right in (A). Scale bar represents 20 μm. Note the detrital grains that have been incorporated into the ferromanganese particle. (C) Ferromanganese particles that have apparently grown on the test of a Foraminifera (*Pyrgo* sp.) recovered from unit G, core EE-283, segment 13, sample 3 (USGS-W-1676-2). Scale bar represents 10 μm.

aggregates of ferromanganese material and sedimentary grains rather than internally laminated nodules.

Semiquantitative elemental analysis was performed on 48 ferromanganese particles. The particles were picked from samples of units A, D, and G (Fig. 2) from cores FI 221, FI 283, and FI 430. X-ray spectra were recorded using the energy-dispersive, X-ray analysis system attached to the scanning electron microscope.

Silicon and aluminum generally are the most abundant elements (Fig. 42). This is explained by the incorporated impurities in the particles. Iron and manganese are normally the next most abundant elements. Iron is more plentiful than manganese in about one-half of the samples, and manganese is more plentiful than iron in the remainder. No definite trends are apparent in the relative abundances of the two elements with depth in the core or between cores. Occasionally, the electron beam would impinge upon pure authigenic material, and iron and manganese would be the most abundant elements almost to the exclusion of others (Fig. 42). Small amounts of copper and nickel also are present in these particles.

X-ray powder photographs were made in an attempt to identify the iron-manganese mineral(s) present in these particles. A large number of particles were ground to a powder and coarse-sized detrital grains were eliminated to purify the sample. Unfortunately, the effort to produce a pure sample was unsuccessful. Quartz, mica, chlorite, and possibly feldspar were identified in the powder photograph. No unique reflections were identified for any form of manganese or iron-manganese minerals. However, the most intense X-ray reflections of todorokite and buttesite, two of the more common minerals found in manganese nodules, would be overlapped by muscovite and chlorite reflections. It is also possible that the ferromanganese mineral or minerals are poorly crystalline.

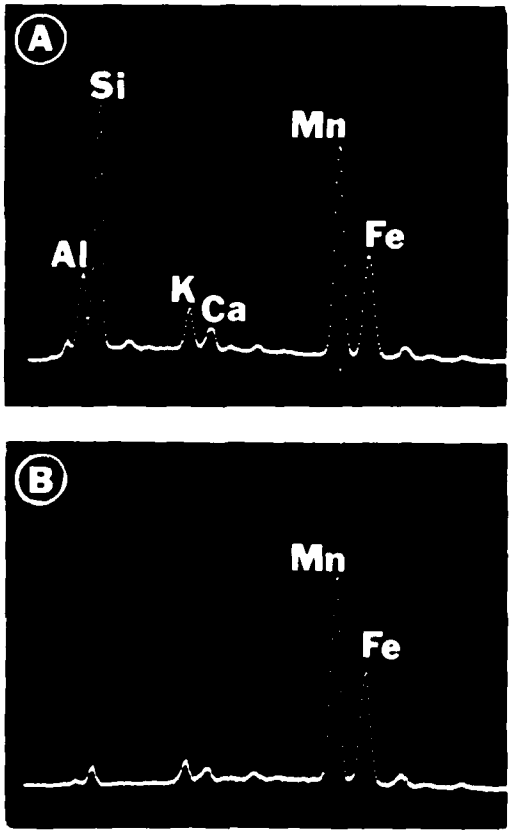

Figure 42. (A) X-ray spectrum of a typical ferromanganese particle from unit A, core FI 221, segment 8, top sample. Elemental peaks other than manganese and iron are probably a result of detrital grains incorporated into the particle. (B) X-ray spectrum for a relatively pure area of one ferromanganese particle from unit A, core FI 221, segment 8, top sample. Manganese and iron are the predominant elements to the near exclusion of all others.

Interpretation

An authigenic origin for these ferromanganese particles is suggested by a combination of facts. The particles are fragile and friable and it is unlikely that they would survive glacial or current transport. The coating on glacial striaties in the cores as well as on Foraminifera tests also is a ferromanganese material and is authigenic. The iron and manganese oxides investigated by Herman (1970) were considered to be precipitates.

It is probable that the iron and manganese are in the oxidized state. The silty lutites are intensely bioturbated which suggests that oxygen was present in sufficient quantity for numerous metazoans to thrive. Because the manganese reacted similarly to iron oxides in chemical reactions, Herman (1970) and Hoffman (1972) assumed that it was in the oxidized state.

Hunkins and others (1971) reported that treatment of the coarse fraction of core 13-67-11 with hydrochloric acid dissolved the "manganese nodules." The ferromanganese particles in this study resisted dissolution in dilute HCl.

Ferromanganese particles are most common in the silty lutites. They reach their maximum abundances in the lower portion of the section in unit A. This distribution contrasts with the findings of Li and others (1969). A core that they studied from the Canada Abyssal Plain showed an irregular but general decrease in manganese in the sediment from the top to the bottom of the core. Our observation of a trend for more ferromanganese particles in the older sediment agrees with the findings of Hunkins and others (1971) who observed that manganese nodules are considerably more abundant in sediment of Matuyama age than they are in sediment of Brunhes age. Herman (1970) and Herman and others (1971) also reported an abundance of iron and manganese oxides in the lower portion of their cores.

Goodell and others (1968) published photographs of the coarse fraction of sediment from Antarctic regions of the Pacific Ocean that show abundant ferromanganese micronodules. These micronodules are similar to the ferromanganese particles described in this study (Fig. 38C). The micronodules from the central Arctic Ocean differ most dramatically from those of the world oceans in lack of layered growth.

MECHANISM OF SEDIMENT DEPOSITION IN THE CENTRAL ARCTIC OCEAN

Introduction

Beneath the Arctic pack ice, sediment is transported by [illegible]

accumulation; (4) ice-rafting; (5) bottom processes involving inorganic or organic activity; and (6) atmospheric dust accumulation (Ericson and others, 1964; Clark, 1971, 1974; Mullen and others, 1972; Darby and others, 1974; Herman, 1974). Three sediment types clearly dominate the upper Miocene to Holocene sediments of the Alpha Cordillera region: (1) arenaceous lutites; (2) silty lutites; and (3) minor amounts of clastic, carbonate-rich, pink-white sediment. Silty lutites comprise about 80% of most sections, but the arenaceous lutites are more distinctive markers and contain a higher percentage of erratics (that is, dropstones). We believe that the origin of all of these units represents a variation on a single theme—ice-rafting.

Evidence of Ice-Rafting

Arenaceous Lutites. Figure 33 illustrates the poor sorting, coarse texture, and ice-rafted pebbles commonly found in the zones of arenaceous lutites. Several large erratics and small, pink-white clasts from unit J are illustrated in Figure 12. The surfaces of the large erratics are faceted and exhibit striae.

The vertical distribution of erratics is listed by unit in Table 1. An increase in the number of erratics per centimetre of section occurs in units J, L, and M. These units contain arenaceous lutite zones and pink-white layers. In addition, the standard deviation of unit thickness for units L and M indicates a greater thickness variability. This may suggest a more sporadic depositional history for these units, such as glacial ice-rafting of a greater magnitude.

The arenaceous lutite in the upper portion of unit J contains small, pink-white clasts of variable texture. These clasts are pelletal *in nature and seem to be very cohesive*; they also occur in most of the pink-white layers. Similar clasts were described by Ovenshine (1970) during a study of recent iceberg rafting in Glacier Bay, Alaska. He concluded:

> Small pellets of poorly sorted sediment are abundant in the material being rafted into Glacier Bay and originally formed between clear ice crystals in foliation bands in glacier ice. They probably owe their coherence to the stress undergone during glacier flow. If present in an ancient sequence, they *testify uniquely to the nearby existence of glaciers* (Ovenshine, 1970, p. 893).

A good correlation exists between arenaceous lutite zones and pink-white layers with increased detrital grains (Fig. 9). Examination of grain microsurfaces with a scanning electron microscope reveals textures and features similar to those commonly observed on microsurfaces of glaciated grains (Krinsley and Doornkamp, 1973). Several grains exhibiting these features are illustrated in Figure 43.

A plot of detrital grains (lithic fragments plus detrital carbonate) versus depth in core is given in Figure 9. There is a good correlation of increase in detrital grains (lithic fragments and detrital carbonate) with sandy lutite zones and pink-white layers. Lithic fragments found hundreds of kilometres from the nearest continental source are probably ice-rafted (Goodell and others, 1968).

Carbonate maxima 1, 3, and 7 (Darby, 1975) correlate with pink-white layers W3, PW2, and PW1, respectively. Arenaceous lutite zones appear to correlate with carbonate maxima 1 and 9 (Fig. 9). Darby interpreted these maxima as detrital units that were derived from glacial icebergs during periods of increased glacial calving.

Figure 12D illustrates the coarse fraction (>63 μm) for the PW1 layer in core FL 270. Poor sorting and faceted pebbles common to these layers are well illustrated in this figure. Most of the pebbles and large grains from these units are angular and exhibit faceting, striae, and other features indicative of glacially derived sediments (Goodell and others, 1968).

Silty Lutites. The silty lutites consist of (1) normal pelagic sediments (slow accumulation of detrital grains, atmospheric dust, and biogenic components), (2) ice-rafted sediments, and (3) authigenic sediments. The silty lutites are characterized by low percentages of coarse sediment (>63 μm). An average value is <5%.

Ice-rafted pebbles are occasionally observed in the silty lutites. However, the frequency is much lower than that of the arenaceous lutites (Table 1; units I and K are primarily silty lutites). Ferromanganese particles are abundant in portions of unit I and all of unit K. Apparent ferromanganese coatings or crusts are also found on detrital grains. Herman (1974) and Hunkins and others (1971) also described authigenic manganese nodules and crusts in several cores from the central Arctic Ocean. They believed that these particles form in areas where the sedimentation rates are extremely low. *The silty lutites are primarily ice-rafted in origin but represent periods of reduced ice-rafting.*

All of these sediment types have been defined stratigraphically and exhibit a continuous distribution across the central Arctic Ocean. There is an apparent dichotomy because it might be assumed that ice-rafted sediments should exhibit a patchy, discontinuous distribution. However, the sedimentation rates indicate that long periods of time are necessary for the deposition of significant amounts of ice-rafted detritus. It seems apparent that the drift of the ice pack over long periods of time, combined with the continual melting and release of ice-rafted detritus into the water, would explain the continuous distribution of ice-rafted sediments in the central Arctic Ocean.

Other Sedimentary Processes

Other clastic sedimentation processes in the ocean are compared in Table 5. The evidence supports the idea that ice-rafting has been the dominant process of central Arctic Ocean sedimentation since the late Miocene. This is not a novel conclusion but has been examined, in part, by Arctic workers (Ericson and others, 1964; Hunkins and others, 1971; Mullen and others, 1972). Studies of ice-rafted sediment are few, and it has been concluded that "there are no generally accepted, quantitatively defined characteristics" for ice-rafted debris (Goodell and others, 1968, p. 47). For this reason, we have considered other possibilities. Middleton and Hampton (1973) listed criteria for distinguishing four mass-flow mechanisms for transportation of sands and coarser sediments into deep water: turbidity currents, fluidized sediment flows, grain flows, and debris flows. Bouma and Hollister (1973) investigated the deposition of sediment by deep ocean currents that produce contourites. Harms (1974) described the characteristics of an unusual deep-water density current deposit from the Permian of west Texas.

Two major factors preclude a sediment-gravity-flow (Middleton and Hampton, 1973) interpretation for the arenaceous lutites: (1) the widespread lateral and vertical distribution of the *arenaceous lutites from the deep margin of the Canada Basin to the* top of the shallow Alpha Cordillera and (2) the lack of any primary sedimentary structures or grain orientation in the arenaceous

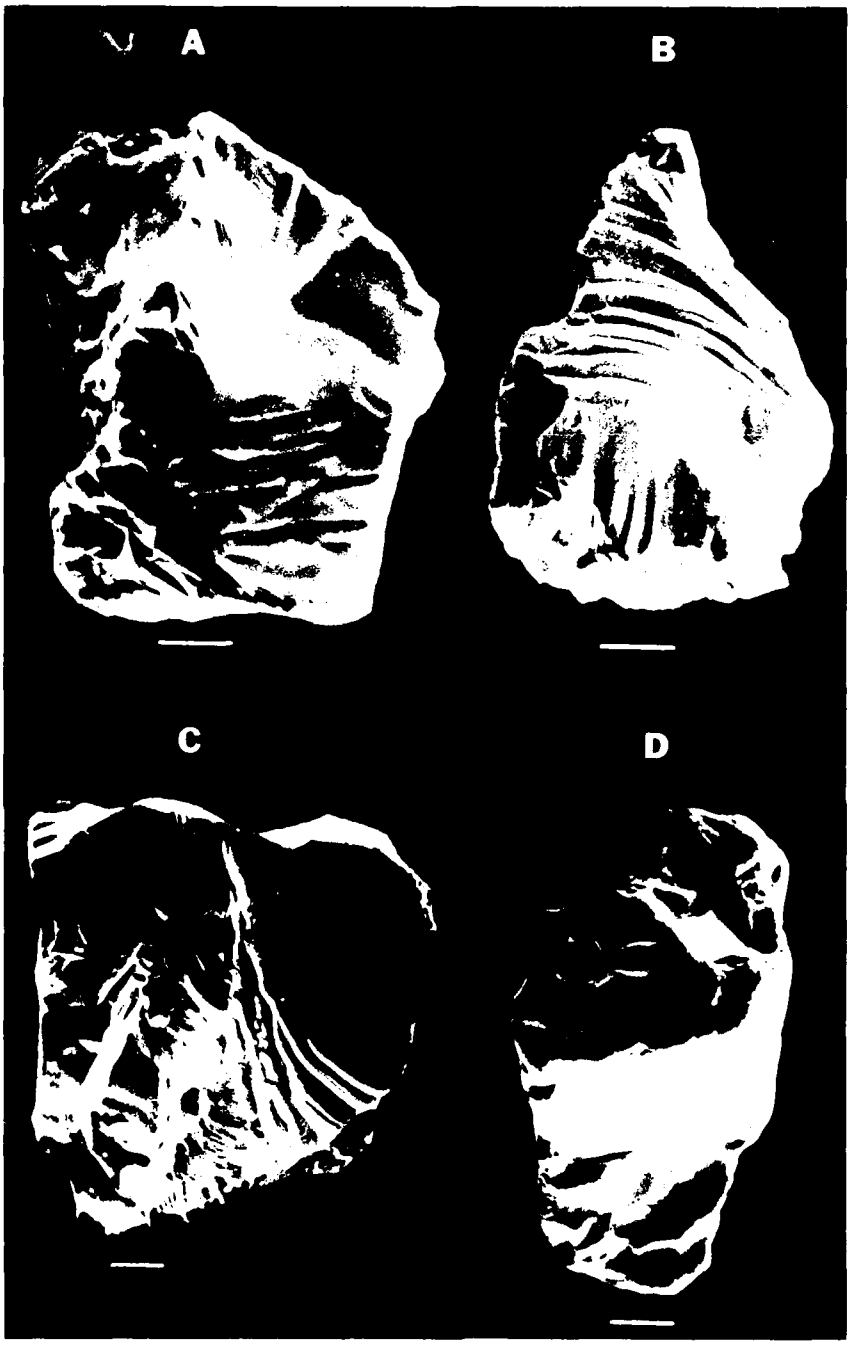

Figure 43. (A) FI-435. Glaciated quartz grain exhibiting high relief, sharp angular outline, conchoidal fractures, semiparallel steplike features, featureless fracture planes, and breakage blocks indicative of primary glacial origin (bar equals 20 μm, UW 1681-1). (B) FI-435. Glaciated quartz grain illustrating high relief, sharp angular outline, large conchoidal fractures, semiparallel steplike features, and breakage blocks characteristic of primary glacial origin (bar equals 40 μm; UW 1681-2). (C) FI-228. Glaciated grain displaying high relief, sharp angular outline, random striations, large conchoidal features, semiparallel steplike fractures, and breakage blocks suggestive of primary glacial origin (bar equals 40 μm UW 1681-3). (D) FI-331. A moderately reworked glacial grain. Note impact pits probably due to transport. This grain exhibits a high relief, sharp angular outline, semiparallel steplike features, and breakage blocks indicative of glacial origin (bar equals 40 μm, UW 1681-4).

lutites (Table 5). A comparison of arenaceous lutite units with the Canada Abyssal Plain turbidite in Figure 6 (Campbell and Clark, 1977) clearly illustrates the differences between an Arctic Ocean turbidite and arenaceous lutites in this study. In addition, X-radiographs failed to reveal primary sedimentary structures in any of the units.

The size sorting and abundance of primary sedimentary structures in contourites (Bouma and Hollister, 1973) and density current deposits (Harms, 1974) eliminate these deposits as possible models for arenaceous lutites in the Arctic.

Table 5 shows that features of arenaceous lutites resemble the expected features of an ice-rafted sediment.

Ice-rafted deposits are generally believed to have been transported by icebergs. Although criteria, notably a striated and polished glacial pavement, have been established for recognition of tillites (Dott, 1961), no characteristic criteria for the identification of ice-rafted sediments were vigorously defined (Holmes and Creager, 1974). Dott (1961) believed that abundant, widespread erratics were best explained by ice-rafting.

Expected features of ice-rafted sediments include poor sorting with abundant matrix and pebbles, variable thicknesses, and a lack of most primary sedimentary structures. In addition, the presence of abundant quartz, chert, and lithic fragments of continental lithologies in the sand-sized fraction of ungraded beds several thousand kilometres from land suggests ice-rafting transport (Goodell and others, 1968). The clockwise drift of ice over the western Arctic Ocean ensures a widespread distribution of detritus.

Conclusions

All of the features expected of ice-rafted sediment are characteristic of arenaceous lutites and, to a great extent, silty lutites of the central Arctic. As indicated, pebble-sized erratics are most abundant in the arenaceous lutites. Evidence that these pebbles were ice-rafted was summarized by Mullen and others (1972). Pebbles reported in other Arctic Ocean cores were also reported as being ice-rafted (Schwarzacher and Hunkins, 1961). Ice-rafting of sediment similar to the arenaceous lutites occurs today in the Arctic Ocean (Stoiber and others, 1960; Hunkins and others, 1969; Schwarzacher and Hunkins, 1961; Holmes and Creager, 1974). The sand-sized fraction of the arenaceous lutites also resembles the sand-sized fraction of sediment interpreted as ice-rafted from other oceans (Kent and others, 1971).

Ice-rafting may also explain the distribution of unit F if the existence of a pack ice cover similar to the present one is assumed. It is possible that the thinning of unit F northward toward the Alpha Cordillera (Fig. 15) is not a function of decreasing water depth but rather a result of thicker and more rigid pack ice nearer the pole. Aagaard and Coachman (1975) reported that summer melting and open water are now restricted primarily to the margins of the Arctic Ocean. Thicker and tighter ice would mean less ice movement with correspondingly less subice deposition compared to areas of thinner, more open ice (Hunkins and others, 1971).

The wealth of evidence for ice-rafting and the lack of convincing evidence for any other depositional mechanism suggest that ice-rafting was the dominant mechanism for deposition of the arenaceous lutites of this study.

The relative contributions of other sediment types to the arenaceous lutites are small. Ferromanganese particles are rare in the arenaceous lutites. Both planktonic and benthic Foraminifera tests are rare. Unfortunately, there is no way to measure the relative contribution to the sediment in the Pliocene and Pleistocene of normal pelagic sedimentation, including atmospheric dust, even though recent atmospheric contributions have been estimated (Mullen and others, 1972; Darby and others, 1974).

One possible objection to the ice-rafting hypothesis is that an ice-rafted sediment might be expected to have a patchy, discontinuous distribution. In contrast, the distribution of the arenaceous lutites in this study is regular. The argument that ice-rafting could explain this pattern is as follows. It would have taken ~46,000 yr for the deposition of unit F (average thickness of 13.76 cm) at an assumed sedimentation rate of 3.0 cm / 1,000 yr. Even if the sedimentation rate was 10.0 mm / 1,000 yr, it would have taken ~14,000 yr to deposit the arenaceous lutites of unit F. It seems probable that the clockwise circulation of rigid pack ice would ensure a widespread and relatively even distribution of glacial ice-rafted sediment averaged over several tens of thousands of years. A rigid ice pack may have even accentuated such a distribution. Bottom photos reveal that much of the Arctic Ocean floor is covered today with glacial ice-rafted gravels (Hunkins and others, 1969; Schwarzacher and Hunkins, 1961).

We conclude that the arenaceous lutite is ice-rafted and that the silty lutite is best explained as a combination of ice-rafted material, pelagic sediment, atmospheric dust, benthic tests, and authigenic ferromanganese particles. For example, in the upper portions of unit G, planktonic Foraminifera tests are a major component of the sediment and suggest a major pelagic contribution to the sediment. Also, authigenic ferromanganese particles are more abundant in the silty lutite.

Summary

While the conclusion that the bulk of the late Cenozoic sediment of the central Arctic is of ice-rafted, glacial-marine origin appears convincing, the age of the initiation of ice-rafting is less firm. Poore and Berggren (1974) concluded that "a major portion of the Labrador Sea experienced significant ice cover during the early Late Pliocene." Berggren (1977) elsewhere concluded that an early Pliocene elevation of the Isthmus of Panama and subsequent mid-Pliocene initiation of polar glaciation and formation of the Labrador current preclude earlier Arctic glaciation. We conclude that there is evidence in the cores that initiation of the central Arctic glacial ice-rafting preceded that of the Labrador Sea by at least a few million years. Our age for initiation is actually a minimum because ice-rafted debris was accumulating in Svalbard as early as the Eocene (Dalland, 1976).

GLACIAL-MARINE SEDIMENTATION PROCESSES

Introduction

Comparison of the grain-size histograms and statistical parameters of East Pacific Ocean pelagic clays and Arctic Ocean clay-rich, glacial-marine sediments (type III) indicates that similarities exist. In fact, it appears that the major textural differences result from the presence of greater relative proportions of silt in the Arctic Ocean sediments. The most striking similarity between the two clay-rich sediments is the occurrence of a pronounced fine mode in the medium- to coarse-clay range. This

TABLE 5. PRINCIPAL CHARACTERISTICS OF SEVEN DEEP-SEA DEPOSITS AND THE ARENACEOUS LUTITES IN THIS STUDY

Characteristic	Turbidites	Fluidized sediment flows	Grain flows
Size sorting	Moderate to poor	Well? to poor	Well? to poor
Bed thickness	Usually 10 to 100 cm	"Thick", 1.5 m+	"Thick", 1.5 m+
Contacts	Top poor, bottom sharp	Sharp	Sharp
Grading	Normal common	Normal rare	Reverse in coarse
Cross laminations	Common	Contorted?	Absent
Horizontal laminations	Common	Common, diffuse	Common, diffuse
Massive bedding	Common	Common, dish structure	Common, dish structure
Grain fabric	None in massive	Absent?	Imbricate up-flow
Matrix (<2μ)	10% to 20%	Absent-minor	Absent-minor
Microfossils	Common, intact	Absent?	Absent?
Plant and skeletal remains	Common, well preserved	Absent?	Absent?
Pebbles	Intraclasts	Intraclasts	Intraclasts
Scour or load structures	Common, ubiquitous	Common	Common
Lateral extent	1 X 10^5 km^2	100's km^2?	Local

Characteristic	Debris flows	Contourites	Density current deposits (Harms, 1974)
Size sorting	Very poor	Well to very well	Well to very well
Bed thickness	"Thick" 1 m+	<5 cm	2 cm to m
Contacts	Sharp	Sharp	Sharp
Grading	Poor reverse	Both	Very uncommon
Cross laminations	Absent	Common with heavy minerals	Common in sands
Horizontal laminations	Not likely?	Common	Common in siltstone
Massive bedding	Common, dish structure	Absent	Common in sands
Grain fabric	Clasts parallel bed?	Parallel to bed	Parallel bed in sands
Matrix (<2μ)	Variable	0% to 5%	Minor
Microfossils	Possible?	Rare, broken	Absent in silt
Plant and skeletal remains	Possible?	Rare, worn, or broken	Common in sands, rare in silts
Pebbles	Common	Absent	Common in sand
Scour or load structures	Possible?	Common?	Common in sand
Lateral extent	Local?	Local?	100's km^2?

Characteristic	Ice rafted	Arenaceous lutites in this study
Size sorting	Poor to very poor	Very poor
Bed thickness	"Thin?" to "Thick?"	2.5 cm to 36.5 cm
Contacts	?	Variable
Grading	Possible?	Absent or very vague
Cross laminations	Doubtful?	Absent
Horizontal laminations	Possible? Varves?	Thin layers and subunits
Massive bedding	Expected	Most common
Grain fabric	Absent?	Absent
Matrix (<2μ)	Abundant	20% to 40%+
Microfossils	Variable	Very rare
Plant and skeletal remains	Both are possible	One wood fragment, no skeletal
Pebbles	Common	Common
Scour or load structures	Absent	Absent
Lateral extent	Extensive?	1 X 10^5 km^2+

size range is characteristic of the fine mode that is present in the histograms of the pelagic clays, the clay-rich glacial-marine sediments (type III), and the bimodal glacial-marine sediments (type II). A secondary mode in this size range also occurs on the fine tail of some slightly bimodal, nonsorted type I glacial-marine sediments.

The presence of the fine mode in the same grain-size interval in all of the pelagic sediments and in the majority of the glacial-marine sediments that were studied suggests that the deposition of clay-sized particles from suspension is similar for all of the deep-sea sediments that were examined. This conclusion, although significant to the understanding of glacial-marine sedimentation, is not too surprising because clay particles, owing to their minute size, are the most likely to be affected by marine processes in the water column and are less susceptible to postdepositional processes (Inman, 1949).

Ice-rafting in the Arctic Ocean releases pebbles, sand, and coarse silt that settle quickly to the sea floor. Finer grains (clays) are more likely to be distributed across the ocean by marine transport processes and mixed with normal pelagic sediments entering the basin. This accounts for the uniform deposition of the fine mode that is found in all but a few of the deep-sea sediments that were examined.

Because the clay distribution is consistent for all Arctic and East Pacific Ocean deposits analyzed, the differences in the silt-clay grain-size distribution of Arctic Ocean glacial-marine surface-sediment types must be interpreted as the result of variations in the medium- to coarse-silt-sized fraction. Other students have pointed out the fact that silt-sized particles are susceptible to transport by ocean currents in the water column and are the most easily eroded from bottom sediment by traction currents (Hjulstrom, 1939; Heezen and Hollister, 1964).

Processes That Modify Silt-Clay Distributions

Silt-distribution variations in surface sediments can be accounted for by changes in the relative proportions of silt and clay in the original ice-rafted sediment, by modifications of grain-size distributions during deposition, and by postdepositional reworking. The relative proportions of silt and clay transported by ice-rafting may differ for different regions of the ocean basin. If it is assumed that the sediment content of glacial ice is not variable, the grain-size distribution must be modified after the sediment is released from the ice. This modification could be accomplished by ocean currents high in the water column, or sediments may be reworked by sea-floor currents.

Reworking by Traction Currents. Entrainment of silt-sized particles by traction currents (bottom currents as opposed to currents occurring high in the water column) may be important. In the Antarctic, continental shelf glacial-marine silt distributions in shelf deposits are the result of entrainment of silt particles by low-intensity traction currents (Anderson and others, 1977b; Barrett, 1975; Chriss and Frakes, 1972). As bottom-current intensity increases, very fine silt to coarse-silt grains are the first size class to be mobilized. Erosion of sediments coarser than coarse silt requires stronger traction currents because of the larger size of these grains. Conversely, the greater cohesiveness and lower bed roughness of clay-sized particles mean that clay-rich deposits also require higher traction-current velocities for entrainment (Inman, 1949).

Few measurements of Arctic Ocean bottom circulation have been reported, but Hunkins and others (1969) measured traction current velocities of 4 to 6 cm/s on the Mendeleyev Ridge. Traction currents in the Canada Abyssal Plain with velocities of 1.5 to 2.6 cm/s also were reported (Galt, 1967). Because so few measurements have been made in such a large ocean basin, it is possible that this data does not give a realistic picture of the Arctic Ocean traction current regime.

According to Hjulstrom's graph (1939), which related flow velocity to erosion and transport of sediment grains, a traction current with a velocity of 45 to 60 cm/s would be required to cause entrainment of the medium- to coarse-silt fraction. This size range is represented by the reduced interval in the bimodal and clay-rich Arctic Ocean surface-sediment distributions (types II and III). Traction currents with velocities of 1.5 to 6 cm/s are not strong enough to entrain sediment of any diameter (Hjulstrom, 1939). They are capable, however, of preventing sedimentation of suspended silt and fine sand. This indicates that the Arctic Ocean bottom currents described by Hunkins and others (1969) and Galt (1967) are not capable of entrainment of silt-sized grains during reworking. These traction currents are capable of redistributing coarse material before deposition, however.

Several authors (Heezen and Hollister, 1964; Chriss and Frakes, 1972) suggested that the relationship between flow velocity and entrainment of marine sediment is shown by the graph constructed by Mavis and others (1935). According to this relationship, the flow velocities required for erosion of incohesive sediments decrease with progressively finer sediment. If this curve applies to Arctic Ocean glacial-marine sediment, traction-current velocities of only 4 to 5.5 cm/s would be sufficient to mobilize the medium- to coarse-silt modal classes missing from types II and III sediment (Heezen and Hollister, 1964). Currents of this intensity also would entrain fine grains, however. Therefore, interaction of traction currents with incohesive sediments probably could not result in a bimodal distribution as found in type II sediments.

Also, the assumption made by Heezen and Hollister (1964) that marine sediments are less cohesive, thus requiring lower flow velocities to cause erosion, probably is not true for glacial-marine sediment. Antarctic glacial-marine deposits have been classified as compacted to overcompacted (Anderson and others, 1977b; Fillon, 1972), which suggests that they might be more cohesive than normal pelagic sediments. No compaction data are available for Arctic Ocean glacial-marine sediment, and the Antarctic sediment has been reworked by ground ice; therefore, a direct comparison probably is not possible.

Anderson and others (1977b) and Barrett (1975) stated that the action of bottom currents results in stratification of continental shelf glacial-marine deposits. Stratification is not common in the Arctic sediment cores. Widespread erosion of marine sediment probably should result in the common occurrence of major unconformities in sediment cores (Fillon, 1972). This is not the case for the Arctic Ocean cores, for which only a few definite unconformities have been recognized (Fig. 28). Although this evidence is not conclusive, it suggests that reworking is minor for the central Arctic sediment.

Reworking Due to Bioturbation or Geochemical Alteration. For Arctic surface sediments, bioturbation may be a factor in silt redistribution. Although burrowing is not extensive in the uppermost centimetres of the Arctic cores, bottom photographs indicate that foraging traces of marine organisms cover a significant portion of the Arctic Ocean floor (Kitchell and Clark,

1979). The effect of marine organisms on sediment silt-clay distributions is not well understood, although recent time-lapse photography of an Atlantic site suggests that modification of sediment is more rapid and temporary than previously thought (Paul and others, 1978).

Barrett (1975) demonstrated that even small amounts of hornblende in unconsolidated sediment is good evidence for no extensive geochemical reworking of that sediment. This unstable mineral is present in small amounts ir smear slides of the Arctic sediment.

Modification of Silt-Clay Patterns by Mid-depth Oceanic Currents. Another oceanographic factor that may be important to glacial-marine sedimentation is the effect of currents that occur high in the water column. As with bottom currents, little information is available on Arctic Ocean mid-depth circulation. Coachman and Aagaard (1974) detected current velocities varying between 0 and 5 cm s at depths of 200 to 900 m. Strong velocity pulses of less than two weeks duration, reaching intensities of 57 cm s, have been measured (Galt, 1967). These measurements suggest that currents high in the water column, capable of affecting sedimentation of silt- and sand-sized particles, are present in the central Arctic Basin (Hjulstrom, 1939; Heezen and Hollister, 1964) but are extremely variable. If we assume that the present input of ice-rafted sediment is constant and that bottom reworking does not alter the silt-clay distribution after deposition, then the variability in position of the coarse mode occurring in types II and IV histograms could be caused by fluctuations in the intensity of currents high in the water column that distribute silt-sized particles. This could explain why the coarse mode ranges in position throughout the very fine silt to coarse-silt ranges (6.35 to 63.0 μm).

Conclusions

Limited data are available, but it appears that mid-depth currents are the most likely factor in modifying grain-size distributions. For this reason, the deposition of Arctic Ocean glacial-marine sediment should be viewed as a complex process dependent on (1) the velocity and depth of currents in the water column, (2) the original grain-size distribution and time of release of ice-rafted sediment, (3) the rate of ice-rafting, and (4) the bathymetric configuration of the basin.

If we accept these variables, the four types of Arctic Ocean glacial-marine sediment in the surface samples are explained in terms of variations in the relative proportion of ice-rafted, medium- to coarse-silt that reaches the sea floor.

Type I Sediment. The deposition of normal pelagic and glacially derived clay and fine silt (fine mode) is considered constant over the entire basin. For deposition of type I sediment to take place, the rate of input of ice-rafted silt must be high enough to reduce the proportion of normal, well-sorted pelagic and glacially derived fine material comprising the fine mode so that a distribution exhibiting little evidence of sorting results.

Type II Sediment. Marine processes have greater impact on type II deposits. As the coarse-sediment particles fall through the water column, portions of the medium- to coarse-silt size classes are separated from the coarser silt and sand by currents that range in intensity. Some of the silt is distributed by these currents and may be deposited with other coarse sediments to form type IV deposits. The silt particles that are too large to be distributed are deposited on the sea floor along with pelagic and glacially derived clays; this results in a bimodal distribution. Thus, the fine mode consists of the pelagic and glacial clay and fine silt that are deposited uniformly over the central Arctic Basin. The coarse mode is composed of particles too large to be distributed by currents higher in the water column.

Type III Sediment. For clay-rich, type III sediments, the amount of ice-rafted debris is small in proportion to the amount of clay being deposited. The fine mode dominates the distribution, which suggests that the rate of ice-rafted silt influx was reduced during deposition of these sediments. Another possibility is that the rate of deposition of ice-rafted silt may have remained the same, but coarse material was diluted by an increase in the rate of deposition of fine-grained pelagic sediment. The addition of fine material, diluting the coarse-silt fraction, results in a histogram exhibiting a mode in the clay fraction. The additional fine sediment may be combined pelagic and glacially derived clay and fine silt or may be sediment transported by turbidity currents.

Type IV Sediment. Type IV sediment is the result of the deposition of a proportionally large amount of medium to coarse silt. In some places, this may result from the removal during sedimentation of fine particles or the addition during sedimentation of medium to coarse silt separated from type II sediment particles by currents in the water column. A more likely explanation for many type IV deposits of the Canada Abyssal Plain is that the well-sorted silt results from deposition at the distal end of turbidity currents. Campbell and Clark (1977) have discussed this type of deposit.

Summary

The bimodal distribution characteristic of type II glacial-marine sediment (and shown by many samples of type I sediment) suggests that the clay-sized to fine-silt-sized fraction and the medium- to coarse-silt-sized fraction of Arctic Ocean surface sediments are deposited on the sea floor by slightly different mechanisms. Normal pelagic and glacially derived fine material are distributed uniformly over much of the central Arctic Basin. This distribution results in the deposition of sediments that make up the fine mode that is observed in most Arctic sea-floor sediments and all East Pacific pelagic clays that were analyzed. Medium- to coarse-silt grains are distributed to a lesser extent owing to their large diameters.

Deposition of coarse-silt grains is a function of several factors. Type I sediment is the least affected by marine processes, whereas type II sediment appears to have been altered slightly by marine currents that removed the fine-silt-fraction, which resulted in a bimodal histogram. Type III sediment results from increases in the relative proportions of normal pelagic and glacially derived clay and fine silt, and type IV sediment is the result of an increase in the relative proportion of medium to coarse silt. The source of the additional silt may be glacial ice-rafting or turbidity currents.

The effects of the reworking of Arctic Ocean sediments by bottom currents are believed to be minimal because of consistently low current velocities reported for the central Arctic Basin and the compacted nature of glacial-marine sediments. This conclusion is supported by the variation in the size classes included in the coarse mode observed in the silt-clay distributions of types II and IV sediments. The lack of unconformities and of stratification in the Arctic cores also suggests that traction currents do not play a major role in Arctic deep-sea sedimentation.

COMPARISON OF ARCTIC SEDIMENT WITH OTHER GLACIAL AND NONGLACIAL SEDIMENT

Introduction

The Arctic Ocean textural categories (I to IV) were compared to non-Arctic glacial-marine sediment, terrestrial glacial tills, and deep ocean pelagic clay to determine similarities and differences. Our purpose was to determine if the Arctic textural categories were unique or the same as those developed in the non-Arctic environment.

Non-Arctic Glacial-Marine Sediment

To provide comparative textural data from non-Arctic, high-latitude seas, 106 samples of sediment described in the *Initial Reports of the Deep Sea Drilling Project* and the core descriptions of the USNS *Eltanin* as having glacial-marine or ice-rafted origins were obtained (Laughton and others, 1972; Talwani and others, 1976; Kulm and others, 1973; Frakes, 1971; Goodell, 1965; Goodell, 1968). Twenty-one samples of glacial-marine sediments also were obtained from Kara Sea cores described by Andrew (1973). Inclusion of these data makes it possible to develop a more generalized definition of glacial-marine sediments and compare depositional processes in Arctic and non-Arctic marine environments.

Sediment samples analyzed in this phase of the research were selected on the basis of information contained in core descriptions supplied in the references listed above. The criteria used to select samples of glacial-marine sediment were poor sorting, lack of primary sedimentary structures, presence of clasts or "pellets" (Ovenshine, 1970), abundant coarse silt and sand, and the occurrence of erratic pebbles described in the core logs as being of glacial ice-rafted origin. The geographic location of the coring site was also considered. Sites selected are near past or present sources of glacial ice. Samples were analyzed from nine cores. Cores were taken from the North Atlantic Ocean, Gulf of Alaska, Greenland Sea, Weddell Sea, Southern Indian Ocean, Ross Sea, Bellingshausen Sea, and Kara Sea. The latitude, longitude, depth, and length of each core sampled during this part of the project are listed in Appendix IF.

The silt-clay grain-size histograms developed from these samples showed three histogram types similar to Arctic Ocean sediment histogram types I, III, and IV. Another histogram type not found in any of the Arctic Ocean sediments also occurs (Fig. 44). The mean statistical parameters and relative proportions of grain-size fractions for the non-Arctic sediment types are summarized in Table 6. In this table, all samples were grouped together to provide statistically significant numbers of each sediment type. This grouping of data makes interpretations of depositional environments represented by individual cores difficult. However, the main purpose of this part of the project was to obtain textural analyses of non-Arctic sediments for comparative purposes rather than to interpret individual cores.

Comparison of the mean statistical parameters (mean grain size, sorting coefficient, and mean percent coarse particles) at the 0.95 confidence level indicated that significant differences were found between Arctic Ocean sediment types III and IV and similar histograms constructed for non-Arctic sediments. For Arctic and non-Arctic type I sediments, the sorting coefficients and coarse

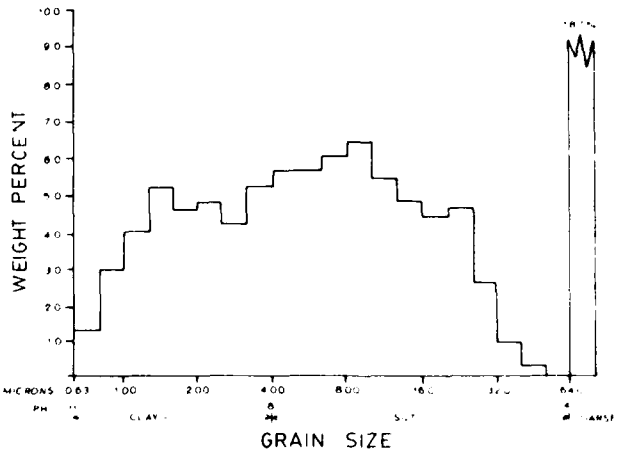

Figure 44. Typical silt-clay grain-size histogram (sample E27-12, 190 to 193 cm) representing a possible fifth sediment type found in some non-Arctic cores. Statistical tests revealed that histograms of this type were not significantly different from non-Arctic type III histograms.

percentages were significantly different ($t = 2.21$ and 7.32 compared to a critical value of 1.98); however, mean grain sizes were not significantly different ($t = 1.69$). Overall, these statistics suggest that the Arctic and non-Arctic type I sediments are significantly different but related.

A fifth histogram type, somewhat similar to Arctic type III, was found in several non-Arctic cores (E27-12, E12-6, NK110, and NK115). Histograms of this type, illustrated in Figure 44, exhibit a unimodal distribution. The mode is in the 3.14- to 10.08-μm (coarse-clay to fine-silt) range. Mean values of mean grain size, sorting coefficient, skewness coefficient, and percent coarse particles for the possible fifth histogram type were found to be intermediate between those parameters describing non-Arctic sediment types III and IV. Statistical tests comparing the mean parameters of non-Arctic type IV and the possible fifth sediment type suggest that these two types are significantly different. This was expected since the possible fifth type appeared to be most closely related to type III histograms. The t test values calculated for comparisons of sediment type III and the possible fifth sediment type based on mean grain size, sorting coefficient, and skewness were 1.98, 1.07, and 1.26, respectively. These values

TABLE 6. NON-ARCTIC GLACIAL-MARINE SEDIMENT TYPES: MEAN STATISTICAL PARAMETERS AND RELATIVE PROPORTIONS OF GRAIN-SIZE FRACTIONS

Sediment type	Mean grain size	Sorting	Skewness	Coarse	Silt	Clay	N
			Mean Values				
I	[illegible]	[illegible]	[illegible]	[illegible]	[illegible]	[illegible]	[illegible]
III	[illegible]	[illegible]	[illegible]	[illegible]	[illegible]	[illegible]	[illegible]
IV	[illegible]	[illegible]	[illegible]	[illegible]	[illegible]	[illegible]	[illegible]
			Standard Deviation				
I	[illegible]	[illegible]	[illegible]	[illegible]	[illegible]	[illegible]	
III	[illegible]	[illegible]	[illegible]	[illegible]	[illegible]	[illegible]	
IV	[illegible]	[illegible]	[illegible]	[illegible]	[illegible]	[illegible]	

are less than the critical value of 2.03, which suggests that the two sediment types are not significantly different.

Bimodal histograms similar to Arctic Ocean type II silt-clay distributions were not observed in any of the non-Arctic sediment cores.

As a group, silt-clay distributions for non-Arctic sediment tend to have lower mean grain sizes than their Arctic counterparts. In addition, non-Arctic sediments generally are better sorted than Arctic sediment types.

Glacial Tills

The comparison of Arctic glacial-marine with nonmarine glacial tills was accomplished by using samples from the upper Pleistocene (Valders) tills collected in eastern Wisconsin. The ease of sample collection motivated this choice.

Most of the Valders tills collected exhibit poorly sorted grain-size distributions (Fig. 45; App. 1C). In many of these poorly sorted histograms, a definite mode occurs in the fine- to medium-silt range (Fig. 46). This type of histogram has some similarities to the grain-size distributions of both type I and type IV Arctic Ocean sediment. Examination of the mean statistical parameters and coarse, silt, and clay mean percentages (Table 7) indicates that the tills are somewhat similar to the nonsorted type I sediment. The significant differences between the Valders till and Arctic type I sediment probably are the result of higher contents of silt and coarse sediment for the tills.

East Pacific Ocean Pelagic Clays

The importance of the clay- to silt-sized material in the Arctic was a factor in the selection of nonglacial, marine sediment for comparison. The East Pacific pelagic clays were used because of similar textures.

Samples of pelagic clay collected from the East Pacific Ocean exhibit grain-size distributions (Fig. 47) and mean statistical parameters (Table 7) similar to those found for Arctic Ocean surface sediment type III (Table 7; App. 1D). The East Pacific pelagic clays are characterized by a unimodal distribution having a strong mode in the medium- to coarse-clay fraction and a coarse

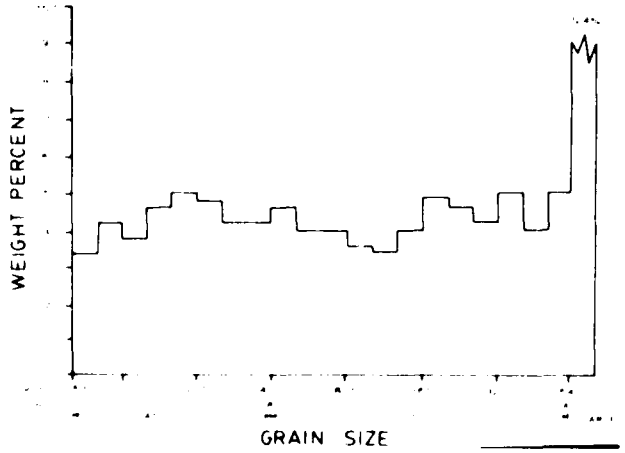

Figure 45. Rectangular silt-clay histogram for a sample of nonsorted glacial till of late Pleistocene age (Valders till sample 119). This histogram is similar to central Arctic Basin type I histograms.

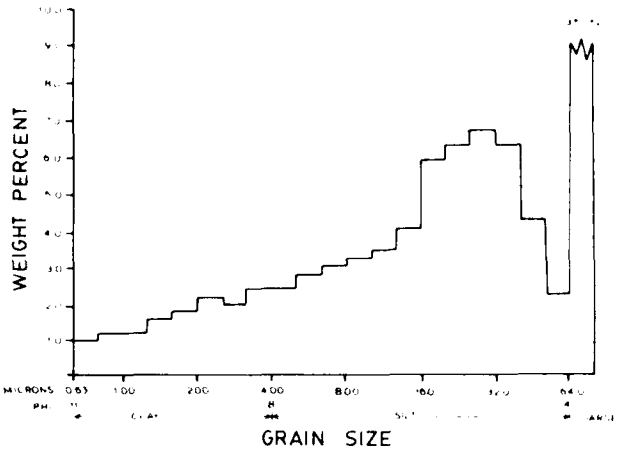

Figure 46. Unimodal silt-clay grain-size histogram representing a sample of silt-rich glacial till of late Pleistocene age (Valders till sample 011). This histogram is similar to central Arctic Basin type IV histograms.

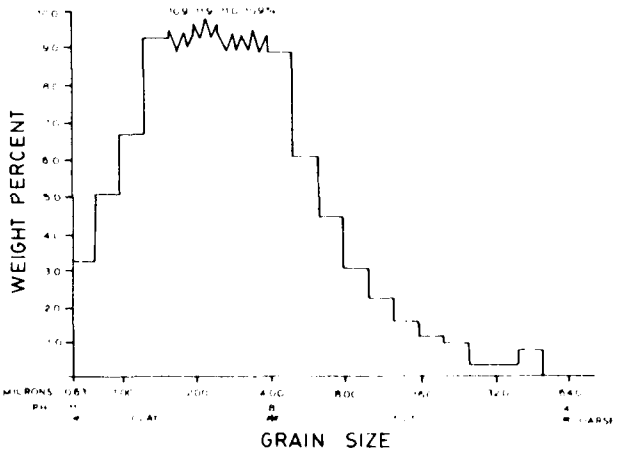

Figure 47. Typical unimodal silt-clay grain-size histogram representing an East Pacific Ocean pelagic clay (sample Mn74-02-12-2). Note the mode in the medium- to coarse-clay (1.26- to 2.52-μm) range. This mode is similar to the fine mode described for central Arctic Basin sediments of types II and III.

tail in the silt range. The mean grain sizes of the pelagic clay and type III sediments of the Canada Abyssal Plain are similar. The standard deviation of the mean grain size of the pelagic clays is lower; this probably indicates a slightly more uniform depositional process. In addition, the sorting-coefficient standard deviations of the two sediment types are different, with the pelagic clays being less variable. The occurrence of a pronounced mode in the clay fraction of both sediment types results in similar mean skewness values.

Discussion

By combining data for each sediment type from all nine non-Arctic cores, general interpretations of average Arctic and non-Arctic sediments can be discussed.

TABLE 7. MEAN STATISTICAL PARAMETERS AND RELATIVE PROPORTIONS OF GRAIN SIZE FRACTIONS FOR SAMPLES OF VALDERS GLACIAL TILL AND EAST PACIFIC OCEAN CLAYS

Mean Values

Sediment type	Mean grain size	Sorting	Skewness	% Coarse	% Silt	% Clay	No.
Valders till	14.9	12.5	0.5	32.7	51.7	15.5	17
East Pacific Ocean pelagic clay	4.5	6.2	0.9	0.1	30.4	69.6	12
East Pacific Ocean hemipelagic clay	6.5	7.6	1.1	0.2	46.9	52.9	3

Standard Deviations

Valders till	2.5	1.9	0.3	13.3	9.9	4.8	
East Pacific Ocean pelagic clay	0.4	1.1	0.1	0.1	1.5	1.6	
East Pacific Ocean hemipelagic clay	0.3	0.6	0.0	0.0	2.1	2.3	

The fine mode that characterized the Arctic Ocean glacial-marine sediments and East Pacific Ocean pelagic clays was not observed in other non-Arctic histograms. This fine mode is assumed to have resulted from deposition of well-sorted clay and fine silt. In Arctic Ocean sediments, the fine mode is composed of normal pelagic and glacially derived fine particles that are distributed uniformly over the enclosed basin. In East Pacific Ocean pelagic clays, the fine mode consists only of pelagic fine sediments.

A marked depth difference exists between Arctic and non-Arctic depositional environments represented in the cores that were sampled. With the exception of the Southern Indian Ocean, Weddell Sea, and North Atlantic sites (E37-7, E12-6, and DSDP-111), the non-Arctic cores were collected from depths less than 1,500 m. The shallowest depth from which an Arctic Ocean core was taken was ~1,860 m. The non-Arctic cores were also collected from locations near large sources of glacial ice and may have been directly beneath floating or ground ice during glacial advances.

Comparison of type III histograms representing samples from the three deep-water, non-Arctic cores with histograms from East Pacific Ocean sediment samples (Fig. 48) of possible hemipelagic origin (Margolis and others, 1975) revealed that these sediments have similar silt-clay distributions. Hemipelagic sediments consist of varying proportions of pelagic and terrestrial components. A complete discussion of hemipelagic environments is given by Shepard (1939). The similarity of East Pacific Ocean hemipelagic clays and type III sediments in the deep-water, non-Arctic cores suggests that deposition of clay-rich sediment in the Weddell Sea, Southern Indian Ocean, and North Atlantic Ocean may be controlled by hemipelagic processes other than glacial ice-rafting.

The poorly sorted, non-Arctic type I and type IV sediments found in the cores from the shallow-water, continental shelf regions of the Ross Sea, Bellinghausen Sea, Kara Sea, Greenland Sea, and Gulf of Alaska are assumed to be of ice-rafted origin. Anderson and others have described continental shelf glacial-marine sedimentation in Antarctica (Anderson, 1972; Anderson and others, 1977a, 1977b; Kellogg and others, 1979). These authors recognized three types of continental shelf glacial-marine sediment: orthotills, compound paratills, and residual paratills. It is important to emphasize that this classification system probably applies only to continental shelf glacial-marine sedimentation. Deposition of Arctic Ocean, deep-sea glacial-marine sediment is assumed to occur in a different manner because of the increased importance of marine processes in distribution of fine-grained glacial and pelagic sediment.

Anderson and others (1977b) described compound paratills as sediments enriched in silt and clay transported by marine currents. For the non-Arctic continental shelf glacial-marine sediments, compound paratills may be represented by type III histograms. Non-Arctic type IV histograms may represent residual paratills, which Anderson and others (1977b) have described as winnowed muddy sands produced by the removal of silt-sized particles by bottom currents. Orthotills are nonsorted, nonstratified marine sediments derived directly from melting grounded glacial ice (Anderson, 1977b). This original, unaltered material may be represented by non-Arctic type I histograms.

An assumption essential to this classification scheme and to much of the literature on Antarctic continental shelf glacial-marine sediment is that the original grain-size distribution of ice-rafted sediment is known to be consistently nonsorted and represented by the rectangular type I histogram. If glacial ice-rafted sediment has properties similar to continental tills, as has been suggested by Barrett (1975), the assumption that the original grain-size distributions of glacial sediments are uniform appears to be incorrect. Textural analyses of till (Gross and Moran, 1971; Drake, 1971) indicate that areal and vertical variations in till grain-size distributions do occur. In addition, the relative proportions of sand, silt, and clay in tills show great variability (Flint, 1947). In part, the grain-size distributions of tills are determined by the nature of the landscape that the glacial ice overrides (Gross and Moran, 1971). For example, glacial abrasion of igneous terrane results in tills with high proportions of gravel- and sand-sized particles. Clays dominate till deposited by glaciers that erode shale and limestone (Flint, 1947). Till samples from eastern Wisconsin (Valders till) exhibited variable silt-clay distributions, as illustrated in Figures 45 and 46. The fact that Arctic and non-Arctic type I grain-size histograms are similar suggests that rectangular, nonsorted silt-clay histograms do not necessarily represent the grain-size distributions of unaltered glacial ice-rafted sediment.

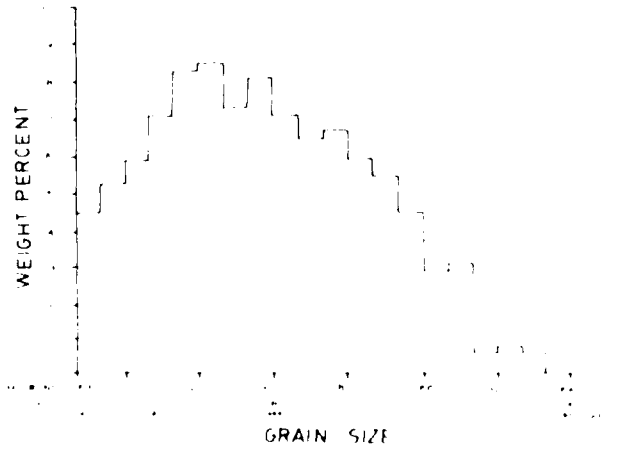

Figure 48. Typical silt-clay grain size histogram representing an east Pacific Ocean hemipelagic sediment (sample Mn74-02-13A-1). This histogram is similar to those constructed for non-Arctic type III glacial-marine sediment.

SEDIMENT MAPS

Introduction

Clay minerals in the marine environment are the result of transportation from a terrestrial source to the ocean as well as diagenesis at sea and in the sediment.

Clay minerals in marine sediment have received considerable attention recently because of the availability of samples provided by the *Glomar Challenger* and the Deep Sea Drilling Project. Millot (1970) summarized much of the early work on marine clays and concluded that differential sedimentation rates and diagenesis may be the most important factors in explaining alteration of terrestrial material in the marine environment. Gorbunova (1976) described the distribution of clay minerals in the Pacific both geographically and for the Miocene to Holocene interval. She reported inverse changes in Miocene to Holocene montmorillonite and chlorite abundances and mapped the Pacific distribution of clay minerals. Gorbunova showed that chlorite was concentrated along the North American, Aleutian, and Japanese coasts and was absent in the equatorial Pacific. In the North Pacific, kaolinite was shown to be of little significance. These data are in harmony with most reports for other oceans of the world (for instance, the summary of Millot, 1970).

Arctic Ocean

To compare the kinds and distribution of clay minerals in the Arctic Ocean with those of other oceans, the upper few centimetres of several hundred central Arctic cores were studied by X-ray diffraction. In addition, data for the shallower, shelf ocean of the Canadian Islands and Alaska were included (Berry and Johns, 1966; Naidu and others, 1971, 1972, 1974, 1975). These data have been compiled into a series of clay-mineral surface maps (Pls. 1 to 7) and a clastic percent map (Pl. 8) for the Amerasian Basin. This is the first compilation for the central Arctic Ocean.

Apparent from the maps of kaolinite, illite, and chlorite (Pls. 2 to 4) is that the abundance pattern is similar to that of most of the world's oceans. All three clay minerals are most abundant in the shallow-shelf, nearshore areas of the Alaskan coast. Chlorite (Pl. 4) has its greatest concentration on the shelves of Greenland and Alaska; this probably reflects proximity to igneous terrane from which it was weathered. Limited data are available for vermiculite and the mixed-layered clays (Pls. 5 to 7), but an interesting pattern

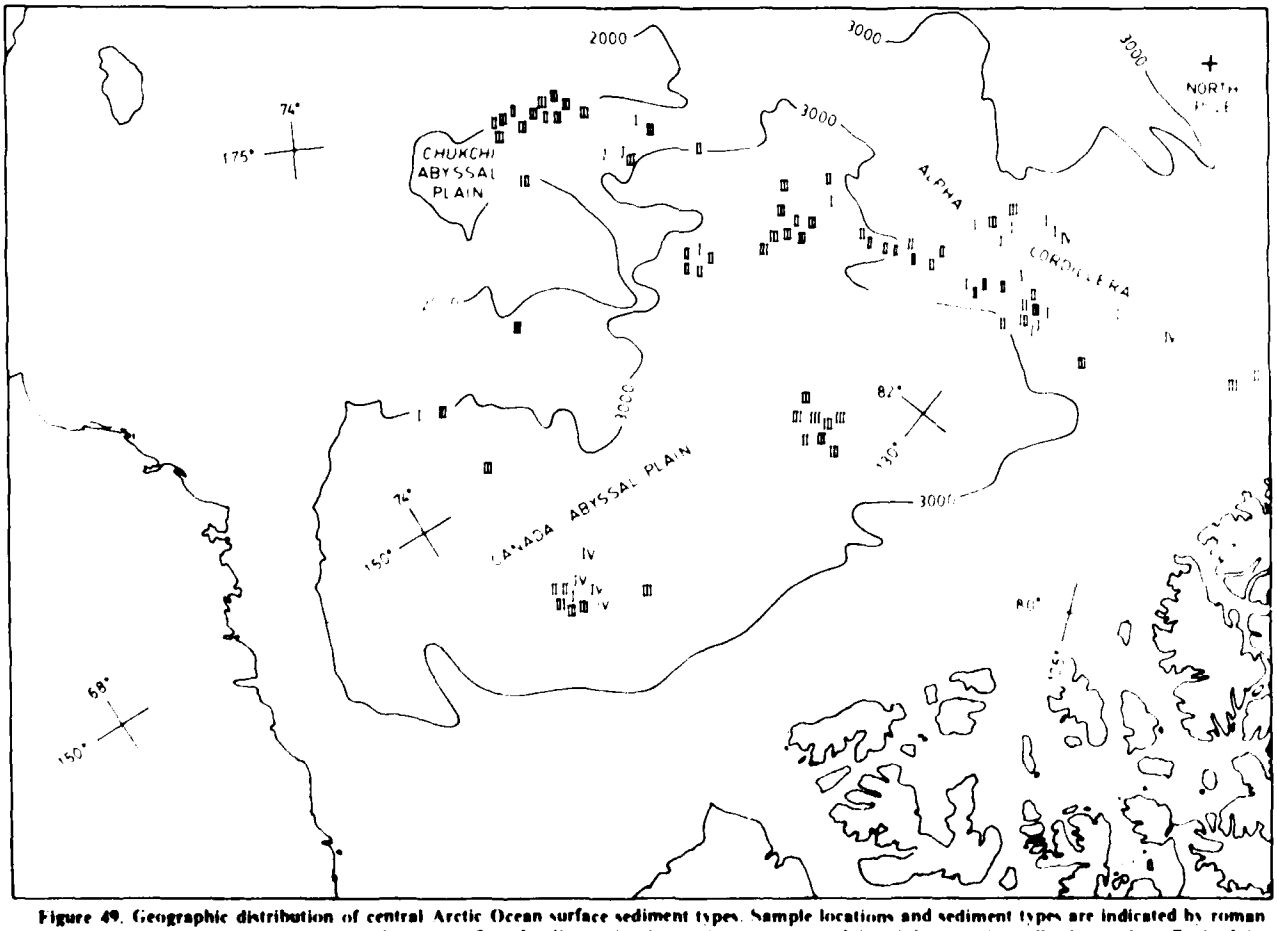

Figure 49. Geographic distribution of central Arctic Ocean surface sediment types. Sample locations and sediment types are indicated by roman numerals. Water-depth contour interval equals 1,000 m. Type I sediment dominates the crest region of the Alpha Cordillera. On the southern flank of the cordillera, sediment types II and III are more abundant.

along the topographically high Alpha Ridge is significant. Because most of the clay minerals were transported by glacial ice, a random pattern might be more easily explained. Diagenesis along the Alpha Ridge may have been the reason for the patterns.

The clastic percent map (Pl. 8) shows a definite belt of coarse material along the Alpha Ridge. This may be a residual effect of unaltered sedimentation, whereas the low clastic percent in the Canadian Basin probably reflects masking by the distal (and finer) ends of turbidites (Campbell and Clark, 1977). Alternately, the circulation pattern of the Arctic ice pack is such that large, sediment-laden icebergs such as T-3 have consistently passed along this route and deposited a higher percentage of coarse sediment.

Because of the glacial-marine nature of the sediment, the maps are unique, and there are no real comparisons. Data from the Eurasian Basin will be of greatest comparative interest.

GEOGRAPHIC DISTRIBUTION OF SURFACE-SEDIMENT TYPES IN THE ARCTIC OCEAN

The geographic distribution of glacial-marine surface-sediment types (I to IV) in the central Arctic Basin is shown in Figure 49. Sediments of types I and II predominate in the region of the Alpha Cordillera. The occurrence of these sediment types indicates that the input of normal pelagic sediment is relatively low and that ice-rafting is the major depositional process contributing sediment to this region.

At the crest of the Alpha Cordillera, near the eastern boundary of the central Arctic Basin, type I sediments occur most frequently. At two sites in this area, type IV sediments are found. Deposition of type IV sediment requires input of a large relative proportion of silt. In the case of these two samples, the silt mode appears to be superimposed on a poorly sorted silt-clay distribution similar to type I. This histogram shape suggests that the rate of influx of ice-rafted silt was high at those two sites; thus, the medium- to coarse-silt-sized fraction diluted the pelagic and glacially derived clay and fine silt that is deposited more or less uniformly over the entire ocean basin. Dilution of the fine fraction reduces the fine mode in the silt-clay histogram relative to the coarse-silt fraction. Therefore, the coarse mode, composed of particles unmodified by marine currents, dominates the histogram. The high rate of influx of ice-rafted sediment on the crest of the Alpha Cordillera, suggested by the occurrence of sediment types I and IV, is supported by the higher percentages of silt and coarse material shown for this area in Figures 50 and 51.

To the west and south of the Alpha Cordillera crest, the frequency of occurrence of type II sediment increases, while the percentages of silt and coarse material shown in Figures 50 and 51 decrease. These trends suggest that the relative proportion of glacial ice-rafted silt is not as great in this area as in the east. Large relative proportions of glacial ice-rafted silt mask the modification of silt-clay distributions caused by mid-depth oceanic currents. A decrease in the rate of input of ice-rafted silt allows modifications of silt-clay distributions to become more apparent. Thus, sediments with bimodal histograms are observed more frequently.

A possible explanation for the suggested higher rates of influx of ice-rafted silt and coarse sediment in the eastern portion of the Alpha Cordillera may be that the present source of the icebergs that transport glacial debris across the central Arctic Basin is the continental glaciers of Greenland and Ellesmere Island (Schwarzacher and Hunkins, 1961). Since the concentration of sediment-bearing icebergs is likely to be higher near the source of glacial ice, the rate of sedimentation of ice-rafted debris might also be expected to increase near the ice front.

The widespread distribution of turbidites in the sediments of the Canada Abyssal Plain (Campbell and Clark, 1977) may explain the occurrence of sediment types III and IV in this region. Turbidity currents are responsible for the deposition of fine-grained material at high sedimentation rates (Clark, 1970). Type III sediments of the Canada Abyssal Plain have significantly lower mean grain sizes, better sorting, lower skewness, lower silt and coarse contents, and higher clay content than those of the Alpha Cordillera. This evidence suggests that the influence of ice-rafted silt input of the Canada Abyssal Plain has been reduced by an influx of fine-grained sediment associated with turbidity current deposition (Bouma and Hollister, 1973). The rapid influx of such fine-grained sediment dilutes the ice-rafted coarse sediment and results in a type III silt-clay distribution. In addition to pelagic fine material, turbidity currents also deposit layers of well-sorted silt on the Canada Abyssal Plain (Campbell and Clark, 1977). These silt layers are probably represented by type IV histograms. The type IV silt-clay distributions of Canada Abyssal Plain sediments show better sorting than those of the Alpha Cordillera and thus reflect dilution of ice-rafted sediment and pelagic clays caused by high rates of input of turbidite silt.

The type III sediments that predominate in the Chukchi Abyssal Plain–Arliss Plateau area have mean statistical parameters and relative proportions of coarse-, silt-, and clay-sized particles intermediate between those of the Canada Abyssal Plain and the Alpha Cordillera. These characteristics may indicate dilution of ice-rafted coarse silt by influx of fine silt and clay carried by turbidity currents originating on the Chukchi Shelf. The effects of dilution by fine turbidite material on the Chukchi Abyssal Plain do not seem to be as great as for the Canada Abyssal Plain. Chukchi Abyssal Plain type III sediments are coarser and less well sorted than their Canada Abyssal Plain counterparts. Perhaps the input rate of ice-rafted coarse silt is greater or the rate of turbidite deposition is lower on the Chukchi Abyssal Plain. The presence of type II (bimodal) sediment in this bathymetric province suggests that deposition of ice-rafted medium to coarse silt modified by currents in the water column may be locally heavy in relation to the proportion of clay- and fine-silt sized turbidite.

The major influence of surface currents on glacial-marine sedimentation is through the dispersal of sediment-laden icebergs. Movement of the Arctic ice pack and accompanying glacial bergs is largely determined by surface circulation patterns. The widespread occurrence of sediment types I and II and high percentages of silt and coarse grains suggest that surface circulation patterns disperse ice-rafted sediment to all areas of the central Arctic Basin. The presence of type II sediment suggests that mid-depth currents modify the silt-clay distributions of sediment settling through the water column. This sediment type is assumed to be at sites where the rate of influx of glacial ice-rafted silt is low enough to allow the effects of weak or fluctuating mid-depth currents to be noticeable. Although these mid-depth oceanic currents undoubtedly affect sedimentation, as do surface currents, no systematic variation in the geographic distribution of sediment types can be directly explained in terms of ocean circulation as described by Coachman and Aagaard (1974) and Hunkins and others (1969).

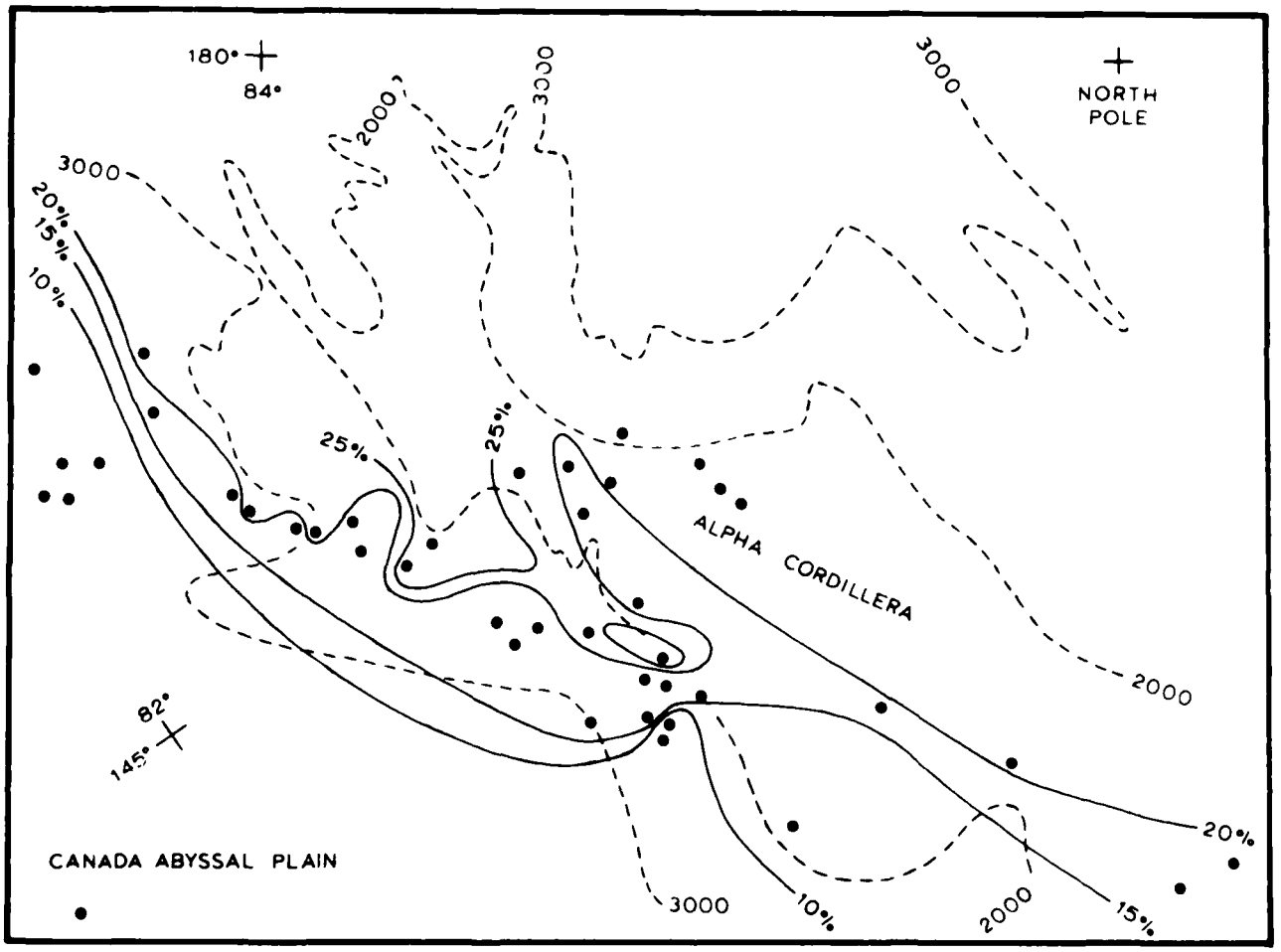

Figure 50. Geographic variation in the relative proportion of coarse sediment. Sample locations are indicated by closed circles. Water-depth contour interval equals 1,000 m. Contour interval for the coarse percentage equals 5%. The percentage of coarse-sized particles decreases to the west and south of the crest of the Alpha Cordillera.

LATE CENOZOIC LITHOSTRATIGRAPHIC UNITS AND GLACIAL-MARINE SEDIMENT TYPES

Introduction

To compare modern glacial-marine sediment with sediment of stratigraphic units A to M, grain size distributions were determined for 191 samples from eight 1-3 cores. The cores used in this phase of the project were selected to provide representative coverage of the 120,000-km^2 area over which the lithostratigraphic units are recognized.

Seven of the cores used in this phase of the research were taken from the crest and southern flank of the Alpha Cordillera in water depths ranging from 1,860 to 3,280 m. The eighth core was taken from the northern slope of the Chukchi Rise at a depth of 3,043 m. Cores from the Alpha Cordillera–Chukchi Rise region were selected because the lithostratigraphic framework applies best to the area.

Two basic lithologies from the cores included silty lutites in units A, B, D, F, G, I, K, and M and arenaceous lutites in units C, E, H, and J. Silty lutites are characterized by low percentages of coarse material, abundant authigenic ferromanganese particles, relatively high abundances of Foraminifera tests, and extensive burrowing. A low mean sedimentation rate of 0.5 mm/1,000 yr was calculated for these units. Sediments of textural types II and III occur most frequently in silty lutite units.

Arenaceous lutites typically have higher percentages of coarse material, have fewer Foraminifera tests and ferromanganese particles, and are less extensively burrowed. The average sedimentation rate of arenaceous lutite layers is about 3.0 mm/1,000 yr. Sediment types I and IV occur most frequently in these units.

All of the sediment types described from surface samples occur at depth in the Arctic cores as well. Mean values of the statistical parameters and relative proportions of grain-size fractions for the down-core sediment types are summarized in Table 8. Comparisons of the mean values for sorting coefficient, percent coarse particles, and mean grain size were made between down-core and surface sediment types at the 0.95 confidence level. This comparison shows that significant differences do not occur between down-core and surface sediments of types I, II, and III on the Alpha Cordil-

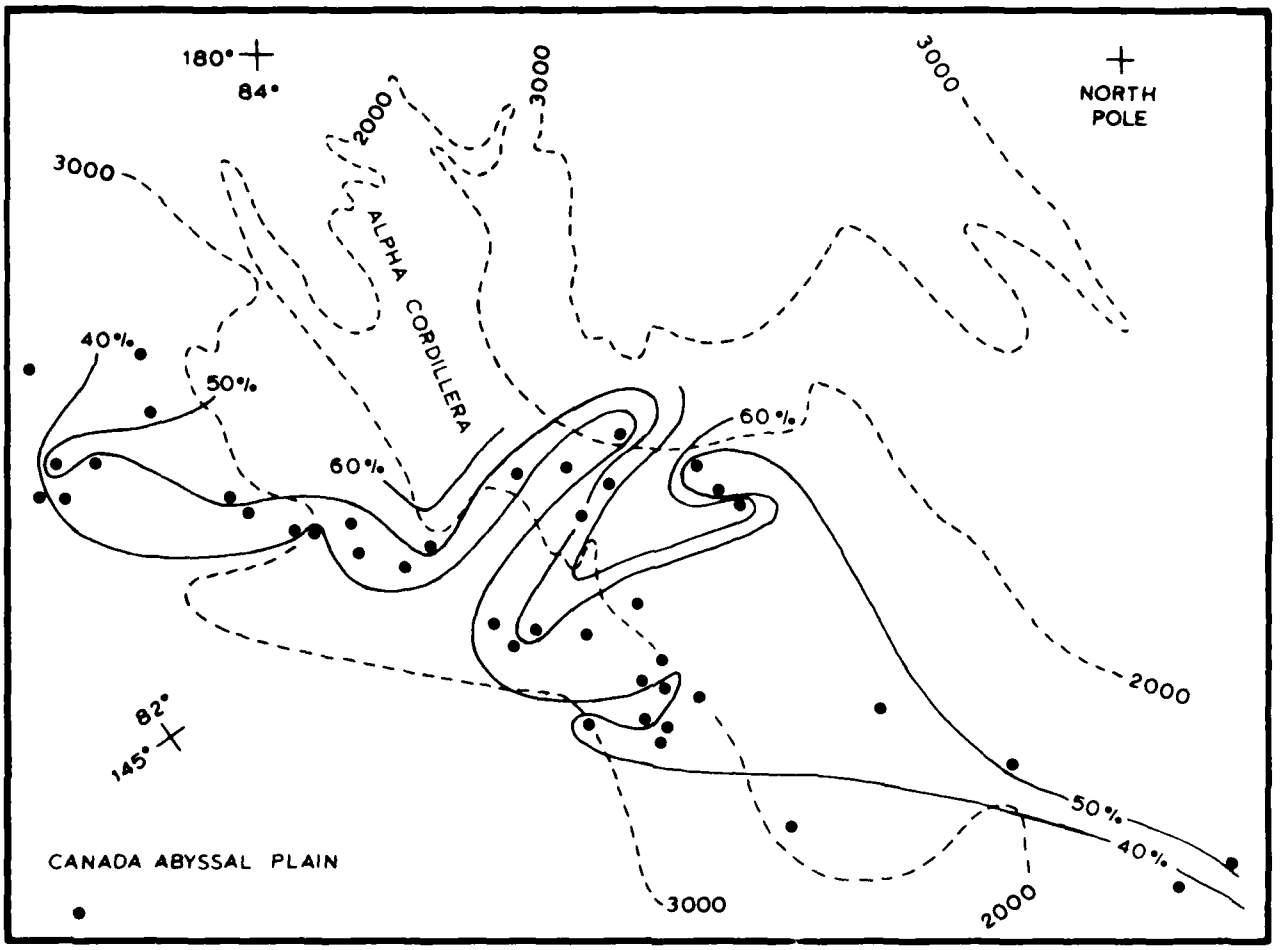

Figure 51. Geographic variation in the relative proportion of silt-sized particles. Sample locations are indicated by closed circles. Water-depth contour interval equals 1,000 m. Contour interval for the silt percentage equals 10%. The percentage of silt-sized particles decreases to the west and south of the Alpha Cordillera crest.

lera. Significant differences in the mean sorting coefficients and mean grain sizes of down-core and type IV surface sediment were suggested by the *t* test. These differences probably reflect sampling error due to the small number (2) of type IV surface samples on the Alpha Cordillera and are probably not indicative of actual differences in the textural characteristics of type IV sediments.

Stratigraphic Distribution of Sediment Types

The relative proportions of the four sediment types in each of the 13 stratigraphic units are shown in Table 9. Although none of the units are characterized by a single sediment type, general trends allow interpretations regarding the depositional environments represented by the units.

The most common sediment in the cores is type I. This is the most abundant in 9 of the 13 stratigraphic units.

For units A, C, E, F, H, and J, sediment types I and IV are dominant. With the exception of units A and F, these units are arenaceous lutites. The suggestion that arenaceous lutites represent periods of increased glacial ice-rafting is supported by the dominance of type I and type IV sediments that are believed to result from relatively higher influx rates of ice-rafted, medium to coarse silt.

Units A and F are somewhat anomalous since they are predominantly silty lutite units dominated by sediment types I and IV. The occurrence of sediments representing high influx rates for ice-rafted coarse silt in stratigraphic units assumed to represent periods of reduced glacial ice rafting seems contradictory. This may be the result of the thin arenaceous lutites in units A and F. In fact, unit F commonly is arenaceous in its upper part.

The silty lutite units, B, C, G, and I, are dominated by type I sediments in combination with either type II or type III sediment. The absence of silt in type III histograms implies a low rate of input of ice-rafted silt. The combination of sediment types I and III in units D and I suggests that input rates of ice-rafted sediment generally were lower during deposition of these units.

In units B and G, sediment types I and II are dominant. The presence of type I sediments in these units implies that ice-rafting of silt was the major depositional process. The presence of type II sediment suggests that mid-depth ocean currents with intensities

TABLE 8. ARCTIC OCEAN DOWN-CORE SEDIMENT TYPES; MEAN STATISTICAL PARAMETERS AND RELATIVE PROPORTIONS OF GRAIN SIZE FRACTIONS

Sediment type	Mean grain size	Sorting	Skewness	% Coarse	% Silt	% Clay	No.
Mean Values							
I	11.7	13.2	1.2	13.6	51.2	35.1	79
II	13.0	14.6	1.2	13.8	50.2	36.3	42
III	8.9	11.9	1.2	12.4	41.3	46.2	35
IV	16.1	14.7	0.7	16.6	59.0	24.2	35
Standard Deviations							
I	2.0	2.0	0.1	7.3	5.1	5.5	
II	2.4	2.1	0.2	6.7	5.5	5.8	
III	1.7	2.2	0.1	6.1	5.8	6.1	
IV	2.9	1.6	0.3	8.6	7.3	5.0	

TABLE 9. RELATIVE PROPORTION OF EACH ARCTIC OCEAN GLACIAL-MARINE SEDIMENT TYPE IN EACH STRATIGRAPHIC UNIT

Unit	% Type I	% Type II	% Type III	% Type IV
A	57.6	14.2	14.2	28.8
B	66.6	22.2	11.1	00.0
C	62.5	12.5	12.5	12.5
D	50.0	13.6	22.7	13.6
E	20.0	00.0	10.0	20.0
F	58.3	00.0	00.0	41.6
G	38.1	38.1	9.5	14.3
H	43.8	18.8	00.0	37.5
I	42.1	15.8	26.3	15.8
J	58.8	11.8	5.9	23.5
K	23.4	35.7	42.8	90.9
L	6.2	37.5	25.0	31.2
M	11.8	47.0	35.2	5.8

great enough to distribute medium to coarse silt played a role. Perhaps the Arctic Ocean ice pack was thin while units B and G were being deposited; this would allow high rates of ice-rafting and increased wind-driven current velocities. For unit G, this hypothesis is supported by the occurrence of abundant Foraminifera tests that may also indicate thin ice cover.

Units K, L, and M are unusual in that they have the lowest relative proportions of type I sediment. Units K and M are dominated by sediment types II and III. The presence of type III sediment suggests that influx rates for ice-rafted silt were low. Relatively high mid-depth current velocities are suggested by the occurrence of type II sediment. If the Arctic ice pack was thin during deposition of these units, which would allow wind-driven circulation to increase, an increase in the rate of ice-rafted sediment influx might also be expected. The presence of type III sediment and absence of sediment types I and IV suggest that this was not the case. An alternate explanation is that the high relative proportion of ice-rafted medium to coarse silt that occurs in many Arctic sediment units masks the effects of mid-depth currents diluting type II deposits. For units K and M, lower rates of ice-rafted silt influx occurred, as indicated by sediment type III; this reduced the masking effect and made modifications of silt-clay distributions more apparent.

Sediment types IV and II dominate unit L. These sediment types indicate a high rate of ice-rafted silt influx and modification of ice-rafted silt distributions. Unit L is similar to units B and G in that the occurrence of dominant sediment types may be explained by high rates of ice-rafting and high wind-driven ocean current intensity, made possible by a thin, less rigid Arctic ice pack. In this unit, high influx rates of ice-rafted coarse material are also indicated by abundant coarse grains and lithic fragments. Thin ice cover is also suggested by the many burrows filled with Foraminifera-rich silty lutite indicating high biologic productivity.

Discussion

The relationships between glacial, oceanic, and biologic processes and glacial-marine deposition are complex. On the Alpha Cordillera, silty lutites are dominated by textural types II and III. Type II sediments represent relatively low rates of ice-rafted silt influx, whereas the lowest rates of influx for ice-rafted medium to coarse silt result in deposition of type III sediment. In some silty lutites, however, glacial-marine sediment types I and IV occur and indicate moderate to high influx rates for ice-rafted silt. The presence of sediment types I and IV in some silty lutites, along with ice-rafted pebbles and sand and abundant Foraminifera tests, suggests that a relationship exists between Foraminifera productivity and rates of ice-rafting. Several authors (Hunkins and others, 1971; Herman and O'Neil, 1975) suggested that a thinner, less rigid Arctic Ocean ice pack might allow a more rapid dispersal of sediment-bearing icebergs across the ocean and result in higher rates of ice-rafted sediment deposition. Thinner ice might also allow deeper penetration of sunlight into the ocean water, resulting in greater Foraminifera productivity (Clark, 1971).

For the arenaceous lutites, which are believed to indicate periods of increased ice-rafting, sediment types I and IV dominate, and Foraminifera abundances are low. This may indicate that high rates of glacial ice rafting occur when ice cover is thick, which results in low Foraminifera productivity. Another possibility is that Foraminifera productivity was high (thin ice) but tests were dissolved after deposition by bottom waters undersaturated with respect to calcium carbonate (Hunkins and others, 1971; Herman and O'Neil, 1975). A third possibility is that high rates of glacial ice rafted sediment influx in the Arctic Ocean resulted in dilution of Foraminifera tests by large relative proportions of coarse sediment.

GEOGRAPHIC DISTRIBUTION OF SEDIMENT TYPES IN STRATIGRAPHIC UNITS A THROUGH M

Discussion

The geographic distributions of the dominant sediment types in the 13 stratigraphic units are illustrated in Figures 52 through 64. Dominant sediment types were established through selection of the type or pair of types having the highest relative abundances observed for each unit in each core.

The Alpha Cordillera crest area is dominated by type I sediment in units A, B, C, J, E, J, and L. Occasional occurrences of sediment types II, III, and IV were found, however. The dominance of type I sediment continues on the southern flank of the cordillera and on the northern flank of the Chukchi Rise. Widespread dominance of type I sediment suggests that moderate rates of glacial ice-rafted medium- to coarse-silt influx occurred over the entire study area during deposition of these units. Because five of these seven units

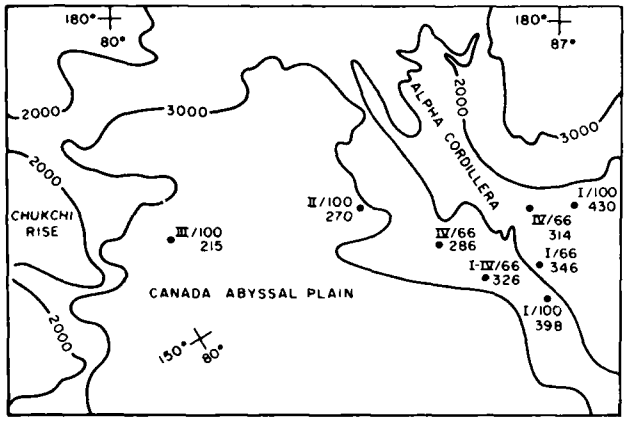

Figure 52. Geographic distribution of dominant glacial-marine sediment types in lithostratigraphic unit A. The locations of the eight cores used in the stratigraphic analysis are indicated by closed circles. Roman numerals at each location indicate the dominant sediment type or pair of types. The numbers accompanying the roman numerals indicate the relative abundance (percent) of the dominant sediment types. Unit A is primarily a silty lutite layer.

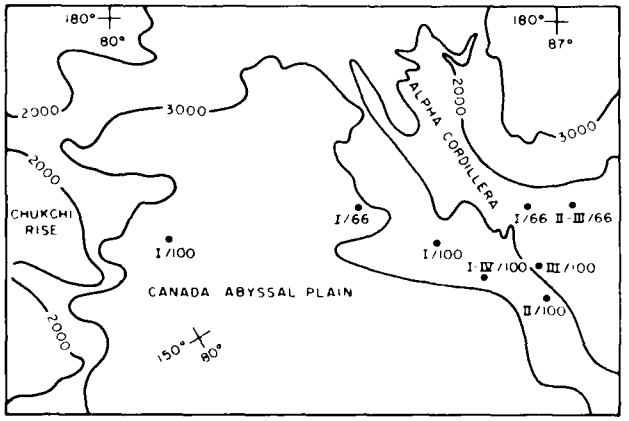

Figure 53. Geographic distribution of dominant sediment types in lithostratigraphic unit D. Unit D is primarily a silty lutite layer.

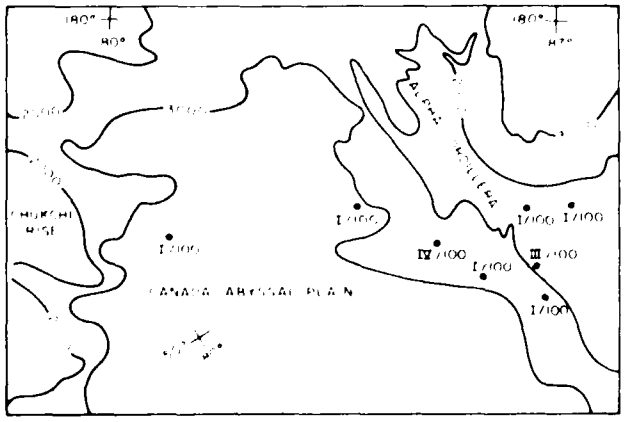

Figure 55. Geographic distribution of dominant sediment types in lithostratigraphic unit F. Unit F is primarily an arenaceous lutite layer.

Figure 56. Geographic distribution of dominant sediment types in lithostratigraphic unit G. Unit G is primarily a silty lutite layer.

Figure 54. Geographic distribution of dominant sediment types in lithostratigraphic unit E. Unit E is primarily a silty lutite layer.

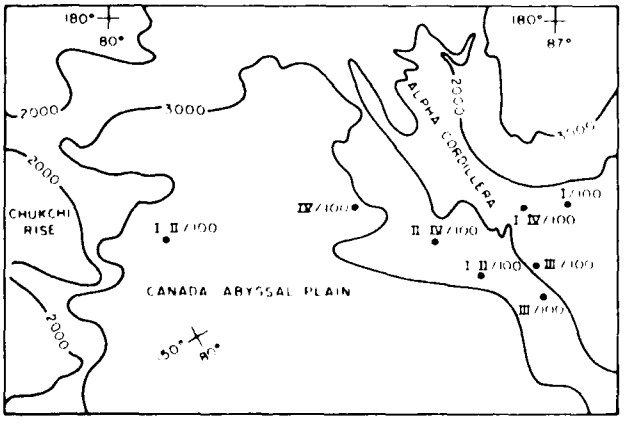

Figure 57. Geographic distribution of dominant sediment types in lithostratigraphic unit H. Unit H is primarily an arenaceous lutite layer.

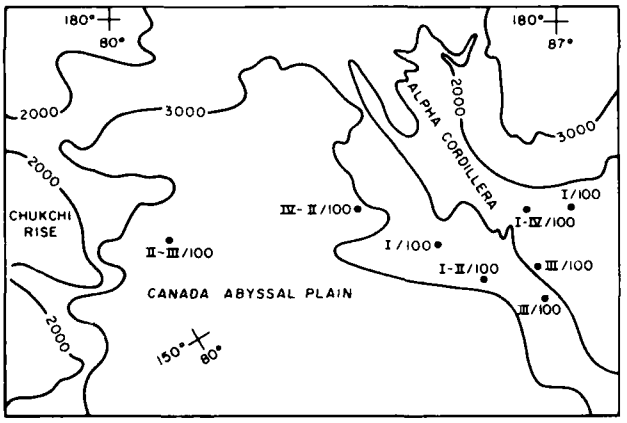

Figure 58. Geographic distribution of dominant sediment types in lithostratigraphic unit I. Unit I is primarily a silty lutite layer.

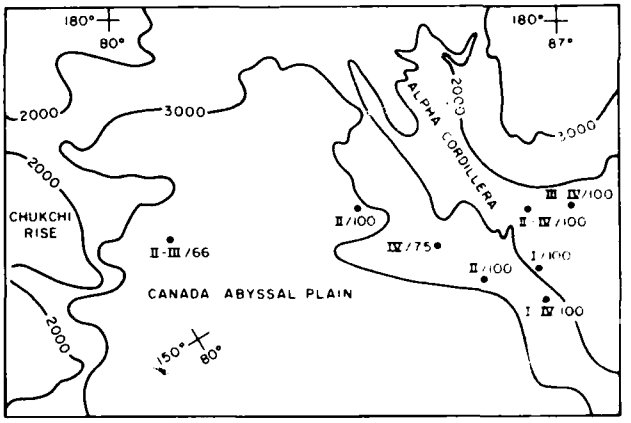

Figure 61. Geographic distribution of dominant sediment types in lithostratigraphic unit L. Unit L is primarily a silty lutite layer.

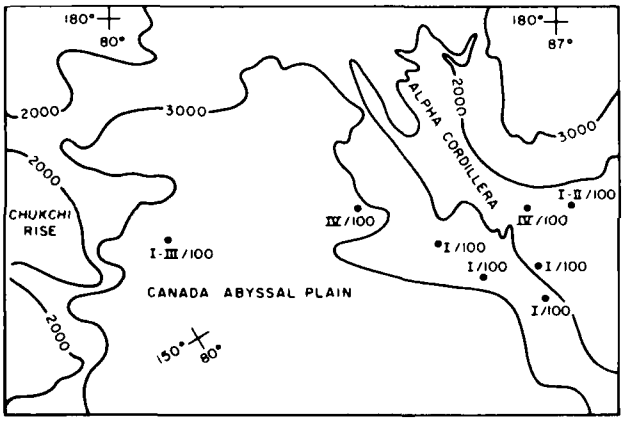

Figure 59. Geographic distribution of dominant sediment types in lithostratigraphic unit J. Unit J is primarily an arenaceous lutite layer.

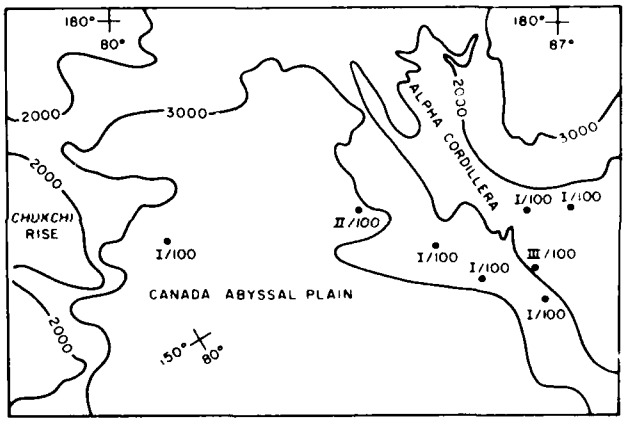

Figure 62. Geographic distribution of dominant sediment types in lithostratigraphic unit B. Unit B is primarily a silty lutite layer.

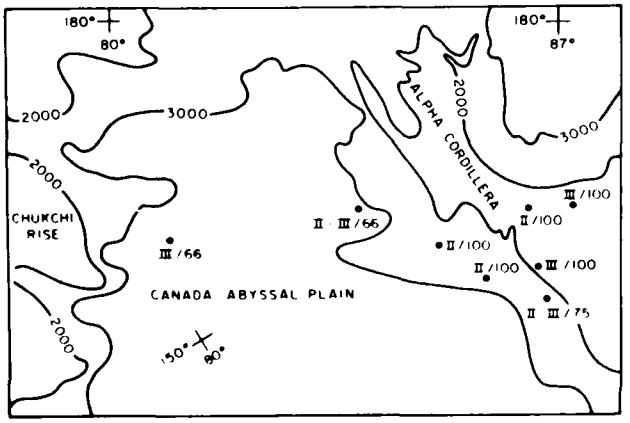

Figure 60. Geographic distribution of dominant sediment types in lithostratigraphic unit K. Unit K is primarily a silty lutite layer.

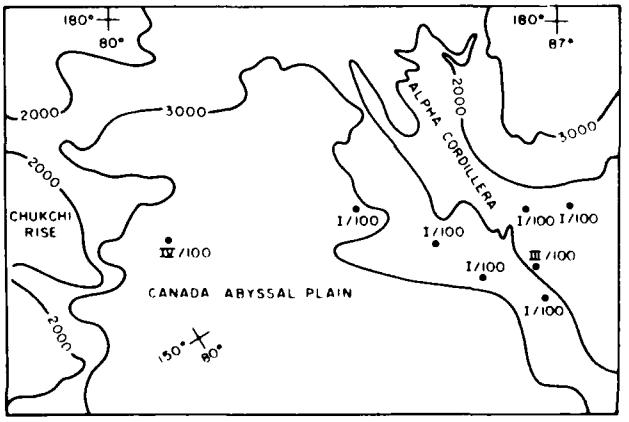

Figure 63. Geographic distribution of dominant sediment types in lithostratigraphic unit C. Unit C is primarily an arenaceous lutite layer.

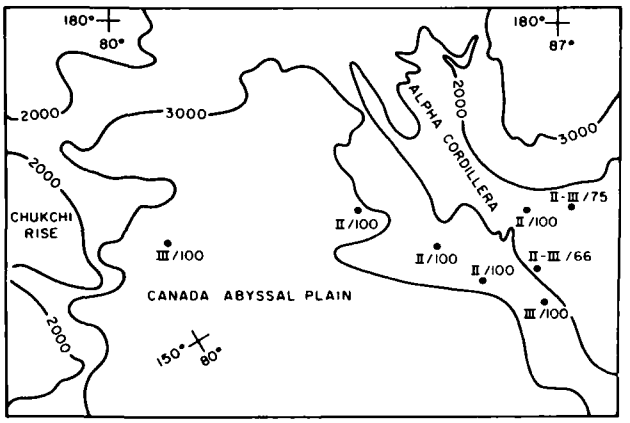

Figure 64. Geographic distribution of dominant sediment types in lithostratigraphic unit M. Unit M is primarily a silty lutite layer.

TABLE 10. ARCTIC OCEAN, ALPHA CORDILLERA, SURFACE AND DOWN-CORE SEDIMENT TYPES; MEAN STATISTICAL PARAMETERS AND RELATIVE PROPORTIONS OF GRAIN SIZE FRACTIONS

Sediment type	Mean grain size	Sorting	Skewness	% Coarse	% Silt	% Clay	No.
			Mean Values				
I	11.7	13.3	1.2	13.7	50.5	35.8	96
II	13.4	15.0	1.2	14.7	49.4	36.1	72
III	9.0	12.2	1.3	12.9	40.6	46.5	43
IV	16.6	14.8	0.7	17.1	59.3	23.7	37
			Standard Deviations				
I	2.0	2.0	0.1	7.1	5.7	5.8	
II	2.8	2.3	0.2	7.3	5.0	7.5	
III	1.6	2.1	0.1	6.1	5.6	6.2	
IV	3.6	1.9	0.4	8.6	7.4	5.4	

have been described as arenaceous lutites (C, F, J, L) or silty lutite containing arenaceous lutite layers (A), the geographic dominance of type I sediment seems to support the theory that arenaceous lutites represent periods of increased glacial ice rafting. No consistent geographic trends in the occurrence of sediment types II, III, and IV were evident in these units, although the locations dominated by sediment types II and III in units A, B, and L tend to be restricted to deeper waters; this suggests lower influx rates for medium to coarse silt and more effective modification of ice-rafted silt distributions at depth.

Sediment types II and III appear as the dominant sediments on the Alpha Cordillera in units D, G, I, K, and M. No consistent geographic patterns were seen in the distribution of sediment types for these units. The dominance of sediment types II and III suggests that influx rates of ice-rafted medium to coarse silt were lower during deposition of these units. Lower rates of ice-rafted silt influx result in deposition of type III sediment and may reduce masking of silt-clay distribution modifications by poorly sorted coarse material; therefore, the occurrence of type II sediment becomes more apparent. Because units D, G, I, K and M are silty lutites, the occurrence of sediment types II and III in these units supports the hypothesis that silty lutite layers represent periods of decreased ice-rafting. Occurrence of sediment types II and III in unit H, an arenaceous lutite, seems somewhat anomalous. This may be the result of unintentional sampling of some of the very thin silty lutite subunits contained within unit H. The subtle changes constituting subunit boundaries were not considered during the sampling process.

Summary

The stratigraphic distribution of sediment types I, II, III, and IV in the Arctic cores supports the hypothesis that deposition of central Arctic arenaceous and silty lutites reflects variations in intensity of ice-rafting. Arenaceous lutite units (C, F, H, J) usually are dominated by type I sediment, which is assumed to reflect relatively high influx rates of ice-rafted medium to coarse silt. The dominance of type III glacial-marine sediment in the silty lutite units (A, B, D, E, G, I, K, M) suggests relatively low rates of input of medium to coarse silt. In addition, low rates of ice-rafting of silt and coarse material may make occurrences of type II sediment more apparent in silty lutites.

Some evidence in a few units (A, B, I) indicates a trend toward lower input rates for ice-rafted medium to coarse silt and increased modifications of those sediments by mid-depth ocean currents in deeper water. No definite geographic pattern was observed in their distributions, however (Figs. 52 through 64). The absence of consistently occurring geographic distribution patterns suggests that conditions governing deposition of glacial-marine sediment were generally uniform over the study area.

Table 10 summarizes the mean statistical parameters and relative proportions of grain-size fractions for Alpha Cordillera surface and down-core sediment types. Abyssal plain sediments were excluded from this analysis because their textural characteristics are influenced by turbidity-current deposition.

LATE CENOZOIC PALEOCLIMATOLOGY

Introduction

The sedimentologic and stratigraphic data for 1-3 cores convince us that the dominant process of sedimentation in the central Arctic since the late Miocene has been ice-rafting. Relating times of increased or decreased ice-rafting in the central Arctic to lower-latitude paleoclimatology has been more difficult.

Major periods of central Arctic glaciation probably were accompanied by intervals of cooler climate in lower latitudes. However, minor periods of glacial growth in the central Arctic may not have been recorded in the lower latitudes. For example, glacial ice rafting is common in the modern Arctic Ocean, but lower latitudes do not reflect this activity to the same extent as the major periods of Arctic cooling have been recorded.

In the central Arctic we identify six major zones of increased ice-rafting during the past 1.2 m.y., the interval for which most comparative lower-latitude data are available (Fig. 65). These intervals of increased ice-rafting are associated with arenaceous lutite units and pink-white layers.

Arenaceous lutites are present in the older parts of the 1-3 cores as well, and in units C, F, and H in particular (the lower, middle,

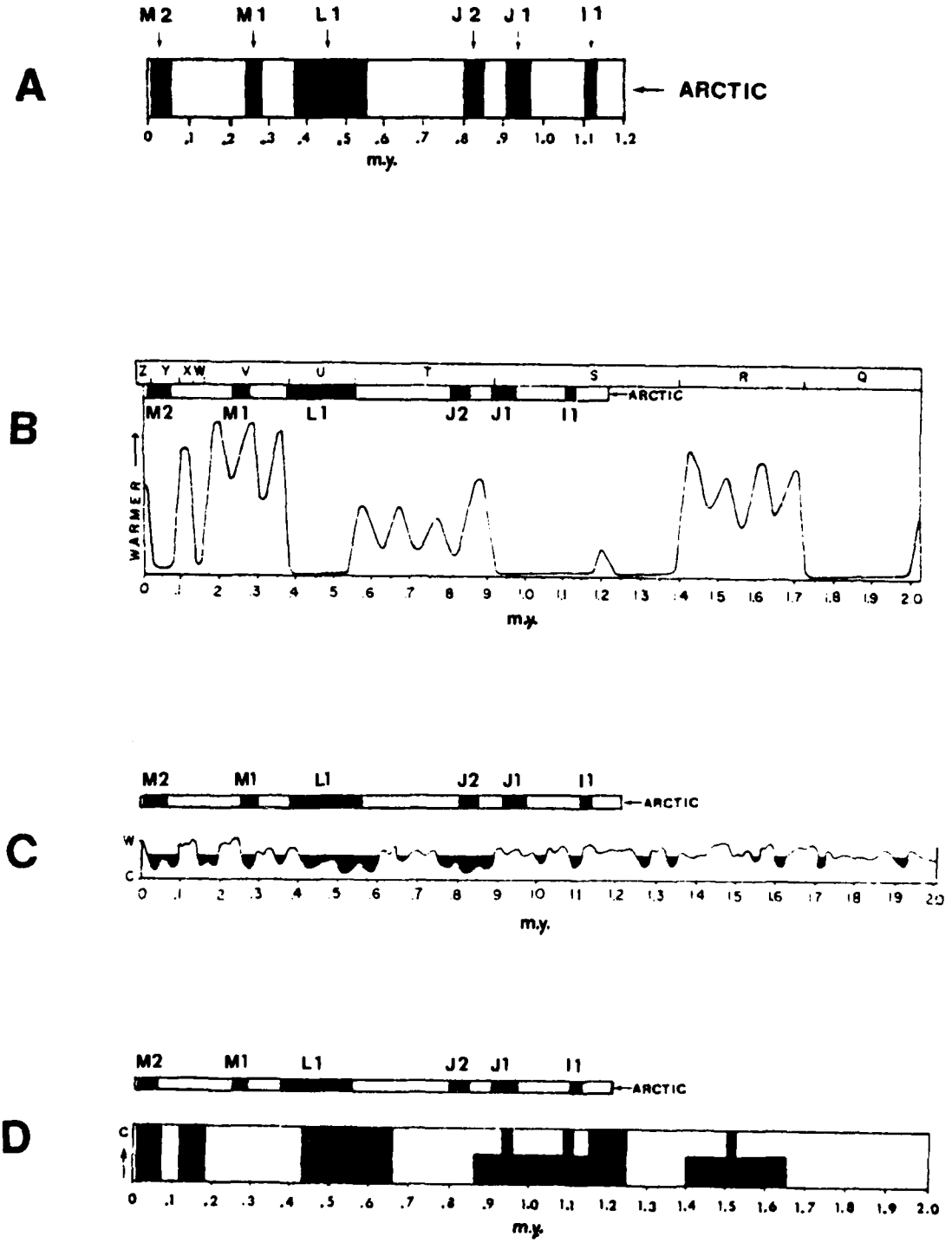

Figure 65. (A) Arctic zones of increased ice-rafting are represented by dark intervals, whereas zones of reduced ice-rafting are indicated by white intervals. Increased ice-rafting zones are labeled by occurrence from bottom to top in each lithostratigraphic unit. The ages of these zones are based on paleomagnetic stratigraphy. (B) Comparison of Arctic glacial ice-rafting zones with the paleoclimatic curve derived by Ericson and Wollin (1968). Letters at top indicate low-latitude climatic stages of Ericson and Wollin. Figure modified from Larson (1975). See text for discussion. (C) Comparison of Arctic glacial ice-rafting zones with Ruddiman's (1971) paleoclimatic curve. Dark areas indicate cooler climate at lower latitudes. Figure modified from Larson (1975). See text for discussion. (D) Comparison of Arctic glacial ice-rafting zones with the paleoclimatic curve derived by Briskin and Berggren (1974; summary in Berggren and Van Couvering, 1974, Fig. 13, p. 140). Dark zones indicate cooler climate at lower latitudes, while light zones indicate warmer climate. See text for discussion.

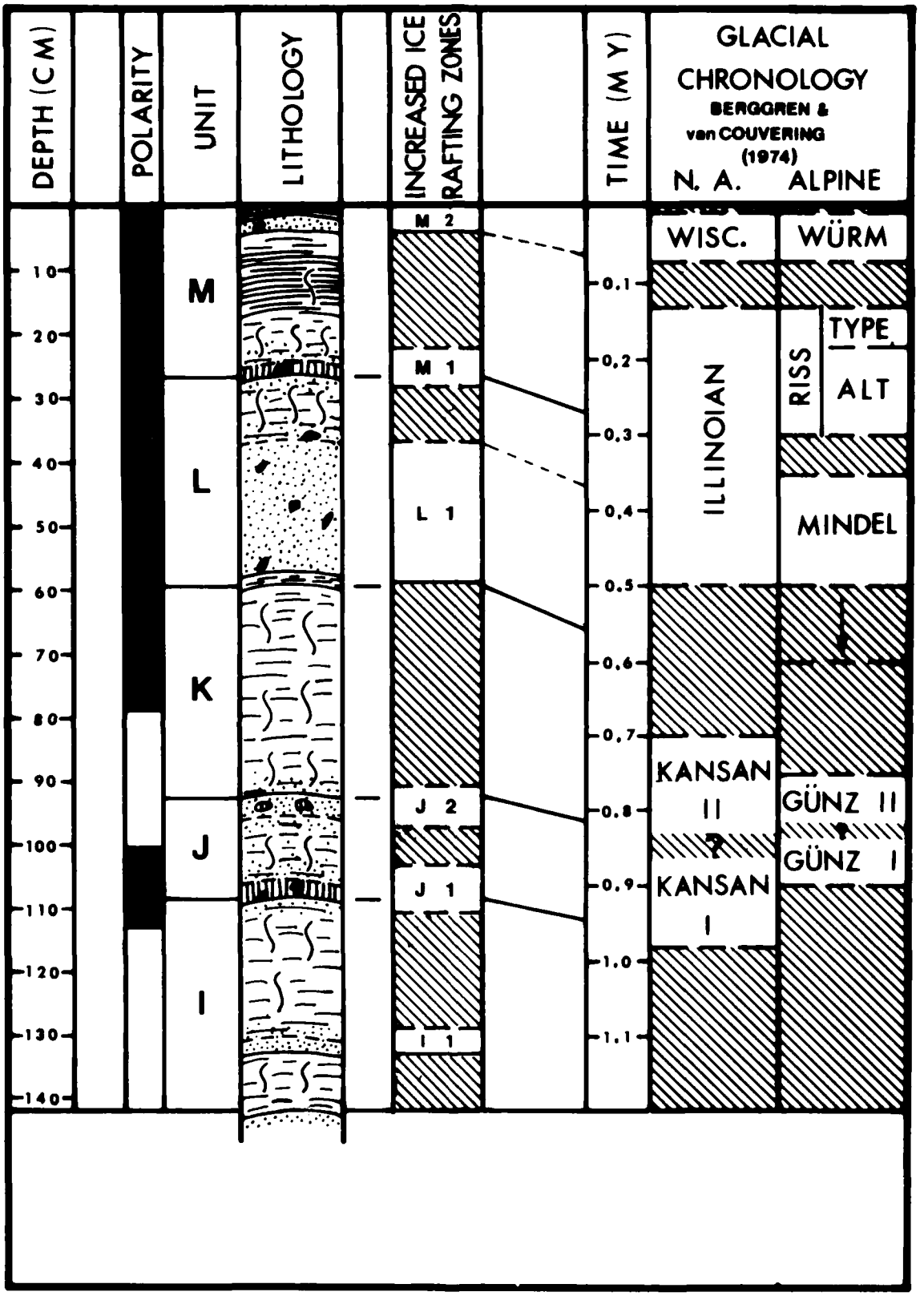

Figure 66. Comparison of times of increased Arctic ice-rafting with the glacial chronology suggested by Berggren and Van Couvering (1974, Fig. 14, p. 144). Black indicates normal polarity. Zones with diagonal lines represent periods of interglacial and/or reduced glacial ice-rafting. White areas indicate periods of glaciation and/or increased ice-rafting. Dashed lines indicate approximate ages as contacts may be gradational and or poorly defined.

and upper coarse units) and must represent the same activity. However, most comparative data, particularly those of oxygen-isotope stratigraphy, appear best defined for only the interval represented in the Arctic cores by units I through M. The central Arctic data can be compared to both the qualitative temperature curves (for example, Ericson and Wollin, 1968; Ruddiman, 1971; Briskin and Berggren, 1974), and oxygen-isotope stratigraphy (Emiliani, 1966, 1972; Shackleton and Opdyke, 1973, 1976).

Qualitative Paleotemperature

Ericson and Wollin (1968), using cores from the equatorial North Atlantic, derived a paleotemperature curve based on the presence or absence of *Globorotalia menardii* for the past 2.0 m.y. Figure 65B illustrates the comparison of Arctic arenaceous lutites and pink-white layers with increased glacial ice rafting. Of particular note is the correlation of Arctic zones I.1 and M2 with Ericson and Wollin's zones U and Y, respectively.

Ruddiman (1971) constructed a paleotemperature curve based on variations in total Foraminifera fauna for the past 2.0 m.y. These data are derived from several cores from the equatorial North Atlantic. A comparison of Arctic zones of increased glacial ice rafting with this paleotemperature curve is illustrated in Figure 65C. There is an apparent correlation of Arctic zone J2 with the low-temperature zone between ~0.75 and 0.9 m.y. Arctic zone I.1 seems to correlate with most of the low-temperature zone between ~0.4 and 0.6 m.y. The youngest low-temperature zone probably is equivalent to Arctic zone M2. This curve is important because it is similar to several other curves derived for the Caribbean and North Atlantic (Ruddiman, 1971; Berggren and van Couvering, 1974).

Briskin and Berggren (1974) used quantitative changes in Foraminifera fauna to develop a paleotemperature curve for the equatorial North Atlantic. A comparison between Arctic zones of increased ice-rafting and this paleotemperature curve is given in Figure 65D. Arctic zones H, J1, and J2 correlate with a general zone of low temperature between ~0.86 and 1.23 m.y. In particular, Arctic zones H and J1 correlate with the temperature minima at ~1.1 and 0.95 m.y., respectively. The temperature minima between 0.42 and 0.65 m.y. seem to correlate with the lower portion of Arctic zone I.1. The youngest temperature zone is probably equivalent to Arctic zone M2.

Comparison between Arctic zones of increased ice-rafting and the three qualitative paleotemperature curves shows a relationship between increased ice-rafting in the Arctic and periods of relatively cooler climate at lower latitudes. This correlation supports the assumption that Arctic zones of increased ice-rafting are related to periods of more intensive glaciation.

A chronology based on both marine and continental sequences for the late Neogene climatic event was proposed by Berggren and Van Couvering (1974). Arctic zones of increased ice-rafting are compared with North American and Alpine periods of glaciation (as interpreted by Berggren and Van Couvering, 1974) in Figure 66. Although Figure 66 could be interpreted to show correlation between zones of increased ice-rafting (arenaceous lutites, coarse pink-white layers) and periods of continental glaciation, such correlation is weakened because of the poor definition of

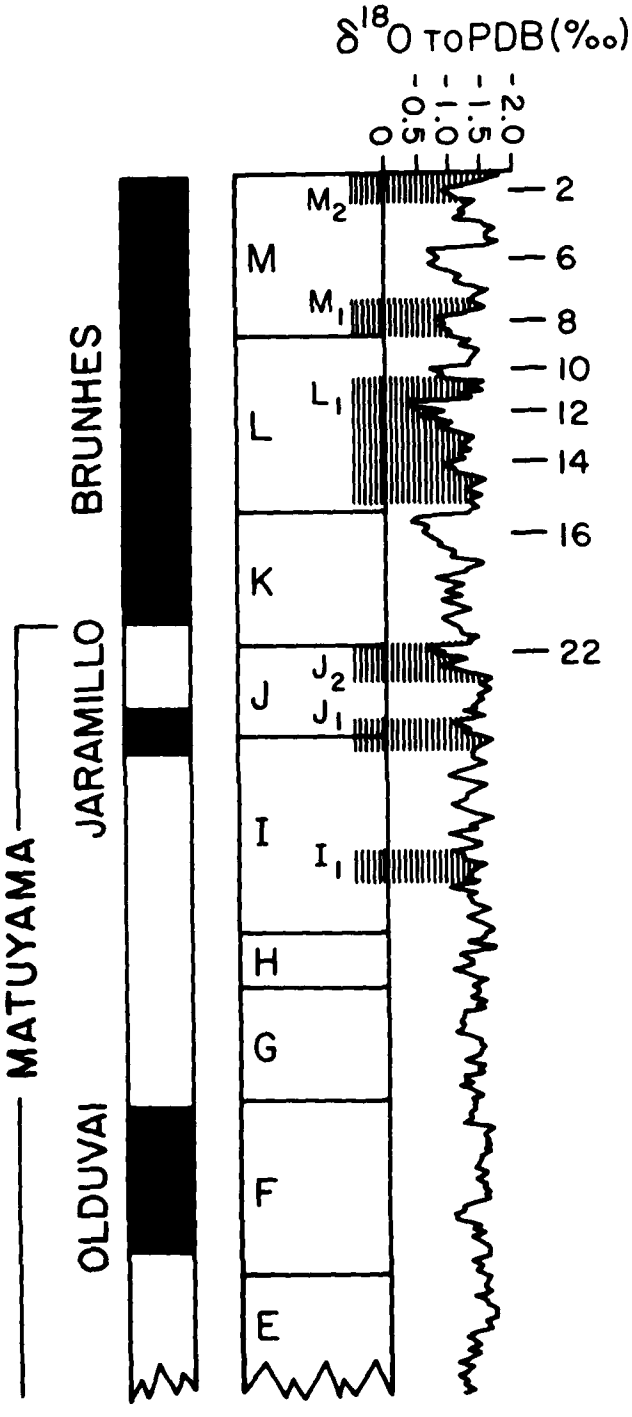

Figure 67. Times of increased ice-rafting in central Arctic Ocean (M$_2$, M$_1$, L$_1$, J$_2$, J$_1$, I$_1$) and correlation with oxygen-isotope stratigraphy and glaciations (2, 6, 8 to 22) of core V 28-239 of Shackleton and Opdyke (1976). Older times of increased central Arctic ice-rafting (during F, H) show less-pronounced correlations with oxygen-isotope excursions.

continental glacial stages. Instead, we think that it is important to note the more positive marine correlations with oxygen-isotope stratigraphy.

Oxygen-Isotope Stratigraphy

Several papers have defined an oxygen-isotope stratigraphy for marine sediments in lower latitudes (Emiliani, 1966, 1972; Shackleton and Opdyke, 1973, 1976; Shackleton and Kennett, 1975). The work of Shackleton and colleagues provides oxygen-isotope data on a magnetic stratigraphy baseline. This is important for our Arctic work for which the magnetic stratigraphy also is available. Thus, direct comparison of our lithostratigraphic units, including intervals of increased ice-rafting, magnetic stratigraphy, and oxygen-isotope stratigraphy of the lower latitudes (Fig. 67), is possible. The older units of increased ice-rafting in the central Arctic (units C, F, and H) are not dramatically represented by oxygen-isotope data. All of the ^{18}O excursions for lower latitudes are of less magnitude during early and middle Matuyama time (~2.4 to 1.4 m.y.). H, in pre-Jaramillo time, correlates with an ^{18}O excursion of about the same magnitude as those of units C, F, and H. J1, in mid-Jaramillo time, correlates with an unnumbered ^{18}O excursion, but J2 shows excellent correlation with glaciation 22, which is the earliest glaciation of duration and intensity in both V28-238 and V28-239. The next major oxygen-isotope recorded glaciation (16) may correlate with an increase in arenaceous texture in the upper part of unit K, but I.1, representing a major time of central Arctic ice-rafting, may be recorded as oxygen-isotope units 10 through 16. M1 shows less positive correlation but probably is represented by parts of glaciation 6 and 8. M2 correlates with glaciation 2.

Because the evidence shows that ice-rafting was a continuous process in the central Arctic, it is possible to correlate arenaceous intervals with most of the oxygen-isotope defined glaciations. The best correlations (for example, M2 with 2, I.1 with 10 through 14, J2 with 22) are those of most-pronounced Arctic ice-rafting with significant ^{18}O excursions.

If the oxygen-isotope stratigraphy is refined for the interval 1.2 to 5 m.y., additional correlations with ice and central Arctic ice-rafting (C, F, H) is possible.

Summary

Clearly, ice-rafting was the dominant sedimentological process during the past 5 m.y. in the central Arctic Ocean. Lower-latitude marine sequences should be expected to show more clearly pronounced climatic sequences alternately between glacial and noglacial climates while the ice-covered Arctic had continuous ice-rafting

CONCLUSIONS

The study of the T-3 cores substantiates the following:

1. Correlation of thin (commonly < 5 cm) sedimentological units is possible in cores that are 600 km apart.

2. Sedimentation of the silty lutite sediments occurred at a very low rate, averaging ~0.5 mm/1,000 yr. Silty lutites makes up most of the cores below the Matuyama-Gauss reversal, which suggests that sedimentation rates were low for most of the Pliocene.

3. Sedimentation of the arenaceous lutite was at a much higher rate, probably >2.0 mm/1,000 yr, and possibly much greater.

4. The approximate ages of the base of the "key" arenaceous lutite units (C, F, and H) are 2.91 m.y., 1.92 m.y., and 1.17 m.y., respectively.

5. The oldest ice-rafted pebble found is in Miocene sediment (Normal Interval 5) and was dated at ~5.26 m.y. by extrapolation from the Gilbert Epoch 5 reversal. Paleomagnetics and sedimentation rates suggest that the oldest sediment recovered has a maximum age of 5.62 m.y.

6. The arenaceous lutite is predominantly the result of an ice-rafting mechanism. This mechanism operated at a greater rate or with more intensity in the late Pliocene–Pleistocene than in the late Miocene–early Pliocene.

A major portion of silty lutite also was deposited by an ice-rafting mechanism. Authigenic, biogenic, and pelagic contributions were probably important.

7. Based on differences in silt-clay histogram shapes, four types of central Arctic Basin glacial-marine sediment can be identified. Comparisons of the *mean* value of statistical parameters describing the histograms indicated that the four histogram types are significantly different.

8. The sediment types represented by the silt-clay histograms reflect variations in environmental factors that influence deposition of glacial-marine sediment.

9. Ice-rafting appears to have been the dominant mechanism contributing sediment to the Alpha Cordillera. This conclusion is based on the distribution of sediment types in the Arctic Ocean surface and down-core samples. In deeper-water environments, such as the Canada and Chukchi Abyssal plains, ice-rafting occurs but is masked by turbidite deposition.

10. The stratigraphic distributions of the four types of Arctic Ocean glacial-marine sediment support the hypothesis that arenaceous lutite represents periods of increased ice-rafting and silty lutite represents periods of reduced ice-rafting.

11. The central Arctic Ocean record is unique. It indicates more or less continuous ice-rafting for the last 5 m.y., during which alternating glacial and interglacial climates affected the sediment record of lower-latitude oceans. Oxygen-isotope determined glacial stages correlate with times of increased ice-rafting in the Arctic Ocean.

APPENDIX 1A. LOCATION, TOTAL LENGTH, AND WATER DEPTH OF CORES, STUDIED IN DETAIL

Core No.	Lat.	Long.	Water depth (m)	Length (cm)
FL 19	83°03.43'	162°49.13'	3417	277
FL 212	80°29.59'	159°37.96'	3642	339
FL 214	80°17.43'	159°30.94'	3021	335
FL 215	80°17.25'	159°25.23'	3043	320
FL 216	80°23.69'	157°41.59'	3576	272
FL 218	80°41.03'	158°21.83'	3654	213
FL 221	80°32.98'	159°38.89'	3638	493
FL 222	80°29.05'	159°12.69'	3633	450
FL 223	80°28.35'	159°06.16'	3616	330
FL 224	80°27.74'	158°48.81'	3467	554
FL 225	80°29.63'	158°42.84'	3610	495
FL 227	80°50.09'	158°25.18'	3641	335
FL 228	80°49.25'	158°49.43'	3632	342
FL 268	83°16.32'	152°58.48'	3062	348
FL 269	83°14.31'	153°13.96'	3097	302
FL 270	83°11.18'	154°00.77'	3280	351
FL 271	83°10.67'	153°53.54'	3254	356
FL 272	83°11.82'	152°56.24'	2384	246
FL 273	83°12.30'	152°56.42'	2323	267
FL 275	83°30.23'	149°58.64'	2884	328
FL 277	83°34.55'	149°26.45'	2871	356
FL 278	83°36.40'	149°08.10'	2725	312
FL 280	83°51.84'	148°22.73'	2639	323
FL 283	83°48.06'	146°12.65'	2639	267
FL 285	83°48.51'	145°27.90'	2653	349
FL 286	84°00.84'	144°02.17'	2316	343
FL 287	84°05.19'	144°01.15'	2430	305
FL 288	84°11.23'	144°28.42'	2414	348
FL 289	84°14.69'	144°16.97'	2357	196
FL 292	84°18.28'	143°41.02'	2330	277
FL 293	84°25.00'	143°04.57'	2058	208
FL 295	84°57.40'	145°30.63'	2214	315
FL 297	84°53.53'	143°10.03'	2223	295
FL 300	85°18.53'	144°02.85'	2082	305
FL 301	85°18.95'	143°36.00'	2100	338
FL 308	85°30.27'	143°08.18'	2252	330
FL 311	85°41.93'	142°21.15'	2332	326
FL 314	85°27.00'	139°23.54'	1927	335
FL 316	85°08.72'	138°13.91'	1785	345
FL 318	84°57.73'	136°13.15'	1982	345
FL 322	84°27.00'	135°18.33'	2446	277
FL 326	84°12.89'	135°41.40'	2653	340
FL 331	84°16.02'	134°37.65'	2659	348
FL 340	84°48.60'	131°17.96'	2290	351
FL 346	84°51.22'	130°42.69'	2372	353
FL 357	84°57.78'	130°20.00'	2213	340
FL 360	84°52.50'	129°55.37'	2398	352
FL 362	84°54.57'	130°10.15'	2385	351
FL 373	84°39.69'	129°52.99'	2493	356
FL 378	84°39.05'	128°57.49'	2299	348
FL 381	84°37.03'	127°24.35'	2585	338
FL 395	84°41.51'	125°53.40'	2502	239
FL 396	84°38.53'	126°04.65'	2589	348
FL 398	84°36.42'	125°48.14'	2596	351
FL 400	84°30.81'	126°21.43'	2690	356
FL 408	84°23.51'	127°52.45'	2758	338
FL 409	84°27.51'	127°00.21'	2742	348
FL 410	84°28.13'	126°52.41'	2737	346
FL 413	84°25.56'	125°15.22'	2390	315
FL 417	84°29.88'	124°06.28'	2381	311
FL 420	84°46.59'	122°55.14'	2240	434
FL 425	85°02.61'	127°54.11'	2282	348
FL 427	86°01.82'	134°44.84'	2216	320
FL 430	85°59.45'	133°20.49'	1860	324
FL 432	85°58.04'	130°51.91'	1674	277
FL 433	85°58.95'	129°51.75'	1624	311
FL 435	86°03.41'	129°32.49'	2272	287

APPENDIX 1B. SURFACE SAMPLES FROM CORE TOPS USED FOR TEXTURAL STUDIES IN ADDITION TO CORES LISTED IN APPENDIX 1A

Sample No. core-segment-sample	Lat.	Long.	Water depth (m)
17-09-1	82°58.99'	159°04.22'	2215
23-18-1	83°02.09'	163°00.39'	3748
24-18-1	82°23.02'	162°06.52'	3743
28-18-1	80°47.93'	140°21.83'	3708
29-16-1	80°29.56'	139°48.16'	3709
32-13-1	80°58.08'	136°13.01'	3698
34-16-1	80°47.41'	136°54.82'	3675
37-13-1	80°40.97'	137°12.79'	3680
39-10-1	80°21.88'	136°46.51'	3680
43-08-1	80°32.58'	134°23.56'	3632
50-14-1	80°31.94'	135°41.72'	3658
54-10-0	76°34.87'	138°06.65'	3605
63-07-1	76°12.85'	142°02.91'	3707
65-15-1	75°33.23'	141°44.21'	3709
66-16-1	75°28.28'	141°14.00'	3703
69-13-T	75°35.23'	140°29.34'	3690
70-05-1	75°44.01'	140°42.47'	3709
73-06-1	75°56.04'	139°41.99'	3703
75-08-1	75°52.54'	139°03.04'	3678
76-15-1	75°32.74'	139°22.79'	3668
77-14-1	75°23.20'	139°50.02'	3681
79-15-1	75°23.25'	140°14.90'	3681
83-12-1	75°23.68'	156°02.43'	2234
87-19-1	75°18.49'	156°07.18'	2903
89-20-1	75°38.49'	151°08.51'	3802
90-20-1	76°59.42'	170°02.33'	2218
92-18-T	77°38.20'	174°43.62'	2078
94-18-T	77°53.03'	175°51.66'	1611
98-18-T	77°43.84'	175°00.21'	1929
100-18-1	77°39.40'	174°23.50'	2099
115-17-1	78°04.26'	174°49.53'	1503
116-16-T	78°05.38'	174°48.49'	1570
122-16-T	78°08.05'	174°22.85'	1837
125-17-T	78°16.15'	175°21.60'	1288
129-17-T	78°34.11'	175°54.80'	1453
133-19-1	78°29.13'	176°14.29'	1222
140-19-1	78°36.93'	176°24.40'	1565
153-18-1	78°40.99'	175°18.16'	1835
165-18-T	78°48.04'	176°08.01'	1490
182-12-1	78°56.61'	175°56.61'	1069
187-13-1	79°33.31'	171°39.64'	2408
193-17-1	80°01.34'	174°02.55'	1753
196-21-1	80°33.93'	171°35.29'	3427
199-23-T	80°11.89'	172°45.27'	2988
204-18-T	79°44.02'	170°57.46'	3157
208-20-1	79°45.18'	170°14.59'	3262
229-23-1	81°40.69'	157°29.49'	3820
231-24-1	81°50.93'	157°32.65'	3812
239-23-1	82°09.02'	156°42.46'	3800
247-24-1	82°13.86'	157°00.42'	3803
259-24-1	82°15.16'	158°19.86'	3804
265-24-1	82°11.27'	157°42.81'	3817
315-20-1	85°11.64'	139°06.72'	1800
325-23-1	84°13.73'	135°29.76'	2654
327-23-1	84°13.49'	135°35.08'	2644
334-21-1	84°36.92'	132°26.68'	2594
344-22-1	85°01.28'	130°57.73'	1769
385-09-1	84°48.33'	126°57.19'	2225
395-16-1	84°41.51'	125°53.40'	2502
416-11-1	84°20.52'	123°29.52'	2682
431-20-1	85°55.63'	132°14.44'	1505
437-19-1	85°59.82'	129°58.76'	1584
476-19-1	85°15.87'	119°00.54'	...
505-16-1	84°16.54'	112°24.07'	...
533-20-1	85°05.90'	98°12.80'	...
552-17-1	...	...	...
559-20-1	84°23.06'	84°04.20'	1280

APPENDIX 1C. VALDERS TILL SAMPLES, EASTERN WISCONSIN (PRINCIPALLY A TILL-SHEET DEPOSITED DURING A GLACIAL ADVANCE)

Sample	Tier	Range	Section	Quarter
001	22N	23E	12	NENESW
002	18	22	10	NWNWNW
003	18	24	7	SESENW
004	17	23	11	SESENE
005	17	23	11	SWSWSE
006	16	23	10	NENWNW
007	16	23	10	SWSESE
008	16	23	34	NENWNE
009	22	24	30	NWSWNW
010	19	22	23	SENENE
011	19	23	18	SWNESE
012	19	22	13	SESWNW
013	19	24	32	SESESW
014	18	23	3	NENWSE
015	19	22	32	SWSWNE
119	20	19	31	NESWNE
126	18	19	6	NENENE

APPENDIX 1D. EAST PACIFIC OCEAN SEDIMENT CORES (SAMPLES AT UNIVERSITY OF WISCONSIN)

Cruise-station-core	Lat. (N)	Long. (W)	Depth	Sediment Type
7401-10-FFC12	19°40'	132°00'	5100 m	pelag. clay
7402-12-FFC12*	30°43'	119°43'	4100	pelag. clay
7402-13A-FFG1	16°00'	125°00'	4210	hemipel. clay
7401-008-FFC9	11°00'	140°00'	4850	calc. ooze
7402-14B-BOX3	04°32'	140°21'	4392	sil. ooze

*Histogram of Figure 45.

APPENDIX 1E. NON-ARCTIC SEDIMENT CORES

Core	Site	Lat.	Long.	Water depth (m)	Core length (m)
Deep-Sea Drilling Project cores					
111	North Atlantic	50°25.57'N	46°22.05'W	1797	74.0
182	Gulf of Alaska	57°52.96'N	148°42.99'W	1411	11.5
346	Greenland Sea	69°53.35'N	8°41.14'W	732	120.4
USNS ELTANIN cores					
12-6	Weddell Sea	65°08.6' S	47°07.3' W	4115	6.45
27-12	Ross Sea	77°14.0' S	169°04.3' W	929	5.01
37-7	Southern Indian Ocean	65°01.1' S	144°57.2' E	3155	11.98
42-9	Bellinghausen Sea	69°59.40'S	80°24.0' W	567	5.65
USNS NORTHWIND cores					
110	Kara Sea	81°34.8' N	79°52.0' E	203	.87
115	Kara Sea	81°35.5' N	67°32.0' E	567	.96

APPENDIX 2. AVERAGES AND RANGES IN VALUES OF THE WEIGHT PERCENT OF THE SAND SIZE FRACTION (>63 MICRONS) FOR SELECTED CORES

Unit	Number of cores	Average (%)	Range (%)
MU	5	18.2	12 to 25
MM	5	9.3	3 to 12
ML	5	20.2	12 to 35
L	5	25.7	18 to 33
K	5	15.3	10 to 30
JU	5	21.4	12 to 29
JL	5	23.1	15 to 25
IM	5	22.4	15 to 30
He	24	26.0	19 to 40
Hd	24	7.8	4 to 15
Hc	22	20.2	15 to 27
Hb	14	33.6	19 to 40
Ha	13	26.6	21 to 31
G	26	9.8	2 to 19
F	22	23.0	9 to 45
E	26	8.6	2 to 15
D	27	6.3	1 to 15
C_t*	22	16.0	12 to 21
C_b†	22	19.7	12 to 28
B	24	6.0	3 to 10
A'§	3	26.3	22 to 30
A	24	5.0	1 to 10

*C_t refers to the Top Lower Coarse layer in unit C.

†C_b refers to the Bottom Lower Coarse layer in unit C.

§A' refers to the arenaceous facies in unit A.

APPENDIX 3. THIN-SECTION MODAL ANALYSIS OF CENTRAL ARCTIC OCEAN STRATIGRAPHIC UNITS

Sample I.D.	Quartz-feldspar	Lithic fragments	Detrital $CaCO_3$	Foram tests	Opaque (FeMn)	Unknown ?
Lower part of unit A						
221-8-T	66.3	6.3	0.8	0.3	20.3	6.0
283-3-4	54.3	8.0	0.4	0.0	21.8	13.8
430-2-3	78.1	8.5	0.8	0.0	4.9	7.7
Average	66.2	7.6	0.6	0.1	15.7	9.2
Upper part of unit A						
214-1-1	44.5	7.5	0.0	0.6	43.4	5.3
283-5-1	46.3	14.6	0.8	0.0	31.1	7.2
430-4-1	56.4	9.3	0.5	0.7	25.5	7.6
Average	49.1	10.5	0.4	0.4	33.3	6.7
Arenaceous portion of unit A						
283-5	87.9	7.1	0.3	0.0	2.1	2.1
381-2	86.8	6.2	0.6	0.0	2.9	3.5
400-1	86.3	6.2	0.3	0.0	2.8	4.4
Average	87.0	6.5	0.4	0.0	2.6	3.3
Unit B						
218-4-8	61.3	13.3	3.8	0.9	16.2	3.8
283-6-1	67.6	12.6	0.0	0.3	15.7	5.4
430-6-1	72.8	10.4	0.0	0.0	9.9	6.9
Average	67.2	12.3	1.3	0.4	13.9	5.4
Lower part of unit C						
221-18	73.6	13.5	5.9	0.0	2.0	5.0
286-9	74.8	14.2	2.7	0.0	1.2	7.1
430-7	75.9	16.1	1.0	1.0	2.9	3.2
Average	74.8	14.6	3.2	0.3	2.0	5.1
Upper part of unit C						
221-18	81.2	9.7	2.6	0.0	2.6	3.8
286-10	79.2	12.5	0.3	0.0	1.4	6.6
430-7	71.7	13.7	0.9	0.0	5.7	8.0
Average	77.4	12.0	1.3	0.0	3.2	6.1
Unit D						
214-3-1	67.6	14.9	5.0	0.0	6.1	6.4
293-9-3	72.5	15.9	2.1	0.0	2.7	6.7
430-9-4	64.5	9.2	2.8	0.8	17.[illegible]	5.1
Average	68.2	13.3	3.3	0.3	8.8	6.1
Unit E						
214-4-1	65.6	12.0	10.8	0.0	3.9	7.8
283-10-3	71.1	14.8	3.3	0.0	5.2	5.5
430-10-4	65.1	13.4	5.5	0.8	8.4	6.8
Average	67.3	13.4	6.4	0.3	5.8	6.7
Unit F						
214-5-2	49.6	21.6	21.0	0.0	2.6	4.7
293-10-1	61.3	18.2	15.4	0.0	1.6	3.6
430-10-2	56.5	23.0	14.2	1.0	1.9	3.4
Average	55.7	20.9	16.9	0.3	2.0	3.9
Lower Foraminifera-poor portion of unit G						
214-7-2	73.1	13.1	7.8	0.3	1.9	3.8
293-11-1	60.6	15.4	10.6	0.3	7.3	5.8
430-11-2	81.4	7.1	3.4	0.9	4.6	2.5
Average	71.7	11.9	7.3	[illegible]	4.6	[illegible]
Upper Foraminifera-rich portion of unit G						
214-9-3	54.6	6.[illegible]	13.4	21.0	1.[illegible]	3.9
293-13-3	73.[illegible]	17.[illegible]	[illegible]	8.6	3.1	[illegible]
430-12-4	49.2	[illegible]	[illegible]	[illegible]	[illegible]	[illegible]
Average	59.1	8.3	[illegible]	18.3	[illegible]	3.9
Unit Ha						
326-13	94.3	3.6		[illegible]	[illegible]	[illegible]
[illegible]	[illegible]	[illegible]	[illegible]	[illegible]	[illegible]	[illegible]
[illegible]	[illegible]	[illegible]	[illegible]	[illegible]	[illegible]	
Average	[illegible]	[illegible]	[illegible]	[illegible]	[illegible]	[illegible]
Unit Hb						
214-[illegible]	[illegible]	[illegible]	[illegible]	[illegible]	[illegible]	[illegible]
286-[illegible]	[illegible]	[illegible]	[illegible]	[illegible]	[illegible]	[illegible]
430-[illegible]	[illegible]	[illegible]	[illegible]	[illegible]	[illegible]	[illegible]
Average	[illegible]	[illegible]	[illegible]	[illegible]	[illegible]	[illegible]
Unit H[illegible]						
214-[illegible]	[illegible]	[illegible]	[illegible]	[illegible]	[illegible]	[illegible]
286-[illegible]	[illegible]	[illegible]	[illegible]	[illegible]	[illegible]	[illegible]
430-[illegible]	[illegible]	[illegible]	[illegible]	[illegible]	[illegible]	[illegible]
Average	[illegible]	[illegible]	[illegible]	[illegible]	[illegible]	[illegible]

APPENDIX 3 (continued)

Sample I.D.	Quartz-feldspar	Lithic fragments	Detrital $CaCO_3$	Foram tests	Opaque (FeMn)	Unknown ?
Unit Hd						
214-11	53.7	16.8	11.1	6.9	3.3	7.[illegible]
286-16	80.3	10.0	0.4	0.4	2.5	6.4
430-13	54.5	3.9	2.6	11.6	22.7	4.[illegible]
Average	62.8	10.2	4.7	6.3	9.5	6.[illegible]
Unit He						
214-11	62.7	10.5	18.8	1.0	1.5	5.0
286-16	92.0	5.1	0.6	0.0	1.2	1.0
430-13	91.9	4.8	0.3	0.0	0.9	[illegible]
Average	82.2	6.8	6.6	0.3	1.1	2.6
Unit J						
228-14-3	59.0	19.0	5.2	0.2	12.5	3.7
270-S-11	67.2	15.4	7.4	0.0	5.8	4.2
331-S-11	68.9	13.7	5.5	1.4	4.5	5.[illegible]
409-S-11	61.8	18.4	7.3	2.3	6.4	4.[illegible]
435-S-11	62.6	19.7	1.5	0.3	5.8	9.8
Average	63.9	17.2	5.5	0.6	7.0	9.6
PW layer of unit J						
228-15-1	43.3	11.0	36.9	0.7	4.6	3.3
270-18-4	42.0	10.0	35.2	1.7	7.0	3.0
331-S-21	45.2	7.3	42.[illegible]	0.8	1.9	[illegible]
409-S-21	48.4	10.5	35.0	0.8	2.4	3.[illegible]
435-S-21	45.6	9.3	38.6	2.0	1.5	3.0
Average	44.9	9.6	37.8	1.2	3.5	2.9
Upper part of unit J with PW clasts						
228-S-52	45.1	15.3	35.0	1.2	1.2	2.2
270-19-4	42.7	11.1	35.6	3.2	4.4	3.0
331-S-22	44.5	12.3	34.0	2.6	3.1	3.4
409-S-22	48.6	11.1	32.5	1.6	3.4	2.8
435-S-22	50.4	10.3	32.6	1.5	1.7	3.[illegible]
Average	46.3	12.0	34.0	2.0	2.8	3.[illegible]
Unit K						
228-17-3	49.5	13.4	16.9	12.9	5.1	1.9
270-19-3	51.5	12.8	17.6	10.2	4.8	2.8
331-18-2	53.7	10.6	12.7	13.5	7.2	[illegible].1
409-12-4	61.1	13.4	9.6	3.8	8.5	1.8
435-12-2	52.8	15.9	17.5	3.9	7.8	1.8
Average	53.7	13.2	14.7	8.8	7.7	2.1
Unit L						
228-21-4	70.9	17.4	5.7	2.1	2.4	1.5
270-22-3	68.2	16.8	8.7	1.[illegible]	2.6	[illegible]
331-20-2	69.8	14.8	6.8	0.3	5.5	[illegible].8
409-15-4	66.0	16.2	10.0	[illegible]	2.8	4.[illegible]
435-14-2	53.3	19.4	8.1	12.9	3.0	3.2
Average	65.6	16.9	7.9	[illegible]	3.3	2.9
409-20-4*	66.6	[illegible]	7.8	2.4	2.4	1.[illegible]
PW2 and W1 layers of unit M						
228-S-51	30.6	10.6	[illegible]	8.[illegible]	[illegible]	[illegible]
270-S-51	39.6	11.[illegible]	38.[illegible]	[illegible]	0.8	3.0
331-S-51	52.0	[illegible]	[illegible]	18.[illegible]	1.9	3.8
409-S-51	30.3	5.9	2[illegible]	[illegible]	[illegible]	[illegible]
435-S-51	33.8	9.9	32.[illegible]	20.[illegible]	1.3	[illegible]
Average	39.2	8.[illegible]	32.[illegible]	17.0	2.[illegible]	[illegible]
Arenaceous infilles of unit M						
228-S-52	67	13.4	9.2	3.9	[illegible]	[illegible]
331-S-52	55.3	8.[illegible]	2[illegible]	[illegible].8	4.9	[illegible]
409-S-52	52.2	13.4	2[illegible]	[illegible]	4.[illegible]	[illegible]
435-19-4	58.9	9.[illegible]	18.[illegible]	[illegible]	[illegible]	[illegible]
Average	58.5	10.[illegible]	[illegible]	[illegible]	4.[illegible]	[illegible]

Note. These analyses were made in order to characterize the sediment of the different units and as a check on the validity of megascopic correlations of units. They do not represent a rigorous sedimentologic study but are used to illustrate general differences between various units. Monocrystalline quartz and polycrystalline quartz, easily differentiated in thin section, are combined with the various plagioclases, because all of these components showed positive correlation. Lithic fragments were also differentiated but combined in this appendix because they are important only as a group (procedure as used in Hollister and Heezen, 1966, and Friedman, 1958).

*This sample is from the olive gray sandy infill containing abundant [illegible] distributed evenly throughout.

REFERENCES CITED

Aagaard, K., and Coachman, L. K., 1975, Toward an ice free Arctic Ocean: EOS (American Geophysical Union Transactions), v. 56, p. 484–486.

Anderson, J. B., 1972, Nearshore glacial-marine deposition from modern sediments of the Weddell Sea: Nature, v. 240, p. 189–192.

Anderson, J. B., Clark, H. C., and Weaver, F. M., 1977a, Sediments and sediment processes on high latitude continental shelves, *in* Proceedings, Ninth Offshore Technology Conference: Houston, p. 91–96.

Anderson, J. B., and others, 1977b, Sedimentation on the Antarctic continental margin, *in* Proceedings, Symposium on Antarctic Geology and Geophysics, 3rd, Abstracts: University of Wisconsin, Madison, p. 11.

Andrew, J. A., 1973, Sediment distribution in deep areas of the northern Kara Sea [Ph.D. thesis]: Madison, University of Wisconsin, 32 p.

Barrett, P. J., 1975, Textural characteristics of Cenozoic preglacial and glacial sediments at site 270, Ross Sea, Antarctica, *in* Hayes, D. E., and others, eds., Initial reports of the deep sea drilling project: Washington, U. S. Government Printing Office, v. 28, p. 757–768.

Berggren, W. A., 1977, North Atlantic Cenozoic foraminifera, *in* Swain, F. M., ed., Stratigraphic micropaleontology of Atlantic basin and borderlands: Amsterdam, Elsevier, p. 389–409.

Berggren, W. A., and Van Couvering, J. A., 1974, The Late Neogene: developments in palaeontology and stratigraphy 2: New York, Elsevier, 216 p.

Berry, R. W., and Johns, W. P., 1966, Mineralogy of the clay-sized fractions of some North Atlantic Arctic Ocean bottom sediments: Geological Society of America Bulletin, v. 77, p. 183–196.

Biscaye, P. E., 1965, Mineralogy and sedimentation of recent deep-sea clay in the Atlantic Ocean and adjacent seas and oceans: Geological Society of America Bulletin, v. 76, p. 803–832.

Bouma, A. H., and Hollister, C. D., 1973, *Deep ocean basin sedimentation*, *in* Middleton, G. V., and Bouma, A. H., cochairman, Pacific Section Short Course Lecture Notes: Society of Economic Paleontologists and Mineralogists, 157 p.

Briskin, Madeleine, and Berggren, W. A., 1974, Pleistocene stratigraphy and quantitative paleo-oceanography of tropical North Atlantic core V16-205, *in* Saito, Tsunemasa, and Burkle, L. H., eds., Late Neogene epoch boundaries: Micropaleontology Press, American Museum of Natural History, New York, p. 167–198.

Campbell, I. S., and Clark, D. L., 1977, Pleistocene turbidites of the Canada Abyssal Plain of the Arctic Ocean: Journal of Sedimentary Petrology, v. 47, p. 657–670.

Chamberlain, C. K., 1975, Trace fossils in DSDP cores of the Pacific: Journal of Paleontology, v. 49, p. 1074–1096.

Chriss, T., and Frakes, L. A., 1972, Glacial marine sedimentation in the Ross Sea, *in* Adie, R. J., ed., Antarctic geology and geophysics: Oslo, Universitetsforlaget, p. 747–762.

Clark, D. L., 1969, Paleoecology and sedimentation in part of the Arctic Basin: Arctic, v. 22, p. 233–245.

1970, Magnetic reversals and sedimentation rates in the Arctic Ocean: Geological Society of America Bulletin, v. 81, p. 3133–3134.

1971, Arctic Ocean ice cover and its late Cenozoic history: Geological Society of America Bulletin, v. 82, p. 3313–3324.

1974, Late Mesozoic and early Cenozoic sediment cores from the Arctic Ocean: Geology, v. 2, p. 41–44.

1975, Geologic history of the Arctic Ocean Basin, *in* Yorath, C. J., and others, eds., Canada's continental margins and offshore petroleum exploration: Canadian Society of Petroleum Geologists, Memoir 4, p. 501–524.

1977a, Climatic factors of the late Mesozoic and Cenozoic Arctic Ocean, *in* Polar Oceans: Dunbar, M. J., ed., Arctic Institute of North America, p. 603–615.

———1977b, Paleontologic response to post-Jurassic crustal plate movements in the Arctic Ocean, *in* Paleontology and plate tectonics, West, R. M., ed., Milwaukee Public Museum, Special Publications in Biology and Geology, no. 2, p. 55–76.

Coachman, L. K., and Aagaard, Knut, 1974, Physical oceanography of the Arctic and Subarctic seas, *in* Herman, Yvonne, ed., Marine geology and oceanography of the Arctic seas: New York, Springer-Verlag, p. 1–72.

Dalland, Arne, 1976, Erratic clasts in the lower Tertiary deposits of Svalbard—evidence of transport by winter ice: Norsk Polarinstitutt Arbok, p. 151–165.

Darby, D. A., 1971, Carbonate cycles and clay mineralogy of Arctic Ocean sediment cores: University of Wisconsin Madison Arctic Ocean sediment studies, Technical Report 8, 43 p.

———1975, An evaluation of Arctic Ocean paleomagnetic stratigraphy, *in* Fisher, R. M., and others, eds., Proceedings, Takesi Nagata Conference, June 1974: University of Pittsburgh, Goddard Space Flight Center, Maryland, p. 230–244.

Darby, D. A., Burckle, L. H., and Clark, D. L., 1974, Airborne dust on the Arctic pack ice: its composition and fallout rate: Earth and Planetary Science Letters, v. 24, p. 166–172.

Dott, R. H., Jr., 1961, Squantum "tillite", Massachusetts—evidence of ancient glaciation or subaqueous mass movements?: Geological Society of America Bulletin, v. 72, p. 1289–1306.

Drake, L. D., 1971, Evidence for ablation and basal till in east-central New Hampshire, *in* Goldthwait, R. P., ed., Till: a symposium: Columbus, Ohio State University Press, p. 73–91.

Emiliani, C., 1966, Paleotemperature analysis of Caribbean cores P6304-8 and P6304-9 and a generalized temperature curve for the past 425,000 years: Journal of Geology, v. 74, p. 109–126.

1972, Quaternary paleotemperatures and the duration of high temperature intervals: Science, v. 178, p. 398–401.

Ericson, D. B., Ewing, Maurice, and Wollin, Goesta, 1964, Sediment cores from the Arctic and subarctic seas: Science, v. 144, p. 1183–1192.

Ericson, D. B., and Wollin, Goesta, 1968, Pleistocene climates and chronology in deep-sea sediments: Science, v. 162, p. 1227–1234.

Fillon, R. H., 1972, Evidence from the Ross Sea for widespread submarine erosion: Nature, v. 238, p. 40–42.

Flint, R. F., 1947, Glacial geology and the Pleistocene epoch: New York, John Wiley and Sons, Inc., 589 p.

Frakes, L. A., 1971, USNS ELTANIN core descriptions, cruises 32 to 45: Sedimentology Research Laboratory contribution no. 33: Florida State University, 105 p.

Friedman, G. M., 1958, Determination of sieve-size distribution from thin-section data for sedimentary studies: Journal of Geology, v. 66, p. 394–416.

Galt, J. A., 1967, Current measurements in the Canada Basin of the Arctic Ocean, summer 1965: University of Washington Department of Oceanography, Technical Report 184, 17 p.

Gamber, L. H., and Clark, D. L., 1978, Distribution of microscopic molluscs, echinoderms and sponges in the central Arctic Ocean: Micropaleontology, v. 24, p. 422–431.

Goodell, H. G., 1965, Marine geology, USNS *Eltanin* cruises 9 to 15: Sedimentology Research Laboratory contribution no. 11: Florida State University, 237 p.

1968, USNS ELTANIN core descriptions, cruises 16 to 22: Sedimentology Research Laboratory contribution no. 25: Florida State University, 247 p.

Goodell, H. G., and others, 1968, The Antarctic glacial history recorded in sediments of the Southern Ocean: Paleogeography, Paleoclimatology, and Paleoecology, v. 5, p. 41–62.

Gorbunova, Z. N., 1976, The history of accumulation of clay minerals in the Pacific Ocean during the Cenozoic according to deep sea drilling data: Oceanology (translation by American Geophysical Union), v. 15, p. 568–571.

Gross, D. L., and Moran, S. R., 1971, Grain size and mineralogical

gradation within tills of the Allegheny Plateau, *in* Goldthwait, R. P., ed., Till: a symposium: Columbus, Ohio State University Press, p. 251–274.

Hall, J. K., 1973, Geophysical evidence for ancient seafloor spreading from the Alpha Cordillera and Mendeleyev Ridge, *in* Pitcher, M. G., ed., Arctic geology: American Association of Petroleum Geologists, Memoir 19, p. 542–561.

Harms, J. C., 1974, Brushy Canyon Formation, Texas; A deep-water density current deposit: Geological Society of America Bulletin, v. 85, p. 1763–1784.

Heezen, B. C., and Hollister, C. D., 1964, Deep-sea current evidence from abyssal sediments: Marine Geology, v. 1, p. 141–174.

Herman, Yvonne, 1964, Temperate water planktonic foraminifera in Quaternary sediments of the Arctic Ocean: Nature, v. 201, p. 386–387.

———1970, Arctic paleo-oceanography in late Cenozoic time: Science, v. 169, p. 474–477.

———1974, Arctic Ocean sediments, microfauna, and the climatic record in late Cenozoic time, *in* Herman, Yvonne, ed., Marine geology and oceanography of the Arctic seas: New York, Springer-Verlag, p. 283-348.

Herman, Yvonne, and O'Neil, J. R., 1975, Arctic paleosalinities during late Cenozoic time: Nature, v. 258, p. 591–595.

Herman, Yvonne, Grazzini, C. V., and Hooper, C., 1971, Arctic paleotemperatures in late Cenozoic time: Nature, v. 232, p. 466–469.

Hjulstrom, F., 1939, Transportation of detritus by moving water, *in* Trask, P. D., ed., Recent marine sediments: a symposium: New York, Dover Publications, Inc., p. 5–31.

Hoffman, T. F., 1972, The origin and stratigraphic significance of pink layers in late Cenozoic sediments of the Arctic Ocean: University of Wisconsin Madison Arctic Ocean sediment studies, Technical Report 11, 74 p.

Hollister, C. D., and Heezen, B. C., 1964, Modern graywacke-type sands: Science, v. 146, p. 1573–1574.

Holmes, M. L., and Creager, J. S., 1974, Holocene history of the Laptev Sea continental shelf, *in* Herman, Yvonne, ed., Marine geology and oceanography of the Arctic seas: New York, Springer-Verlag, p. 211–229.

Howard, J. D., 1975, The sedimentological significance of trace fossils, *in* Frey, R. W., ed., The study of trace fossils: New York, Springer-Verlag, p. 131–146.

Hunkins, K. L., 1968, Geomorphic provinces of the Arctic Ocean, *in* Sater, J. E., coordinator, Arctic drifting stations: a report on activities supported by the Office of Naval Research: The Arctic Institute of North America, p. 366–376.

Hunkins, K. L., and Kutschale, Henry, 1967, Quaternary sedimentation in the Arctic Ocean, *in* Sears, Mary, ed., Progress in oceanography, v. 4: Pergamon Press, p. 89–94.

Hunkins, K. L., Thorndike, E. M., and Mathieu, Guy, 1969, Nepheloid layers and bottom currents in the Arctic Ocean: Journal of Geophysical Research, v. 74, p. 6995–7008.

Hunkins, K. L., and others, 1971, The late Cenozoic history of the Arctic Ocean, *in* Turekian, K. K., ed., The late Cenozoic glacial ages: Yale University Press, p. 215–237.

Inman, D. L., 1949, Sorting of sediments in the light of fluid mechanics: Journal of Sedimentary Petrology, v. 19, p. 51–70.

Johns, W. D., Grim, R. E., and Bradley, W. F., 1954, Quantitative estimates of clay minerals by diffraction methods: Journal of Sedimentary Petrology, v. 24, p. 242–251.

Joy, J. A., and Clark, D. L., 1977, The distribution, ecology and systematics of the benthic Ostracoda of the central Arctic Ocean: Micropaleontology, v. 23, p. 129–154.

Kellogg, T. B., Truesdale, R. S., and Osterman, L. E., 1979, Late Quaternary extent of the West Antarctic ice sheet: new evidence from Ross Sea cores: Geology, v. 7, p. 249–253.

Kent, D. V., Opdyke, N. D., and Ewing, M., 1971, Climate change in the North Pacific using ice-rafted detritus as a climatic indicator: Geological Society of America Bulletin, v. 82, p. 2741–2754.

Kitchell, J. A., 1979, Deep-sea foraging pathways: an analysis of randomness and resource exploitation: Paleobiology, v. 5, p. 107–125.

Kitchell, J. A., and Clark, D. L., 1979, A multivariate approach to biofacies analysis of deep-sea traces from the central Arctic: Journal of Paleontology, v. 53, p. 1045–1067.

Kitchell, J. A., and others, 1978a, Deep-sea foraging behavior: its bathymetric potential in the fossil record: Science, v. 200, p. 1289–1291.

Kitchell, J. A., and others, 1978b, Abyssal traces and megafauna: comparison of productivity, diversity, and density in the Arctic and Antarctic: Paleobiology, v. 4, p. 177–180.

Krinsley, D. H., and Doornkamp, J. C., 1973, Atlas of quartz sand surface textures: Cambridge University Press, 91 p.

Ku, T., and Broecker, W. S., 1967, Rates of sedimentation in the Arctic Ocean, *in* Sears, M., ed., Progress in Oceanography, v. 4: Pergamon Press, p. 95–104.

Ku, T., Broecker, W. S., and Opdyke, Neil, 1968, Comparison of sedimentation rates measured by paleomagnetic and the ionium methods of age determination: Earth and Planetary Science Letters, v. 4, p. 1–16.

Kulm, L. D., and others, 1973, Initial reports of the deep sea drilling project, Leg 18: Washington, U. S. Government Printing Office, v. 18, 1077 p.

LaBrecque, J. L., Kent, D. V., and Cande, S. C., 1977, Revised magnetic polarity time scale for late Cretaceous and Cenozoic time: Geology, v. 5, p. 330–335.

Lagoe, M. B., 1976, Species diversity of deep-sea benthic foraminifera from the central Arctic Ocean: Geological Society of America Bulletin, v. 87, p. 1678–1683.

———1977, Recent benthic foraminifera from the central Arctic Ocean: *Journal of Foraminifera Research*, v. 7, p. 106–129.

Larson, J. A., 1975, Arctic Ocean foraminifera abundance and its relationship to equatorial Pacific Ocean solution cycles: Geology, v. 3, p. 491–492.

Laughton, A. S., and others, 1972, Initial reports of the deep sea drilling project: Washington, U. S. Government Printing Office, v. 12, 1243 p.

Li, Y. H., Bischoff, James, and Mathieu, Guy, 1969, The migration of manganese in the Arctic Basin sediment: Earth and Planetary Science Letters, v. 7, p. 265–270.

Margolis, S. V., Bowser, C. J., and others, 1975, Ferromanganese deposits of the ocean floor: cruise report Mn-74-02, R. V. MONA WAVE: Hawaii Institute for Geophysics Technical Report H16-75-17, p. 12–14.

Mavis, F. T., Ho, C., and Lu, Y. C., 1935, The transportation of detritus by flowing water: Iowa University Studies in Engineering Bulletin, no. 5, 53 p.

Middleton, G. V., and Hampton, M. A., 1973, Sediment gravity flows: mechanics of flow and deposition, *in* Middleton, G. V., and Bouma, A. H., cochairmen, Pacific Section Short Course Lecture Notes: Society of Economic Paleontologists and Mineralogists, 157 p.

Millot, Georges, 1970, Geology of clays: translated by Farrand, W. R., and Paquet, Helene: New York, Springer-Verlag, 429 p.

Moore, W. S., 1973, Accumulation rates of manganese crusts on rocks exposed on the sea floor, *in* Phase I report, inter-university program of research on ferromanganese deposits of the ocean floor: National Science Foundation, Washington [unpublished].

Mullen, R. E., Darby, D. A., and Clark, D. L., 1972, Significance of atmospheric dust and ice rafting for Arctic Ocean sediment: Geological Society of America Bulletin, v. 83, p. 205–212.

Naidu, A. S., and Mowatt, T. C., 1975, Depositional environments and sediment characteristics of the Colville and adjacent deltas, northern Arctic Alaska, *in* Broussard, M. L. S., ed., Deltas: models for

exploration: Houston Geological Society, p. 283–309.

Naidu, A. S., Burrell, D. C., and Hood, D. W., 1971, Clay mineral composition and geologic significance of some Beaufort Sea sediments: Journal of Sedimentary Petrology, v. 41, p. 691–694.

Naidu, A. S., Mowatt, T. C., and Sharma, G. D., 1972, Texture, mineralogy and chemistry of Arctic Ocean sediments: Institute of Marine Science, University of Alaska–Fairbanks, Rept. R 72-12, 31 p.

Naidu, A. S., and others, 1974, Clay mineralogy and geochemistry of some Arctic Ocean sediments: significance of paleoclimate interpretations, *in* Weller, G., and Bowling, S. A., eds., Climate of the Arctic: Fairbanks, Geophysical Institute, University of Alaska, p. 59–67.

Ovenshine, A. T., 1970, Observations of iceberg rafting in Glacier Bay, Alaska, and the identification of ancient ice-rafted deposits: Geological Society of America Bulletin, v. 81, p. 891–894.

Paul, A. Z., Thorndike, E. M., Sullivan, L. G., Heezen, B. C., and Gerard, R. D., 1978, Observations of the deep-sea floor from 202 days of time lapse photography: Nature, v. 276, p. 812–814.

Poore, R. Z., and Berggren, W. A., 1974, Pliocene biostratigraphy of the Labrador Sea: calcareous plankton: Journal of Foraminiferal Research, v. 4, p. 91–108.

Ruddiman, W. F., 1971, Pleistocene sedimentation in the equatorial Atlantic; stratigraphy and faunal paleoclimatology: Geological Society of America Bulletin, v. 82, p. 238–302.

Schwarzacher, W., and Hunkins, K. L., 1961, Dredged gravels from the central Arctic Ocean, *in* Raasch, G. O., ed., Geology of the Arctic, V. 1: University of Toronto Press, p. 666–677.

Shackleton, N. J., and Opdyke, N. D., 1973, Oxygen isotope and paleomagnetic stratigraphy of equatorial Pacific core V28-238: oxygen isotope tmeperatures and ice volumes on a 10^5 and 10^6 year scale: Quaternary Research, v. 3, p. 39–55.

———1976, Oxygen-isotope and paleomagnetic stratigraphy of Pacific core V28-239, late Pliocene to latest Pleistocene, *in* Cline, R. M., and Hays, J. D., eds., Investigation of late Quaternary paleoceanography and paleoclimatology: Geological Society of America Memoir 145, p. 449–464.

Shackleton, N. J., and Kennett, J. P., 1975, Paleotemperature history of the Cenozoic and the initiation of Antarctic glaciation: oxygen and carbon isotope analyses in DSDP sites 277, 279, and 281, *in* Kennett, J. P., ed., Initial Reports of the DSDP, v. 29, p. 247–254.

Shepard, F. P., 1939, Continental shelf sediments, *in* Trask, P. D., ed., Recent marine sediments: a symposium: New York, Dover Publications, p. 219–229.

Steuerwald, B. A., Clark, D. L., and Andrew, J. A., 1968, Magnetic stratigraphy and faunal patterns in Arctic Ocean sediments: Earth and Planetary Science Letters, v. 5, p. 79–85.

Stoiber, R. E., and others, 1960, Petrographic evidence on the source area and age of T-3, *in* Bushnell, Vivian, ed., Scientific studies at Fletcher's Ice Island, T-3 (1952-1955), v. 3: Air Force Cambridge Research Center, ASTIA Doc. No. AD-216815.

Talwani, Manik, and others, 1976, Initial reports of the deep sea drilling project: Washington, U. S. Government Printing Office, v. 38, 1256 p.

Van Der Plas, L., and Tobi, A. C., 1965, A chart for judging the reliability of point counting results: American Journal of Science, v. 263, p. 87–90.

Watkins, N. D., and Kennett, J. P., 1977, Erosion of deep sea sediments in the southern ocean between longitude 70° E and 190° E and contrast in maganese nodule development, *in* Symposium on Antarctic Geology and Geophysics, 3rd, Abstracts: Madison, University of Wisconsin, p. 154

Manuscript Received by the Society September 10, 1979
Manuscript Accepted October 11, 1979

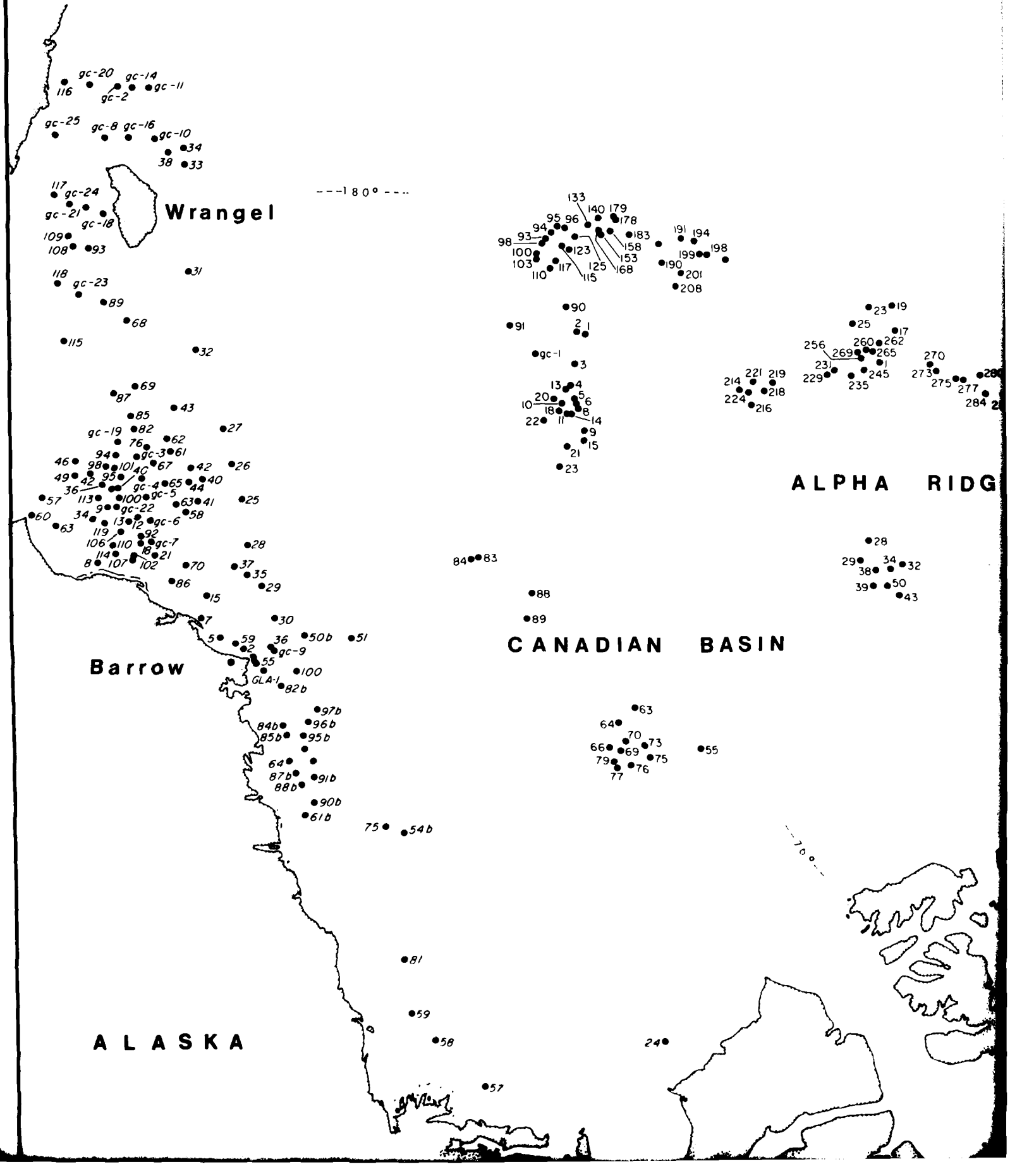
Wrangel
---180°---
ALPHA RIDG
CANADIAN BASIN
Barrow
ALASKA
-70°
gc-20
gc-14
gc-11
gc-2
116
gc-25
gc-8
gc-16
gc-10
34
38
33
117
gc-24
gc-21
gc-18
109
108
93
118
gc-23
89
68
115
31
32
69
87
43
85
gc-19
82
27
76
62
94
gc-3
61
46
98
101
40
67
42
26
49
42
95
36
gc-4
65
44
40
113
100
gc-5
63
41
25
57
9
gc-22
58
60
34
13
12
gc-6
63
119
92
106
110
gc-7
28
114
18
21
8
107
102
70
37
35
86
29
15
7
30
5
59
36
50b
51
2
gc-9
55
GLA-1
100
82b
97b
84b
96b
85b
95b
64
87b
91b
88b
90b
61b
75
54b
81
59
58
57
133
140
179
95
96
178
94
183
98
93
158
191
194
100
123
153
199
198
103
125
168
190
110
117
115
201
208
90
91
2
1
gc-1
3
13
4
20
5
6
10
18
8
14
22
11
9
15
21
23
23
19
25
17
256
260
262
269
265
231
1
229
245
235
270
273
275
277
214
221
219
224
218
216
28
29
34
32
38
39
50
43
84
83
88
89
63
64
70
66
69
73
79
75
77
76
55
24

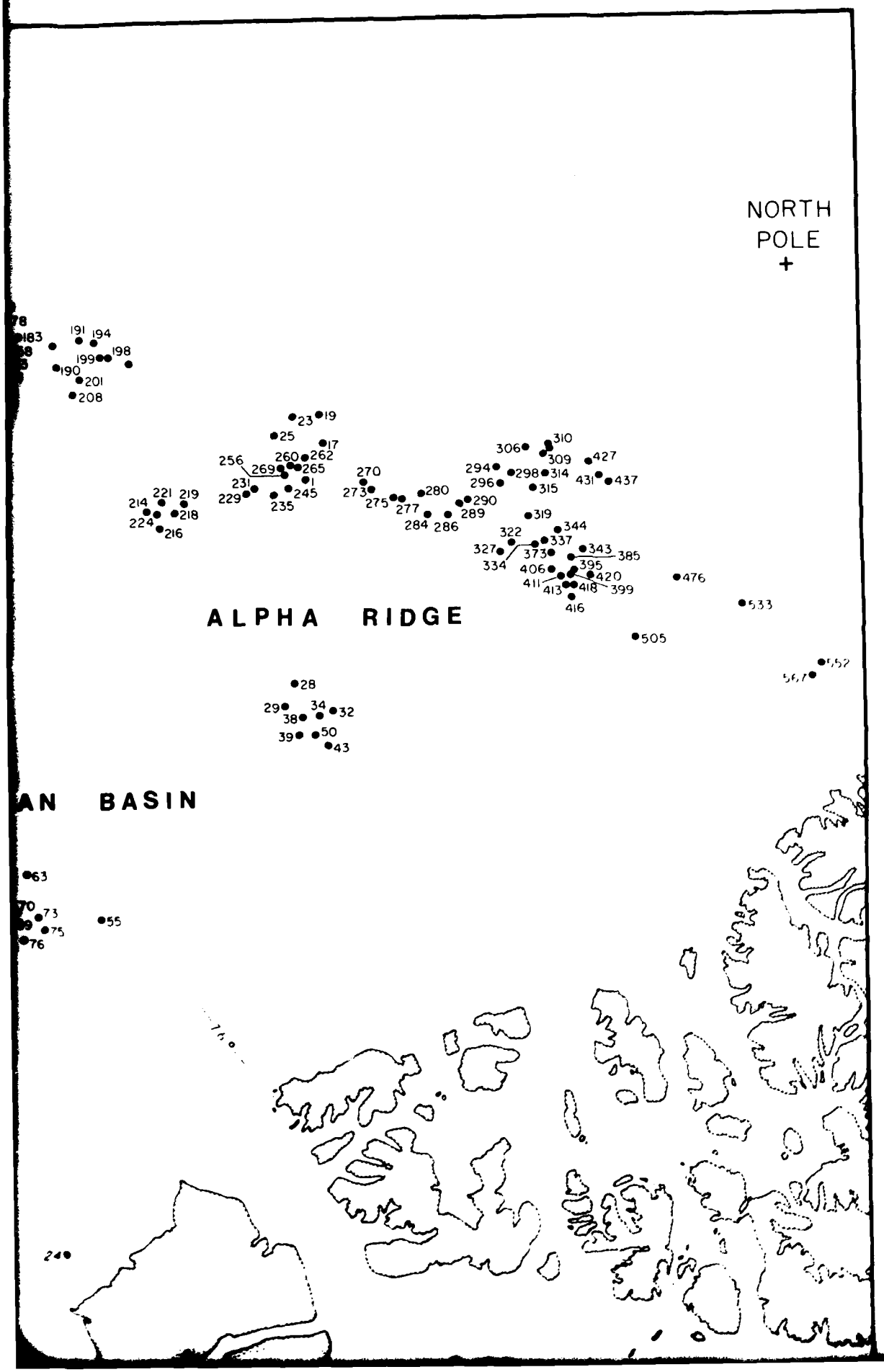
NORTH
POLE
+
ALPHA RIDGE
AN BASIN
78
183
191
194
198
199
190
201
208
23
19
25
17
256
260
262
269
265
231
1
229
245
235
270
273
280
275
277
284
286
290
289
319
306
310
309
427
294
298
314
431
437
296
315
322
344
337
327
373
343
385
334
395
406
420
411
413
418
399
416
476
533
505
56,7
52
28
29
34
38
32
39
50
43
63
70
73
55
75
76
240

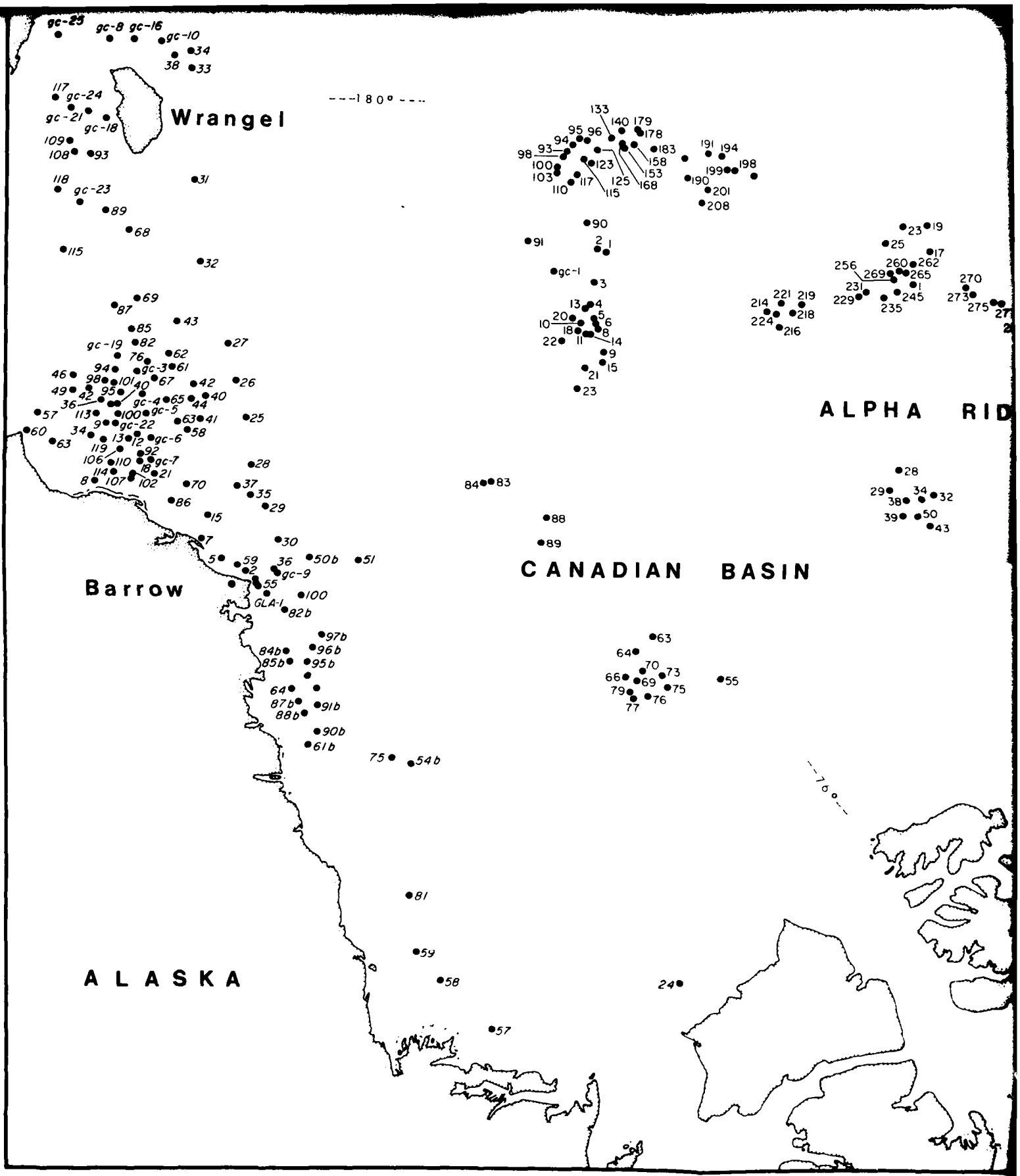

Plate 1. Index map showing location of the samples used in the mineralogic and textural data compilations that follow on Plates 2 to 8. All central Arctic Ocean points are T-3 cores (for example, No. 1-567). The points along the continental shelf east to the Canadian Arctic (letters followed by numbers and numbers followed by letters) are from Berry and Johns (1966), Biscaye (1965), Naidu and others (1971), Naidu and others (1974), Naidu and Sharma (1972), Naidu and Mowatt (1975), and the NOAA Computer Printout of Arctic Ocean Sediment Grain Size Data. Mineralogic data for the maps were taken from X-ray diffraction data usi continental shelf data have been recalcula and others (1954). This results in uniform different workers. This means that the co because of difficulties in converting data

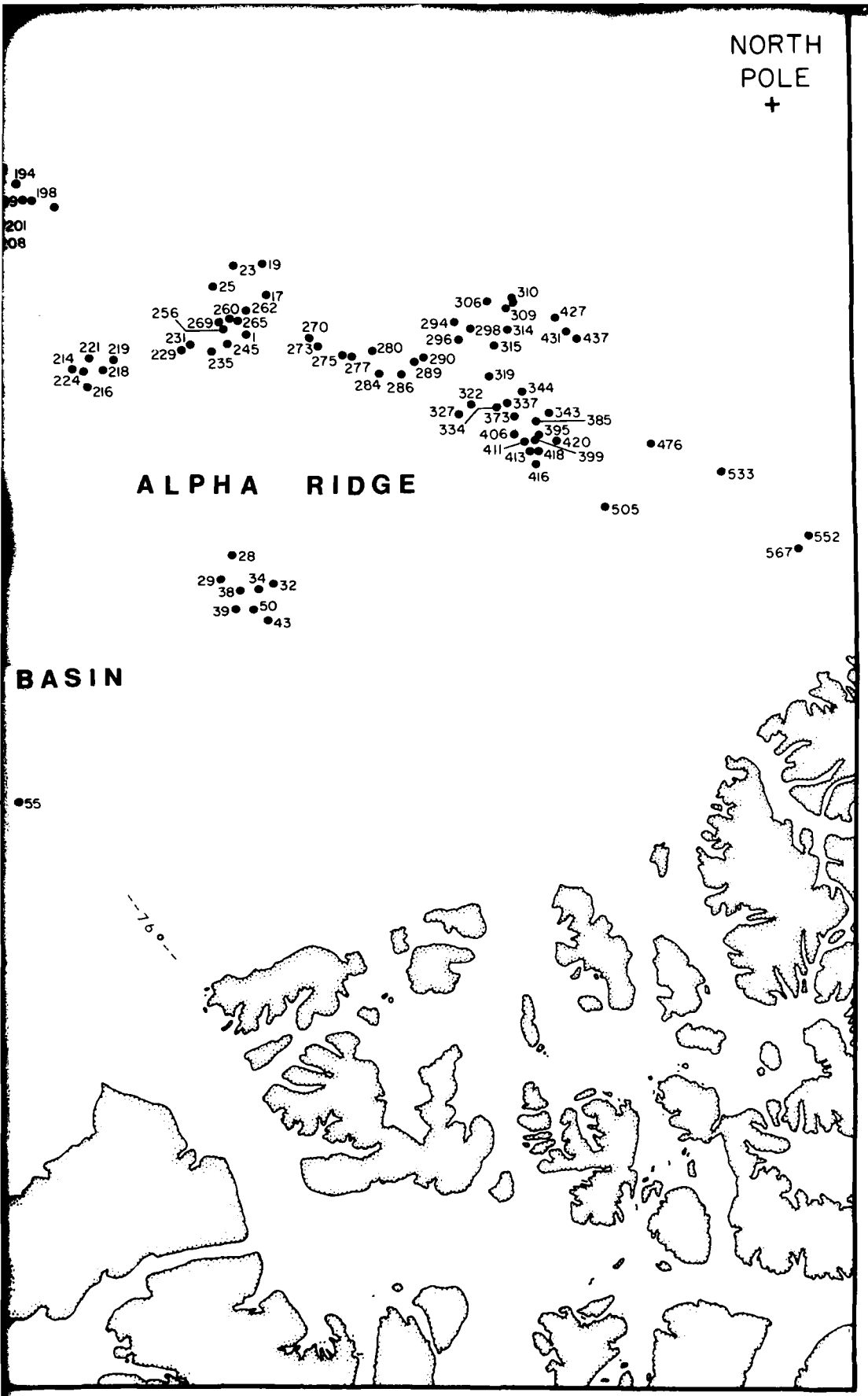

taken from X-ray diffraction data using the technique outlined by Biscaye (1965). Much of the continental shelf data have been recalculated using techniques and methods of Biscaye (1965) and Johns and others (1954). This results in uniform data for illite, but the nonillite clays were treated differently by different workers. This means that the continental shelf data for the nonillite clays are only approximate because of difficulties in converting data from different sources.

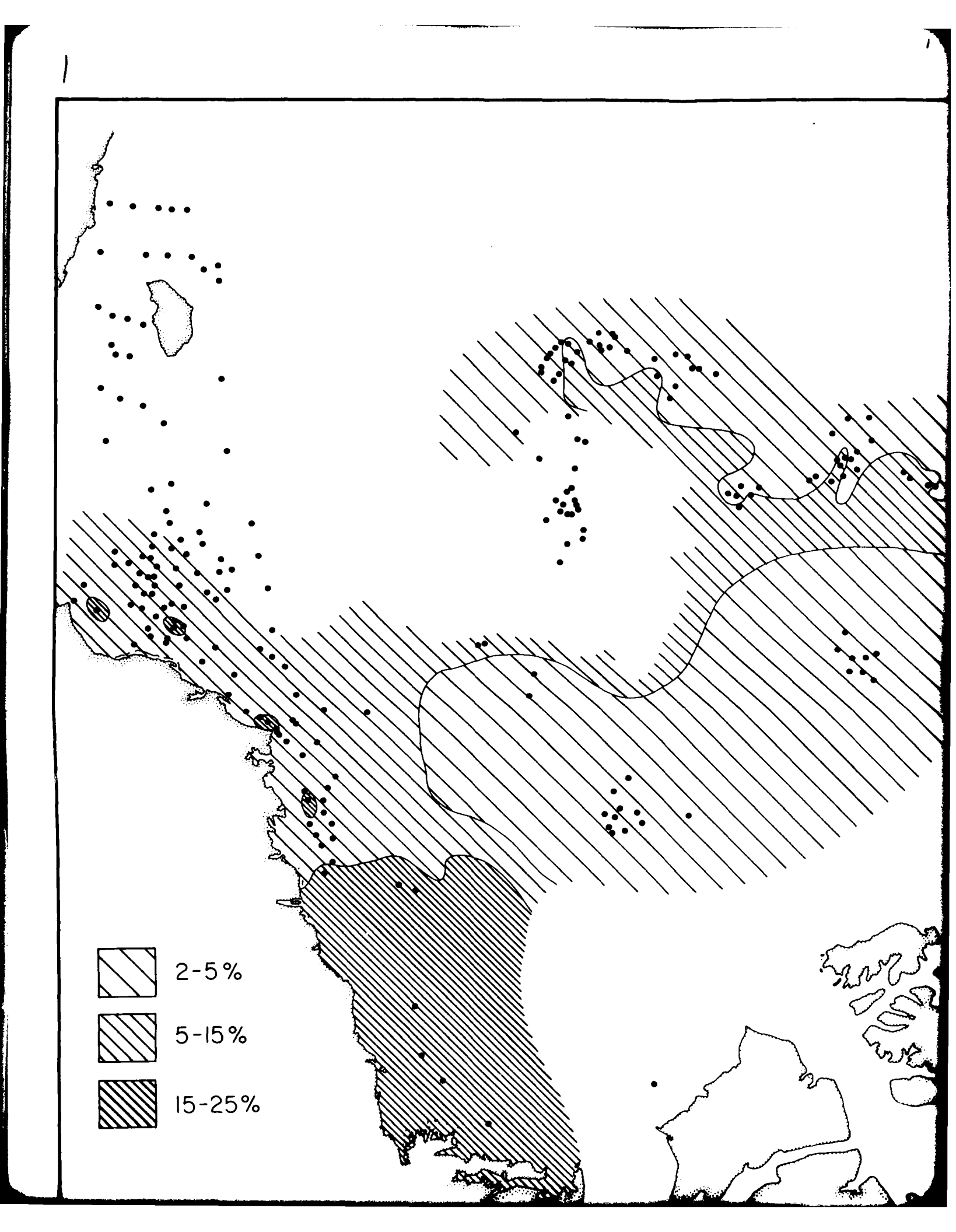
2-5%
5-15%
15-25%

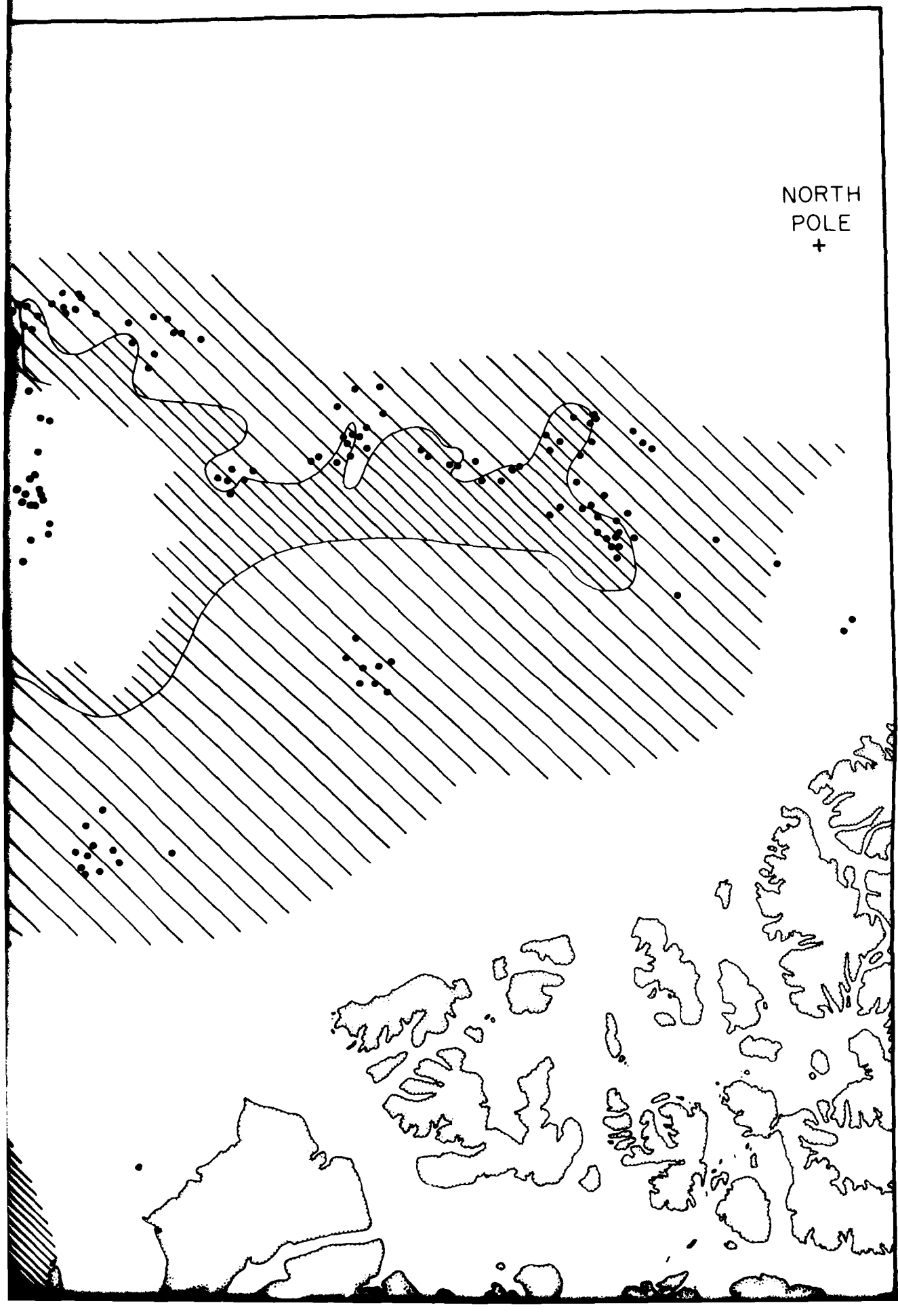
NORTH
POLE

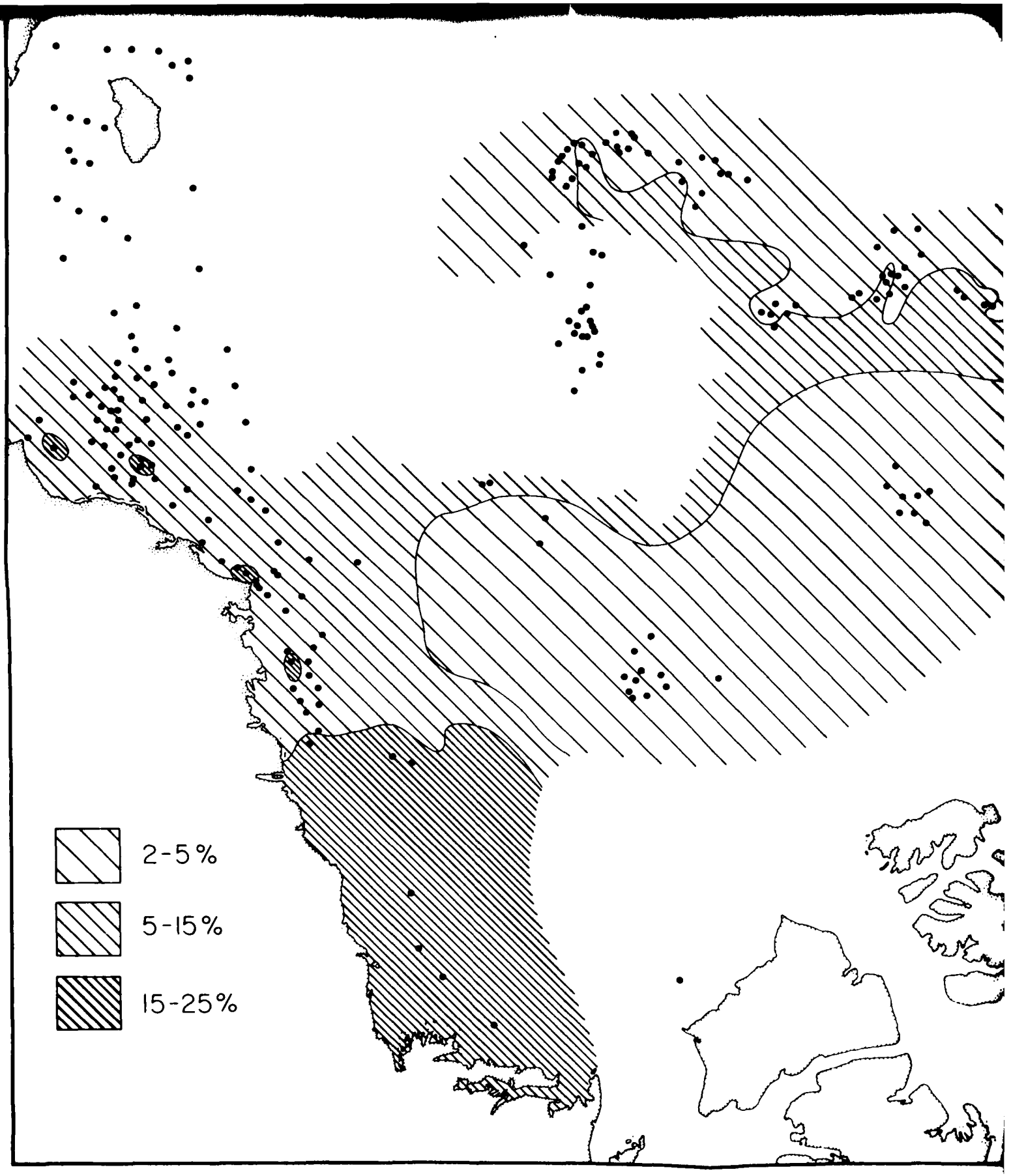

Plate 2. Percent kaolinite in surface sediment of the Arctic Ocean. See Plate 1 explanation for sample-number data and geographic information.

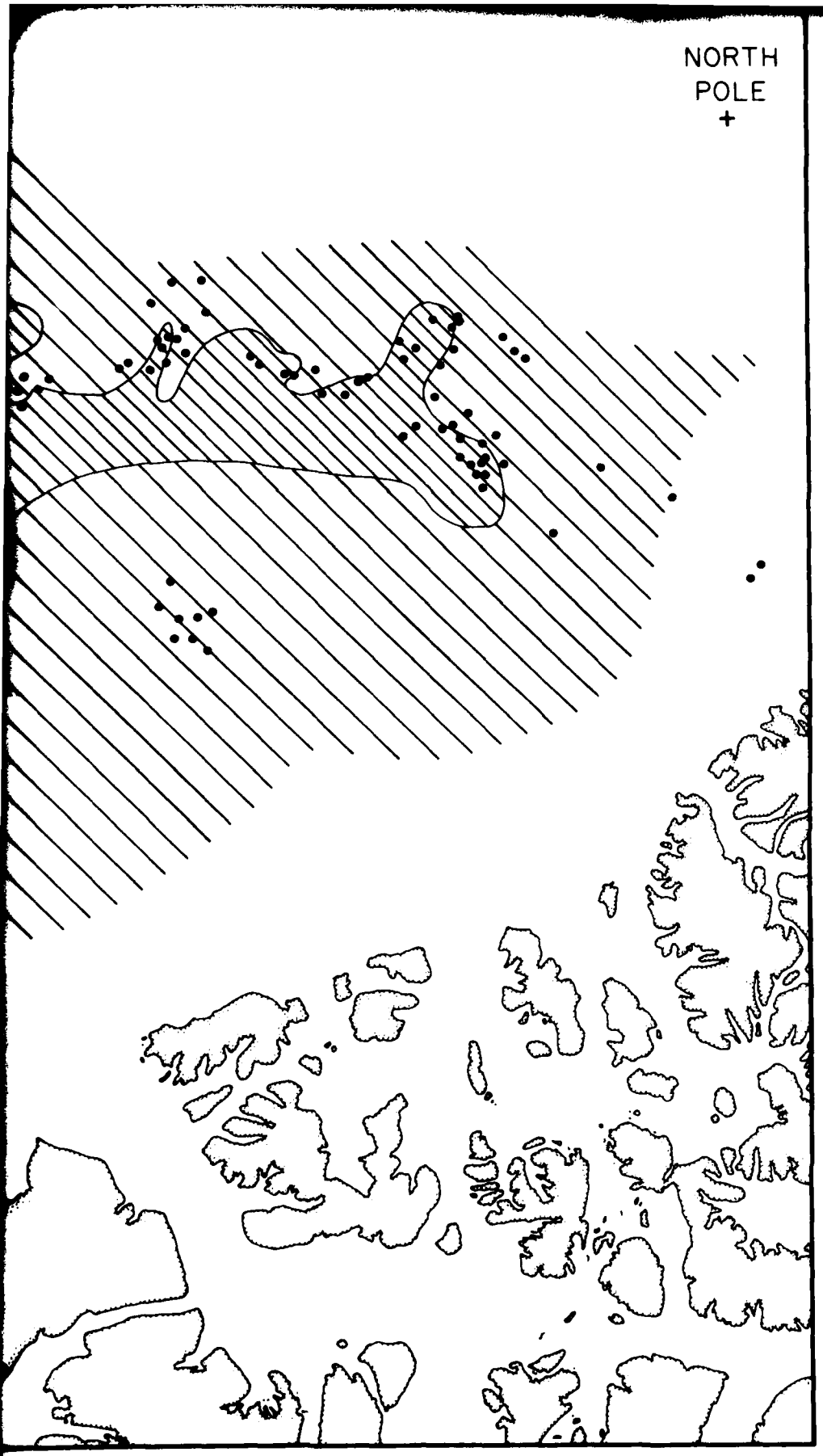

of the Arctic Ocean. See Plate 1
information.

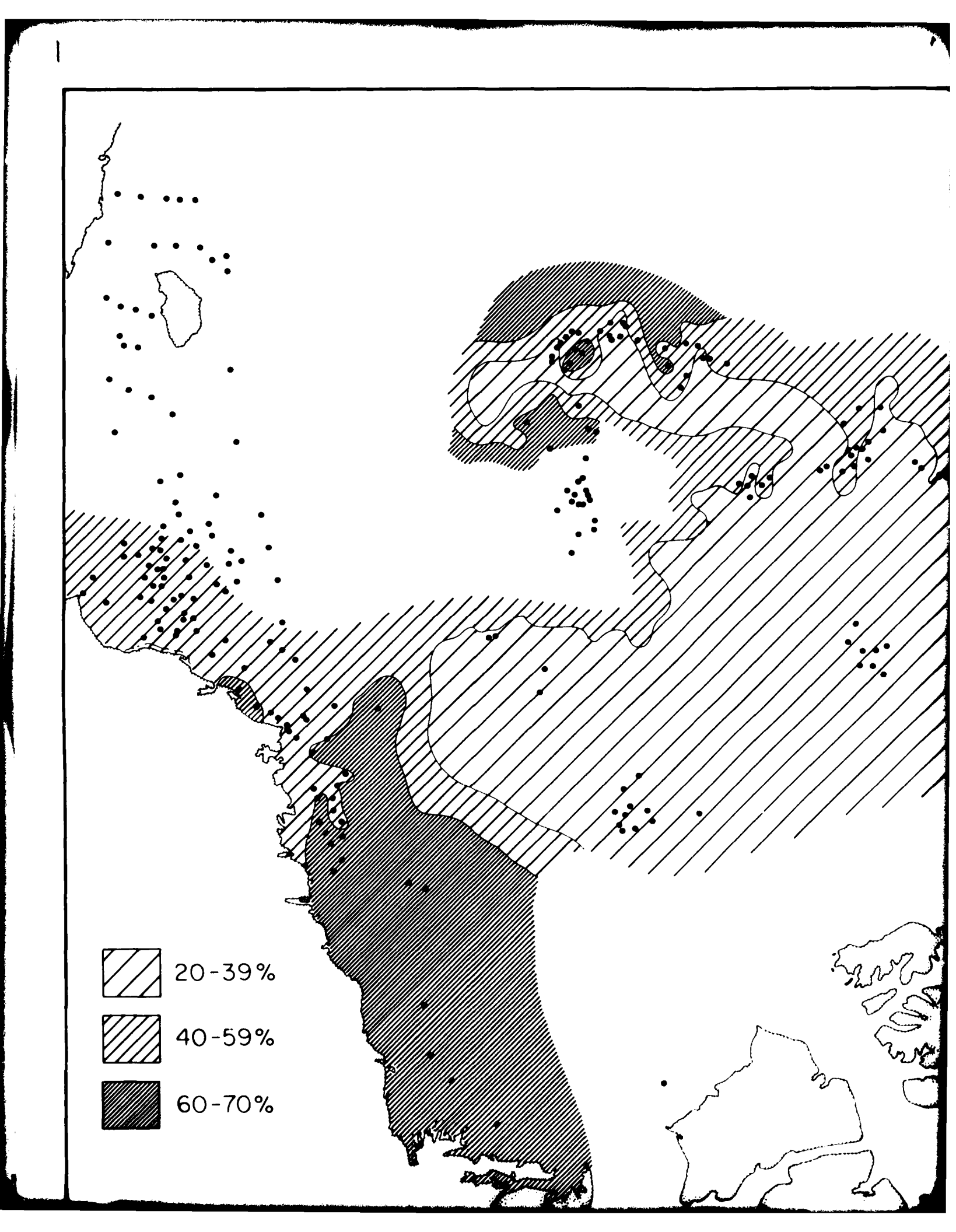
20-39%
40-59%
60-70%


NORTH
POLE

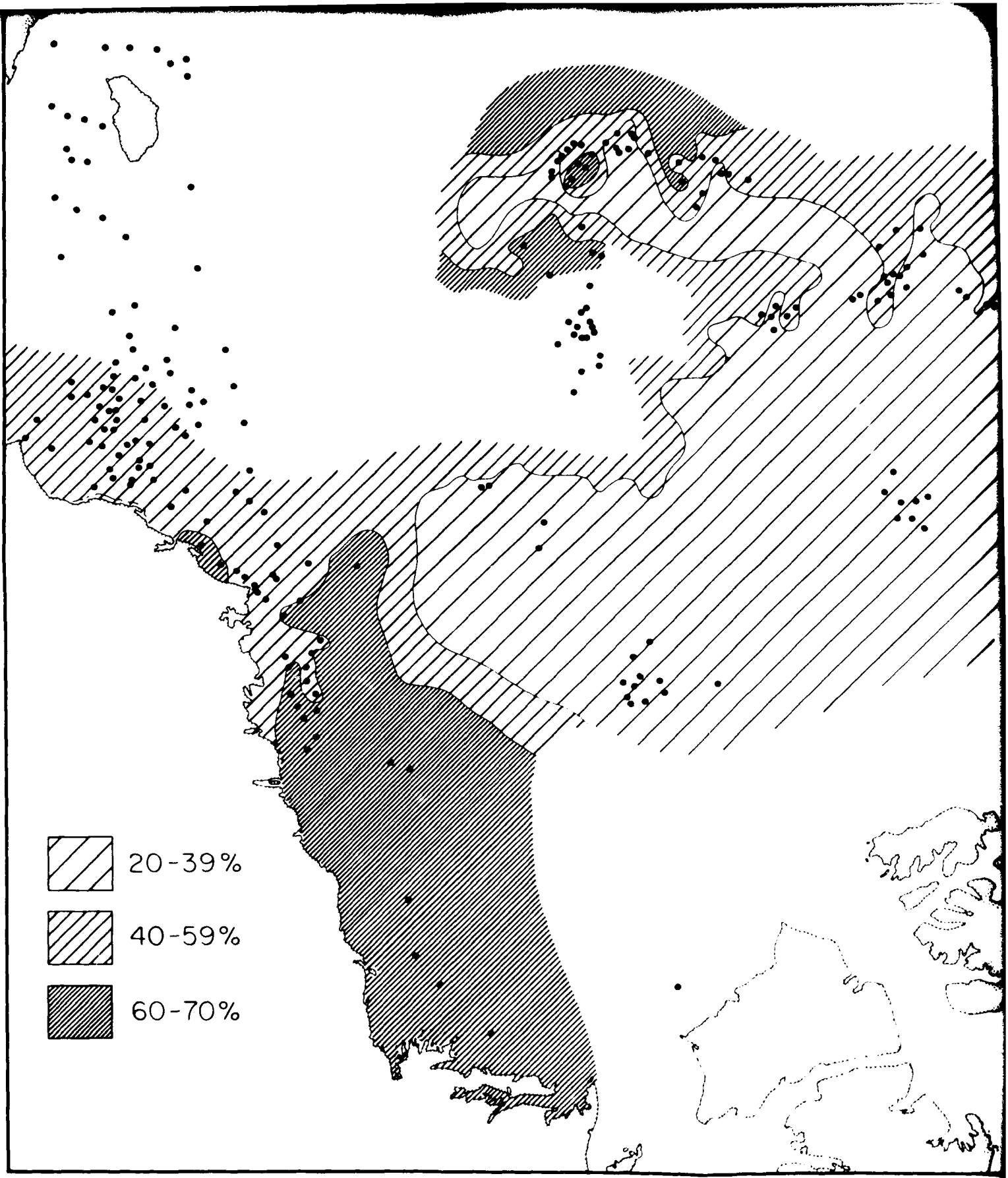

Plate 3. Percent illite in Arctic Ocean surface sediment. See Plate 1 explanation fo
sample-number data and geographic information

Plate 1 explanation for

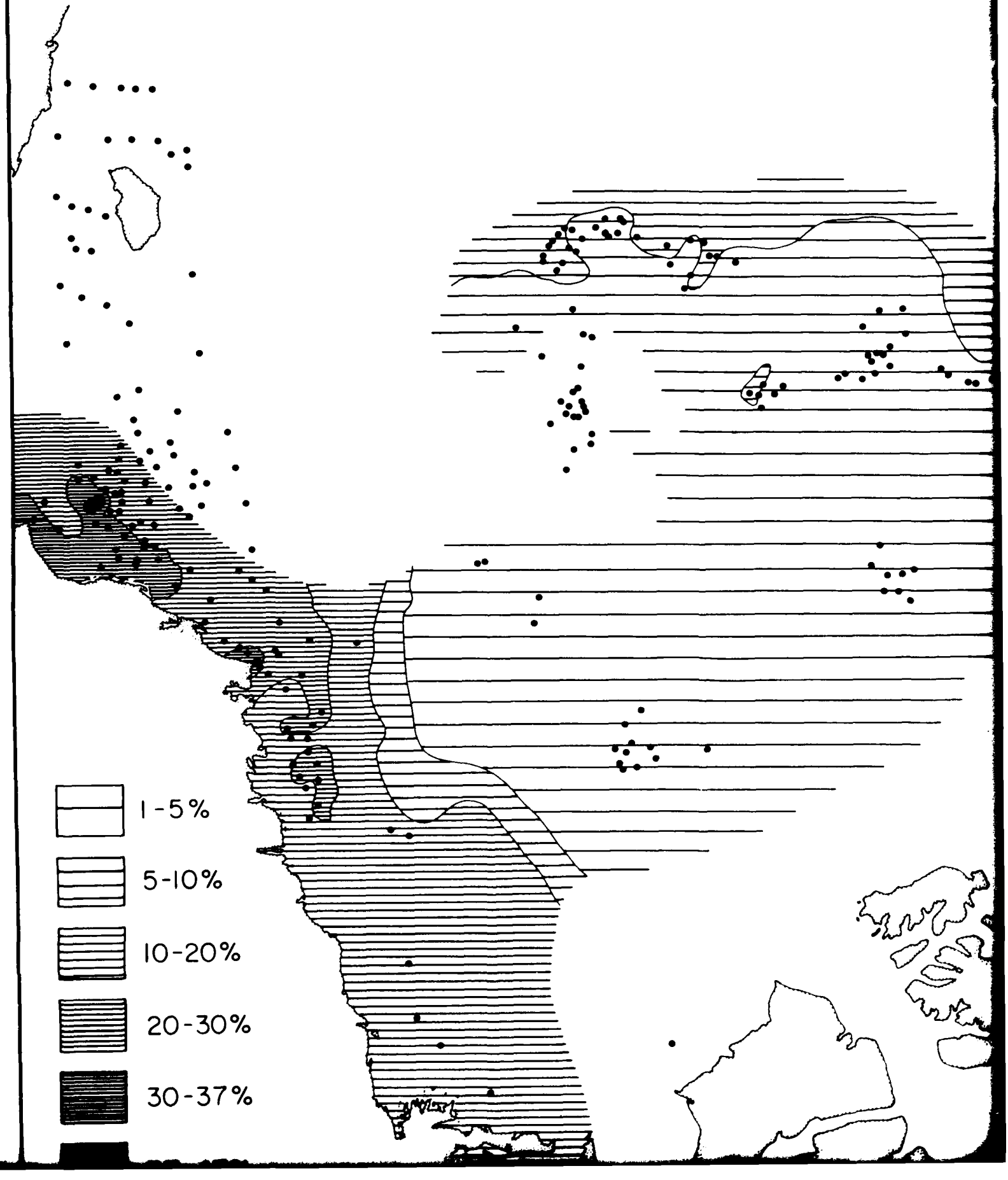
1-5%
5-10%
10-20%
20-30%
30-37%

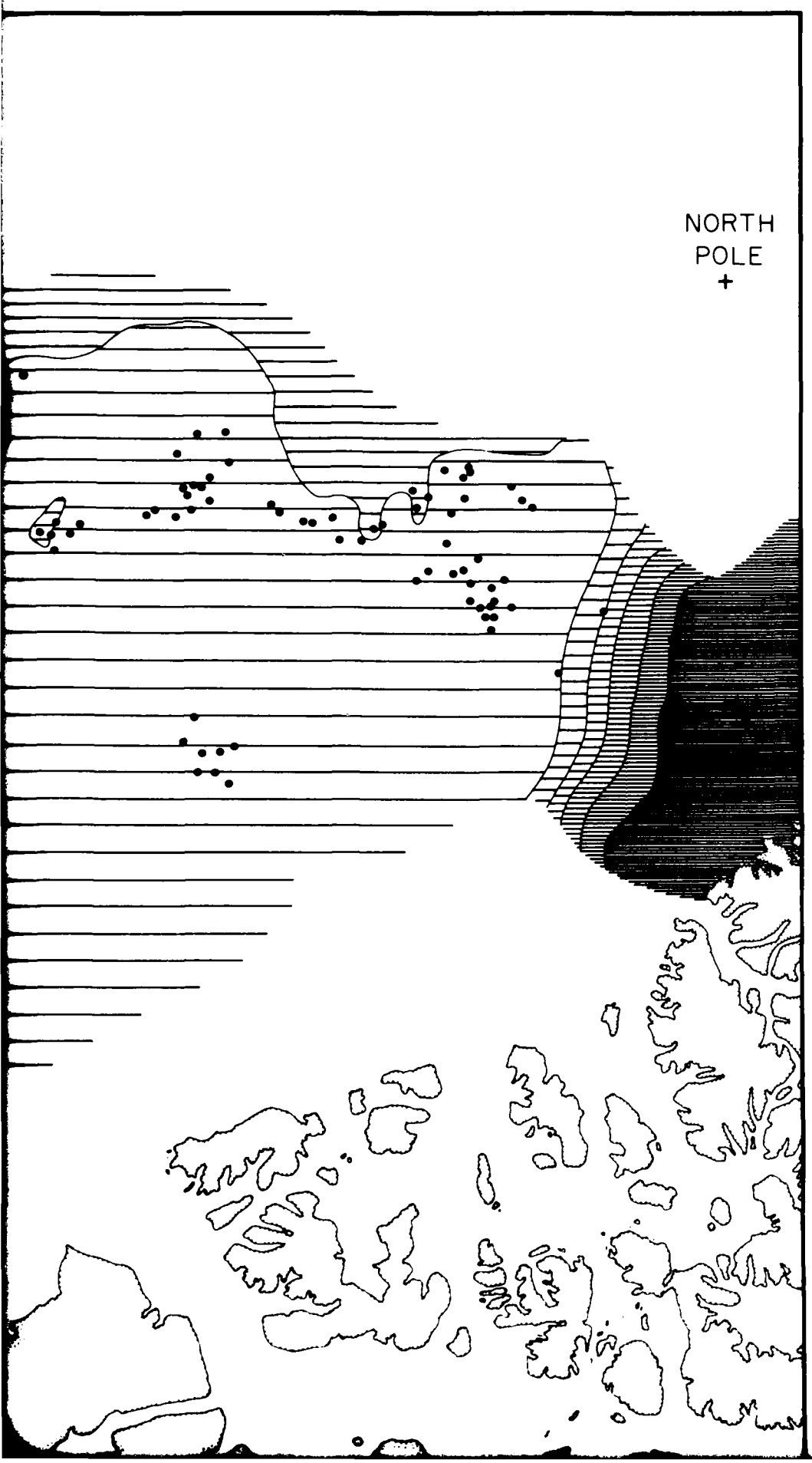
NORTH
POLE

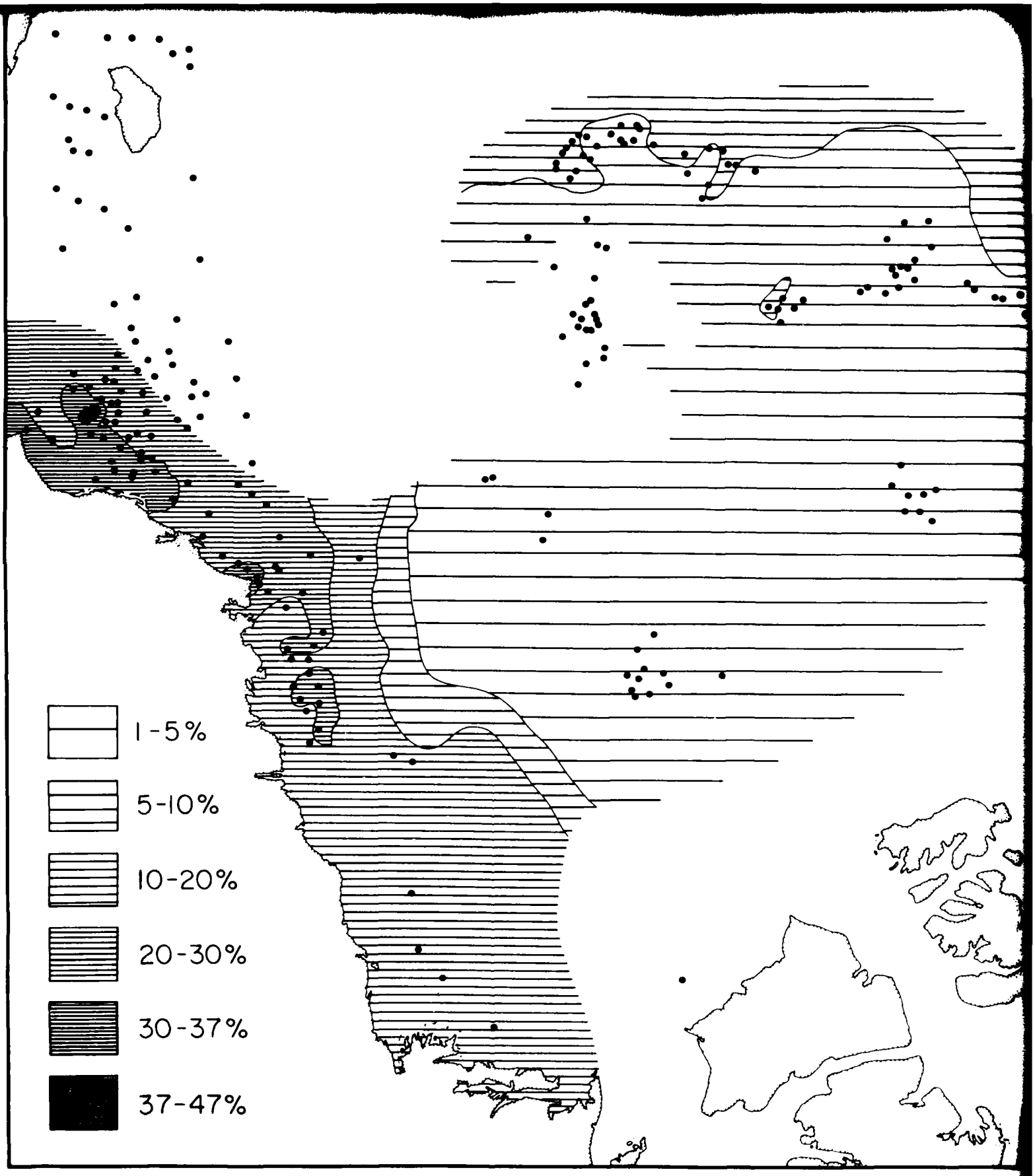

Plate 4. Percent chlorite in Arctic Ocean surface sediment. See Plate 1 explanation for sample-number data and geographic information.

3

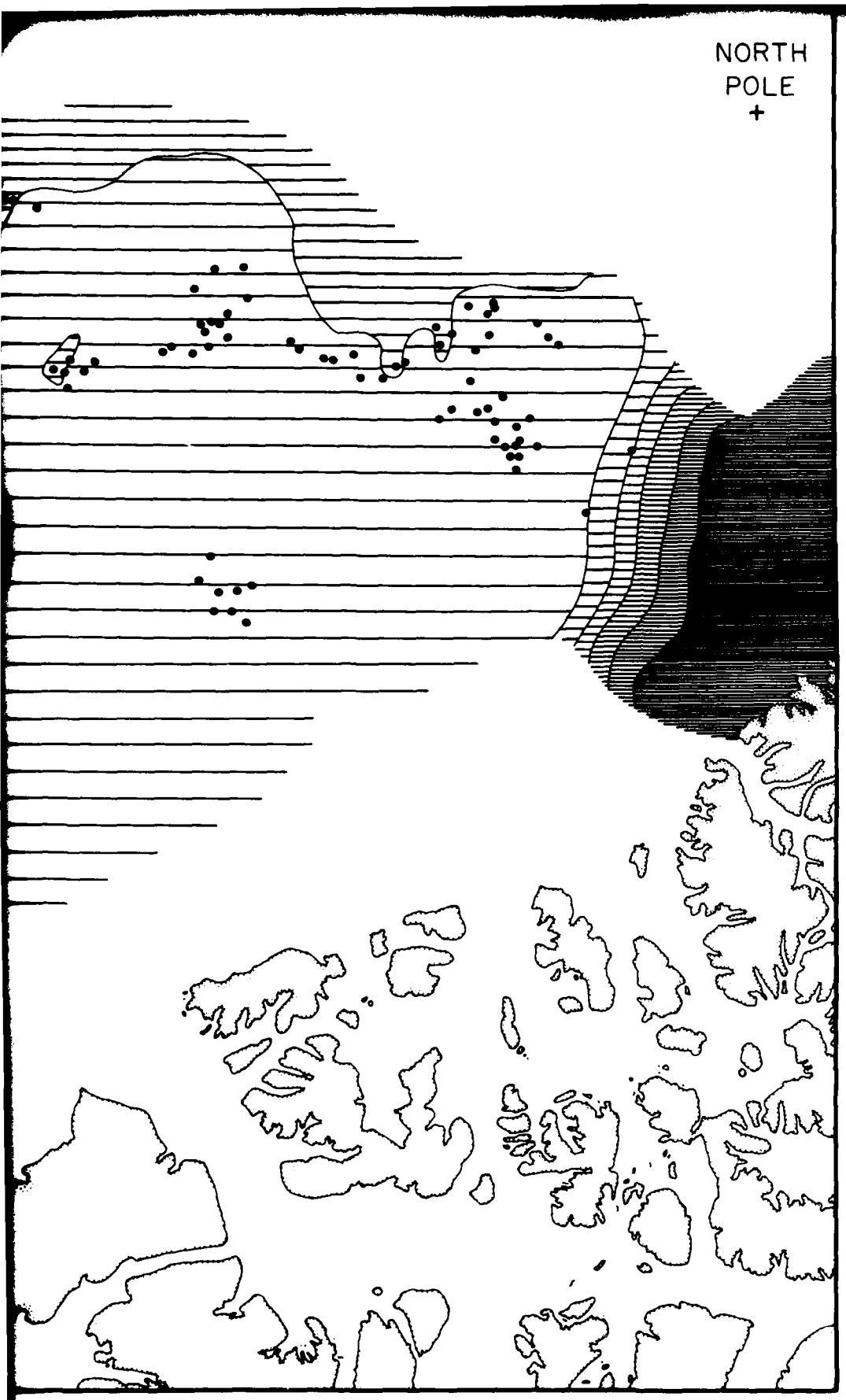

ice sediment. See Plate 1 explanation for
s.

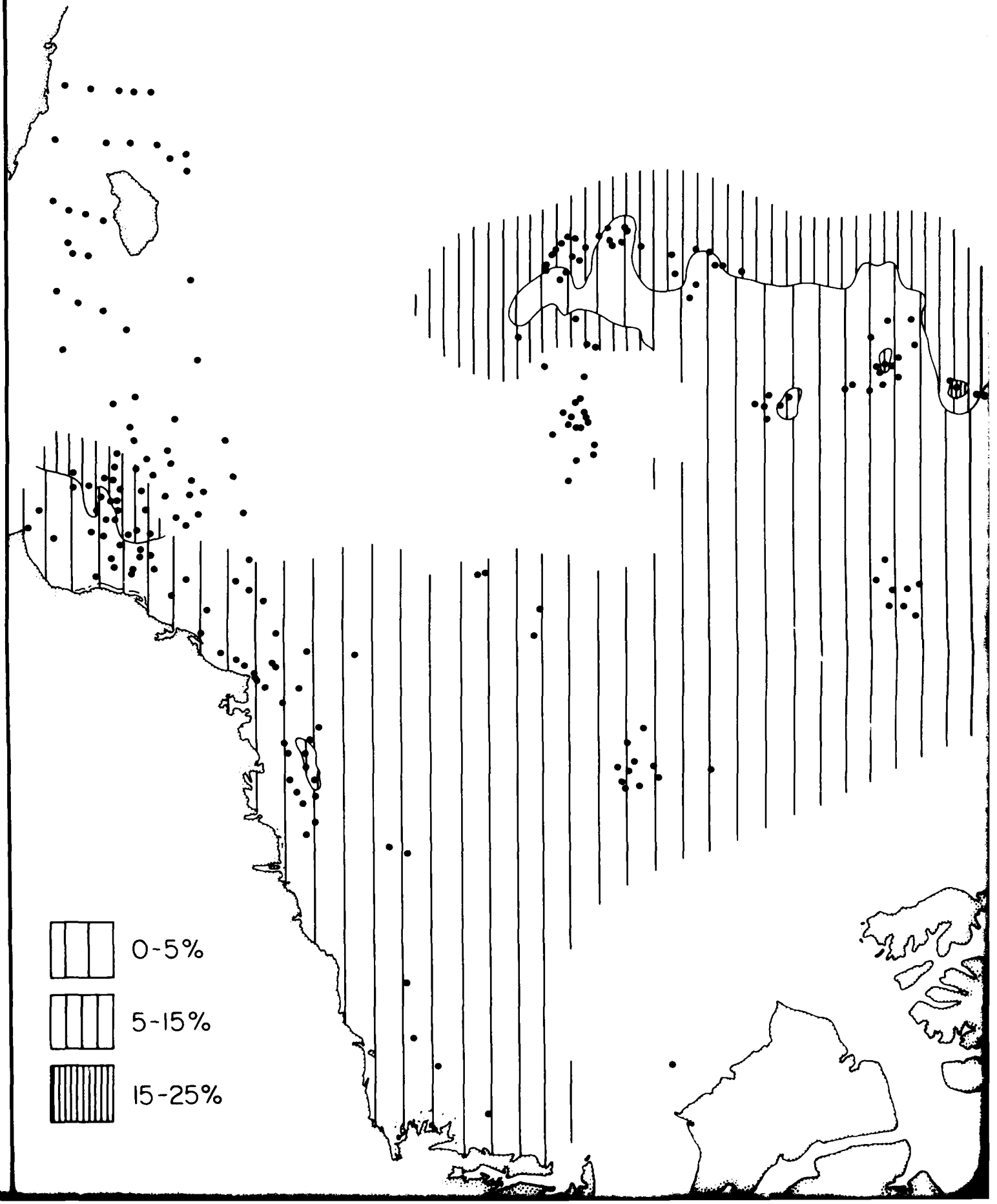
0-5%
5-15%
15-25%

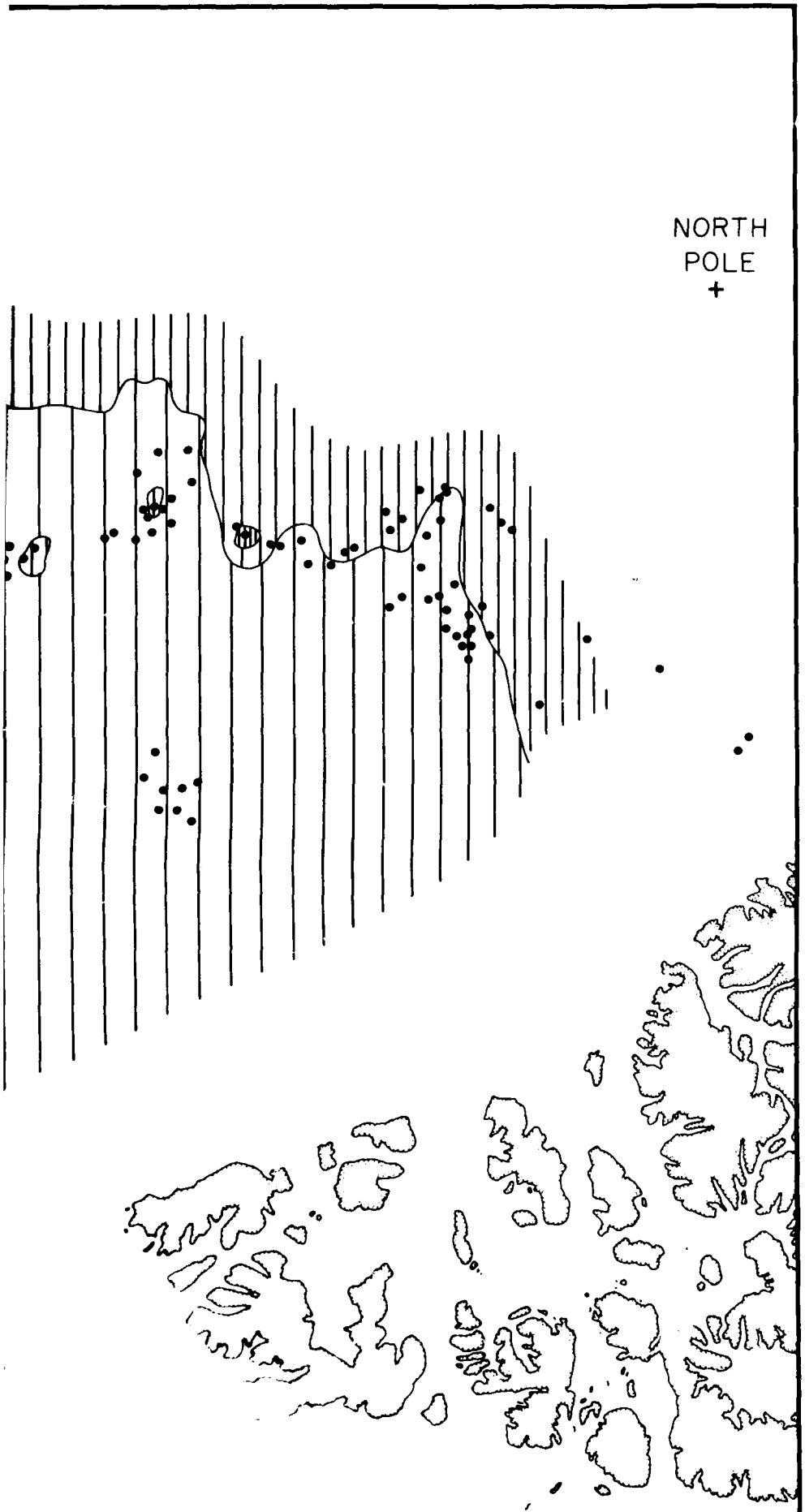
NORTH
POLE

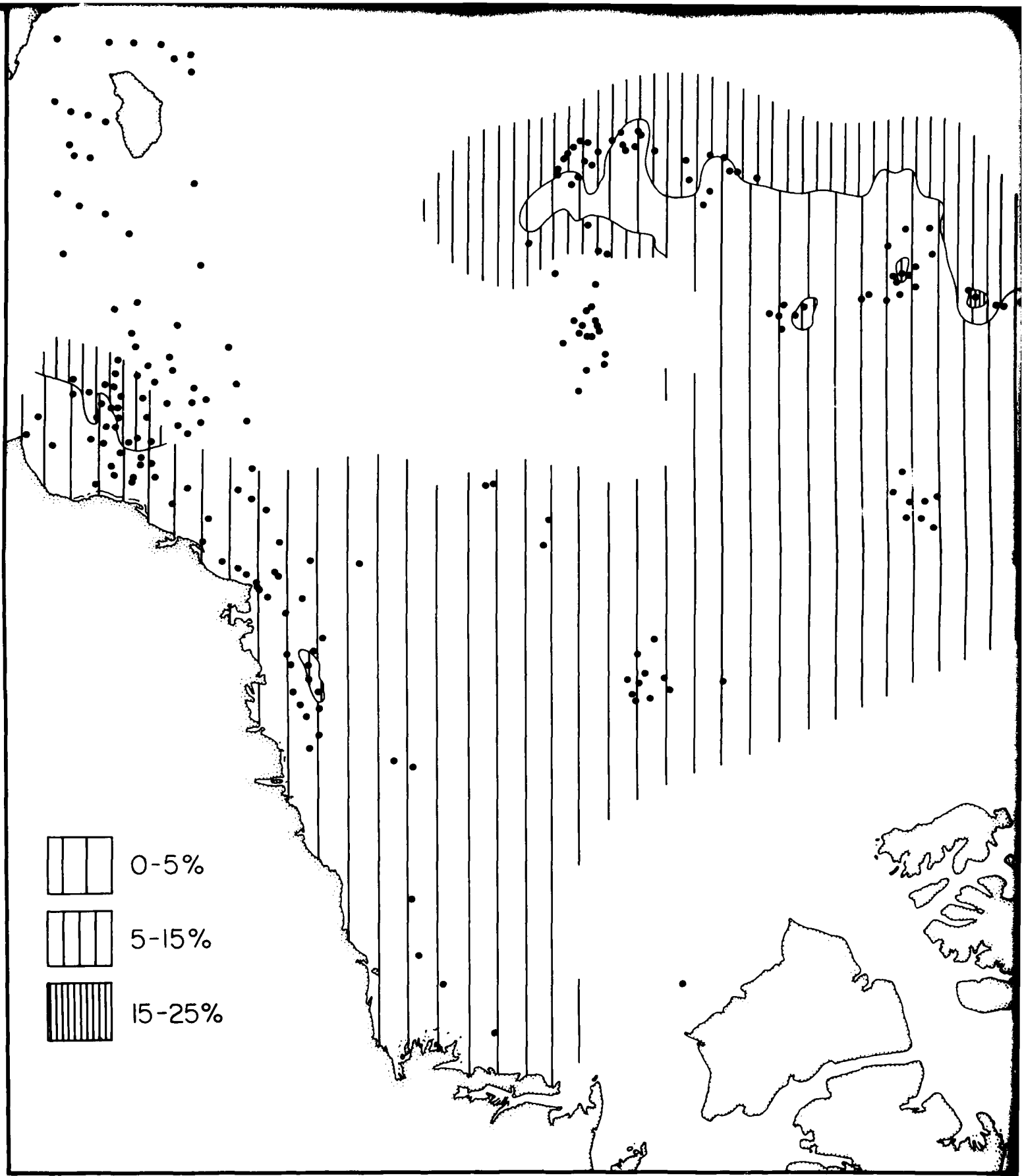

Plate 5. Percent smectite in Arctic Ocean surface sediment. See Plate 1 explanation fo
sample-number data and geographic information.

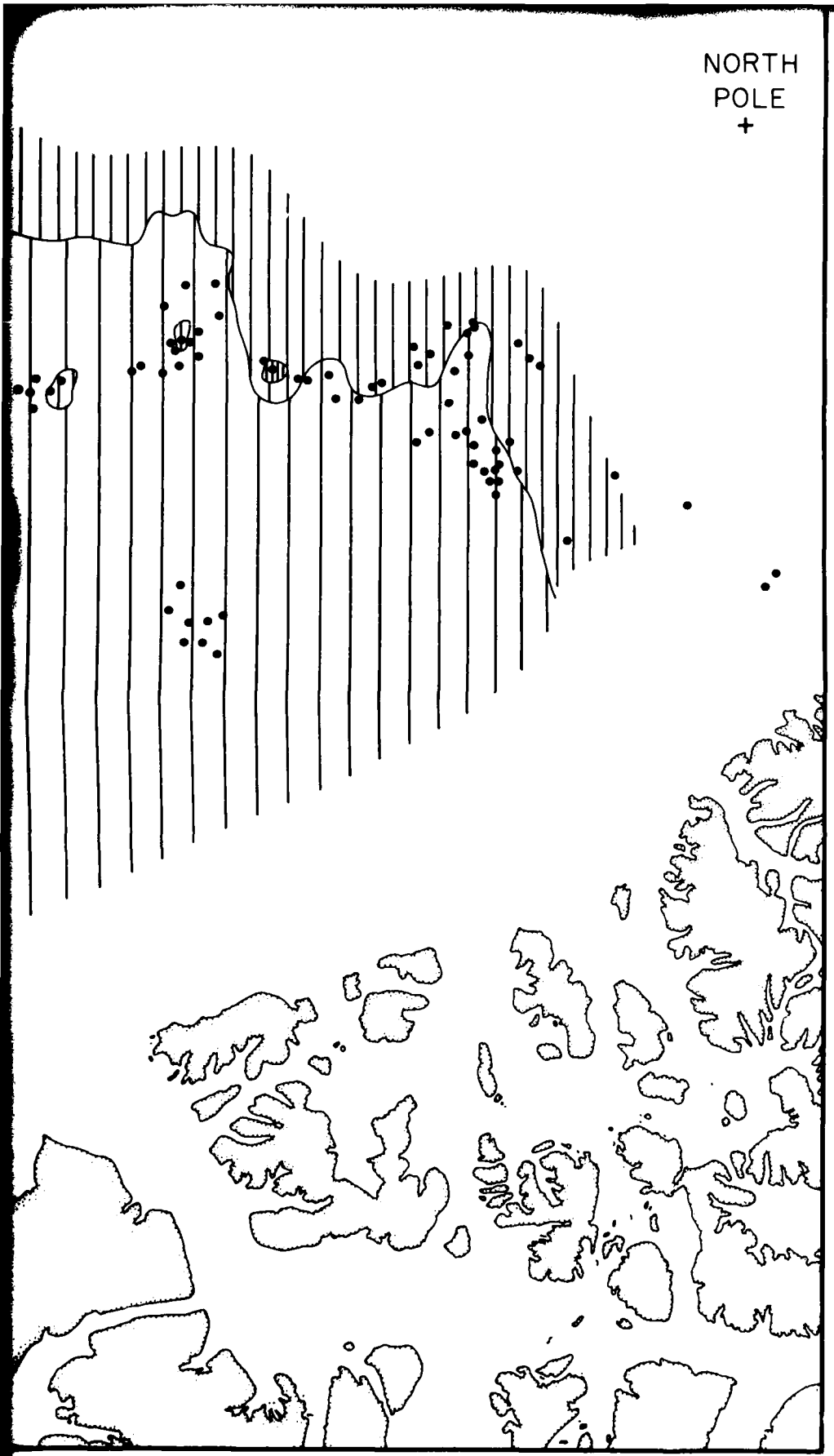

ediment. See Plate 1 explanation for

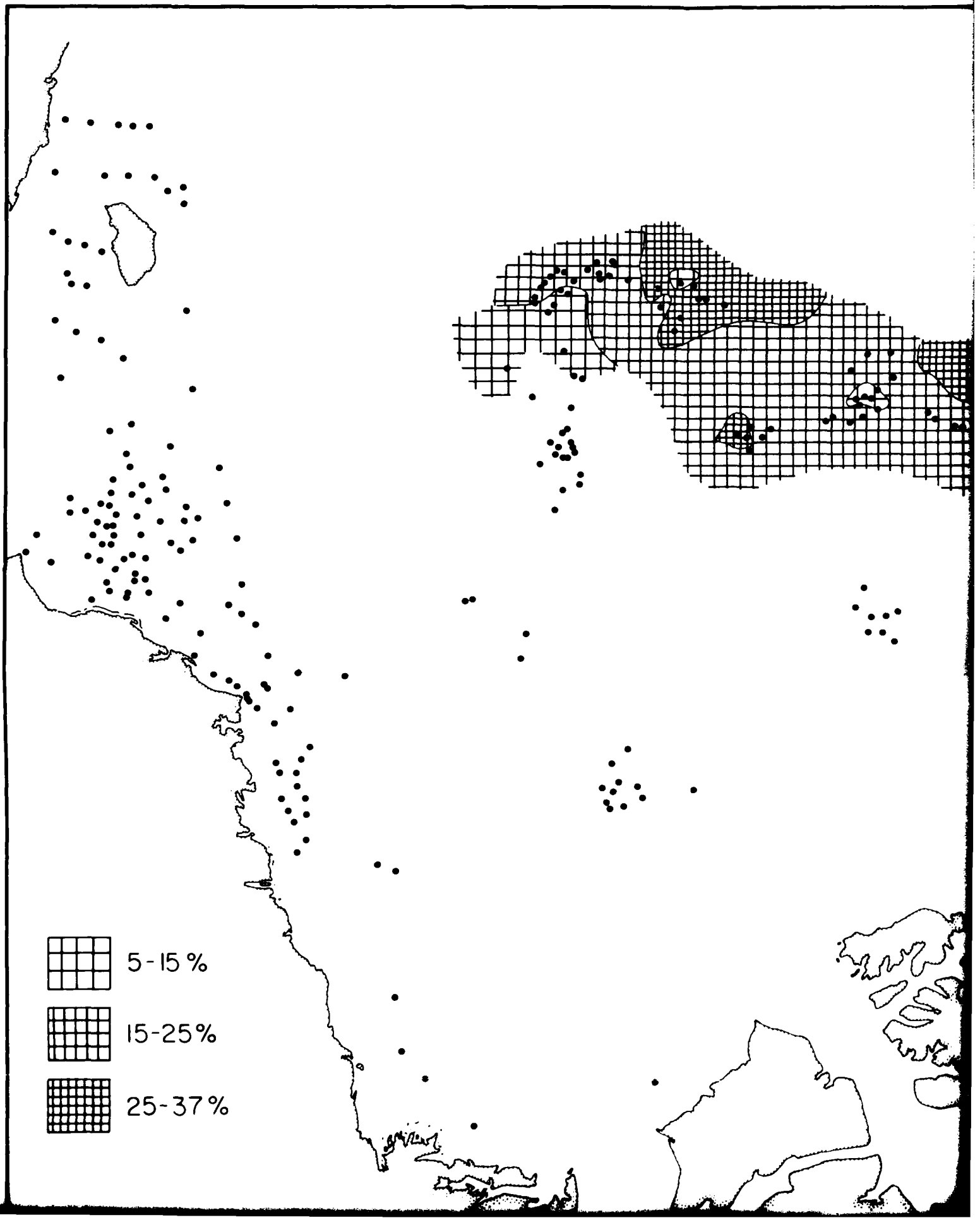
5-15%
15-25%
25-37%

'2

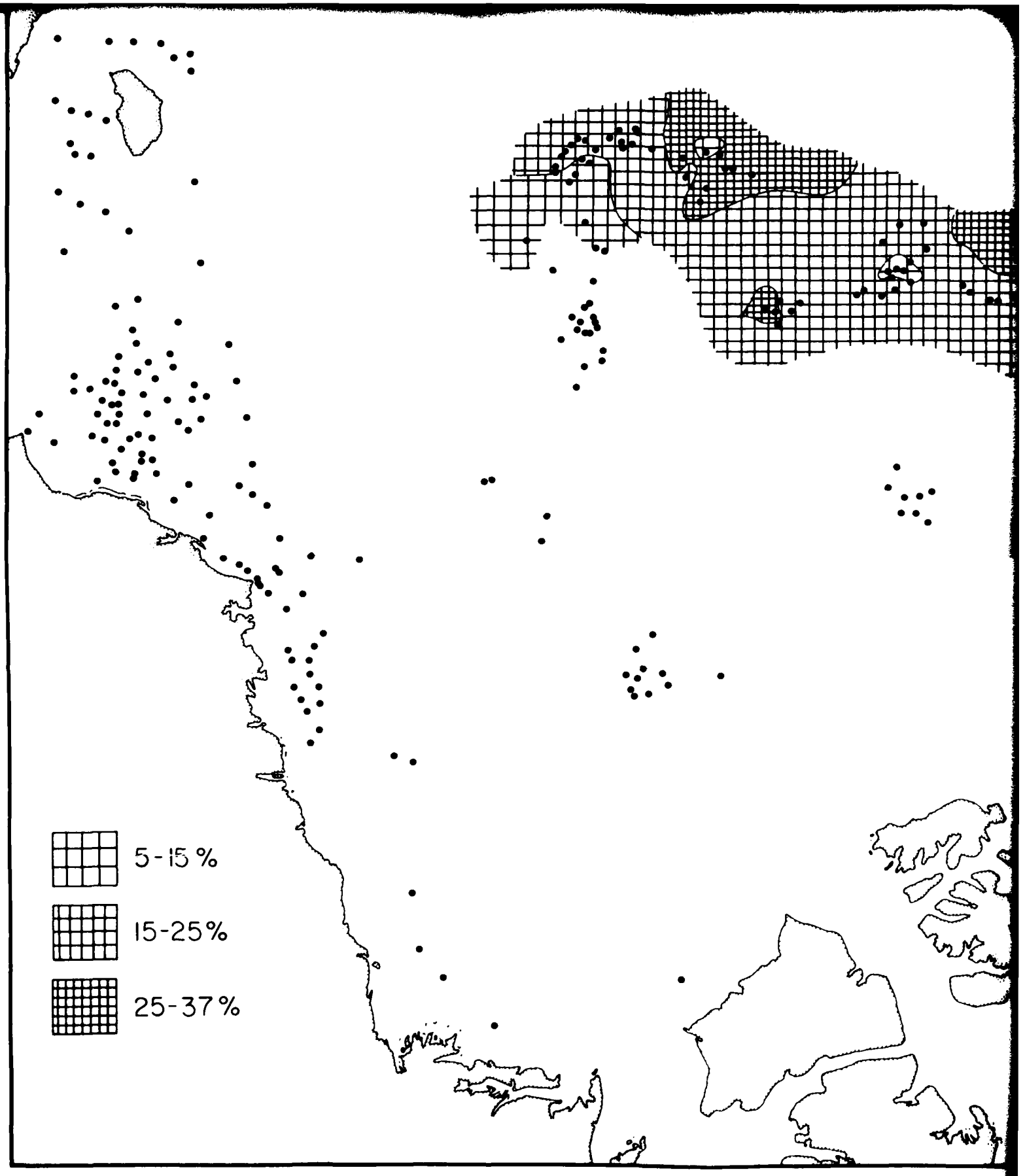

Plate 6. Percent mixed-layers collapsible in Arctic Ocean surface sediment. See Plate 1 explanation for sample-number data and geographic information.

Ocean surface sediment. See Plate 1
information.

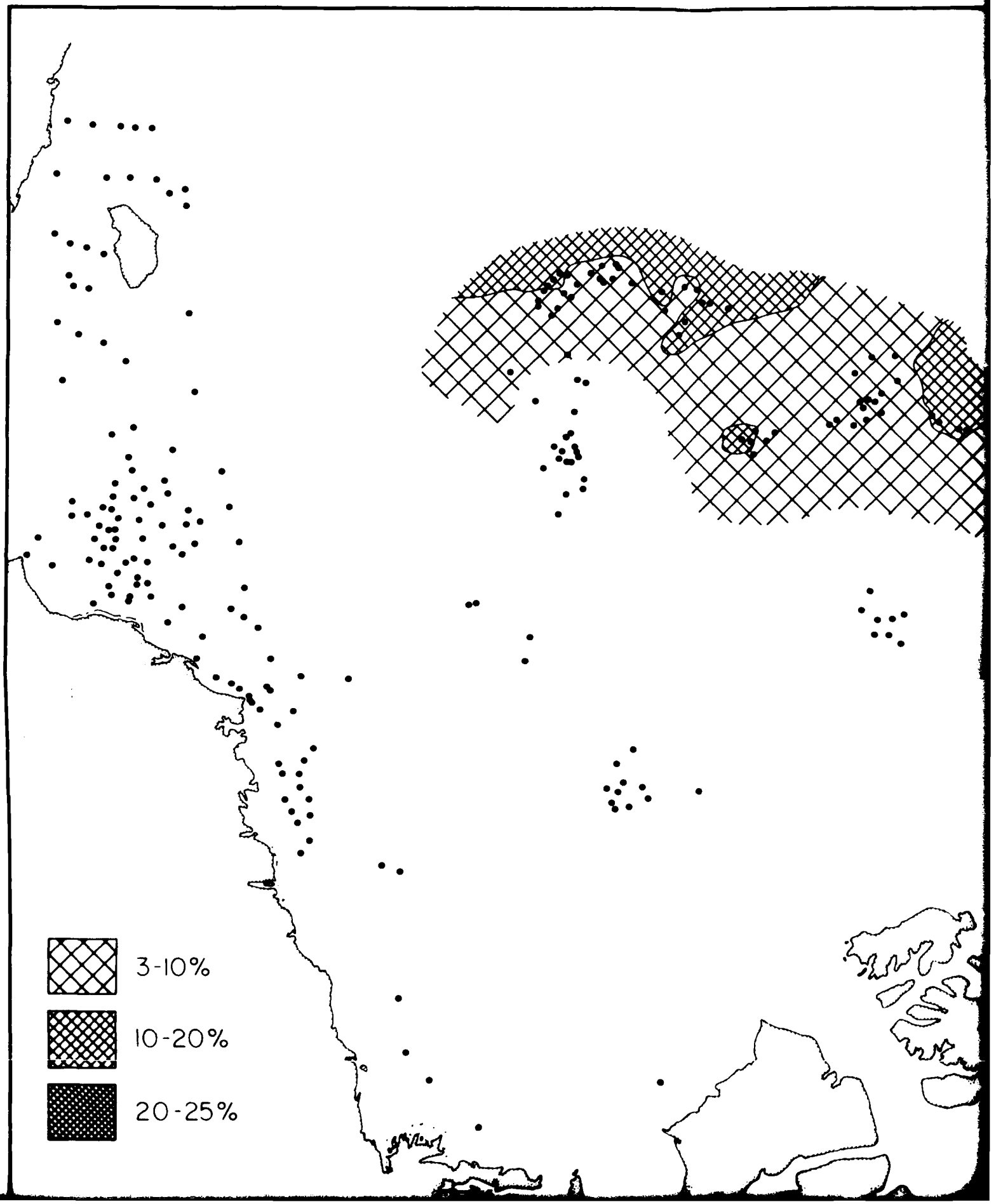
3-10%
10-20%
20-25%

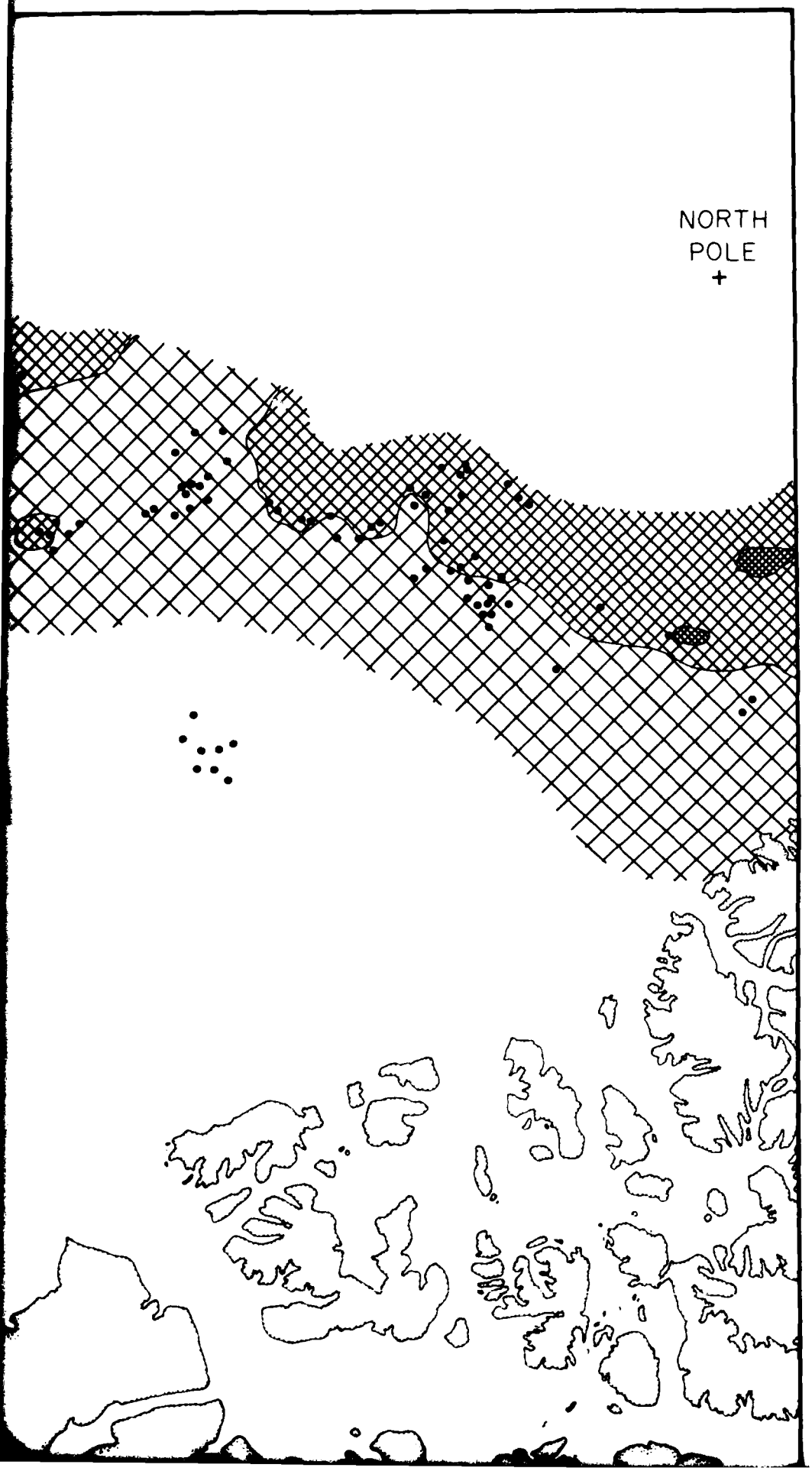
NORTH
POLE

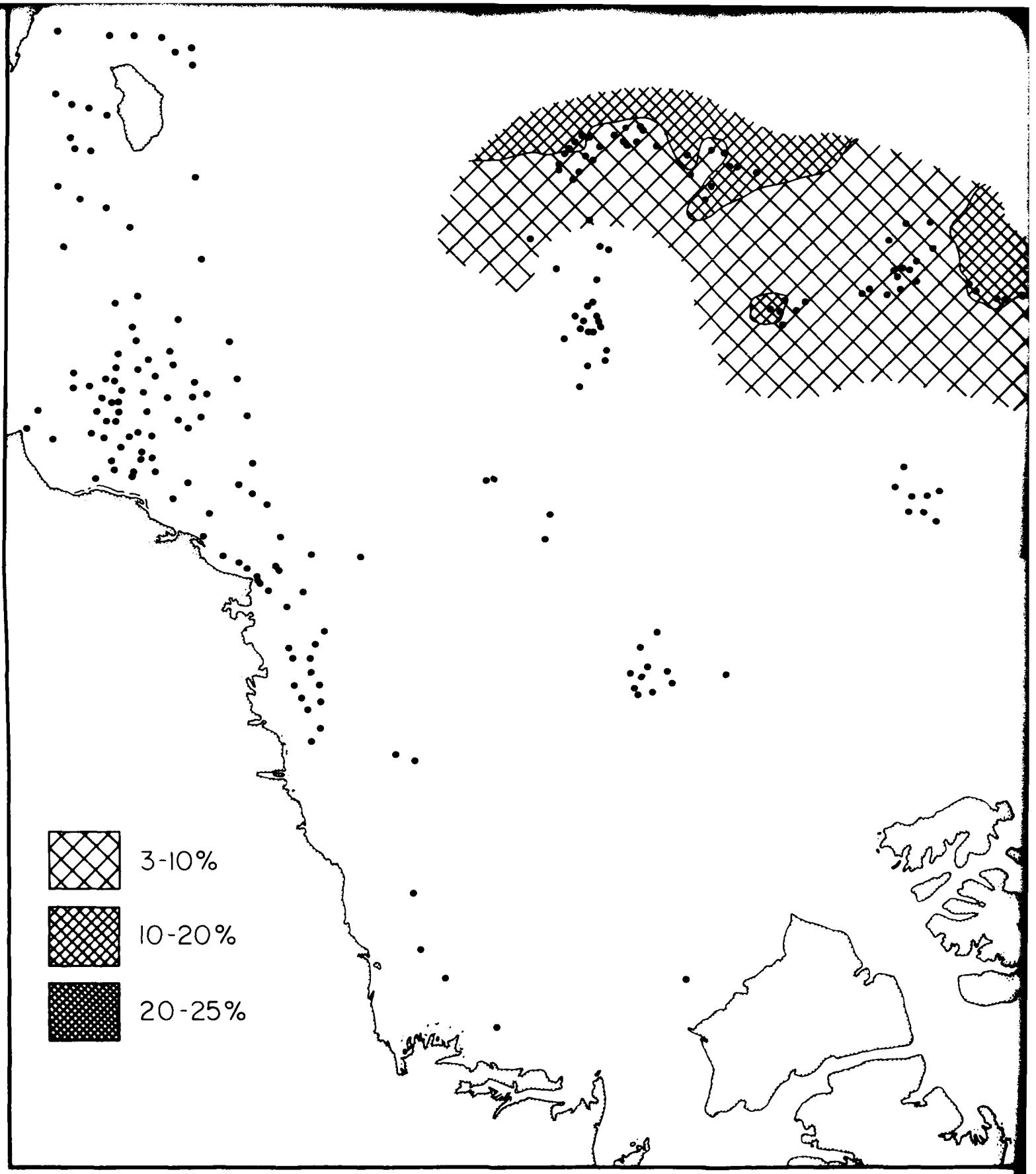

Plate 7. Percent mixed-layers expandable in Arctic Ocean surface sediment. See Plate 1 explanation for sample-number data and geographic information.

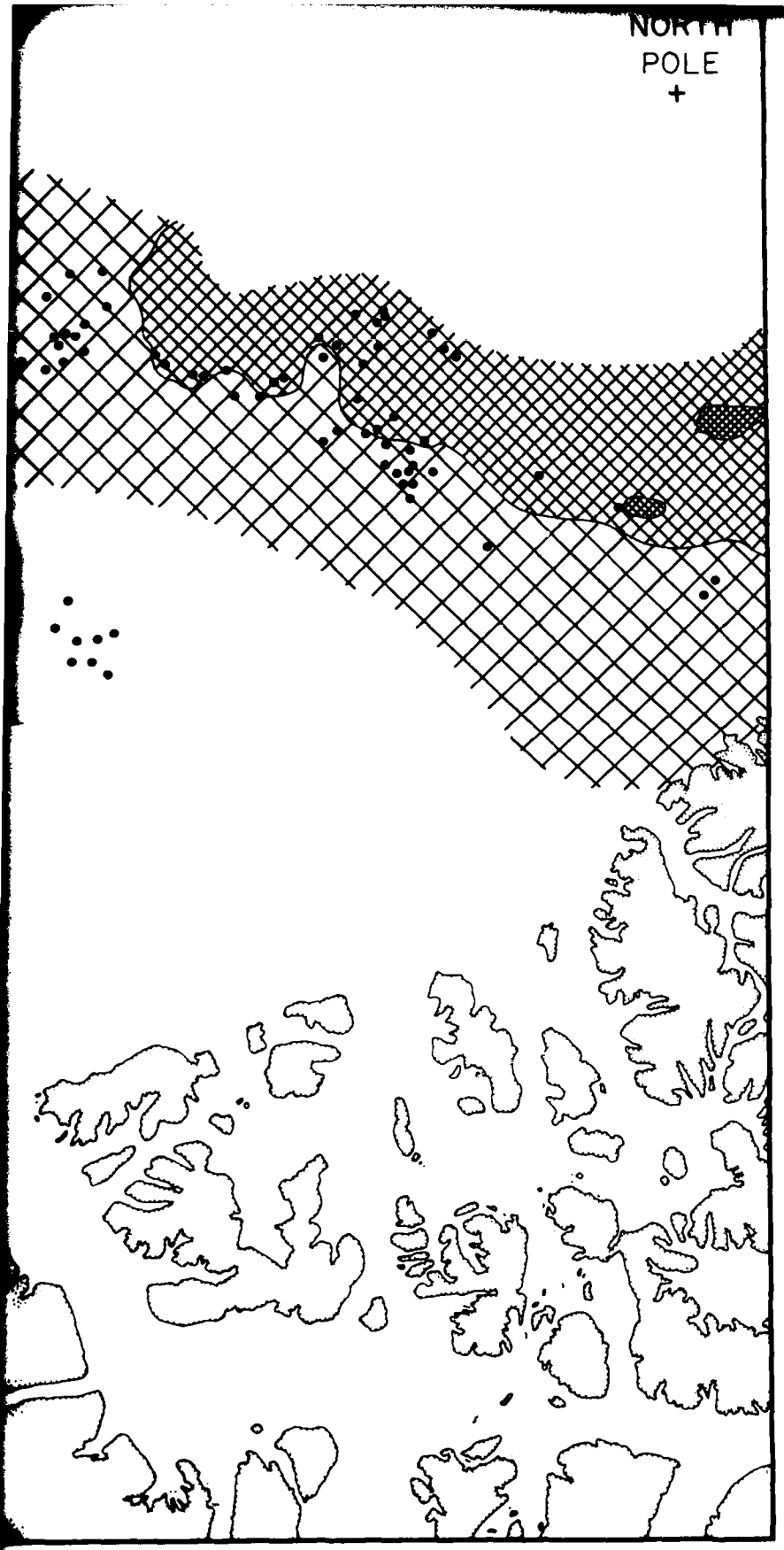

ace sediment. See Plate 1


10
10
10
20
0

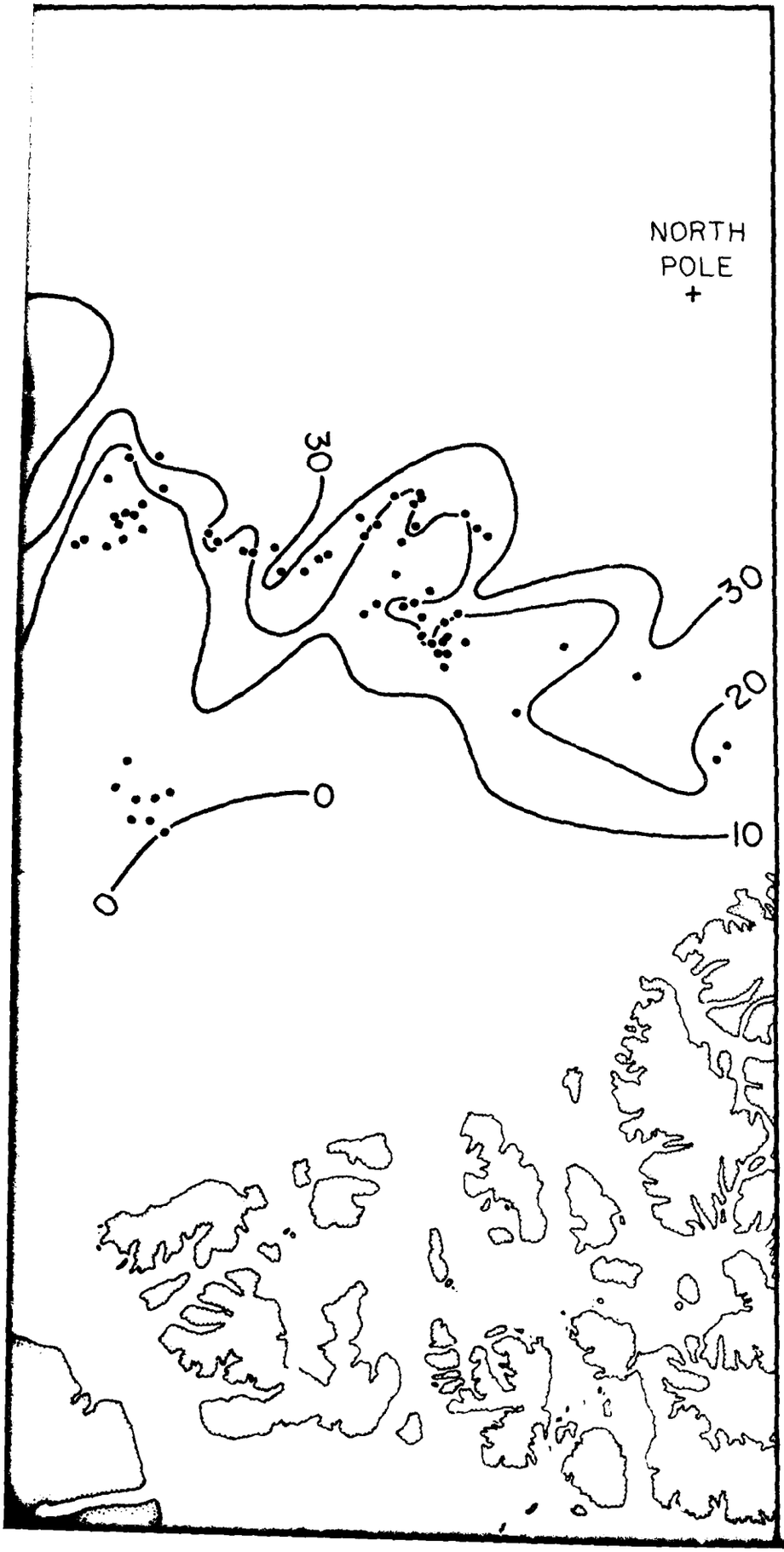
NORTH
POLE
30
30
20
10
0
0

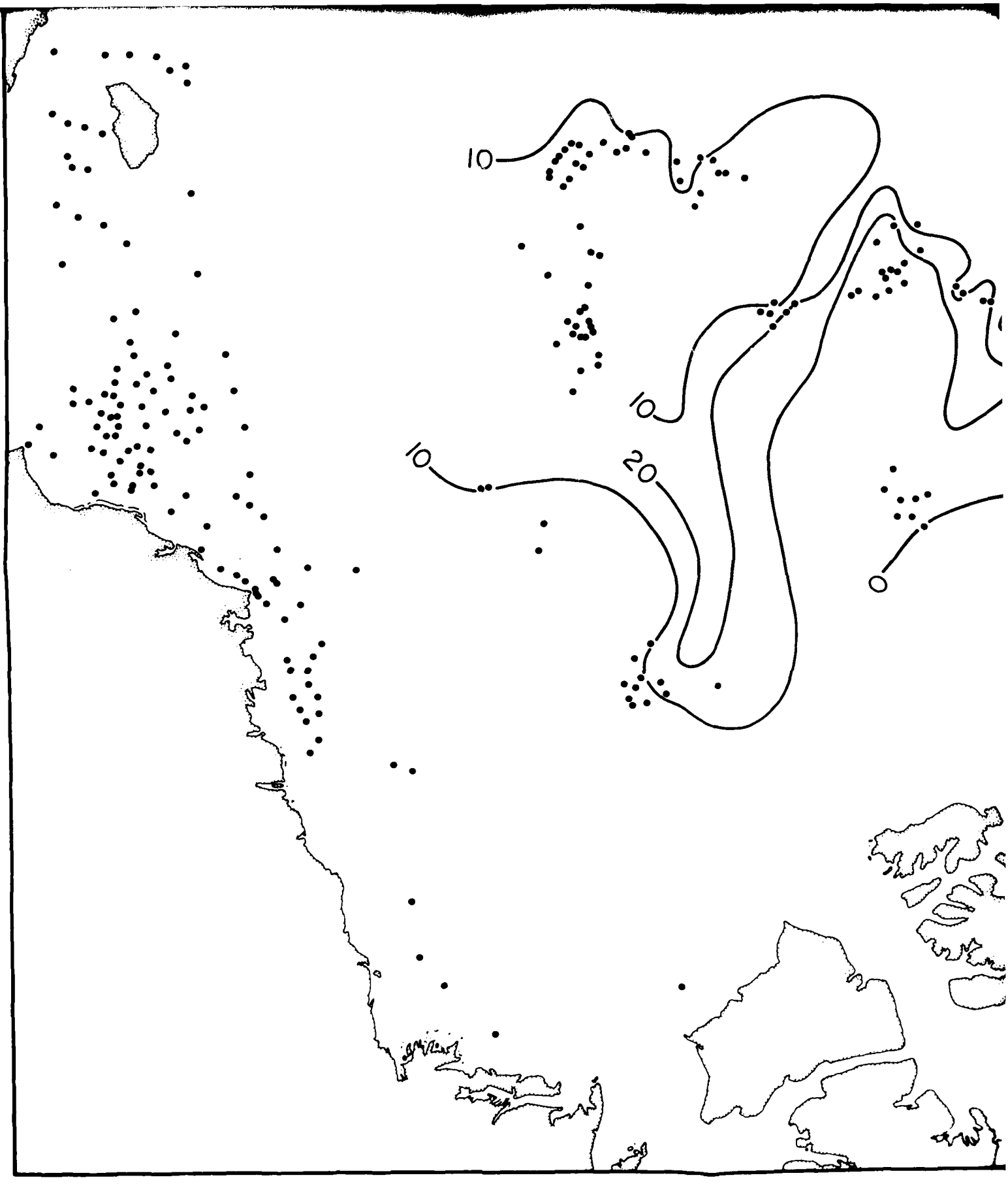

Plate 8. Isopach map of percent sand (<62 μm) in Arctic Ocean surface sediment
Plate 1 explanation for sample-number data and geographic information

3

AD-A096 078 WISCONSIN UNIV-MADISON DEPT OF GEOLOGY AND GEOPHYSICS F/G 8/10
STRATIGRAPHY AND GLACIAL-MARINE SEDIMENTS OF THE AMERASIAN BASI--ETC(U)
FEB 81 D L CLARK, R R WHITMAN, K A MORGAN N00014-76-C-0005

UNCLASSIFIED NL

2 OF 2

END
DATE FILMED
4-81
DTIC

Ocean surface sediment. See
information.


N
DATE
ILME